

DISS. ETH NO. 26365

***UNDERSTANDING THE STRUCTURE,
ACTIVITY AND INITIATION OF ACTIVE
SITES IN TUNGSTEN OXO BASED OLEFIN
METATHESIS CATALYSTS***

A thesis submitted to attain the degree of
DOCTOR OF SCIENCES of ETH ZURICH
(Dr. sc. ETH Zurich)

presented by
KA WING CHAN

M. Phil. (Chem), The Hong Kong University of Science and Technology

born on 24.12.1991

citizen of
Hong Kong, China

accepted on the recommendation of
Prof. Dr. Christophe Copéret, examiner
Prof. Dr. Peter Chen, co-examiner
Dr. Olga Safonova, co-examiner
Prof. Dr. Richard R. Schrock, co-examiner

2019

Acknowledgments

First of all, I would like to acknowledge Prof. Christophe Copéret and Dr. Olga Safonova for giving me the opportunity to conduct my PhD study under their supervisions. Both of them have provided me a lot of freedom in conducting my research studies, and, at the same time, given me numerous suggestions and valuable guidance. I have to thank their patience in teaching and helping me throughout my PhD study, in addition to the encouraging environment that they have provided. I am grateful for all the projects that we completed together and for the exciting research that I could conduct.

I would like to thank Prof. C. Copéret, Prof. P. Chen, Dr. O. Safonova and Prof. R. R. Schrock for being the juries of my PhD and their time for reviewing my thesis.

Secondly, I would like to thank my collaborators, who contributed experimentally to the research projects: Prof. V. Mougel (who started the project on W(VI)-oxo species and offered me helps when I started my PhD), Dr. G. Siddiqi (who helped me on XAS), Dr. F. Allouche (who measured single crystal XRD), E. Lam (who taught me DFT calculations) and Dr. D. Mance (who measured ssNMR).

In addition, I would like to thank those former and current group members who have helped me during my PhD (in my XAS runs, scientific discussions and experiments etc.): Pavel (for all the fruitful and not so fruitful discussions), Nicolas, Jordan Meyet (for driving back and forth between PSI and ETH for 24 h), Keith (for fruitful discussions), Kim (for proper Swagelok training), Christopher (for NMR), Gina, Patrick, Wei-Chih (for NMR, EPR), Tsung-Han, Hsueh-Ju, Dima (for XRD, TEM), Maxence (for teaching me how to do an important but painful experiment in my PhD), Julia (for XAS run), Margherita (for fixing the GC), Keishi and Masami (for the reductants). I would also like to acknowledge Dr. M. Nachtegaal for his helps in SuperXAS.

It was my pleasure to work in the Copéret group, where I have learned and experienced a lot. I have to thank the rest of the group and former members that I had met, in particular, Shohei (for being so funny), Jorge, Hung-Kun and Reinhard.

Lastly, I need to thank my family for always providing me with great support.

Abstract	vii
-----------------------	------------

Zusammenfassung	viii
------------------------------	-------------

Chapter 1. Introduction

1.1 General Introduction	1
1.2 Olefin Metathesis.....	1
1.3 Heterogeneous Metathesis Catalysts	4
1.3.1 W-based Heterogeneous Catalysts	4
1.3.2 Mo-based Heterogeneous Catalysts	5
1.3.3 Re-based Heterogeneous Catalysts	6
1.4 Initiation Mechanisms of Supported Metal Oxide Catalysts	6
1.4.1 Initiation of W-based Catalysts	7
1.4.2 Initiation of Mo-based Catalysts	8
1.4.3 Initiation of Re-based Catalysts	8
1.5 Homogeneous Metathesis Catalysts.....	9
1.5.1 Oxo Ligand-based W and Mo Alkylidenes	9
1.5.2 Formation of Alkylidenes from Reduced Metal Complexes.....	10
1.6 Well-defined Heterogeneous Metathesis Catalyst Prepared by Surface Organometallic Chemistry	13
1.7 Strategy and Outline	15
1.8 References	17

Chapter 2. Preparation of Well-defined Silica-supported Tungsten-oxo Species and Metathesis Activity upon Activation by Organosilicon Reducing Agents

2.1 Introduction	25
2.2 Result and Discussion.....	26
2.2.1 Synthesis of Well-Defined Silica Supported Tungsten-oxo Species	26
2.2.2 Activation at Low Temperature with Organosilicon Reducing Agents	27
2.2.3 Characterization of Activated Catalysts 1-(Red) ₂	29
2.2.4 Catalytic Activity of Activated Materials.....	31
2.2.5 Investigation of Reaction Intermediates and Initiation Mechanism.....	33
2.3 Conclusion.....	34
2.4 Experimental Details.....	35
2.4.1 General procedures	35

2.4.2	Synthesis of the molecular precursors	36
2.4.3	Synthesis of the supported materials	36
2.4.4	Catalytic test	38
2.4.5	Exposure of 1-(Red) ₂ to ethylene	38
2.5	References	39

Chapter 3. Olefin Metathesis Initiated by Molecular Tungsten(IV)-oxo Complex

3.1	Introduction	42
3.2	Result and Discussion.....	43
3.2.1	Synthesis of WO(OR) ₂ (py) ₃	43
3.2.2	Catalytic Activity and Reactivity of WO(OR) ₂ (py) ₃	44
3.2.3	Reactions of WO(O <i>t</i> BuF ₆) ₂ (py) ₃ with <i>trans</i> - β -(methyl- <i>d</i> ₃)styrene and Allylbenzene.....	49
3.2.4	DFT Computational Studies of the Initiation Mechanisms.....	50
3.3	Conclusion.....	53
3.4	Experimental Details.....	54
3.4.1	General procedures	54
3.4.2	Syntheses of 1a-1b, 2a-2c, 3a-C ₂ H ₄ , 3a-C ₃ H ₆	54
3.4.3	Catalytic tests	57
3.4.4	Reaction with olefins.....	58
3.4.5	Kinetic studies on the reaction of 2a and <i>trans</i> - β -methylstyrene in the presence of B(C ₆ F ₅) ₃	58
3.4.6	Computational details.....	59
3.5	References	60

Chapter 4. Well-defined Silica-supported Tungsten(IV)-oxo Complex: Olefin Metathesis Activity, Initiation and Role of Brønsted Acid Sites

4.1	Introduction	63
4.2	Result and Discussion.....	64
4.2.1	Synthesis and Characterization of (\equiv SiO)WO(O <i>t</i> BuF ₆)(py) ₃	64
4.2.2	Catalytic Activity	65
4.2.3	Effect of Surface OH Density	66
4.2.4	Investigation of Reaction Intermediates Formed Upon Reaction of F6@SiO ₂₋₂₀₀ with Styrene.....	68
4.2.5	Brønsted Acid Site in F6@SiO ₂₋₂₀₀ Probed by ¹⁵ N-pyridine	69
4.2.6	Proposed Initiation Mechanism for the Formation of Alkylidenes.....	70
4.3	Conclusion.....	71

4.4	Experimental Details	73
4.4.1	General procedures.....	73
4.4.2	Syntheses and characterizations of supported Species (F6@SiO _{2-x}).....	74
4.4.3	Catalytic activity measurements.....	75
4.4.4	Reactions of F6@SiO ₂₋₂₀₀ with styrene- α , β - ¹³ C ₂	77
4.4.5	Reaction of ¹⁵ N-F6@SiO ₂₋₂₀₀ with ¹⁵ N-py/B(C ₆ F ₅) ₃	77
4.5	References	78

Chapter 5. Effects of Preparation Methods and Organosilicon Reductants on the Olefin Metathesis Activity of Silica-supported W(VI)-oxo Species

5.1	Introduction	80
5.2	Result and Discussion	80
5.2.1	Effects of Precursors and Preparation Methods on the Structure of Supported W-oxo Species.....	80
5.2.2	Effects of Reductants on the Catalytic Activities of W-oxo Species Prepared by Different Approaches.....	82
5.2.3	Origins of the Difference in Activities between Various Systems.....	85
5.3	Conclusion	91
5.4	Experimental Details	93
5.4.1	General procedures.....	93
5.4.2	Synthesis of 1-WO.....	94
5.4.3	Synthesis of 1-WO ₂ -Red1.....	94
5.4.4	Synthesis of 1-WO ₂ -SA500.....	94
5.4.5	Catalytic activity measurements.....	95
5.4.6	Titration experiments with ethene and 2-butene.....	96
5.5	References	97

Chapter 6. Conclusion and Perspective99

Appendixes

	Appendix to Chapter 2.....	103
	Appendix to Chapter 3.....	132
	Appendix to Chapter 4.....	154
	Appendix to Chapter 5.....	174
	Curriculum Vitae.....	185

Abstract

Silica-supported tungsten-oxo catalyst (WO_3/SiO_2) is an important heterogeneous metathesis catalyst, which is used in one of the largest industrial processes nowadays for the production of propene via olefin metathesis. However, understanding in the nature of active sites and their formation mechanisms in WO_3/SiO_2 is very limited, despite years of research. In this PhD thesis, we address these questions by tailoring and investigating well-defined molecular and supported model systems prepared by Surface Organometallic Chemistry (SOMC). We prepared a silica-supported molecularly-defined W(VI)-oxo material as a model for WO_3/SiO_2 . In addition, we show that upon low-temperature activation with organosilicon reducing agents, reduced W(IV) species are generated. These W(IV) centers serve as highly active precatalysts for metathesis. Investigations with molecular W(IV)-oxo complex provided further information on the structure of the active precatalyst and its initiation mechanism. Further studies with well-defined silica-supported W(IV)-oxo system reveal the role of oxide support, especially the surface Brønsted acidic sites, in the initiation and the dependence of initiation mechanisms on the types of olefins used. Comparison of the WO_3/SiO_2 system with the molecularly-defined W(VI)-oxo species prepared by SOMC, allows us to bridge the gap between the well-defined model systems and the ill-defined heterogeneous catalyst. This study shows the effects of preparation methods, conditions and organosilicon reductants on the metathesis activity of the W(VI)-oxo species, which is closely related to their reducibility.

Zusammenfassung

Der Wolfram-Oxo Katalysator auf Siliziumdioxid Trägeroberflächen (WO_3/SiO_2) ist ein wichtiger heterogener Katalysator für die Olefinmetathese Reaktion und wird heutzutage in einem der grössten industriellen Prozesse für die Produktion von Propen verwendet. Das Verständnis der Struktur der aktiven Zentren sowie deren Entstehungsmechanismus ist jedoch trotz jahrelanger Forschung sehr limitiert. Diese Dissertation befasst sich mit dieser Problematik durch die Erzeugung und Untersuchung von wohldefinierten molekularen und auf Siliziumdioxid-Trägeroberflächen aufgebrachten Modellsystemen, hergestellt durch metallorganische Oberflächenchemie (SOMC). Auf molekularer Ebene wohldefinierte, auf Siliziumdioxid aufgebrachte, W(VI)-Oxo Materialien wurden als Modell für WO_3/SiO_2 hergestellt. Diese W(VI) Spezies wurden mittels Organosilizium Reduktionsmitteln bei tiefer Temperatur aktiviert. Die entstandenen W(IV) Zentren sind sehr reaktive Katalysator-Vorstufen für die Metathese Reaktion. Untersuchungen an molekularen W(IV)-oxo Komplexen lieferten weitere Informationen über die Struktur der Vorstufe sowie deren Initiierungsmechanismus. Weitere Untersuchungen mit wohldefinierten W(IV)-oxo Systemen unterstützt auf Siliziumoxid offenbarten die Rolle der Oxid-Trägeroberfläche. Dabei wurde die Funktion von Brønsted Säuren auf der Oberfläche für die Initiierung und die Abhängigkeit des Initiierungsmechanismus von verschiedenen Typen von Olefinen untersucht. Der Vergleich zwischen WO_3/SiO_2 Systemen und auf molekularer Ebene wohldefinierten Siliziumdioxid-unterstützten W(VI)-oxo Gruppen hergestellt durch SOMC erlaubte, einen Zusammenhang zwischen wohldefinierten Modellsystemen und schlecht-definierten heterogenen Katalysatoren herzustellen. Diese Studie zeigt den Effekt der Organosilizium Reduktionsmitteln sowie der Herstellungsmethode des Katalysators auf die Aktivität für die Metathese Reaktion von den W(VI)-oxo Gruppen, die im Zusammenhang mit deren Reduzierbarkeit steht.

Chapter 1. Introduction

1.1 General Introduction

Olefin metathesis is a reaction that has been widely used over the past decades in different industries, ranging from petrochemical to pharmaceutical applications. Nowadays, due to the increasing demand of propylene, its production via cross-metathesis of ethylene and 2-butene has become one of the largest scale industrial processes. This process is catalyzed by a heterogeneous catalyst: tungsten oxide supported on silica (WO_3/SiO_2).

Supported metal oxide metathesis catalysts prepared by conventional impregnation methods generally have a very small amount of active sites, and therefore, any structural investigation by spectroscopic technique is very challenging. In fact, despite years of research, the structures of active species, reaction intermediates and their formation mechanisms remain elusive and they are still the key questions in this field.

In order to develop a better understanding of the heterogeneous catalysts, one of the approaches is to synthesize well-defined supported catalysts via Surface Organometallic Chemistry (SOMC). This approach provides structural control at a molecular-level by grafting well-defined molecular complexes on partially dehydroxylated oxide supports. Grafting mainly proceeds through the reaction with the surface hydroxyl groups and generates supported catalysts with close to 100 % active sites, hence they are often coined “single-site catalysts”. The presence of a dominant surface species facilitates spectroscopic studies, thus leading to a better understanding of the supported systems.

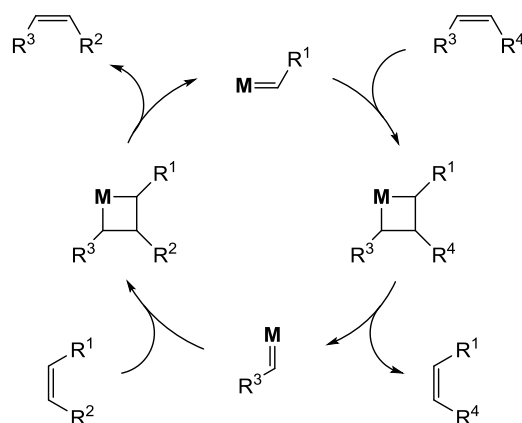
This PhD thesis is devoted in understanding tungsten-oxo based olefin metathesis catalysts, in particular, the initiation process involved in transforming the tungsten-oxo species into active catalysts. This includes conducting detailed investigations on molecular models, well-defined supported catalysts and related supported model systems prepared by SOMC, as well as the classical WO_3/SiO_2 catalyst.

1.2 Olefin Metathesis

Olefin metathesis is a reaction that allows the exchange of alkylidene fragments between different olefins. It was discovered in 1955 by industrial chemists at DuPont when they polymerized norbornene to form polynorbornene using TiCl_4 and lithium aluminum tetrabutyl.¹ In 1964, R. L. Banks and G. C. Bailey of Phillips Petroleum reported the first disproportionation of linear olefin catalyzed by heterogeneous molybdenum and tungsten

based catalysts dispersed on oxide supports.² In the same year, G. Natta reported the ring opening polymerization of cyclopentene catalyzed by WCl_6 or $MoCl_5$ with $Al(C_2H_5)_3$.³ It was only in 1967, that the homogeneous version of disproportionation of linear olefin was reported by N. Calderon at Goodyear, demonstrating the production of 3-hexenes and 2-butenes from 2-pentenes catalyzed by $WCl_6/EtOH/EtAlCl_2$.⁴ Since then, the term “metathesis” was introduced and the disproportionation of olefin and ring opening polymerization were considered to be the same type of reaction. Nowadays, olefin metathesis catalysts are mainly based on group VI-VIII (molybdenum, tungsten, rhenium and ruthenium) transition-metal complexes and the corresponding supported group VI-VII metal oxide.⁵⁻⁶

In 1971, the reaction mechanism of olefin metathesis (Scheme 1.1) was proposed by Chauvin,⁷ who shared the 2005 Nobel Prize of Chemistry with R. G. Grubbs and R. R. Schrock.⁸⁻¹⁰ The Chauvin mechanism involves metal alkylidene as the key moiety, which can undergo [2+2] cycloaddition with an olefin to form a metallacyclobutane; subsequent cycloreversion yields the metathesis products.



Scheme 1.1. Chauvin mechanism for olefin metathesis.

Chauvin mechanism is now widely accepted. In fact, different experimental and computational studies have further supported that mechanism and revealed more details regarding the active species and the reaction mechanism. It is now generally accepted that a catalytically active metal alkylidene complex should be a 14 valence electron tetra-coordinated species, which is consistent with the ubiquitous high valent d^0 Schrock type alkylidenes (Figure 1.1.A).¹¹ In the case of d^6 Grubbs type carbene (Figure 1.1.B), such as $RuCl_2L_2(=CHR)$, the dissociation of one of the L type ligands is required to generate the metathesis active species.¹²⁻¹⁵ Meanwhile, a metathesis active metallacyclobutane intermediate is shown to have a trigonal bipyramidal geometry (TBP), while square pyramidal

(SP) geometry of metallacyclobutane is shown to be an off-cycle species in d^0 systems (Scheme 1.2) and is a high energy (and never observed) intermediate in the Ru-based catalysts.¹⁶⁻¹⁸ Computational studies have also shown that additional steps, for instance, olefin coordination could require a relatively high energy barrier for d^0 catalysts that is mostly associated with the distortion to trigonal pyramidal geometry. Thus, this step could play an important role in controlling the rate of metathesis.¹⁹⁻²²

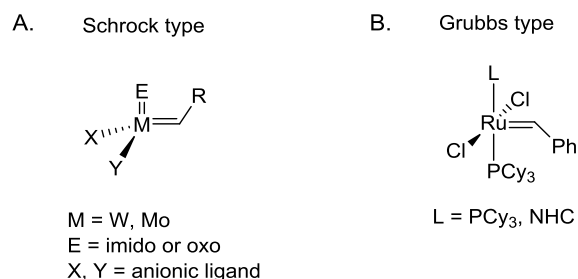
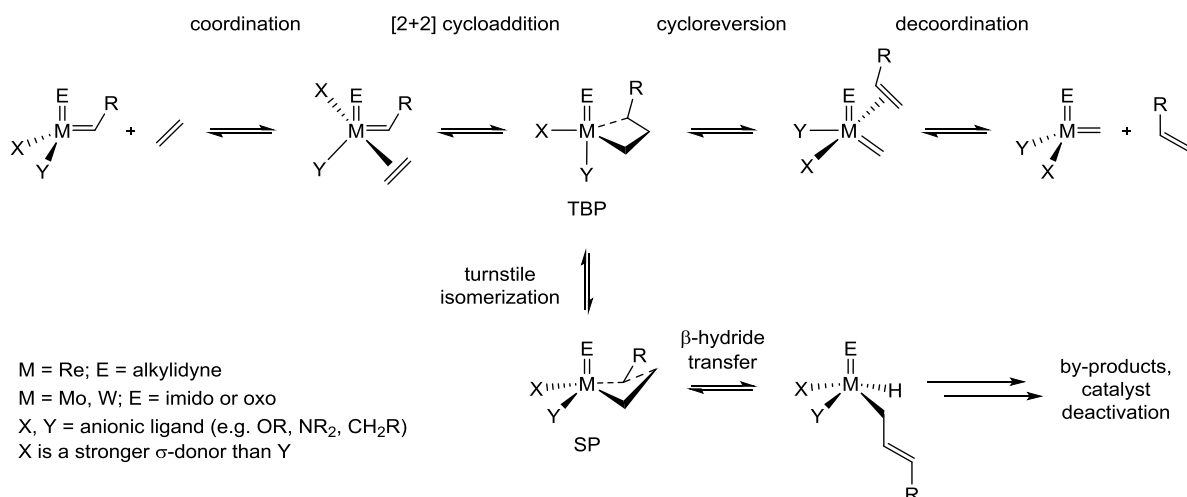
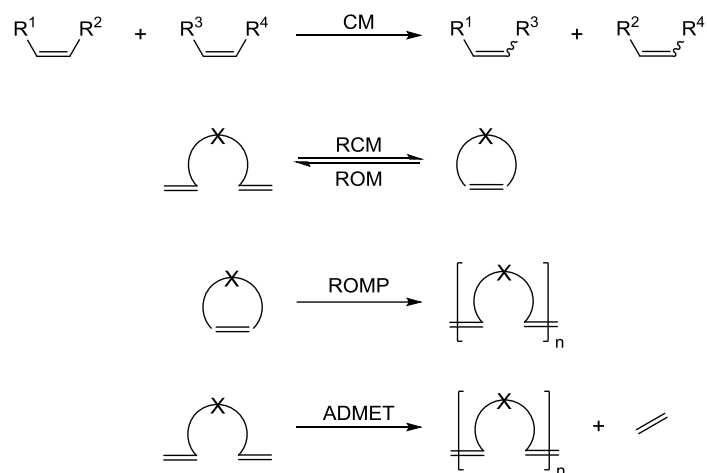


Figure 1.1.A. General structures of Schrock type and **1.1.B.** Grubbs type olefin metathesis catalysts.



Scheme 1.2. Elementary steps and decomposition pathways involved in olefin metathesis catalyzed by d^0 alkylidene complexes of Mo, W and Re.

Olefin metathesis reaction can be sub-divided into several major classes (Scheme 1.3) including Self-/ Cross-Metathesis (CM) for acyclic olefins, Ring Opening Metathesis (ROM) for transforming cyclic olefins into acyclic products, Ring Closing Metathesis (RCM) which is the reverse of ROM,²³ Ring Opening Metathesis Polymerization (ROMP) for forming acyclic polymers from cyclic olefins and Acyclic Diene Metathesis (ADMET) for polymerization of dienes.²⁴⁻²⁵



Scheme 1.3. Major classes in olefin metathesis reactions.

1.3 Heterogeneous Metathesis Catalysts

Heterogeneous metathesis catalysts are mainly based on tungsten, molybdenum or rhenium oxides supported on high surface area (ca. 100 – 500 m²/g) oxide supports, such as silica (SiO₂) and alumina (Al₂O₃) as well as silica-alumina (SiO₂–Al₂O₃). Typically, these catalysts are prepared by impregnation followed by calcination at high temperatures. They are known to have a small amount of active sites (< 5%). In addition, the nature and the formation mechanism of the active sites are still under debate. The supported W(VI), Mo(VI) or Re(VII) oxides, which can be present as monomeric metal-oxo species, oligomers, clusters or crystalline nanoparticles, are believed to be the precursors for active site formation. While the supports are inactive for metathesis, their acidity has been shown to affect the metathesis activity and product selectivity by promoting side reactions, for instance, isomerization and coke formation.²⁶

1.3.1 W-based Heterogeneous Catalysts

Silica-supported tungsten oxide (WO₃/SiO₂) is the most commonly used industrial olefin metathesis catalyst. It is used in the Olefin Conversion Technology (OCT) process, which produces propylene from ethenolysis of 2-butene.⁶ The W-based catalyst has higher resistance towards oxygenate poisons in the feeds; it displays longer lifetime compared to the Mo- or Re-based catalysts and is easily regenerated to remove coke.²⁷ However, it typically operates at temperatures above 400 °C.

A number of studies had been carried out to investigate the surface structure of WO₃/SiO₂ via various in situ spectroscopic methods including Raman, IR and UV-Vis spectroscopy as well as Diffuse Reflectance Spectroscopy (DRS), and X-ray Absorption Spectroscopy (XAS).²⁸⁻²⁹ Under fully oxidizing and anhydrous conditions, di-oxo

$(\equiv\text{SiO})_2\text{W}(=\text{O})_2$ and mono-oxo $(\equiv\text{SiO})_4\text{W}(=\text{O})$ sites are observed, in addition to the WO_3 nanoparticles/clusters (Figure 1.2). The relative amounts of these species depend on the W loading. For 2 – 6 wt % of WO_x , di-oxo $(\equiv\text{SiO})_2\text{W}(=\text{O})_2$ species is reported to be the dominant species, which is also proposed to be the source of active sites. From 8 wt % of WO_x or above, crystalline WO_3 nanoparticles are also present but they are shown to be inactive for metathesis.³⁰

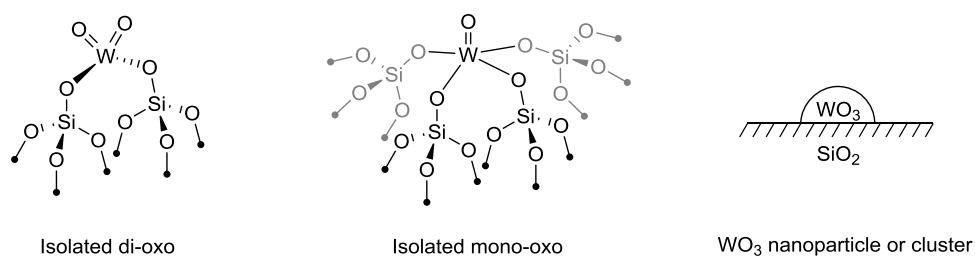


Figure 1.2. Various surface species present on WO_3/SiO_2 .

In contrast, supported $\text{WO}_3/\text{Al}_2\text{O}_3$ has received less attention in the literature since its activity is lower than that of $\text{MoO}_3/\text{Al}_2\text{O}_3$ or $\text{ReO}_x/\text{Al}_2\text{O}_3$. It has been shown that the $\text{SiO}_2\text{--Al}_2\text{O}_3$ mixed oxide support with a suitable composition could enhance the metathesis activity, while the product selectivity is also influenced by the $\text{SiO}_2/\text{Al}_2\text{O}_3$ ratio. For instance, the ethylene and hexene selectivities from 1-butene metathesis decrease with an increasing SiO_2 to Al_2O_3 ratio.³¹⁻³³

1.3.2 Mo-based Heterogeneous Catalysts

$\text{MoO}_3/\text{Al}_2\text{O}_3$, which has an operation temperature of 100 – 200 °C, is used in the Shell Higher Olefin Process (SHOP). This process converts ethylene into linear higher α -olefins by using a combination of oligomerization, isomerization and metathesis catalysts.⁶

The molecular structure of surface MoO_3 species on Al_2O_3 has been established by different spectroscopic studies³⁴⁻³⁶, such as Raman, UV-Vis, DRS, XAS, and DFT computations.³⁷⁻³⁹ Although the findings are similar to the supported W oxide species, it has been shown that only isolated di-oxo $(-\text{O})_2\text{Mo}(=\text{O})_2$ species is present at low surface coverage (≤ 1 Mo atoms/ nm^2). Oligomeric mono-oxo $(-\text{O})_4\text{Mo}(=\text{O})$ and crystalline MoO_3 nanoparticles only appear at 1 – 4.5 and above 4.6 Mo atoms/ nm^2 , respectively. In addition, recent in-situ studies suggested that the oligomeric mono-oxo $(-\text{O})_4\text{Mo}(=\text{O})$ sites, which are anchored at the more acidic $\mu_{1/3}\text{-Al}_{\text{V/VI}}$ sites, are more ready to be transformed into active sites compared to the isolated $(-\text{O})_2\text{Mo}(=\text{O})_2$ at the more basic $\mu_1\text{-Al}_{\text{IV}}$.⁴⁰

Similar structures of the surface species are also identified in $\text{MoO}_3/\text{SiO}_2$, however this catalyst is an order of magnitude less active than $\text{MoO}_3/\text{Al}_2\text{O}_3$.²⁶ Noteworthy, $\text{MoO}_3/\text{SiO}_2\text{-Al}_2\text{O}_3$ has a higher catalytic activity compared to $\text{MoO}_3/\text{Al}_2\text{O}_3$ or $\text{MoO}_3/\text{SiO}_2$, and it is proposed that the optimal level of Brønsted acidity of the support contributes to the high activity.⁴¹⁻⁴²

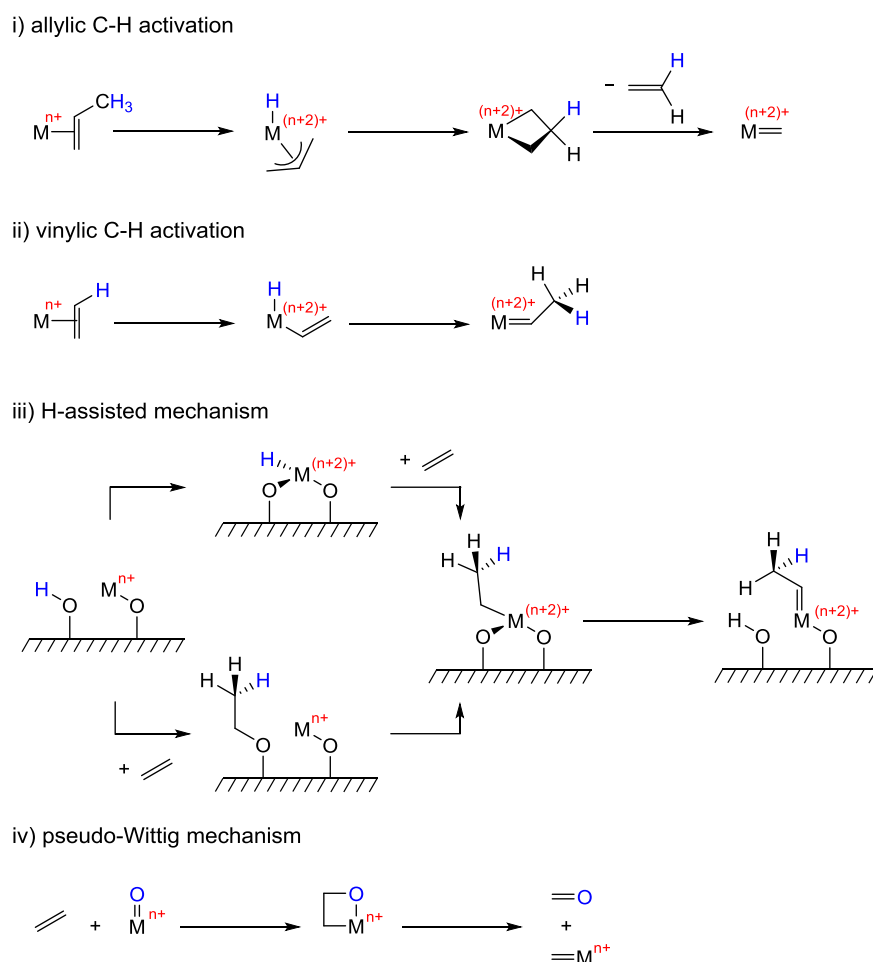
1.3.3 Re-based Heterogeneous Catalysts

$\text{Re}_2\text{O}_7/\text{Al}_2\text{O}_3$ and related systems are the only supported oxide catalysts that can perform olefin metathesis at room temperature. Furthermore, $\text{Re}_2\text{O}_7/\text{Al}_2\text{O}_3$ is compatible with functional olefin in the presence of promoters such as Me_4Sn .⁴³ However, the expensive cost and volatility of Re oxide have limited its applications in industry. The low melting point (297 °C) of crystalline Re_2O_7 ensure homogeneously dispersed Re sites after calcination at high temperature. The structures of surface Re sites on Al_2O_3 are found to be isolated tetra-coordinated $(\text{O}=\text{O})_2\text{ReO}_2$ with two terminal oxo ligands by a combination of detailed experimental and computational studies.⁴⁴⁻⁴⁵ There are two distinct $(\text{O}=\text{O})_2\text{ReO}_2$ species, anchored either on basic $\mu_1\text{-Al}_{\text{IV}}$ site or acidic $\mu_2\text{-Al}_{\text{VI}}$ and $\mu_3\text{-Al}_{\text{VI}}$ sites. At low Re coverage, the anchoring on basic $\mu_1\text{-Al}_{\text{IV}}$ site is preferable leading to the formation of distorted $(\text{O}=\text{O})_2\text{ReO}_2$ species, which are inactive in metathesis. In fact, metathesis activity is only observed with Re coverage above $0.74 \text{ Re}/\text{nm}^2$ when anchoring of $(\text{O}=\text{O})_2\text{ReO}_2$ takes place on acidic alumina sites. In contrast, $\text{Re}_2\text{O}_7/\text{SiO}_2$ is inactive for metathesis⁴⁶ and $\text{Re}_2\text{O}_7/\text{SiO}_2\text{-Al}_2\text{O}_3$ is more active than $\text{Re}_2\text{O}_7/\text{Al}_2\text{O}_3$ at low loading ($< 0.5 \text{ Re}/\text{nm}^2$) with a decrease in activity as the loading increases.⁴⁷

1.4 Initiation Mechanisms of Supported Metal Oxide Catalysts

All supported metal oxide catalysts are in fact precatalysts and need to undergo an initiation step to generate the corresponding metal alkylidenes, which are the active states of the olefin metathesis catalysts. However, due to the small quantity of active sites ($< 5\%$), understanding the initiation mechanism has been a great challenge. Many studies have been focused on investigating different pre-treatment conditions and their effects on the duration of induction period and metathesis activity. In addition, by analyzing the initiation products formed during the induction period, different initiation mechanisms have been proposed over the years. The most commonly proposed initiation mechanisms include i) allylic C–H activation,⁴⁸⁻⁵¹ ii) vinylic C–H activation,⁵²⁻⁵³ iii) H-assisted mechanism⁵⁴ and iv) pseudo-Wittig mechanism⁵⁵⁻⁵⁷ (Scheme 1.4). Among these mechanisms, only pseudo-Wittig

mechanism does not involve a reduced metal center as the starting precursor, while all the other mechanisms involve a change in the formal oxidation state of metal center.



Scheme 1.4. Proposed initiation mechanisms for heterogeneous olefin metathesis catalysts.

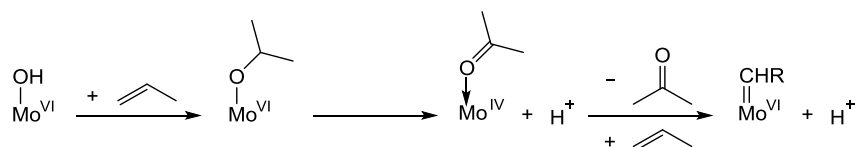
1.4.1 Initiation of W-based Catalysts

During the induction period of propene metathesis catalyzed by WO_3/SiO_2 , it has been reported that trace amounts of acetone and acetaldehyde are formed. While pre-treatments under H_2 or N_2 can reduce the amount of acetone formed, the amount of acetaldehyde remains the same suggesting two separate processes are involved. Moreover, the detection of non-stoichiometric $\text{WO}_{2.9}$ suggested a reduction of the surface W sites.⁵⁸ More recent studies by Lwin et. al. also reported the formation of oxygenate products, including acetaldehyde, formaldehyde, water and carbon dioxide, but no acetone was observed during the induction period.³⁰ In addition, they showed that highly active sites can only be generated by using propylene or 2-butene but not ethylene.⁵⁹ Howell et. al. reported the formation of acetone during the induction period, while acetone is not present when the catalyst is pre-treated with

He.⁶⁰ The presence of oxygenate products could be related to the reduction of metal centers or pseudo-Wittig mechanism, in the case of acetaldehyde and formaldehyde formed from propylene, depending on the identities of the oxygenate products. However, due to their variations in different studies, no consensus has been reached so far.

1.4.2 Initiation of Mo-based Catalysts

While MoO₃/SiO₂ is known to be less active compared to MoO₃/Al₂O₃,²⁶ most of the studies regarding initiation have been conducted on MoO₃/SiO₂. Early studies had shown that MoO₃/SiO₂ can be reduced by photoreduction in the presence of H₂ or CO, which subsequently lead to the formation of CO₂. Moreover, by poisoning test with N₂O, Mo with +4 oxidation state was proposed to be the species that leads to active site formation.⁶¹ Further studies on the photoreduced species revealed the formation of propylene via self-metathesis of ethylene, and in combination with the kinetic isotopic effect observed, vinylic C–H activation mechanism was proposed.⁶² Studies on the MoO₃/SBA-15 in the presence of propylene by IR spectroscopy suggested the formation of isopropoxyl group, which induces the formation of Mo +4 site and acetone (Scheme 1.5). These reduced Mo +4 centers were proposed to undergo vinylic C–H activation mechanism, based on the earlier reports, resulting in the formation of Mo alkylidene.⁶³ Kinetic study of the Mo(IV)/Al₂O₃ by isotope labeling of propylene also pointed to the vinylic C–H activation mechanism.⁵³ All the reported studies on supported Mo catalysts seem to suggest the generation of Mo +4 species followed by vinylic C–H activation mechanism to form the Mo alkylidenes.



Scheme 1.5. Proposed initiation mechanism for MoO₃/SBA-15 via Mo(IV) species.

1.4.3 Initiation of Re-based Catalysts

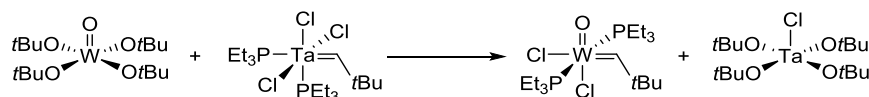
Re₂O₇/Al₂O₃ is known to be inactive for ethylene self-metathesis at room temperature.^{50, 56, 64} While early study had suggested allylic C–H activation mechanism by pulsing experiment of propylene and analysis of the first formed alkene,⁵⁰ later it has been shown that allylic C–H bond is not needed to initiate the metathesis activity as this catalyst can promote the cross-metathesis of *cis*-stilbene and ethylene.⁵⁶ In the same study, both vinylic C–H activation and H-assisted mechanisms were also ruled out by the absence of 3-

methyl-2-pentene in the self-metathesis of *cis*-2-butenes leaving pseudo-Wittig mechanism to be the most probably mechanism.

1.5 Homogeneous Metathesis Catalysts

Nowadays, some of the most widely used homogeneous metathesis catalysts are based on high valent Mo and W alkylidene complexes, which are also known as the Schrock-type catalysts.

In fact, the early development of these catalysts was inspired by the group 5 Tantalum chemistry. In 1974, Schrock discovered the first high valent alkylidene (*t*BuCH₂)₃Ta(=CH*t*Bu), which demonstrated the importance of using sterically hindered neopentyl ligands for stabilizing the tetra-coordinated highly electron deficient metal center. In addition, it showed that alkylidene moieties were accessible via α -H abstraction.⁶⁵ Later, the alkoxide complex Ta(=CH*t*Bu)(O*t*Bu)₂Cl(PMe₃) was shown to catalyze metathesis.⁶⁶



Eq. 1.1. Reaction of WO(O*t*Bu)₄ with TaCl₃(PEt₃)₂(=CH*t*Bu).

The first metathesis active group 6 alkylidene WO(PEt₃)₂Cl₂(=CH*t*Bu) was synthesized by reacting WO(O*t*Bu)₄ with TaCl₃(PEt₃)₂(=CH*t*Bu) (Eq. 1.1).⁶⁶⁻⁶⁷ However, this catalyst displays only a very slow metathesis activity in the absence of AlCl₃. Attempts to replace the Cl⁻ ligands by the more bulky alkoxide ligands e.g. *t*BuO⁻ led to the formation of WO(O*t*Bu)₂(=CH*t*Bu)(PEt₃). However, this complex decomposes in solution or in the solid-state at room temperature suggesting the oxo ligand is not bulky enough to prevent bimolecular decomposition.⁶⁸ Thereafter, the main research focus switched to the isoelectronic bulky imido ligands, instead of the oxo ligands. Imido ligands (NAr) containing a 2,6-disubstituted aryl group, such as 2,6-diisopropylaryl imido ligand, have shown to be a great success in synthesizing various tetra-coordinated W- and Mo-based alkylidenes.^{11, 69-70} Meanwhile, the synthesis of metathesis active Re(VII) alkylidene was also reported.⁷¹⁻⁷³

1.5.1 Oxo Ligand-based W and Mo Alkylidenes

Alkylidene complexes bearing an oxo ligand are fundamentally interesting since they are the closest model structures for the active sites in heterogeneous catalysts. However, due to the highly reactive nature of the oxo alkylidene complexes and the long and indirect synthetic route involved, they received much less attention in the literature compared to their

imido counterparts until more recently. In 2011, the syntheses of the tetra-coordinated $W(O)(CH-t-Bu)(OHIPT)(Me_2Pyr)$ (Pyr = 2,5-dimethylpyrrolide; OHIPT = *O*-2,6-(2,4,6-*i*-Pr₃C₆H₂)₂C₆H₃) and $W(O)(CH-t-Bu)(OHMT)(Me_2Pyr)(PMe_2Ph)$ (OHMT = *O*-2,6-dimesitylphenoxide) were reported (Figure 1.3.A).⁷⁴ The latter is shown to be a highly Z-selective catalyst.

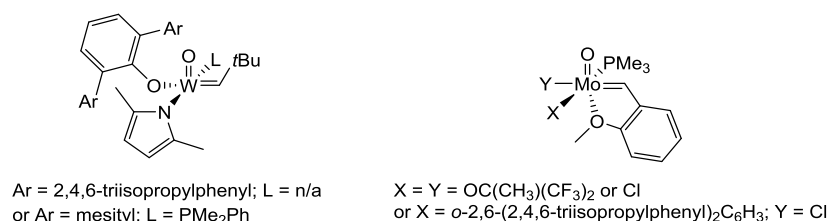
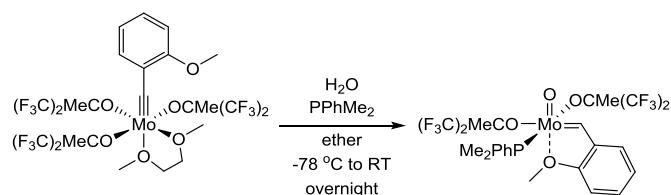


Figure 1.3.A. First well-defined tetra-coordinated W oxo alkylidene complexes; **1.3.B.** First metathesis active Mo oxo alkylidene complexes.

Afterwards, a new synthetic route for synthesizing $W(O)(CHR)Cl_2(PMe_2Ph)_2$ (R = *t*Bu or CMe_2Ph) was reported, which facilitates the syntheses of various W oxo alkylidene complexes.⁷⁵ Furthermore, the presence of oxo ligand allows investigation of the effect of Lewis acids e.g. $B(C_6F_5)_3$ in metathesis reaction to be conducted at a molecular-level.⁷⁶ Thereafter, the cationic W oxo alkylidenes stabilized by N-Heterocyclic Carbene (NHC) ligands were synthesized and they were shown to be highly active in metathesis.⁷⁷ The most recent development has led to the synthesis of the first well-defined Mo oxo alkylidenes (Figure 1.3.B) that are highly active in metathesis. It is worth noting that a key step in their syntheses involves the reaction between water and alkylidyne as illustrated in Eq. 1.2.⁷⁸⁻⁷⁹



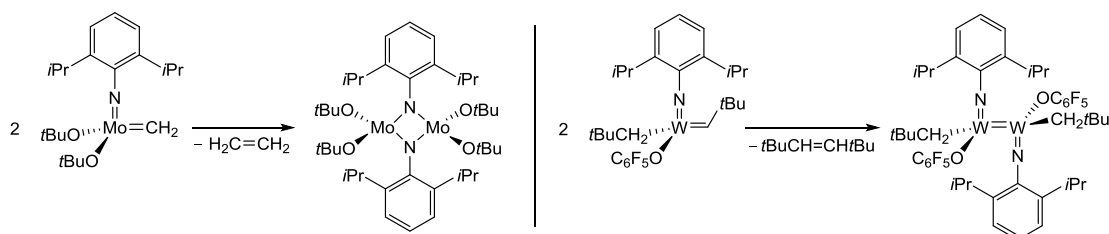
Eq. 1.2. Reaction of $Mo(CAr)[OCMe(CF_3)_2]_3(DME)$ (Ar = *o*-(OMe) C_6H_4) with water in the presence of $PPhMe_2$.

1.5.2 Formation of Alkylidenes from Reduced Metal Complexes

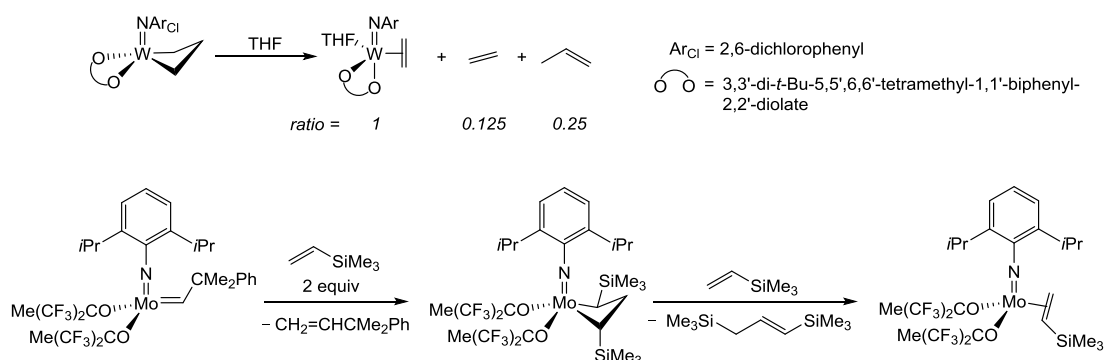
Common decomposition pathways of high valent alkylidenes include bimolecular coupling of the alkylidene moieties forming dimeric species (Scheme 1.6.A) and rearrangement of the metallacyclobutanes yielding reduced metal centers (Scheme 1.6.B).¹¹,

⁸⁰⁻⁸⁶ For example, Mo(IV) olefin complexes were identified as the decomposition products of Mo(VI) alkylidenes.⁸⁵⁻⁸⁷ Meanwhile, [ReCp(NO)(PPh₃)(=CH₂)]PF₆ complex was proposed to undergo bimolecular coupling followed by rearrangement to yield an ethylene π complex.⁸⁶ All these decomposition pathways involve the loss of the alkylidene moieties. Therefore, if one can regenerate the alkylidene moieties from these reduced metal complexes (the decomposition products), this would be a way to regenerate the metathesis active catalysts. Such alkylidene formation pathways might also be closely related to how active species are generated in the corresponding heterogeneous metal oxide catalysts (for more details, please refer to section 1.4).

A) Bimolecular decomposition



B) Rearrangement of metallacyclobutane or alkylidene

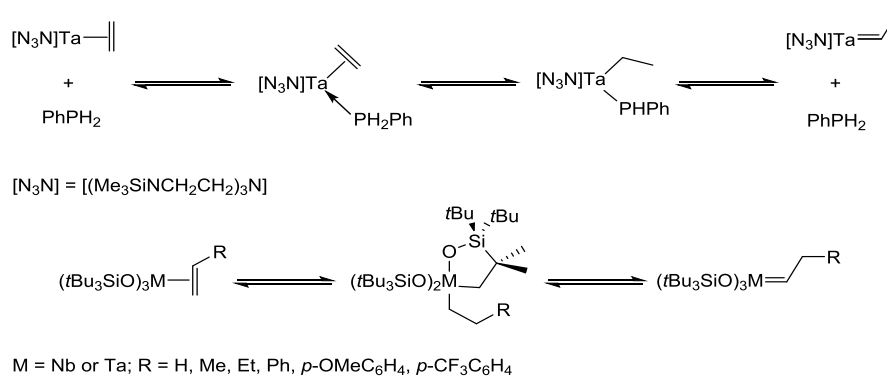


Scheme 1.6.A. Examples of dimers formation via bimolecular coupling of alkylidenes. **1.6.B.**

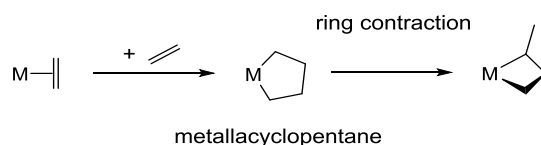
Examples of reduced W and Mo species formed via rearrangement of metathesis active species.

There are several reports on generating alkylidenes by using alkylidene transfer reagents, such as alkylidene phosphorane⁸⁸⁻⁹⁰ and diazomethane-based reagents⁹¹, on Ta(III) and W(IV), but the resulting complexes only show little to no activity in metathesis. Besides, these reagents might further react with the metal alkylidene formed leading to undesirable products.⁹² Alternatively, strained 3,3-diphenylcyclopropene has been used to generate vinylalkylidenes from reduced metal centers.⁹³⁻⁹⁶ Additionally, other pathways may operate. For instance, the rearrangement of olefins, which are coordinated to the M(III) (M = Ta or Nb) centers, into alkylidene moieties has been shown to be catalyzed by the presence of external proton source

or proton from the ligand (Scheme 1.7).⁹⁷⁻⁹⁸ Another potential route involves the formation of metallacyclopentane, which then undergo ring contraction to form metallacyclobutane (Eq 1.3), as proposed in the Ta and Re systems.⁹⁹⁻¹⁰⁰ This mechanism is also proposed for the unusual homologation of a vinyl tin species to an allyl tin species catalyzed by Mo(IV) ethylene complex.¹⁰¹

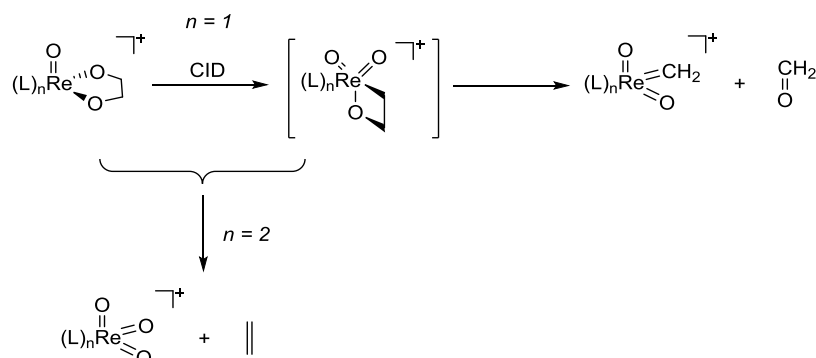


Scheme 1.7. Rearrangement of olefin complexes into alkylidenes for Ta(III) and Nb(III).



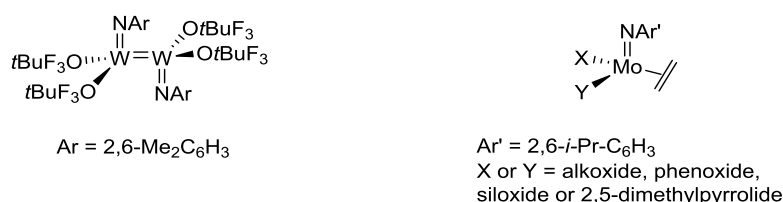
Eq. 1.3. Formation of metallacyclopentane followed by ring contraction.

Meanwhile, the formation of metathesis active Re alkylidene was observed from Re(V) diolate via Collision Induced Dissociation (CID) and metallaooxetane was proposed to be the intermediate, which could undergo cycloreversion to give the Re alkylidene and aldehydes (Scheme 1.8).^{57, 102-103} This study also provided a molecular evidence for the formation of alkylidenes by pseudo-Wittig mechanism, which has been proposed in the initiation of Re₂O₇/Al₂O₃.



Scheme 1.8. Formation of Re alkylidene from Re(V) diolate via Collision Induced Dissociation.

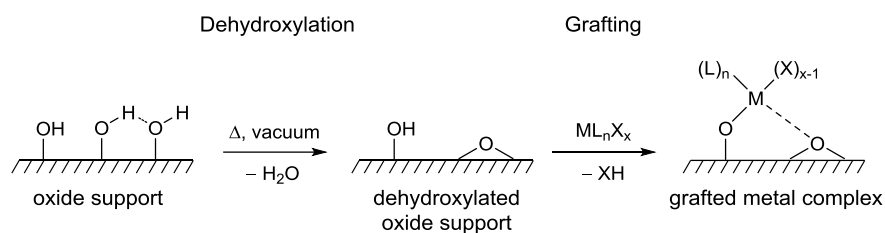
Although the formation mechanism of a metal alkylidene from an olefin and a reduced metal center is still under debate, there are several examples showing that low valent W¹⁰⁴ or Re¹⁰⁵ complexes could catalyze ROMP of strained olefins and that reduced M(IV) (M = Mo or W) complexes could slowly catalyze metathesis reaction. Notably, it has been reported that dimeric complexes containing unsupported M=M double bond such as [Mo(NAr)(CH₂-*t*-Bu)(OC₆F₅)]₂ (Ar = 2,6-*i*-Pr₂C₆H₃) and {W(NAr')[OCMe₂(CF₃)]₂ (Ar' = 2,6-Me₂C₆H₃) (Scheme 1.9.A) can slowly catalyze metathesis.¹⁰⁶ However, the amounts of alkylidenes formed in these systems were estimated to be less than 2 – 3 % and no spectroscopic evidence for the formation of alkylidene species has been reported. Similarly, various monomeric Mo(IV) olefin complexes (Scheme 1.9.B) have been reported to catalyze metathesis slowly including metathesis of acyclic olefins but the active alkylidene species have not been observed.⁸⁷



Scheme 1.9.A. Dimeric {W(NAr')[OCMe₂(CF₃)]₂ (Ar' = 2,6-Me₂C₆H₃) with unsupported W=W bond. **1.9.B.** Monomeric Mo(IV) olefin complexes.

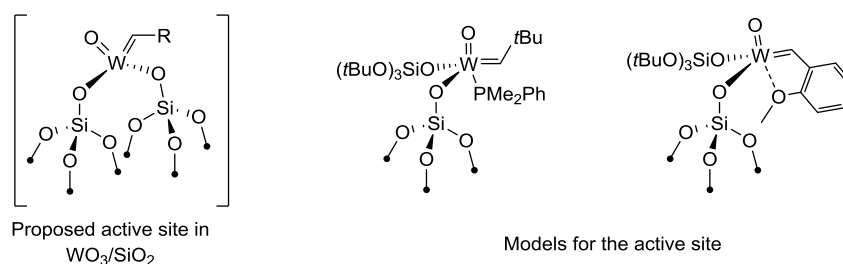
1.6 Well-defined Heterogeneous Metathesis Catalysts Prepared by Surface Organometallic Chemistry

Surface Organometallic Chemistry (SOMC) has emerged as a powerful approach to synthesize well-defined supported surface species, which helps to strengthen the connection between homogeneous and heterogeneous catalysts.¹⁰⁷⁻¹⁰⁹ Typically, high surface area oxides, such as silica (SiO₂) and alumina (Al₂O₃), are used as the supports. These supports provide the surface hydroxyl groups (HO-) as anchoring groups; they serve as the anionic surface O- ligands at the supported metal center (Scheme 1.10). In SOMC, the density of the OH groups on the supports is controlled by the dehydroxylation temperature. For instance, silica partially dehydroxylated at 700 °C under high vacuum results in the formation of isolated ≡SiOH groups (ca. 0.8 ≡SiOH nm⁻²) that can be exploited to generate isolated organometallic complexes on the surface.¹¹⁰⁻¹¹¹



Scheme 1.10. Formation of grafted metal complex by surface organometallic chemistry approach.

Grafting of molecular olefin metathesis catalysts does not only provide models for the active sites in heterogeneous metathesis catalysts, but it also shuts down the typical bimolecular decomposition pathways observed in homogeneous systems.¹¹² Hence, the catalytic performances of these supported catalysts are generally improved with respect to their molecular counterparts. The first fully-characterized grafted metathesis active alkylidene is $(\equiv\text{SiO})\text{Re}(=\text{CH}t\text{Bu})(\equiv\text{C}t\text{Bu})(\text{CH}_2t\text{Bu})$.¹¹³ The characteristic alkylidene moiety was observed spectroscopically by ^1H and ^{13}C solid-state NMR. Since then, a series of well-defined supported metathesis active alkylidenes were prepared via grafting.¹¹⁴⁻¹²⁷ In 2008, Blanc et. al. reported the first observation of metathesis reaction intermediates including methylidene and metallacyclobutanes (both TBP and SP) by solid-state NMR, upon contacting $[(\equiv\text{SiO})\text{W}(=\text{NAr})(=\text{CH}t\text{Bu})(2,5\text{-Me}_2\text{NC}_4\text{H}_2)]$ with ^{13}C -dilabeled ethylene.¹²⁸ The well-defined nature of the supported alkylidenes also allows systematic studies of the ligand influence on the metathesis activity and helps to establish a structure-activity relationship of supported catalysts.^{17, 117, 129} Besides, the recent development of oxo alkylidenes in homogeneous catalysts also brought forward the syntheses of supported oxo alkylidenes leading to a more realistic model for the active site in classical heterogeneous catalyst (Scheme 1.11).¹³⁰⁻¹³² Moreover, the supported W oxo alkylidenes were shown to be highly active in metathesis at room temperature. The large difference in the metathesis activity of these supported models versus the heterogeneous catalysts is believed to come from the different amounts of active sites and the difficulties in initiating the classical heterogeneous metal oxides catalysts.



Scheme 1.11. Proposed structure of the active site in WO_3/SiO_2 and the structural mimics generated by SOMC approach.

On the other hand, various supported metal alkyl complexes were also prepared by SOMC approach; they were shown to be metathesis active and presumably involved the generation of alkylidene moieties via α -H abstraction.¹³³⁻¹³⁹ While most of the catalysts were supported on SiO₂, there are few examples of grafting CH₃ReO₃ on Al₂O₃, which have been used as the model for Re₂O₇/Al₂O₃.¹⁴⁰⁻¹⁴⁴

1.7 Strategy and Outline

WO₃/SiO₂ is used for the production of propylene in the OCT process, which is one of the largest industrial processes. Despite the discovery of this catalyst more than 50 years ago, understanding of the nature of active sites and their formation mechanisms is still very limited. Therefore, this thesis is devoted to understand the initiation process involved in silica-supported W-oxo based olefin metathesis catalysts. This includes the identification of active species and detailed investigation in the initiation mechanism involved in transforming W-oxo (W=O) species into W alkylidenes (W=CHR).

The biggest challenges in studying heterogeneous catalysts are the small amounts of active sites and the presence of a variety of surface species. In order to tackle these problems, SOMC approach is used for generating well-defined surface species, which serve as a model system for WO₃/SiO₂. The uses of complementary spectroscopic techniques (e.g. solid-state NMR, IR and X-ray Absorption Spectroscopy) as well as molecular mimics allow molecular-level understanding of the surface species to be established. In particular, we focus on tailoring molecular precursors as structural mimics for the proposed surface species in WO₃/SiO₂. The reactivities of the tailored molecular precursors are investigated by experimental approaches assisted by DFT computations. Furthermore, the supported analogues of these molecular precursors are prepared via SOMC to yield the well-defined supported model systems, in which the activities and reactivities are further investigated. This strategy allows us to achieve a fundamental understanding of different surface species that are present in the WO₃/SiO₂ catalytic system and their initiation mechanisms, and hence, allowing rational improvement in the supported metathesis catalysts.

Chapter 2 focuses on preparing a well-defined silica-supported W-oxo catalyst and investigates its activation with organosilicon reducing agents. This study helps to understand the molecular structures of the surface W-oxo species and how they are being activated. The efficient activation with organosilicon reductants also allows us to characterize the activated species, and thus, answer the long-standing question regarding the nature of the active sites.

The results obtained also hint us to potential initiation mechanism, which is further investigated in the following chapters.

Based on these findings, well-defined molecular W(IV)-oxo complex is tailored as a model compound for investigating its reactivity and initiation in olefin metathesis, which is discussed in **Chapter 3** to provide a molecular-level understanding on the reduced W(IV) species. The combination of both experimental and DFT computational studies in this chapter provides unprecedented details into the initiation mechanism.

In **Chapter 4**, we relate the molecular model system back to the supported W(IV)-oxo species by using SOMC. By investigating the reactivity of the supported species and comparing it to the molecular system, the role of the silica support is revealed.

With all the knowledge and understanding obtained through these different studies, the effects of preparation methods and organosilicon reductants on the metathesis activity of supported W(VI)-oxo species are investigated and rationalized in **Chapter 5**.

This thesis is end with a general conclusion and perspective in **Chapter 6**.

1.8 References

1. Anderson, A. W. M., N. G., Polymeric bicyclo-(2, 2, 1)-2-heptene. *U.S. Patent 2721189 (A)* **1955**.
2. Banks, R. L.; Bailey, G. C., Olefin Disproportionation. A New Catalytic Process. *Ind. Eng. Chem. Prod. Res. Dev.* **1964**, *3*, 170-173.
3. Natta, G.; Dall'Asta, G.; Mazzanti, G., Stereospecific Homopolymerization of Cyclopentene. *Angew. Chem. Int. Ed.* **1964**, *3*, 723-729.
4. Calderon, N.; Chen, H. Y.; Scott, K. W., Olefin metathesis - A novel reaction for skeletal transformations of unsaturated hydrocarbons. *Tetrahedron Lett.* **1967**, *8*, 3327-3329.
5. Grubbs, R. H.; Wenzel, A. G.; O'Leary, D. J.; Khosravi, E., *Handbook of Metathesis*, 3 Vol. Set, 2nd ed. Wiley VCH: Weinheim: 2015.
6. Mol, J. C., Industrial applications of olefin metathesis. *J. Mol. Catal. A: Chem.* **2004**, *213*, 39-45.
7. Jean-Louis Hérisson, P.; Chauvin, Y., Catalyse de transformation des oléfines par les complexes du tungstène. II. Télomérisation des oléfines cycliques en présence d'oléfines acycliques. *Makromol. Chem.* **1971**, *141*, 161-176.
8. Chauvin, Y., Olefin Metathesis: The Early Days (Nobel Lecture). *Angew. Chem. Int. Ed.* **2006**, *45*, 3740-3747.
9. Grubbs, R. H., Olefin-Metathesis Catalysts for the Preparation of Molecules and Materials (Nobel Lecture). *Angew. Chem. Int. Ed.* **2006**, *45*, 3760-3765.
10. Schrock, R. R., Multiple Metal-Carbon Bonds for Catalytic Metathesis Reactions (Nobel Lecture). *Angew. Chem. Int. Ed.* **2006**, *45*, 3748-3759.
11. Schrock, R. R., Recent Advances in High Oxidation State Mo and W Imido Alkylidene Chemistry. *Chem. Rev.* **2009**, *109*, 3211-3226.
12. Weskamp, T.; Kohl, F. J.; Hieringer, W.; Gleich, D.; Herrmann, W. A., Highly Active Ruthenium Catalysts for Olefin Metathesis: The Synergy of N-Heterocyclic Carbenes and Coordinatively Labile Ligands. *Angew. Chem. Int. Ed.* **1999**, *38*, 2416-2419.
13. Romero, P. E.; Piers, W. E.; McDonald, R., Rapidly Initiating Ruthenium Olefin-Metathesis Catalysts. *Angew. Chem. Int. Ed.* **2004**, *43*, 6161-6165.
14. Torker, S.; Merki, D.; Chen, P., Gas-Phase Thermochemistry of Ruthenium Carbene Metathesis Catalysts. *J. Am. Chem. Soc.* **2008**, *130*, 4808-4814.
15. Jović, M.; Torker, S.; Chen, P., Non-innocent Character of Oxyanions in Ruthenium Metathesis Catalysts. *Organometallics* **2011**, *30*, 3971-3980.
16. Feldman, J.; Davis, W. M.; Thomas, J. K.; Schrock, R. R., Preparation and reactivity of tungsten(VI) metallacyclobutane complexes. Square pyramids versus trigonal bipyramids. *Organometallics* **1990**, *9*, 2535-2548.
17. Mougél, V.; Copéret, C., Magnitude and consequences of OR ligand σ -donation on alkene metathesis activity in d^0 silica supported $(\equiv\text{SiO})\text{W}(\text{NAr})(=\text{CHtBu})(\text{OR})$ catalysts. *Chem. Sci.* **2014**, *5*, 2475-2481.
18. Gordon, C. P.; Yamamoto, K.; Liao, W.-C.; Allouche, F.; Andersen, R. A.; Copéret, C.; Raynaud, C.; Eisenstein, O., Metathesis Activity Encoded in the Metallacyclobutane Carbon-13 NMR Chemical Shift Tensors. *ACS Cent. Sci.* **2017**, *3*, 759-768.
19. Solans-Monfort, X.; Clot, E.; Copéret, C.; Eisenstein, O., d^0 Re-Based Olefin Metathesis Catalysts, $\text{Re}(\equiv\text{CR})(\text{CHR})(\text{X})(\text{Y})$: The Key Role of X and Y Ligands for Efficient Active Sites. *J. Am. Chem. Soc.* **2005**, *127*, 14015-14025.
20. Solans-Monfort, X.; Coperet, C.; Eisenstein, O., Shutting Down Secondary Reaction Pathways: The Essential Role of the Pyrrolyl Ligand in Improving Silica Supported d^0 - ML_4 Alkene Metathesis Catalysts from DFT Calculations. *J. Am. Chem. Soc.* **2010**, *132*, 7750-7757.
21. Solans-Monfort, X.; Copéret, C.; Eisenstein, O., Oxo vs Imido Alkylidene d^0 -Metal Species: How and Why Do They Differ in Structure, Activity, and Efficiency in Alkene Metathesis? *Organometallics* **2012**, *31*, 6812-6822.
22. Poater, A.; Solans-Monfort, X.; Clot, E.; Copéret, C.; Eisenstein, O., Understanding d^0 -Olefin Metathesis Catalysts: Which Metal, Which Ligands? *J. Am. Chem. Soc.* **2007**, *129*, 8207-8216.
23. Hoveyda, A. H.; Zhugralin, A. R., The remarkable metal-catalysed olefin metathesis reaction. *Nature* **2007**, *450*, 243.

24. Bielawski, C. W.; Grubbs, R. H., Living ring-opening metathesis polymerization. *Prog. Polym. Sci.* **2007**, *32*, 1-29.
25. Mutlu, H.; de Espinosa, L. M.; Meier, M. A. R., Acyclic diene metathesis: a versatile tool for the construction of defined polymer architectures. *Chem. Soc. Rev.* **2011**, *40*, 1404-1445.
26. Lwin, S.; Wachs, I. E., Olefin Metathesis by Supported Metal Oxide Catalysts. *ACS Catal.* **2014**, *4*, 2505-2520.
27. van Schalkwyk, C.; Spamer, A.; Moodley, D. J.; Dube, T.; Reynhardt, J.; Botha, J. M.; Vosloo, H. C. M., Factors that could influence the activity of a WO₃/SiO₂ catalyst: Part III. *Appl. Catal., A* **2003**, *255*, 143-152.
28. Lee, E. L.; Wachs, I. E., In Situ Spectroscopic Investigation of the Molecular and Electronic Structures of SiO₂ Supported Surface Metal Oxides. *J. Phys. Chem. C* **2007**, *111*, 14410-14425.
29. Ross-Medgaarden, E. I.; Wachs, I. E., Structural Determination of Bulk and Surface Tungsten Oxides with UV-vis Diffuse Reflectance Spectroscopy and Raman Spectroscopy. *J. Phys. Chem. C* **2007**, *111*, 15089-15099.
30. Lwin, S.; Li, Y.; Frenkel, A. I.; Wachs, I. E., Nature of WO_x Sites on SiO₂ and Their Molecular Structure-Reactivity/Selectivity Relationships for Propylene Metathesis. *ACS Catal.* **2016**, *6*, 3061-3071.
31. Liu, N.; Ding, S.; Cui, Y.; Xue, N.; Peng, L.; Guo, X.; Ding, W., Optimizing activity of tungsten oxides for 1-butene metathesis by depositing silica on γ -alumina support. *Chem. Eng. Res. Des.* **2013**, *91*, 573-580.
32. Debecker, D. P.; Stoyanova, M.; Rodemerck, U.; Colbeau-Justin, F.; Boissère, C.; Chaumonnot, A.; Bonduelle, A.; Sanchez, C., Aerosol route to nanostructured WO₃-SiO₂-Al₂O₃ metathesis catalysts: Toward higher propene yield. *Appl. Catal., A* **2014**, *470*, 458-466.
33. Mol, J. C.; van Leeuwen, P. W. N. M., *Metathesis of Alkenes. Handbook of Heterogeneous Catalysis*. Wiley-VCH: Weinheim: 2008; Vol. 14, p 3240-3256.
34. Hu, H.; Wachs, I. E.; Bare, S. R., Surface Structures of Supported Molybdenum Oxide Catalysts: Characterization by Raman and Mo L₃-Edge XANES. *J. Phys. Chem.* **1995**, *99*, 10897-10910.
35. Chen, K.; Xie, S.; Bell, A. T.; Iglesia, E., Structure and Properties of Oxidative Dehydrogenation Catalysts Based on MoO₃/Al₂O₃. *J. Catal.* **2001**, *198*, 232-242.
36. Tian, H.; Roberts, C. A.; Wachs, I. E., Molecular Structural Determination of Molybdena in Different Environments: Aqueous Solutions, Bulk Mixed Oxides, and Supported MoO₃ Catalysts. *J. Phys. Chem. C* **2010**, *114*, 14110-14120.
37. Chempath, S.; Zhang, Y.; Bell, A. T., DFT Studies of the Structure and Vibrational Spectra of Isolated Molybdena Species Supported on Silica. *J. Phys. Chem. C* **2007**, *111*, 1291-1298.
38. Handzlik, J.; Sautet, P., Structure of Isolated Molybdenum(VI) Oxide Species on γ -Alumina: A Periodic Density Functional Theory Study. *J. Phys. Chem. C* **2008**, *112*, 14456-14463.
39. Handzlik, J.; Sautet, P., Structure of Dimeric Molybdenum(VI) Oxide Species on γ -Alumina: A Periodic Density Functional Theory Study. *J. Phys. Chem. C* **2010**, *114*, 19406-19414.
40. Chakrabarti, A.; Wachs, I. E., Molecular Structure-Reactivity Relationships for Olefin Metathesis by Al₂O₃-Supported Surface MoO_x Sites. *ACS Catal.* **2018**, *8*, 949-959.
41. Debecker, D. P.; Stoyanova, M.; Colbeau-Justin, F.; Rodemerck, U.; Boissière, C.; Gaigneaux, E. M.; Sanchez, C., One-Pot Aerosol Route to MoO₃-SiO₂-Al₂O₃ Catalysts with Ordered Super Microporosity and High Olefin Metathesis Activity. *Angew. Chem. Int. Ed.* **2012**, *51*, 2129-2131.
42. Goelden, V.; Linke, D.; Kondratenko, E. V., Investigation of the Enhancing Effect of Solid Cocatalysts on Propene Formation in Ethene/*trans*-2-Butene Metathesis over MoO_x/SiO₂-Al₂O₃. *ACS Catal.* **2015**, *5*, 7437-7445.
43. Mol, J. C., Metathesis of functionalized olefins. *J. Mol. Catal.* **1982**, *15*, 35-45.
44. Lwin, S.; Keturakis, C.; Handzlik, J.; Sautet, P.; Li, Y.; Frenkel, A. I.; Wachs, I. E., Surface ReO_x Sites on Al₂O₃ and Their Molecular Structure-Reactivity Relationships for Olefin Metathesis. *ACS Catal.* **2015**, *5*, 1432-1444.
45. Lwin, S.; Li, Y.; Frenkel, A. I.; Wachs, I. E., Activation of Surface ReO_x Sites on Al₂O₃ Catalysts for Olefin Metathesis. *ACS Catal.* **2015**, *5*, 6807-6814.
46. Lin, C. J.; Aldag, A. W.; Clark, A., Adsorption and disproportionation of ethylene on supported rhenium oxide catalysts. *J. Catal.* **1976**, *45*, 287-296.

47. Mol, J. C., Olefin metathesis over supported rhenium oxide catalysts. *Catal. Today* **1999**, *51*, 289-299.
48. Farona, M. F.; Tucker, R. L., Studies on the mechanism of olefin metathesis promoted by a heterogeneous catalyst. *J. Mol. Catal.* **1980**, *8*, 85-90.
49. Grubbs, R. H.; Swetnick, S. J., Mechanism of olefin metathesis over a supported molybdenum catalyst. *J. Mol. Catal.* **1980**, *8*, 25-36.
50. McCoy, J. R.; Farona, M. F., Olefin metathesis over a $\text{Re}_2\text{O}_7/\text{Al}_2\text{O}_3$ metathesis catalyst: Mechanism for initial metallacarbene formation. *J. Mol. Catal.* **1991**, *66*, 51-58.
51. Ephritikhine, M.; Green, M. L. H.; MacKenzie, R. E., Some η^1 and η^3 -allylic and metallocyclobutane derivatives of molybdenum and tungsten. *J. Chem. Soc., Chem. Commun.* **1976**, 619-621.
52. Iwasawa, Y.; Hamamura, H., Mechanism for initial carbene formation in olefin metathesis over fixed Mo catalysts. *J. Chem. Soc., Chem. Commun.* **1983**, 130-132.
53. Iwasawa, Y.; Kubo, H.; Hamamura, H., Olefin metathesis over Al_2O_3 or SiO_2 -attached molybdenum catalysts: active structures and mechanism for initial carbene formation. *J. Mol. Catal.* **1985**, *28*, 191-208.
54. Lavery, D. T.; Rooney, J. J.; Stewart, A., Possible role of hydrido-metal complexes in metathesis, isomerization, dimerization, and polymerization of alkenes. *J. Catal.* **1976**, *45*, 110-113.
55. Rappe, A. K.; Goddard, W. A., Olefin metathesis - a mechanistic study of high-valent Group VI catalysts. *J. Am. Chem. Soc.* **1982**, *104*, 448-456.
56. Salameh, A.; Copéret, C.; Basset, J.-M.; Böhm, V. P. W.; Röper, M., Rhenium(VII) Oxide/Aluminum Oxide: More Experimental Evidence for an Oxametallacyclobutane Intermediate and a Pseudo-Wittig Initiation Step in Olefin Metathesis. *Adv. Synth. Catal.* **2007**, *349*, 238-242.
57. Chen, X.; Zhang, X.; Chen, P., Metallaoxetanes and Carbenes from Diolates in High-Valent Rhenium Oxo Chemistry: The Importance of the Coordination Number. *Angew. Chem. Int. Ed.* **2003**, *42*, 3798-3801.
58. Basrur, A. G.; Patwardhan, S. R.; Was, S. N., Propene metathesis over silica-supported tungsten oxide catalyst—Catalyst induction mechanism. *J. Catal.* **1991**, *127*, 86-95.
59. Lwin, S.; Wachs, I. E., Catalyst Activation and Kinetics for Propylene Metathesis by Supported WO_x/SiO_2 Catalysts. *ACS Catal.* **2017**, *7*, 573-580.
60. Howell, J. G.; Li, Y.-P.; Bell, A. T., Propene Metathesis over Supported Tungsten Oxide Catalysts: A Study of Active Site Formation. *ACS Catal.* **2016**, *6*, 7728-7738.
61. Shelimov, B. N.; Elev, L. V.; Kazansky, V. B., Use of photoreduction for activation of silica-molybdena catalysts for propylene metathesis: Comparison with thermal reduction. *J. Catal.* **1986**, *98*, 70-81.
62. Shelimov, B. N.; Elev, I. V.; Kazansky, V. B., Spectroscopic study of formation of active metal-carbene species in photoreduced silica-molybdena catalysts for olefin metathesis. *J. Mol. Catal.* **1988**, *46*, 187-200.
63. Amakawa, K.; Wrabetz, S.; Kröhnert, J.; Tzolova-Müller, G.; Schlögl, R.; Trunschke, A., In Situ Generation of Active Sites in Olefin Metathesis. *J. Am. Chem. Soc.* **2012**, *134*, 11462-11473.
64. Olsthoorn, A. A.; Boelhouwer, C., An infrared spectroscopic study of the $\text{Re}_2\text{O}_7/\text{Al}_2\text{O}_3$ metathesis catalyst: II. Catalytic properties. *J. Catal.* **1976**, *44*, 207-216.
65. Schrock, R. R., Alkylcarbene complex of tantalum by intramolecular α -hydrogen abstraction. *J. Am. Chem. Soc.* **1974**, *96*, 6796-6797.
66. Schrock, R.; Rocklage, S.; Wengrovius, J.; Rupprecht, G.; Fellmann, J., Preparation and characterization of active niobium, tantalum and tungsten metathesis catalysts. *J. Mol. Catal.* **1980**, *8*, 73-83.
67. Wengrovius, J. H.; Schrock, R. R.; Churchill, M. R.; Missert, J. R.; Youngs, W. J., Multiple metal-carbon bonds. 16. Tungsten-oxo alkylidene complexes as olefins metathesis catalysts and the crystal structure of $\text{W}(\text{O})(\text{CHCMe}_3)(\text{PEt}_3)\text{Cl}_2$. *J. Am. Chem. Soc.* **1980**, *102*, 4515-4516.
68. Wengrovius, J. H.; Schrock, R. R., Synthesis and characterization of tungsten oxo neopentylidene complexes. *Organometallics* **1982**, *1*, 148-155.
69. Schrock, R. R.; Hoveyda, A. H., Molybdenum and Tungsten Imido Alkylidene Complexes as Efficient Olefin-Metathesis Catalysts. *Angew. Chem. Int. Ed.* **2003**, *42*, 4592-4633.

70. Schrock, R. R., Recent advances in olefin metathesis by molybdenum and tungsten imido alkylidene complexes. *J. Mol. Catal. A: Chem.* **2004**, *213*, 21-30.
71. Toreki, R.; Schrock, R. R., A well-defined rhenium(VII) olefin metathesis catalyst. *J. Am. Chem. Soc.* **1990**, *112*, 2448-2449.
72. Schofield, M. H.; Schrock, R. R.; Park, L. Y., Rhenium(VII) monoimido alkylidene complexes: synthesis, structure, and Lewis-acid-cocatalyzed olefin metathesis. *Organometallics* **1991**, *10*, 1844-1851.
73. Toreki, R.; Vaughan, G. A.; Schrock, R. R.; Davis, W. M., Metathetical reactions of rhenium(VII) alkylidene-alkylidyne complexes of the type $\text{Re}(\text{CR}')(\text{CHR}')[\text{OCMe}(\text{CF}_3)_2]_2$ ($\text{R}' = \text{CMe}_3$ or CMe_2Ph) with terminal and internal olefins. *J. Am. Chem. Soc.* **1993**, *115*, 127-137.
74. Peryshkov, D. V.; Schrock, R. R.; Takase, M. K.; Müller, P.; Hoveyda, A. H., Z-Selective Olefin Metathesis Reactions Promoted by Tungsten Oxo Alkylidene Complexes. *J. Am. Chem. Soc.* **2011**, *133*, 20754-20757.
75. Peryshkov, D. V.; Schrock, R. R., Synthesis of Tungsten Oxo Alkylidene Complexes. *Organometallics* **2012**, *31*, 7278-7286.
76. Peryshkov, D. V.; Forrest, W. P.; Schrock, R. R.; Smith, S. J.; Müller, P., $\text{B}(\text{C}_6\text{F}_5)_3$ Activation of Oxo Tungsten Complexes That Are Relevant to Olefin Metathesis. *Organometallics* **2013**, *32*, 5256-5259.
77. Schowner, R.; Frey, W.; Buchmeiser, M. R., Cationic Tungsten-Oxo-Alkylidene-N-Heterocyclic Carbene Complexes: Highly Active Olefin Metathesis Catalysts. *J. Am. Chem. Soc.* **2015**, *137*, 6188-6191.
78. Bukhryakov, K. V.; Schrock, R. R.; Hoveyda, A. H.; Tsay, C.; Müller, P., Syntheses of Molybdenum Oxo Alkylidene Complexes through Addition of Water to an Alkylidyne Complex. *J. Am. Chem. Soc.* **2018**, *140*, 2797-2800.
79. Zhai, F.; Bukhryakov, K. V.; Schrock, R. R.; Hoveyda, A. H.; Tsay, C.; Müller, P., Syntheses of Molybdenum Oxo Benzyldiene Complexes. *J. Am. Chem. Soc.* **2018**, *140*, 13609-13613.
80. Schrock, R. R.; DePue, R. T.; Feldman, J.; Yap, K. B.; Yang, D. C.; Davis, W. M.; Park, L.; DiMare, M.; Schofield, M., Further studies of imido alkylidene complexes of tungsten, well-characterized olefin metathesis catalysts with controllable activity. *Organometallics* **1990**, *9*, 2262-2275.
81. Tsang, W. C. P.; Hultsch, K. C.; Alexander, J. B.; Bonitatebus, P. J.; Schrock, R. R.; Hoveyda, A. H., Alkylidene and Metalacyclic Complexes of Tungsten that Contain a Chiral Biphenoxide Ligand. Synthesis, Asymmetric Ring-Closing Metathesis, and Mechanistic Investigations. *J. Am. Chem. Soc.* **2003**, *125*, 2652-2666.
82. Lopez, L. P. H.; Schrock, R. R., Formation of Dimers That Contain Unbridged W(IV)/W(IV) Double Bonds. *J. Am. Chem. Soc.* **2004**, *126*, 9526-9527.
83. Lopez, L. P. H.; Schrock, R. R.; Müller, P., Dimers that Contain Unbridged W(IV)/W(IV) Double Bonds. *Organometallics* **2006**, *25*, 1978-1986.
84. Arndt, S.; Schrock, R. R.; Müller, P., Synthesis and Reactions of Tungsten Alkylidene Complexes That Contain the 2,6-Dichlorophenylimido Ligand. *Organometallics* **2007**, *26*, 1279-1290.
85. Robbins, J.; Bazan, G. C.; Murdzek, J. S.; O'Regan, M. B.; Schrock, R. R., Reduction of molybdenum imido-alkylidene complexes in the presence of olefins to give molybdenum(IV) complexes. *Organometallics* **1991**, *10*, 2902-2907.
86. Merrifield, J. H.; Lin, G. Y.; Kiel, W. A.; Gladysz, J. A., Mechanism of coupling of methylidene to ethylene at a homogeneous (triphenylphosphine)nitrosyl(eta-cyclopentadienyl)rhenium(+) [(eta-C5H5)Re(NO)(PPh3)]⁺ center. Remarkable enantiomer self-recognition. *J. Am. Chem. Soc.* **1983**, *105*, 5811-5819.
87. Marinescu, S. C.; King, A. J.; Schrock, R. R.; Singh, R.; Müller, P.; Takase, M. K., Simple Molybdenum(IV) Olefin Complexes of the Type $\text{Mo}(\text{NR})(\text{X})(\text{Y})(\text{olefin})$. *Organometallics* **2010**, *29*, 6816-6828.
88. Sharp, P. R.; Schrock, R. R., Multiple metalcarbon bonds: XIV. Preparation of alkylidenetantalum complexes by alkylidene transfer from phosphoranes. The first ethylidene complex and how it decomposes. *J. Organomet. Chem.* **1979**, *171*, 43-51.

89. Johnson, L. K.; Virgil, S. C.; Grubbs, R. H.; Ziller, J. W., Facile tungsten alkylidene synthesis: alkylidene transfer from a phosphorane to a tungsten imido complex. *J. Am. Chem. Soc.* **1990**, *112*, 5384-5385.
90. Johnson, L. K.; Frey, M.; Ulibarri, T. A.; Virgil, S. C.; Grubbs, R. H.; Ziller, J. W., Alkylidene transfer from phosphoranes to tungsten(IV) imido complexes. *J. Am. Chem. Soc.* **1993**, *115*, 8167-8177.
91. Joost, M.; Transue, W. J.; Cummins, C. C., Diazomethane umpolung atop anthracene: an electrophilic methylene transfer reagent. *Chem. Sci.* **2018**, *9*, 1540-1543.
92. Tonzetich, Z. J.; Schrock, R. R.; Müller, P., Reaction of Phosphoranes with Mo(N-2,6-*i*-Pr₂C₆H₃)(CHCMe₃)[OCMe(CF₃)₂]₂: Synthesis and Reactivity of an Anionic Imido Alkylidyne Complex. *Organometallics* **2006**, *25*, 4301-4306.
93. Binger, P.; Müller, P.; Benn, R.; Mynott, R., Vinylcarbene Complexes of Titanocene. *Angew. Chem. Int. Ed.* **1989**, *28*, 610-611.
94. Johnson, L. K.; Grubbs, R. H.; Ziller, J. W., Synthesis of tungsten vinyl alkylidene complexes via the reactions of WCl₂(NAr)(PX₃)₃ (X = R, OMe) precursors with 3,3-disubstituted cyclopropenes. *J. Am. Chem. Soc.* **1993**, *115*, 8130-8145.
95. Flatt, B. T.; Grubbs, R. H.; Blanski, R. L.; Calabrese, J. C.; Feldman, J., Synthesis, Structure, and Reactivity of a Rhenium Oxo-Vinylalkylidene Complex. *Organometallics* **1994**, *13*, 2728-2732.
96. de la Mata, F. J.; Grubbs, R. H., Synthesis and Reactions of Tungsten Oxo Vinylalkylidene Complexes: Reactions of WCl₂(O)(PX₃) (X = OMe, R) Precursors with 3,3-Diphenylcyclopropene. *Organometallics* **1996**, *15*, 577-584.
97. Freundlich, J. S.; Schrock, R. R.; Davis, W. M., Synthetic and Mechanistic Investigations of Trimethylsilyl-Substituted Triamidoamine Complexes of Tantalum That Contain Metal-Ligand Multiple Bonds. *J. Am. Chem. Soc.* **1996**, *118*, 3643-3655.
98. Hirsekorn, K. F.; Veige, A. S.; Marshak, M. P.; Koldobskaya, Y.; Wolczanski, P. T.; Cundari, T. R.; Lobkovsky, E. B., Thermodynamics, Kinetics, and Mechanism of (silox)₃M(olefin) to (silox)₃M(alkylidene) Rearrangements (silox = *t*Bu₃SiO; M = Nb, Ta). *J. Am. Chem. Soc.* **2005**, *127*, 4809-4830.
99. McLain, S. J.; Sancho, J.; Schrock, R. R., Metallacyclopentane to metallacyclobutane ring contraction. *J. Am. Chem. Soc.* **1979**, *101*, 5451-5453.
100. Yang, G. K.; Bergman, R. G., Synthesis, molecular structure, and thermal chemistry of (η⁵-cyclopentadienyl)dicarbonylrhenacyclopentane. *Organometallics* **1985**, *4*, 129-138.
101. Schrock, R. R.; Duval-Lungulescu, M.; Tsang, W. C. P.; Hoveyda, A. H., Catalytic Homologation of Vinyltributylstannane to Allyltributylstannane by Mo(IV) Complexes in the Presence of Ethylene. *J. Am. Chem. Soc.* **2004**, *126*, 1948-1949.
102. Zhang, X.; Chen, X.; Chen, P., Mass Spectrometric Study of the Conversion of Rhenium Diolates to Metallaoxetanes and Carbenes. Coordination Number, Polar, and Steric Effects. *Organometallics* **2004**, *23*, 3437-3447.
103. Narancic, S.; Chen, P., Computational Study of Low-Coordinate Rhenium Diolates, Metallaoxetanes, Oxo Complexes, and Carbenes. *Organometallics* **2005**, *24*, 10-12.
104. Bencze, L.; Bíró, N.; Szabó-Ravasz, B.; Mihichuk, L., Chemical transformations of cis-W(CO)₄(C₃H₅N)₂ in the ring-opening metathesis polymerization of norbornene. *Can. J. Chem.* **2004**, *82*, 499-503.
105. Frech, C. M.; Blacque, O.; Schmalte, H. W.; Berke, H.; Adlhart, C.; Chen, P., Unprecedented ROMP Activity of Low-Valent Rhenium-Nitrosyl Complexes: Mechanistic Evaluation of an Electrophilic Olefin Metathesis System. *Chem. Eur. J.* **2006**, *12*, 3325-3338.
106. Schrock, R. R.; Lopez, L. P. H.; Hafer, J.; Singh, R.; Sinha, A.; Müller, P., Olefin Metathesis Reactions Initiated by d² Molybdenum or Tungsten Complexes. *Organometallics* **2005**, *24*, 5211-5213.
107. Coperet, C.; Allouche, F.; Chan, K. W.; Conley, M. P.; Delley, M. F.; Fedorov, A.; Moroz, I. B.; Mougél, V.; Pucino, M.; Searles, K.; Yamamoto, K.; Zhizhko, P. A., Bridging the Gap between Industrial and Well-Defined Supported Catalysts. *Angew. Chem. Int. Ed.* **2018**, *57*, 6398-6440.
108. Copéret, C.; Chabanas, M.; Petroff Saint-Arroman, R.; Basset, J.-M., Homogeneous and Heterogeneous Catalysis: Bridging the Gap through Surface Organometallic Chemistry. *Angew. Chem. Int. Ed.* **2003**, *42*, 156-181.

109. Copéret, C.; Comas-Vives, A.; Conley, M. P.; Estes, D. P.; Fedorov, A.; Mougél, V.; Nagae, H.; Núñez-Zarur, F.; Zhizhko, P. A., Surface Organometallic and Coordination Chemistry toward Single-Site Heterogeneous Catalysts: Strategies, Methods, Structures, and Activities. *Chem. Rev.* **2016**, *116*, 323-421.
110. Rascón, F.; Wischert, R.; Copéret, C., Molecular nature of support effects in single-site heterogeneous catalysts: silicavvs.alumina. *Chem. Sci.* **2011**, *2*, 1449-1456.
111. Zhuravlev, L. T., The surface chemistry of amorphous silica. Zhuravlev model. *Colloids Surf. A Physicochem. Eng. Asp.* **2000**, *173*, 1-38.
112. Blanc, F.; Copéret, C.; Thivolle-Cazat, J.; Basset, J.-M.; Lesage, A.; Emsley, L.; Sinha, A.; Schrock, R. R., Surface versus Molecular Siloxy Ligands in Well-Defined Olefin Metathesis Catalysts: $[(\text{RO})_3\text{SiO}]\text{Mo}(=\text{NAr})(=\text{CH}t\text{Bu})(\text{CH}_2t\text{Bu})$. *Angew. Chem. Int. Ed.* **2006**, *45*, 1216-1220.
113. Chabanas, M.; Baudouin, A.; Copéret, C.; Basset, J.-M., A Highly Active Well-Defined Rhenium Heterogeneous Catalyst for Olefin Metathesis Prepared via Surface Organometallic Chemistry. *J. Am. Chem. Soc.* **2001**, *123*, 2062-2063.
114. Rhers, B.; Quadrelli, E. A.; Baudouin, A.; Taoufik, M.; Copéret, C.; Lefebvre, F.; Basset, J.-M.; Fenet, B.; Sinha, A.; Schrock, R. R., Understanding the reactivity of $[\text{WNAr}(\text{CH}_2t\text{Bu})_2(\text{CH}t\text{Bu})]$ ($\text{Ar}=2,6\text{-}i\text{PrC}_6\text{H}_3$) with silica partially dehydroxylated at low temperatures through a combined use of molecular and surface organometallic chemistry. *J. Organomet. Chem.* **2006**, *691*, 5448-5455.
115. Rhers, B.; Salameh, A.; Baudouin, A.; Quadrelli, E. A.; Taoufik, M.; Copéret, C.; Lefebvre, F.; Basset, J.-M.; Solans-Monfort, X.; Eisenstein, O.; Lukens, W. W.; Lopez, L. P. H.; Sinha, A.; Schrock, R. R., A Well-Defined, Silica-Supported Tungsten Imido Alkylidene Olefin Metathesis Catalyst. *Organometallics* **2006**, *25*, 3554-3557.
116. Chabanas, M.; Copéret, C.; Basset, J.-M., Re-Based Heterogeneous Catalysts for Olefin Metathesis Prepared by Surface Organometallic Chemistry: Reactivity and Selectivity. *Chem. Eur. J.* **2003**, *9*, 971-975.
117. Blanc, F.; Berthoud, R.; Salameh, A.; Basset, J.-M.; Copéret, C.; Singh, R.; Schrock, R. R., Dramatic Improvements of Well-Defined Silica Supported Mo-Based Olefin Metathesis Catalysts by Tuning the N-Containing Ligands. *J. Am. Chem. Soc.* **2007**, *129*, 8434-8435.
118. Blanc, F.; Thivolle-Cazat, J.; Basset, J.-M.; Copéret, C.; Hock, A. S.; Tonzetich, Z. J.; Schrock, R. R., Highly Active, Stable, and Selective Well-Defined Silica Supported Mo Imido Olefin Metathesis Catalysts. *J. Am. Chem. Soc.* **2007**, *129*, 1044-1045.
119. Allouche, F.; Mougél, V.; Copéret, C., Activating Thiolate-Based Imidoalkylidene Tungsten(VI) Metathesis Catalysts by Grafting onto Silica. *Asian J. Org. Chem.* **2015**, *4*, 528-532.
120. Mougél, V.; Pucino, M.; Copéret, C., Strongly σ Donating Thiophenoxide in Silica-Supported Tungsten Oxo Catalysts for Improved 1-Alkene Metathesis Efficiency. *Organometallics* **2015**, *34*, 551-554.
121. Pucino, M.; Mougél, V.; Schowner, R.; Fedorov, A.; Buchmeiser, M. R.; Copéret, C., Cationic Silica-Supported N-Heterocyclic Carbene Tungsten Oxo Alkylidene Sites: Highly Active and Stable Catalysts for Olefin Metathesis. *Angew. Chem. Int. Ed.* **2016**, *55*, 4300-4302.
122. Blanc, F.; Rendón, N.; Berthoud, R.; Basset, J.-M.; Copéret, C.; Tonzetich, Z. J.; Schrock, R. R., Dramatic enhancement of the alkene metathesis activity of Mo imido alkylidene complexes upon replacement of one *t*BuO by a surface siloxy ligand. *Dalton Trans.* **2008**, 3156-3158.
123. Rendón, N.; Berthoud, R.; Blanc, F.; Gajan, D.; Maishal, T.; Basset, J.-M.; Copéret, C.; Lesage, A.; Emsley, L.; Marinescu, S. C.; Singh, R.; Schrock, R. R., Well-Defined Silica-Supported Mo-Alkylidene Catalyst Precursors Containing One OR Substituent: Methods of Preparation and Structure-Reactivity Relationship in Alkene Metathesis. *Chem. Eur. J.* **2009**, *15*, 5083-5089.
124. Gajan, D.; Rendón, N.; Wampler, K. M.; Jean-Marie, B.; Copéret, C.; Lesage, A.; Emsley, L.; Schrock, R. R., Synthesis and reactivity of molybdenum imido alkylidene bis-pyrazolide complexes. *Dalton Trans.* **2010**, *39*, 8547-8551.
125. Pucino, M.; Inoue, M.; Gordon, C. P.; Schowner, R.; Stöhr, L.; Sen, S.; Hegedüs, C.; Robé, E.; Tóth, F.; Buchmeiser, M. R.; Copéret, C., Promoting Terminal Olefin Metathesis with a Supported Cationic Molybdenum Imido Alkylidene N-Heterocyclic Carbene Catalyst. *Angew. Chem. Int. Ed.* **2018**, *57*, 14566-14569.
126. Zhizhko, P. A.; Mougél, V.; De Jesus Silva, J.; Copéret, C., Benchmarked Intrinsic Olefin Metathesis Activity: Mo vs. W. *Helv. Chim. Acta* **2018**, *101*, e1700302.

127. Valla, M.; Stadler, D.; Mougél, V.; Copéret, C., Switching on the Metathesis Activity of Re Oxo Alkylidene Surface Sites through a Tailor-Made Silica–Alumina Support. *Angew. Chem. Int. Ed.* **2015**, *55*, 1124-1127.
128. Blanc, F.; Berthoud, R.; Copéret, C.; Lesage, A.; Emsley, L.; Singh, R.; Kreickmann, T.; Schrock, R. R., Direct observation of reaction intermediates for a well defined heterogeneous alkene metathesis catalyst. *Proc. Natl. Acad. Sci.* **2008**, *105*, 12123.
129. Mougél, V.; Santiago, C. B.; Zhizhko, P. A.; Bess, E. N.; Varga, J.; Frater, G.; Sigman, M. S.; Copéret, C., Quantitatively Analyzing Metathesis Catalyst Activity and Structural Features in Silica-Supported Tungsten Imido–Alkylidene Complexes. *J. Am. Chem. Soc.* **2015**, *137*, 6699-6704.
130. Mougél, V.; Copéret, C., Isostructural Molecular and Surface Mimics of the Active Sites of the Industrial WO₃/SiO₂ Metathesis Catalysts. *ACS Catal.* **2015**, *5*, 6436-6439.
131. Conley, M. P.; Mougél, V.; Peryshkov, D. V.; Forrest, W. P.; Gajan, D.; Lesage, A.; Emsley, L.; Copéret, C.; Schrock, R. R., A Well-Defined Silica-Supported Tungsten Oxo Alkylidene Is a Highly Active Alkene Metathesis Catalyst. *J. Am. Chem. Soc.* **2013**, *135*, 19068-19070.
132. Conley, M. P.; Forrest, W. P.; Mougél, V.; Copéret, C.; Schrock, R. R., Bulky Aryloxide Ligand Stabilizes a Heterogeneous Metathesis Catalyst. *Angew. Chem. Int. Ed.* **2014**, *53*, 14221-14224.
133. Blanc, F.; Chabanas, M.; Copéret, C.; Fenet, B.; Herdweck, E., Reactivity differences between molecular and surface silanols in the preparation of homogeneous and heterogeneous olefin metathesis catalysts. *J. Organomet. Chem.* **2005**, *690*, 5014-5026.
134. Mazoyer, E.; Merle, N.; Mallmann, A. d.; Basset, J.-M.; Berrier, E.; Delevoye, L.; Paul, J.-F.; Nicholas, C. P.; Gauvin, R. M.; Taoufik, M., Development of the first well-defined tungsten oxo alkyl derivatives supported on silica by SOMC: towards a model of WO₃/SiO₂ olefin metathesis catalyst. *Chem. Commun.* **2010**, *46*, 8944-8946.
135. Merle, N.; Girard, G.; Popoff, N.; De Mallmann, A.; Bouhoute, Y.; Trébosc, J.; Berrier, E.; Paul, J.-F.; Nicholas, C. P.; Del Rosal, I.; Maron, L.; Gauvin, R. M.; Delevoye, L.; Taoufik, M., On the Track to Silica-Supported Tungsten Oxo Metathesis Catalysts: Input from ¹⁷O Solid-State NMR. *Inorg. Chem.* **2013**, *52*, 10119-10130.
136. Bouhoute, Y.; Grekov, D.; Szeto, K. C.; Merle, N.; De Mallmann, A.; Lefebvre, F.; Raffa, G.; Del Rosal, I.; Maron, L.; Gauvin, R. M.; Delevoye, L.; Taoufik, M., Accessing Realistic Models for the WO₃–SiO₂ Industrial Catalyst through the Design of Organometallic Precursors. *ACS Catal.* **2016**, *6*, 1-18.
137. Dey, R.; Samantaray, M. K.; Poater, A.; Hamieh, A.; Kavitate, S.; Abou-Hamad, E.; Callens, E.; Emwas, A.-H.; Cavallo, L.; Basset, J.-M., Synthesis and characterization of a homogeneous and silica supported homoleptic cationic tungsten(VI) methyl complex: application in olefin metathesis. *Chem. Commun.* **2016**, *52*, 11270-11273.
138. Grekov, D.; Bouhoute, Y.; Szeto, K. C.; Merle, N.; De Mallmann, A.; Lefebvre, F.; Lucas, C.; Del Rosal, I.; Maron, L.; Gauvin, R. M.; Delevoye, L.; Taoufik, M., Silica-Supported Tungsten Neosilyl Oxo Precatalysts: Impact of the Podality on Activity and Stability in Olefin Metathesis. *Organometallics* **2016**, *35*, 2188-2196.
139. Merle, N.; Le Quémener, F.; Bouhoute, Y.; Szeto, K. C.; De Mallmann, A.; Barman, S.; Samantaray, M. K.; Delevoye, L.; Gauvin, R. M.; Taoufik, M.; Basset, J.-M., Well-Defined Molybdenum Oxo Alkyl Complex Supported on Silica by Surface Organometallic Chemistry: A Highly Active Olefin Metathesis Precatalyst. *J. Am. Chem. Soc.* **2017**, *139*, 2144-2147.
140. Rost, A. M. J.; Schneider, H.; Zoller, J. P.; Herrmann, W. A.; Kühn, F. E., Methyltrioxorhenium heterogenized on commercially available supporting materials as cyclooctene metathesis catalyst. *J. Organomet. Chem.* **2005**, *690*, 4712-4718.
141. Salameh, A.; Joubert, J.; Baudouin, A.; Lukens, W.; Delbecq, F.; Sautet, P.; Basset, J. M.; Copéret, C., CH₃ReO₃ on γ -Al₂O₃: Understanding Its Structure, Initiation, and Reactivity in Olefin Metathesis. *Angew. Chem. Int. Ed.* **2007**, *46*, 3870-3873.
142. Salameh, A.; Baudouin, A.; Basset, J.-M.; Copéret, C., Tuning the Selectivity of Alumina-Supported (CH₃)ReO₃ by Modifying the Surface Properties of the Support. *Angew. Chem. Int. Ed.* **2008**, *47*, 2117-2120.

143. Salameh, A.; Baudouin, A.; Soulivong, D.; Boehm, V.; Roeper, M.; Basset, J.-M.; Copéret, C., CH₃-ReO₃ on γ -Al₂O₃: Activity, selectivity, active site and deactivation in olefin metathesis. *J. Catal.* **2008**, *253*, 180-190.
144. Valla, M.; Wischert, R.; Comas-Vives, A.; Conley, M. P.; Verel, R.; Copéret, C.; Sautet, P., Role of Tricoordinate Al Sites in CH₃ReO₃/Al₂O₃ Olefin Metathesis Catalysts. *J. Am. Chem. Soc.* **2016**, *138*, 6774-6785.

Chapter 2. Preparation of Well-defined Silica-supported Tungsten-oxo Species and Metathesis Activity upon Activation by Organosilicon Reducing Agent

Reproduced in part with permission from: Mougel, V.; Chan, K.-W.; Siddiqi, G.; Kawakita, K.; Nagae, H.; Tsurugi, H.; Mashima, K.; Safonova, O.; Copéret, C., Low Temperature Activation of Supported Metathesis Catalysts by Organosilicon Reducing Agents. *ACS Cent. Sci.* **2016**, *2*, 569-576. Copyright 2016 American Chemical Society.

2.1 Introduction

Silica-supported tungsten oxide WO_3/SiO_2 is one of the most commonly used heterogeneous olefin metathesis catalysts in petrochemical industry.^{1,2} Its active sites have been proposed to be isolated W-oxo alkylidene species, in their highest oxidation state, formed under the harsh operating conditions of ca. 400 °C (Figure 2.1.A).^{2,3} Major research efforts have been conducted in the past 40 years to generate the corresponding well-defined molecular and surface mimics (Figure 2.1.B).^{2,4-8} Such catalysts display very high activity at room temperature (> 100 turnover number (TON)/ min)^{9,10} in contrast to industrial catalysts, showing that the low activity of the industrial WO_3/SiO_2 catalysts is presumably due to the difficulty to generate the active oxo alkylidene from the oxo surface species rather than an intrinsic low activity of W-oxo alkylidene moieties.

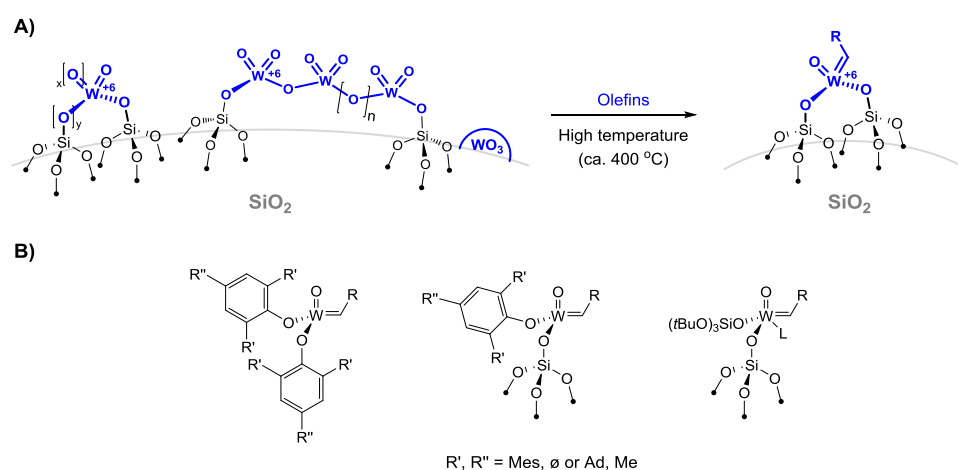


Figure 2.1.A. In WO_3/SiO_2 metathesis catalyst catalysts, the putative active sites (isolated metal oxo alkylidene moieties in +6 oxidation state) are formed at high temperature in presence of olefin. **2.1.B.**

Well-defined isostructural molecular and silica-supported mimics of the putative active site.

Most activation strategies for industrial catalysts involve high temperature treatments under gas atmospheres (alkenes, inert gases, air, H₂) or the use of alkylating agents such as R₄Sn.¹¹⁻¹⁴ However, the performance of these activated industrial catalysts is still far from that of the well-defined molecular and surface mimics. The activation processes are proposed to involve either redox or non-redox mechanisms,^{2,15} which are still largely debated and hinder the rational development of activation strategies for these industrial catalysts.

One of the biggest challenges in developing a molecular-level understanding in the activation processes is the complexity of a mixture of surface species in classical WO₃/SiO₂. Therefore, in this chapter, we develop a synthetic method by combining the Surface Organometallic Chemistry (SOMC) and Thermolytic Molecular Precursor (TMP) approach¹⁶ for synthesizing molecularly-defined isolated tungsten(VI) oxo surface sites on silica. Such an approach consists of grafting a molecular complex containing (*t*BuO)₃SiO– ligands followed by a thermolysis step that removes all organic moieties leaving isolated W(VI) oxo sites. We then further investigate the activation of these supported W(VI) oxo sites by using organosilicon reducing agents.

2.2 Result and Discussion

2.2.1 Synthesis and Characterization of Well-Defined Silica Supported Tungsten-oxo Species

We grafted [W(O)₂(OSi(*Ot*Bu)₃)₂(DME)]^{17,18} on silica partially dehydroxylated at 700 °C (SiO₂₋₇₀₀), followed by a thermal treatment under high vacuum (10⁻⁵ mbar) to afford the material **1** (Figure 2.2.A). A tungsten loading of 3.15 wt% was determined by elemental analysis, corresponding to a site density of ca. 0.5 W/nm² and indicating a partial reaction of the molecular complex with the surface silanols, which was corroborated by IR spectroscopy (Figure 2.2.B).

Further characterization of the material **1** by X-ray Absorption Spectroscopy (XAS) indicates material **1** presents a W L_{III}-edge XANES white line energy of 10210.93 eV, very similar to the white line energy value of the molecular precursors [W(O)(OSi(*Ot*Bu)₃)₄] and [WO₂(OSi(*Ot*Bu)₃)₂(DME)] (10210.97 and 10210.87 eV respectively), confirming that the tungsten centers are present in the +6 oxidation state. The W L_{III}-edge EXAFS spectra of material **1** is shown in Figure 2.2.C. Fitting this spectrum with scattering paths from the nearest oxygen neighbors shows that the presence of a single surface species like the dioxo [(≡SiO)₂WO₂] or the monooxo [(≡SiO)₄WO] is not possible. The best fit shows the number of O atoms at 1.70 Å and 1.89 Å are 1.5 and 2.9, respectively (Table A.2.5), in agreement with a

ca. 1:1 mixture of $[(\equiv\text{SiO})_2\text{WO}_2]$ and $[(\equiv\text{SiO})_4\text{WO}]$ species, as shown in Figure 2.2.A. In addition, the absence of intense peaks at high R values indicates the isolated nature of the tungsten centers in our material (W–W scattering path being typically observed at ca. 3.7 Å for bulk crystalline WO_3 reference, Figure A.2.18).

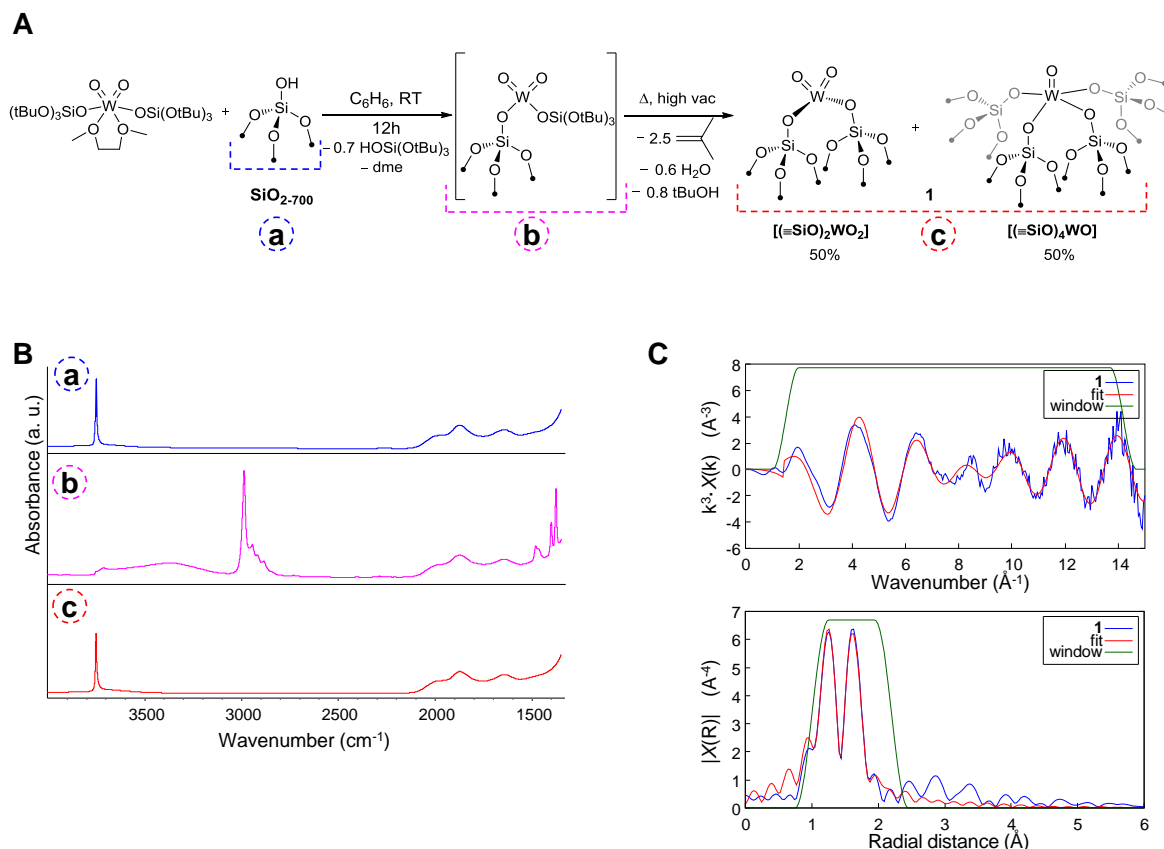


Figure 2.2.A. Synthetic route for **1**. **2.2.B.** The IR spectra of SiO_{2-700} (top), the material after grafting of $[\text{W}(\text{O})_2(\text{OSi}(\text{O}t\text{Bu})_3)_2(\text{DME})]$ (middle) and after thermal decomposition to generate **1** (bottom).

2.2.C. The fit of the EXAFS spectrum in k space and R space of **1** in W L_{III} edge.

The absence of crystalline WO_3 in our sample was further confirmed by powder X-ray diffraction of the material (Figure A.2.16). UV-Vis Diffuse reflectance spectra (UV-DRS) of the material **1** (Figure A.2.14) reveals only one strong transition centered at 230 nm associated to an electronic edge energy (E_g) of 4.2 eV. This single LMCT band is typical for distorted mono-tungstate species¹⁹ and together with the EXAFS data confirm the presence of isolated tungsten centers.

2.2.2 Activation at Low Temperature with Organosilicon Reducing Agents

These well-defined isolated tungsten oxo sites are however only active above 400 °C in propene metathesis, with very modest TOF and TON (initial TOF at 500 °C = 0.05 min⁻¹,

TON = 60 after 24 h), (Figure A.2.26) further illustrating that low activity is probably due to the difficulty in generating the putative alkylidene active sites from isolated metal oxo species.

To overcome the low activity and need of elevated temperatures, we explored the use of organic reducing agents for low temperature activation. Reduction of supported metal complexes is complicated by the fact that most of the typically used reducing agents in molecular inorganic/organometallic chemistry (e.g. alkali metals, organometallic reagents) generate salts or metallic co-products upon reduction. These byproducts stay adsorbed on the surface, which hinders the understanding of the activity of the surface sites and the efficient recycling/reactivation of the catalyst. In that context, reduction of surface complexes with (metal/salt-free) organosilicon reagents, recently demonstrated to be very efficient for the reduction of molecular complexes,²⁰⁻²³ appear as promising alternatives to classical reducing agents. We thus examined the activation of **1** using 2,3,5,6-tetramethyl-1,4-bis(trimethylsilyl)-1,4-diaza-2,5-cyclohexadiene (**Red4**) (Figure 2.3.A).²⁴

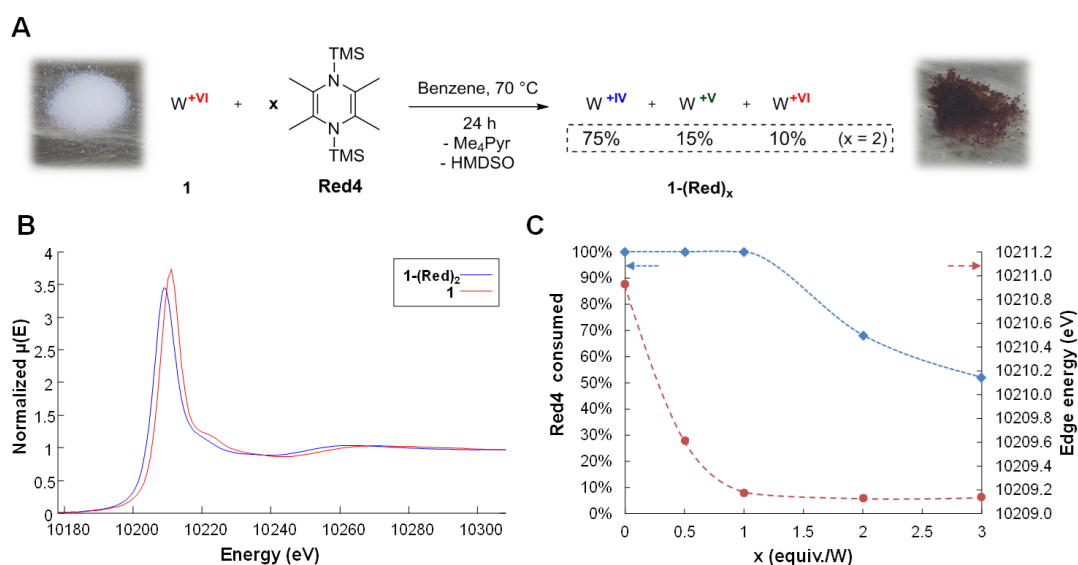


Figure 2.3.A. The reaction of **1** with x equiv. of the organosilicon reducing agent **Red4** results in the partial reduction of the material. Ratio of the W(IV), W(V) and W(VI) species are indicated for x = 2. **2.3.B.** Bulk W L_{III}-edge XANES spectra before and after reduction of **1** with 2 equiv. of **Red4**. **2.3.C.** Changes in the amount of **Red4** consumed (blue diamonds) and XANES white line position (red dots) after reduction of **1** with x equiv. of **Red4**.

The addition of 1 equiv. of **Red4** to a suspension of **1** in benzene at 70 °C afforded a dark purple solid (Figure 2.3.A). Based on proton NMR spectra of the filtrate, **Red4** reacted quantitatively; 0.5 equiv. of 2,3,5,6-tetramethylpyrazine and 0.03 equiv. of HMDSO were

released in solution, and reduction of the material was confirmed by a shift of the XANES white line to lower energy (Figure 2.3.B). The activity of this material in alkene metathesis was investigated using *cis*-4-nonene as a prototypical substrate. In contrast to **1**, inactive in similar conditions, the catalysts activated with **Red4** converted 1000 equiv. of *cis*-4-nonene to thermodynamic conversion at 70 °C in 6 h.

Analysis of the reduced materials by IR spectroscopy revealed that upon addition of **Red4** new C–H stretches were formed and remaining isolated silanols were consumed, likely indicating a passivation of the surface upon exposure to the organosilicon reducing agent (Figure A.2.4). As the passivation of surface silanols by **Red4**—observed even on neat SiO₂-700 (see Appendix for details)—could prevent full use of the reductant for the reduction of the W centers, we investigated the optimal amount of reductant required for quantitative reduction of the tungsten sites. Reductions in similar conditions as described above with x = 0.5, 1, 2, and 3 equiv. of **Red4** per W sites were evaluated by NMR spectroscopy of the filtrate and XANES spectroscopy of the materials, thereafter coined **1-(Red)_x** (Figure 2.3.C).

Proton NMR spectra of the filtrate after addition of **Red4** revealed that **Red4** is quantitatively consumed until one equivalent, and increasing amount of unreacted **Red4** are observed with 2 and more equivalents. The activated materials were analyzed by XANES, monitoring the variation of the tungsten white line energy. The latter gradually decreases with addition of reductant from 10210.93 eV for **1** to 10209.14 eV for **1-(Red)₂**, (see Appendix for details) this value remaining similar for materials activated with 2 equiv. or more of **Red4**. This, combined with the presence of unreacted reductant when more than 2 equiv. are used, indicates that the use of a larger amount of the reductant is not necessary to fully reduce the material. For this reason, we choose to characterize and focus our further studies on **1** reduced with 2 equiv. of **Red4**, **1-(Red)₂**.

2.2.3 Characterization of Activated Catalysts **1-(Red)₂**

Clear information of the oxidation state of the sample is difficult, as very few similar low valent W references are available. We could however observe that the W L_{III} white line energy of the most reduced sample (10209.1 eV for **1-(Red)₂** (Figure 2.3.B) is lower in energy than W(VI) and W(V) reference materials (10211.0 eV for [W(O)(OSi(O*t*Bu)₃)₄], 10210.9 eV for [W(O)₂(OSi(O*t*Bu)₃)₂(DME)] and 10209.5 eV for W(OEt)₅/SiO₂²⁵ respectively), indicating that the main oxidation state of the material is likely to be lower than +5. In particular, the XANES spectra of **1** and **1-(Red)₂** are very close to the spectra of Na₂WO₄ and WO₂ reference materials respectively, consistent with their proposed oxidation state (Figure A.2.21).

To confirm the oxidation state assignment in **1-(Red)₂**, chemical titration of the reduced material using an excess [(Cp₂Fe)(PF₆)] in d₈-THF was carried out. Quantification of released byproducts by proton NMR of the filtrate revealed the release of 1.66 equiv. of ferrocene, 0.1 equiv. of 2,3,5,6-tetramethylpyrazine and 0.8 equiv. of TMS moieties (see Appendix for details). This indicates that the main oxidation state of W is close to +4, but with the presence of some species in higher oxidation states (+5 or +6). In fact, EPR studies of **1-(Red)₂** revealed the presence of W(V) centers, (Figure 2.4) which were determined to represent ca. 0.15 equiv. of the W sites according to spin counting (see Appendix for details).

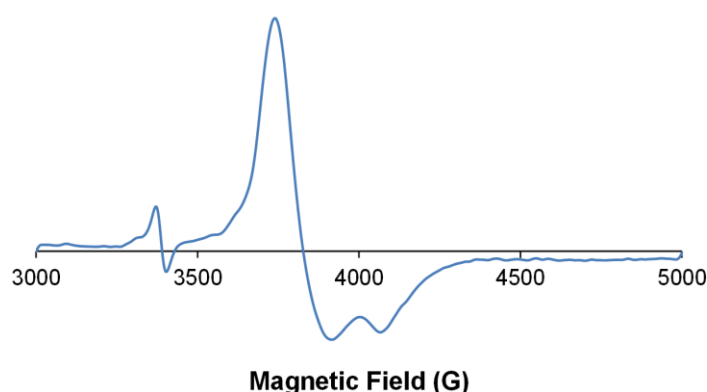


Figure 2.4. EPR spectra of **1-(Red)₂**

Hence, W(IV) species probably account for 75% of the surface species, together with 15% of W(V) species and 10% of non-reduced W(VI) species, in agreement with the XANES shift described above. As both the dioxo [(=SiO)₂WO₂] and monooxo [(=SiO)₄WO] surface sites are present in a 1:1 ratio in **1**, this indicates that both species can be reduced by **Red4**. UV-DRS of **1-(Red)₂** presents strong absorbance in all the 200-800 nm region, similar to what is observed for H₂ treated tungsten oxides,²⁶ the shifts above 400 nm being typical for d-d transition of W(V) species, but may also arise from other reduced W species.³ EXAFS studies of **1-(Red)₂** show that the numbers of oxygen atoms at ca. 1.70 Å decreased together with an increase in the numbers of oxygen neighbors at ca. 1.90 Å with respect to **1**, that is in agreement with an average of less W=O double bonds and more W–O single bonds. From the quantitative analysis, the number of W=O bond before and after reaction drop from 1.5 to 0.8 while the numbers of W–O bonds increases from 2.9 to 3.1 (see Figure A.2.19, Table A.2.5 and A.2.7). This is consistent with the reduction of the tungsten sites and the TMS functionalization of the oxo moieties upon reaction with the organosilicon reducing agent.

This information is consistent with the C, H, N and W elemental analysis of **1-(Red)₂** indicating the presence of ca. 0.5 equiv. of 2,3,5,6-tetramethylpyrazine and ca. 2.9 equiv. of TMS moieties per surface tungsten center (13 C, 1 N and 33 H atoms per W center), the latter accounting also for the presence of at least 1.4 ($\equiv\text{SiOTMS}$) moieties per W center resulting from silica passivation.²⁷ This is consistent with amount of 2,3,5,6-tetramethylpyrazine and HMDSO recovered in the filtrate after the reduction procedure.

At this stage however, it is not possible to propose a defined structure after reduction, as the reduced material is likely composed of several surface species with tungsten in +IV (75%), +V (15%) and +VI (10%) oxidation state.

2.2.4 Catalytic Activity of Activated Materials

In order to evaluate the potential of the most reduced catalyst **1-(Red)₂** in alkene metathesis of liquid olefins in batch conditions, we evaluated its activity with *cis*-4-nonene. The reduced catalyst showed good activity in the metathesis of *cis*-4-nonene, converting 1000 equiv. of *cis*-4-nonene to thermodynamic conversion at 70 °C in less than 12 h. However, as shown in Figure 2.5 (dark blue diamonds), an induction period of 3 h took place before metathesis started. Interestingly, we noticed that this induction period was affected by the amount of **Red4** used, as shorter induction periods were observed for **1-(Red)₁** and **1-(Red)_{0.5}** (Figure 2.5, light blue squares and purple dots).

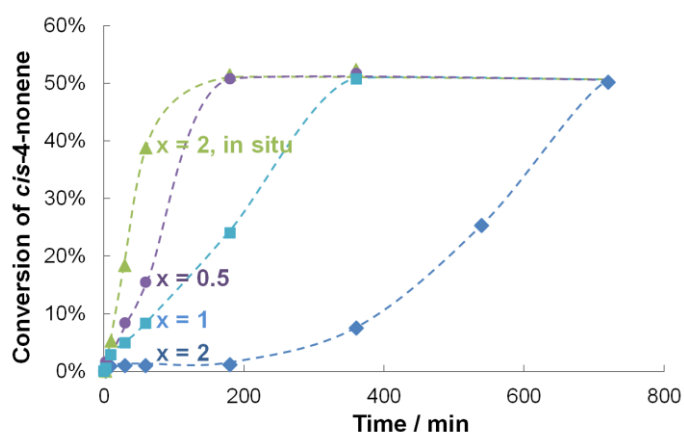


Figure 2.5. Conversion vs time, *cis*-4-nonene homometathesis, 0.1 mol% W, 70 °C for **1-(Red)₂** (blue diamonds), **1-(Red)₁** (blue squares), **1-(Red)_{0.5}** (purple dots) and in situ addition of 0.2 mol% **Red4** to **1** (green triangles). Dashed lines have been added as a guide to the eyes.

We reasoned that this induction period might be due to the reversible poisoning of some active sites by 2,3,5,6-tetramethylpyrazine released upon activation of the catalysts with the

reducing agent. To test this hypothesis, we looked into directly activating the material under catalytic conditions. When 2 equiv. of **Red4** were added to the materials in presence of 1000 equiv. of *cis*-4-nonene, full conversion was observed in less than 3 h, without observing an induction period (Figure 2.5, green triangles).²⁸ This activity is comparable with some well-defined silica-supported tungsten alkylidene catalysts.²⁹

This high activity prompted us to investigate the catalytic activity with a broader range of substrates, including ethyl oleate, a prototypical functionalized substrate from biomass (Table 2.1). The catalyst was proven efficient with 1-nonene, albeit with lower TOF, reaching equilibrium conversion in 24 h at 1 mol% loading. With ethyl oleate equilibrium conversion is also observed at 1 mol% loading in 24 h. Ring opening metathesis was realized with a TON of 100 with cyclooctene. The molecular dioxo and monoxo analogues of the surface species ($[W(O)_2(OSi(OtBu)_3)_2(DME)]$ and $[W(O)(OSi(OtBu)_3)_4]$) were found to be inactive under the same conditions reaction. The good activity displayed by **1** in the presence of 2 equiv. of **Red4** at low temperatures, including for functionalized substrates, is unprecedented for supported tungsten oxide catalysts.

Table 2.1. Metathesis of various substrates by **1** in presence of 2 equiv. of **Red4** at 70 °C.

<i>Substrate</i>	<i>Mol %</i>	<i>TOF_{max} (min⁻¹)^a</i>	<i>Time to final conversion^b</i>
<i>cis</i> -4-nonene	0.1	8 (10 min)	3 h (500)
1-nonene	1	3 (360 min)	24 h (84)
Ethyl Oleate	1	4 (3 min)	24 h (48)
Cyclooctene	1	10 (5 min)	20 min (100)

^a Maximum TOF value measured during the test, at the time indicated in parentheses. ^b TON are given in parentheses

Meanwhile, we also investigated the possibility of catalyst recycling and reactivation. After initial activation of **1** with 2 equiv. of **Red4** in presence of 1000 equiv. of *cis*-4-nonene and thermodynamic conversion is observed, the catalyst can be recovered by filtration. A new portion of 1000 equiv. can be converted to thermodynamic conversion with this recycled catalyst, however at the expense of much slower TOF, equilibrium conversion being reached in about 24 h (vs. 3 h for the initial cycle, Figure A.2.27). This significant aging of the catalyst is likely due to the deactivation of active sites with the feed impurities, the most common impurities in the olefin feed are adventitious traces of water, dioxygen and alcohol.³⁰⁻³² Interestingly, it can be noticeably reduced by addition of 1 equiv. of **Red4** to the second

portion of *cis*-4-nonene added, equilibrium conversion being then reached in about 10 h (Figure A.2.28). This highlights the potential of the reductant to reactivate the deactivated sites (see Appendix for details). We thus investigated the reactivation of poisoned catalyst with dioxygen, water and ethanol. Metathesis of *cis*-4-nonene was initiated using **1** at 0.1 mol% loading in presence of 2 equiv. of **Red4**; after 1.5 h, and ensuring that the catalytic reaction took place, H₂O, dry air or ethanol (1 equiv., excess and 1 equiv. respectively) were added to the reaction mixtures (see Appendix for details). After 1.5 h, the deactivated catalysts were separated from the solution phase to remove the contaminant, and exposed to a new portion of 1000 equiv. of *cis*-4-nonene. No catalytic activity was observed with these poisoned catalysts, confirming their complete deactivation. These poisoned catalysts were then reactivated with 2 equiv. of **Red4** and display full conversions in all the three cases (observed after 100 h for O₂ poisoned catalyst and 48 h for H₂O and ethanol). This unprecedented reactivation of poisoned catalysts paves the way towards continuous regeneration of the catalyst in flow conditions.

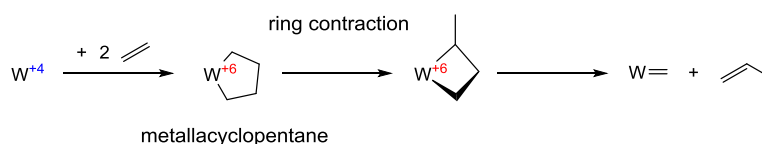
2.2.5 Investigation of Reaction Intermediates and Initiation Mechanism

In order to investigate the changes occurring at the metal sites in catalytic conditions, we investigated the changes in the XANES of **1-(Red)₂** before and after catalytic tests with *cis*-4-nonene in the conditions described above (1000 equiv. of *cis*-4-nonene in toluene at 70 °C for 24 h). The XANES white line energy of the catalyst **1-(Red)₂** before and after exposure to the olefin increased from 10209.1 eV to 10209.4 eV, this increase in the white line energy being consistent with the partial reoxidation of the material upon exposure to alkenes.

Moreover, EPR studies of **1-(Red)₂** before and after exposure to *cis*-4-nonene in catalytic conditions show that the signal attributed to W(V) sites is barely affected in terms of shape and intensity (Figure A.2.23), indicating that these are likely spectator species in the catalytic reaction. The presence of these remaining W(V) sites after exposure to olefins could be a reason why the value of the tungsten white-line energy after exposure is still lower than that of the parent W(VI) precursor **1** (10209.4 eV for **1-(Red)₂** after exposure to 1000 equiv. of *cis*-4-nonene vs. 10210.9 eV for **1**).

Based on both XANES and EPR studies, the results suggest the formation of W(VI) alkylidenes (metathesis active species) likely resulted from the W(IV) sites. To further probe this hypothesis, **1-(Red)₂** was exposed to 60 equiv. of ethylene at 100 °C for 12 h. GC-MS characterization of the gas phase after reaction revealed the release of ca. 0.5 equiv. of propene and 0.04 equiv. of but-2-enes. ¹³C Cross Polarisation Magic Angle Spinning (CP MAS) and HETCOR NMR spectrum of a sample prepared analogously with ¹³C dilabeled

ethylene revealed the appearance of peaks at 74, 38, 34 and 21 ppm correlating to ^1H signals at 3.2, 3.5, 2.0 and 2.6 ppm respectively (Figures A.2.11 – A.2.13). The set of signals at 38 and 21 ppm are reminiscent from SP metallacyclobutane units,^{29, 33, 34} while the signals at 74 ppm and 34 ppm can be tentatively assigned to a metallacyclopentane moiety. To confirm this hypothesis, a suspension of this sample in CH_2Br_2 was contacted with Br_2 ; GC-MS analysis of the product solution revealed the presence of 1,4-dibromobutane, in agreement with the presence of the proposed metallacyclopentane complex (see Appendix for details). One way to explain the formation of metallacyclopentane, metallacyclobutane and propene is that metallacyclopentane is formed from W(IV) olefin adducts, similar to the reported Ta, Mo, W³⁵⁻⁴⁰ examples (for molecular complexes). Then, a subsequent ring contraction generates the metallacyclobutane and finally the carbene species (Eq 2.1).^{41,42}



Eq. 2.1. Possible mechanism for the observation of metallacyclopentane and propene.

2.3 Conclusion

Using a molecularly-defined tungsten oxo model of the surface species existing in WO_3/SiO_2 catalysts, we have identified a simple activation process via the reduction of the surface sites with organosilicon reductants at low temperatures. This process allows the generation of highly active catalysts, notably through the in-situ reduction of the catalyst in presence of the substrate. By showing evidence for the generation of metathesis active sites from W(IV) centers, this approach builds bridges between molecular and classical heterogeneous metal oxide metathesis catalysts. This activation process paves the way towards simple improvement of existing alkene metathesis processes by allowing lower temperature operation and improved selectivity.

2.4 Experimental Details

2.4.1 General procedures

All experiments were carried out under dry and oxygen free argon atmosphere using standard Schlenk, high vacuum lines (10^{-5} mbar) or glove-box techniques for organometallic synthesis. Pentane, toluene and diethyl ether were purified using double MBraun SPS alumina column, and were degassed using three freeze-pump-thaw cycles before being used. DME and THF were distilled from Na/Benzophenone. Silica (Aerosil Degussa, $200 \text{ m}^2 \cdot \text{g}^{-1}$) was compacted with distilled water, calcined at $500 \text{ }^\circ\text{C}$ under air for 4 h and treated under vacuum (10^{-5} mbar) at $500 \text{ }^\circ\text{C}$ for 6 h and then at $700 \text{ }^\circ\text{C}$ for 10 h (support referred to as SiO_{2-700}) and contained 0.26 mmol of OH per g as measured by titration with PhCH_2MgCl . All infrared (IR) spectra were recorded using a Bruker α -T spectrometer placed in an Ar glovebox, equipped with OPUS software. A typical experiment consisted in the measurement of transmission in 32 scans in the region from 4000 to 400 cm^{-1} . The ^1H and ^{13}C solid state NMR spectra were obtained on Bruker Avance III 400 MHz Bruker spectrometers equipped with a 4 mm probe. Cross polarization magic angle spinning (CPMAS) and spin echo type experiments were used to measure ^{13}C and ^1H , respectively. The radio frequency (RF) field of proton was always set to 100 kHz while the ^1H decoupling was set to 80 kHz. The solution spectra were recorded in C_6D_6 at room temperature. The electronic structures of the catalysts were obtained with a Varian Cary UV-vis spectrophotometer employing a Praying Mantis integration sphere. The UV-vis spectra were processed with Microsoft Excel software, consisting of calculation of the Kubelka-Monk function, $F(R_\infty)$, which was extracted from the UV-vis DRS absorbance. The edge energy (E_g) for allowed transitions was determined by finding the intercept of the straight line in the low-energy rise of a plot of $[F(R_\infty)h\nu]^2$.¹⁹ Continuous Wave (CW) EPR spectra were measured at X band (9.5-GHz microwave frequency) on a Bruker EMX spectrometer at 110 K. Powder XRD experiments were performed on a STOE Padi Diffractometer in Debye-Scherrer Mode (2θ) with a Dectris Mythen 1K area detector using Cu $K\alpha_1$ radiation. The sample was prepared and measured in a sealed quartz capillary. X-ray absorption spectroscopy (XAS) at the W L_{III} -edge was measured at the SuperXAS beamline at the Swiss Light Source (SLS; Paul Scherrer Institute, Villigen, Switzerland). Calibration of the beamline energy was performed using Pt reference foil (Pt L_{III} -edge position at 11564 eV). XAS spectra in transmission mode were measured at room temperature using ionization chambers filled with He- N_2 gas mixtures. To avoid contact with air, all samples were sealed in a Ar glovebox. Each pellet of samples (with optimized thickness for transmission detection) was placed in two aluminized plastic bags using an

impulse sealer inside a glovebox; one sealing layer was removed just before the measurements. Multiple extended X-ray absorption fine structure (EXAFS) scans (10207–11207 eV) were averaged using new spots for each scan, with a scan time of ca. 30 min. EXAFS data were analyzed using the Ifeffit program package. The EXAFS data were fitted in R-space (1–2.2 Å) after a Fourier transform ($k = 1.5\text{--}14.2 \text{ \AA}^{-1}$) using a k-weight of 3.

Compounds $\text{WO}_2\text{Cl}_2(\text{DME})$,⁴³ $\text{WOCl}_3(\text{bipy})$,⁴⁴ 2,3,5,6-tetramethyl-1,4-bis(trimethylsilyl)-1,4-diaza-2,5-cyclohexadiene (**Red4**),²¹ were synthesized according to literature procedures.

2.4.2 Synthesis of the molecular precursors

Synthesis of $[\text{W}(\text{O})(\text{OSi}(\text{OtBu})_3)_4]$

$[\text{W}(\text{O})(\text{OSi}(\text{OtBu})_3)_4]$ was synthesized following the procedure described by Tilley.¹⁷ XRD suitable crystals were obtained upon cooling at $-40 \text{ }^\circ\text{C}$ a saturated toluene solution of the complex.

Synthesis of $[\text{W}(\text{O})_2(\text{OSi}(\text{OtBu})_3)_2(\text{DME})]$

$[\text{W}(\text{O})_2(\text{OSi}(\text{OtBu})_3)_2(\text{DME})]$ was synthesized using a modification of the procedure described by Tilley.¹⁷ A solution of $\text{LiOSi}(\text{OtBu})_3$ (2.87 g, 10.6 mmol, 2 equiv.) in cold toluene (15 mL, $-40 \text{ }^\circ\text{C}$) was added dropwise to a suspension of $\text{WO}_2\text{Cl}_2(\text{DME})$ (2.00 g, 5.3 mmol, 1 equiv.) in toluene (20 mL, $-78 \text{ }^\circ\text{C}$) containing 200 μL of DME under vigorous stirring. After 1 hour stirring at $-78 \text{ }^\circ\text{C}$ and 2 h at room temperature, the solution was filtered through a short Celite® pad to afford a colorless solution. Crystallization of the product from this solution at $-40 \text{ }^\circ\text{C}$ afforded 3.2 g (3.8 mmol, 72 %) of the title product as large colorless needle shaped crystals suitable for XRD (collected in two crops).

$^1\text{H-NMR}$ (300 MHz, C_6D_6) δ 1.38 (s, 54H, $(\text{OtBu})_3$), 3.15 (s, 6H, DME), 3.33 (s, 4H, DME). IR (KBr, cm^{-1}): 703(m), 830(m), 858(m), 902(m), 948(m), 962(m), 1028(m), 1066(s), 1191(m), 1243(m), 1366(m), 1390(m), 1473(w), 2975(m).

2.4.3. Synthesis of the supported materials

Synthesis of $[(\equiv\text{SiO})\text{W}(\text{O})_2(\text{OSi}(\text{OtBu})_3)]$

A solution of 1.00 g of $\text{WO}_2[\text{OSi}(\text{OtBu})_3]_2(\text{DME})$ (1.25 mmol, 1.05 equiv.) in benzene (6 mL) was added to a suspension of $\text{SiO}_{2-(700)}$ (4.61 g, 1.19 mmol, 1 equiv.) in benzene (3 mL) at room temperature. The suspension was slowly stirred at room temperature for 12 h. The white solid was collected by filtration, and was washed by five suspension/filtration cycles in benzene (5 x 2 mL). The resulting solid was dried thoroughly under high vacuum (10^{-5} mbar) at room temperature for 3 h to afford 4.55 g of the title compound. All the filtrate solutions were collected and analyzed by $^1\text{H NMR}$ spectroscopy in C_6D_6 using ferrocene as

internal standard, indicating that 1.7 mmol of $(t\text{BuO})_3\text{SiOH}$ and 0.47 mmol of DME were released upon grafting (0.70 $(t\text{BuO})_3\text{SiOH}/W_{\text{surf}}$ and 0.40 $\text{DME}/W_{\text{surf}}$). Additional 0.65 mmol of DME were quantified in the volatiles collected upon high vacuum drying, indicating that > 95% of DME was not retained on the silica surface.

Elemental Analysis: W 3.12%, H 0.64%, C 2.97% corresponding to 14.5 C/W (12 expected), 38 H/W 39 expected).

IR and solid state NMR spectra of the material are given in Figure A.2.3, A.2.7 – A.2.8, respectively.

*Thermal decomposition of $[(\equiv\text{SiO})\text{WO}_2(\text{OSi}(\text{OtBu})_3)]$: preparation of **1***

$[(\equiv\text{SiO})\text{WO}_2(\text{OSi}(\text{OtBu})_3)]$ (3.0 g) was loaded into a reactor and placed under high vacuum (10^{-5} mbar) and heated to 200 °C (1 °C/min) and held at this temperature for 3 h then heated at 400 °C (1 °C/min) and held at this temperature for 6 h. The reactor was cooled to ambient temperature under vacuum, and **1** was stored in an Ar filled glovebox. The volatiles evolved during this process were quantified by ^1H NMR in C_6D_6 using ferrocene as an internal standard, indicating the release of 2.5 equiv. of isobutylene, 0.6 equiv. of water and 0.8 equiv. of $t\text{BuOH}$ per surface W complex.

Elemental analysis: W 3.15 %.

IR spectrum, UV-DRS and powder XRD pattern of the material are given in Figure A.2.3; A.2.14 and A.2.16, respectively.

*Reductions of **1***

A solution of 5.4 mg of **Red4** (19.4 μmol , 2 equiv.) in benzene (0.5 mL) was added to a suspension of **1** (50 mg, 9.7 μmol) in benzene (0.5 mL) at room temperature. The suspension was slowly stirred at 70 °C for 12 h, resulting in color change of the material from colorless to dark violet. The solid was collected by filtration, and was washed by four suspension/filtration cycles in benzene (4 x 1 mL). The resulting dark violet solid was dried thoroughly under high vacuum (10^{-5} mbar) at room temperature for 3 h to afford 45 mg of the title compound. All the filtrate solutions were collected and analyzed by ^1H NMR spectroscopy in C_6D_6 using ferrocene as internal standard, indicating consumption of 13.1 μmol of **Red4** and that 9.7 μmol of 2,3,5,6-tetramethylpyrazine and 1.2 μmol of HMDSO were released upon reacting (0.18 equiv. 2,3,5,6-tetramethylpyrazine / W_{surf}).

Elemental Analysis: W 2.93 %, C 2.57 %, H 0.54%, N 0.24 % corresponding to 13 C/W, 33 H/W and 1 N/W.

IR, UV-DRS and solid state NMR spectra of the material are given in Figure A.2.4; A.2.15, and Figure A.2.9 – A.2.10, respectively.

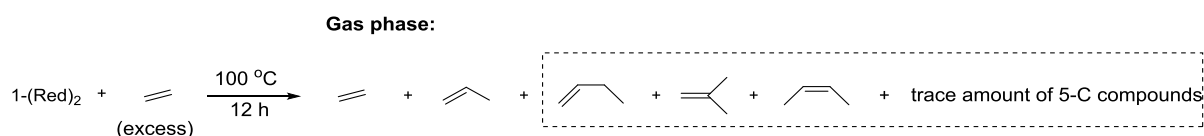
2.4.4. Catalytic test

General procedure for metathesis of liquid olefin substrate in batch

At $t=0$ a ca. 1.0 M solution of olefin in toluene containing heptane as internal standard (ca. 0.1 M) was added to the catalyst introduced in a conical base vial containing a wing shaped magnetic stirring bar. The reaction mixture was stirred at 600 rpm and kept at 70 °C using an aluminum heating block. 5 μL aliquots of the solution were sampled, diluted with pure toluene (100 μL) and quenched by the addition of 1 μL of wet ethyl acetate. The resulting solution was analyzed by GC/FID (Agilent Technologies 7890 A) equipped with an HP-5 (Agilent Technologies) column. Conversion is shown by eq (1).

$$\text{Product conversion}_t = \frac{\Sigma[\text{products}]_t}{[\text{substrate}]_{\text{ini}}} \quad (1)$$

2.4.5. Exposure of 1-(Red)₂ to ethylene



1-(Red)₂ (62.1 mg) was loaded in a 26 mL glass reactor and contacted with ethylene (9.4 equiv. per W metal center). After 12 h at 100 °C, the gas phase was analyzed by GC-FID and GC-MS showing the presence of unreacted ethylene, propylene (0.5 equiv.) and a mixture of four-carbon containing hydrocarbons (1-butene, cis-2-butene, trans-2-butene and *iso*-butene; in total 0.03 equiv.). Good reproducibility in the amount of olefin released was confirmed while reproducing twice this experiment on different samples of **1-(Red)₂**.

2.5 References

1. Grubbs, R. H.; Wenzel, A. G.; O'Leary, D. J.; Khosravi, E., Handbook of Metathesis. In *Handbook of Metathesis*, Wiley-VCH Verlag GmbH & Co. KGaA: Weinheim, Germany, 2015; pp I-XVII.
2. Lwin, S.; Wachs, I. E., Olefin Metathesis by Supported Metal Oxide Catalysts. *ACS Catal.* **2014**, *4*, 2505-2520.
3. Lwin, S.; Li, Y.; Frenkel, A. I.; Wachs, I. E., Nature of WO_x Sites on SiO₂ and Their Molecular Structure–Reactivity/Selectivity Relationships for Propylene Metathesis. *ACS Catal.* **2016**, *6*, 3061-3071.
4. Wengrovius, J. H.; Schrock, R. R.; Churchill, M. R.; Missert, J. R.; Youngs, W. J., Multiple metal-carbon bonds. 16. Tungsten-oxo alkylidene complexes as olefins metathesis catalysts and the crystal structure of W(O)(CHCMe₃)(PEt₃)Cl₂. *J. Am. Chem. Soc.* **1980**, *102*, 4515–4516.
5. Yermakov, Y. I.; Kuznetsov, B. N.; Zakharov, V. A., *Catalysis by Supported Complexes*. Elsevier: Amsterdam, 1981.
6. Iwasawa, Y.; Kubo, H.; Hamamura, H., Olefin metathesis over Al₂O₃ or SiO₂-attached molybdenum catalysts: active structures and mechanism for initial carbene formation. *J. Mol. Catal.* **1985**, *28*, 191-208.
7. Peryshkov, D. V.; Schrock, R. R., Synthesis of Tungsten Oxo Alkylidene Complexes. *Organometallics* **2012**, *31*, 7278-7286.
8. Copéret, C.; Comas-Vives, A.; Conley, M. P.; Estes, D.; Nunez-Zarur, F.; Fedorov, A.; Mougél, V.; Nagae, H.; Zhizhko, P. A., Surface Organometallic and Coordination Chemistry towards Single-Site Heterogeneous Catalysts: Strategies, Methods, Structures, and Activities. *Chem. Rev.* **2016**, *116*, 323-421.
9. Mougél, V.; Copéret, C., Isostructural Molecular and Surface Mimics of the Active Sites of the Industrial WO₃/SiO₂ Metathesis Catalysts. *ACS Catal.* **2015**, *5*, 6436-6439.
10. Conley, M. P.; Mougél, V.; Peryshkov, D. V.; Forrest, W. P.; Gajan, D.; Lesage, A.; Emsley, L.; Copéret, C.; Schrock, R. R., A Well-Defined Silica-Supported Tungsten Oxo Alkylidene Is a Highly Active Alkene Metathesis Catalyst. *J. Am. Chem. Soc.* **2013**, *135*, 19068-19070.
11. Rodriguezramos, I.; Guerrerorruiz, A.; Homs, N.; Delapiscina, P. R.; Fierro, J. L. G., Reactions of propene on supported molybdenum and tungsten-oxides. *J. Mol. Catal. A-Chem.* **1995**, *95*, 147-154.
12. Andreini, A.; Mol, J. C., Activity of Supported Tungsten-Oxide Catalysts for the Metathesis of Propene. *J Chem Soc Farad T 1* **1985**, *81*, 1705-1714.
13. Basrur, A. G.; Patwardhan, S. R.; Vyas, S. N., Propene metathesis over silica-supported tungsten-oxide catalyst catalyst induction mechanism. *J. Catal.* **1991**, *127*, 86-95.
14. Lokhat, D.; Starzak, M.; Stelmachowski, M., Gas-phase metathesis of 1-hexene over a WO₃/SiO₂ catalyst: Search for optimal reaction conditions. *Appl. Catal., A* **2008**, *351*, 137-147.
15. Amakawa, K.; Wrabetz, S.; Kröhnert, J.; Tzolova-Müller, G.; Schlögl, R.; Trunschke, A., In Situ Generation of Active Sites in Olefin Metathesis. *J. Am. Chem. Soc.* **2012**, *134*, 11462-11473.
16. Furdala, K. L.; Tilley, T. D., Design and synthesis of heterogeneous catalysts: the thermolytic molecular precursor approach. *J. Catal.* **2003**, *216*, 265-275.
17. Jarupatrakorn, J.; Coles, M. P.; Tilley, T. D., Synthesis and Characterization of MO[OSi(OtBu)₃]₄ and MO₂[OSi(OtBu)₃]₂ (M = Mo, W): Models for Isolated Oxo-Molybdenum and -Tungsten Sites on Silica and Precursors to Molybdena- and Tungsta-Silica Materials. *Chem. Mat.* **2005**, *17*, 1818-1828.
18. Crystal structure of the precursor was collected during the course of this study. Details are given in Appendix.
19. Ross-Medgaarden, E. I.; Wachs, I. E., Structural determination of bulk and surface tungsten oxides with UV-vis diffuse reflectance spectroscopy and Raman spectroscopy. *J. Phys. Chem. C* **2007**, *111*, 15089-15099.
20. Arteaga-Müller, R.; Tsurugi, H.; Saito, T.; Yanagawa, M.; Oda, S.; Mashima, K., New Tantalum Ligand-Free Catalyst System for Highly Selective Trimerization of Ethylene Affording 1-Hexene: New Evidence of a Metallacycle Mechanism. *J. Am. Chem. Soc.* **2009**, *131*, 5370-5371.
21. Saito, T.; Nishiyama, H.; Tanahashi, H.; Kawakita, K.; Tsurugi, H.; Mashima, K., 1,4-Bis(trimethylsilyl)-1,4-diaza-2,5-cyclohexadienes as Strong Salt-Free Reductants for Generating Low-

- Valent Early Transition Metals with Electron-Donating Ligands. *J. Am. Chem. Soc.* **2014**, *136*, 5161-5170.
22. Tsurugi, H.; Saito, T.; Tanahashi, H.; Arnold, J.; Mashima, K., Carbon Radical Generation by d^0 Tantalum Complexes with α -Diimine Ligands through Ligand-Centered Redox Processes. *J. Am. Chem. Soc.* **2011**, *133*, 18673-18683.
23. Tsurugi, H.; Tanahashi, H.; Nishiyama, H.; Fegler, W.; Saito, T.; Sauer, A.; Okuda, J.; Mashima, K., Salt-Free Reducing Reagent of Bis(trimethylsilyl)cyclohexadiene Mediates Multielectron Reduction of Chloride Complexes of W(VI) and W(IV). *J. Am. Chem. Soc.* **2013**, *135*, 5986-5989.
24. Kaim, W., Effects of cyclic 8π -electron conjugation in reductively silylated nitrogen heterocycles. *J. Am. Chem. Soc.* **1983**, *105*, 707-713.
25. Alphazan, T.; Bonduelle-Skrzypczak, A.; Legens, C.; Gay, A.-S.; Boudene, Z.; Girleanu, M.; Ersen, O.; Copéret, C.; Raybaud, P., Highly Active Nonpromoted Hydrotreating Catalysts through the Controlled Growth of a Supported Hexagonal WS_2 Phase. *ACS Catal.* **2014**, *4*, 4320-4331.
26. Aliev, R. K.; Tsitovskaya, I. L.; Kadushin, A. A.; Krylov, O. V., Investigation of supported WO_3 catalysts for propene metathesis by Diffuse Reflectance Spectroscopy. *React. Kinet. Catal. Lett.* **1978**, *8*, 257-261.
27. Silica passivation could result from reaction of **Red4** and HMDSO with surface silanols, as both react with surface OH in the condition used for reduction. We have quantified the passivation of silica in **1-(Red)₂** by titrating the numbers of surface SiOH before (2.33 equiv. SiOH/W) and after addition of two equivalents of **Red4** (0.94 equiv. SiOH/W). See the Appendix for details.
28. Interestingly, applying similar strategy to the molecular catalysts $[W(O)_2(OSi(OtBu)_3)_2(DME)]$ and $[W(O)(OSi(OtBu)_3)_4]$ or the grafted complexes $[(\equiv SiO)W(O)_2(OSi(OtBu)_3)]$ and $[(\equiv SiO)W(O)(OSi(OtBu)_3)_3]$ did not afford active alkene metathesis catalysts (see Appendix for details).
29. Mougél, V.; Santiago, C. B.; Zhizhko, P. A.; Bess, E. N.; Varga, J.; Frater, G.; Sigman, M. S.; Copéret, C., Quantitatively Analyzing Metathesis Catalyst Activity and Structural Features in Silica-Supported Tungsten Imido-Alkylidene Complexes. *J. Am. Chem. Soc.* **2015**, *137*, 6699-6704.
30. Amigues, P.; Chauvin, Y.; Commereuc, D.; Hong, C. T.; Lai, C. C.; Liu, Y. H., Methathesis of ethylene-butene mixtures to propylene with rhenium on alumina catalysts. *J. Mol. Catal.* **1991**, *65*, 39-50.
31. Behr, A.; Schüller, U.; Bauer, K.; Maschmeyer, D.; Wiese, K. D.; Nierlich, F., Investigations of reasons for the deactivation of rhenium oxide alumina catalyst in the metathesis of pentene-1. *Appl. Catal., A* **2009**, *357*, 34-41.
32. UOP *Purification of olefin and polymer process streams*; Honeywell UOP: 2012. <http://www.uop.com/wp-content/uploads/2012/12/UOP-Adsorbents-for-purification-of-olefin-and-polymer-process-streams-brochure.pdf>.
33. Blanc, F.; Berthoud, R.; Copéret, C.; Lesage, A.; Emsley, L.; Singh, R.; Kreickmann, T.; Schrock, R. R., Direct observation of reaction intermediates for a well defined heterogeneous alkene metathesis catalyst. *Proc. Nat. Acad. Sci. U.S.A.* **2008**, *105*, 12123-12127.
34. Mougél, V.; Copéret, C., Magnitude and consequence of OR ligand σ -donation on alkene metathesis activity in d^0 silica supported $(\equiv SiO)W(NAr)(=CHtBu)(OR)$ catalysts. *Chem. Sci.* **2014**, *5*, 2475-2481.
35. McLain, S. J.; Wood, C. D.; Schrock, R. R., Preparation and characterization of tantalum(III) olefin complexes and tantalum(V) metallacyclopentane complexes made from acyclic α . olefins. *J. Am. Chem. Soc.* **1979**, *101*, 4558-4570.
36. Wang, S. Y. S.; VanderLende, D. D.; Abboud, K. A.; Boncella, J. M., Metallacyclopentane formation: A deactivation pathway for a tungsten(VI) alkylidene complex in olefin metathesis reactions. *Organometallics* **1998**, *17*, 2628-2635.
37. Tsang, W. C. P.; Jamieson, J. Y.; Aeilts, S. L.; Hultsch, K. C.; Schrock, R. R.; Hoveyda, A. H., Investigations of Reactions between Chiral Molybdenum Imido Alkylidene Complexes and Ethylene: Observation of Unsolvated Base-Free Methylene Complexes, Metalacyclobutane and Metalacyclopentane Complexes, and Molybdenum(IV) Olefin Complexes. *Organometallics* **2004**, *23*, 1997-2007.

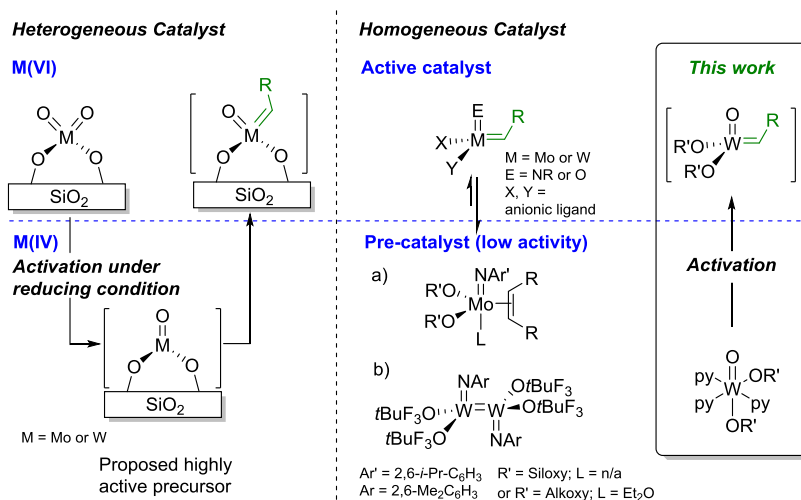
38. Schrock, R. R.; Duval-Lungulescu, M.; Tsang, W. C. P.; Hoveyda, A. H., Catalytic Homologation of Vinyltributylstannane to Allyltributylstannane by Mo(IV) Complexes in the Presence of Ethylene. *J. Am. Chem. Soc.* **2004**, *126*, 1948-1949.
39. Leduc, A. M.; Salameh, A.; Soulivong, D.; Chabanas, M.; Basset, J. M.; Copéret, C.; Solans-Monfort, X.; Clot, E.; Eisenstein, O.; Bohm, V. P. W.; Roper, M., β -H transfer from the metallacyclobutane: A key step in the deactivation and byproduct formation for the well-defined silica-supported rhenium alkylidene alkene metathesis catalyst. *J. Am. Chem. Soc.* **2008**, *130*, 6288-6297.
40. Solans-Monfort, X.; Copéret, C.; Eisenstein, O., Shutting Down Secondary Reaction Pathways: The Essential Role of the Pyrrolyl Ligand in Improving Silica Supported d^0 -ML₄ Alkene Metathesis Catalysts from DFT Calculations. *J. Am. Chem. Soc.* **2010**, *132*, 7750-7757.
41. Yang, G. K.; Bergman, R. G., Synthesis, molecular structure, and thermal chemistry of (η^5 -cyclopentadienyl)dicarbonylrhenacyclopentane. *Organometallics* **1985**, *4*, 129-138.
42. McLain, S. J.; Sancho, J.; Schrock, R. R., Metallacyclopentane to metallacyclobutane ring contraction. *J. Am. Chem. Soc.* **1979**, *101*, 5451-5453.
43. Dreisch, K.; Andersson, C.; Stalhandske, C., Synthesis and structure of dimethoxyethane-dichlorodioxo-tungsten(VI)—a highly soluble derivative of tungsten dioxodichloride. *Polyhedron* **1991**, *10*, 2417-2421.
43. Rice, C. A.; Kroneck, P. M. H.; Spence, J. T., Tungsten(V)-oxo and tungsten(VI)-dioxo complexes with oxygen, nitrogen, and sulfur ligands. Electrochemical, infrared, and electron paramagnetic resonance studies. *Inorg. Chem.* **1981**, *20*, 1996-2000.

Chapter 3. Olefin Metathesis Initiated by Molecular Tungsten(IV)-oxo Complex

Reproduced with permission from: Chan, K. W.; Lam, E.; D'Anna, V.; Allouche, F.; Michel, C.; Safonova, O. V.; Sautet, P.; Copéret, C., C–H Activation and Proton Transfer Initiate Alkene Metathesis Activity of the Tungsten(IV)–Oxo Complex. *J. Am. Chem. Soc.* **2018**, *140*, 11395-11401. Copyright 2018 American Chemical Society.

3.1 Introduction

We have shown that low-temperature activation of well-defined silica-supported tungsten-oxo species with organosilicon reductants generates highly active species, which can catalyze olefin metathesis at 70 °C (as discussed in Chapter 2). We hypothesize that W(IV) species bearing an oxo ligand, which is formed upon reduction, is the highly active species and can be transformed into alkylidene species in the presence of alkenes.^{1,2} Previous works in homogeneous catalysis have shown that Mo(IV)(NAr)(X)(Y)(alkene) and dimeric {W(NAr')[OCMe₂(CF₃)₂]₂}₂ complexes (Scheme 3.1), which can be formed from the alkylidenes during metathesis, can also reinitiate metathesis, albeit with a very low efficiency.^{3,4} In fact, the numbers of active species generated under these conditions have been reported to be very small (< 3 %). Thus, understanding how alkylidenes can be regenerated in situ from M(IV) molecular species would be valuable as it could help to design methods for reactivation and ways to improve overall catalyst performance.⁵



Scheme 3.1. Transformation of M(IV) pre-catalysts to active M(VI) alkene metathesis catalysts.

In view of the reported metathesis activities of reduced group 6 metal centers in homogeneous systems and the high activities of the putative W(IV)–oxo sites in supported systems, we reason that molecular W(IV) complexes bearing oxo and alkoxide ligands would be an ideal system to probe the initiation step and a source of potentially efficient catalyst precursors.

There are only a few W(IV)–oxo complexes known: (i) $\text{WOCl}_2(\text{PX}_3)_3$ ($\text{PX}_3 = \text{P}(\text{OMe})_3, \text{PMe}_2\text{Ph}, \text{PMePh}_2$),^{6,7} which can react with strained cyclopropenes to form metathesis active vinylalkylidenes, and (ii) $\text{WO}(\text{OR})_2(\text{alkene})$ ($\text{OR} = 2,6\text{-dimesitylphenoxide}$ or $2,6\text{-diadamantyl-4-methylphenoxide}$), which can be formed upon decomposition of the corresponding alkylidenes, but which has not been reported to engage in olefin metathesis.⁸ In this chapter, we synthesize monomeric d^2 W(IV)–oxo complexes bearing electron-withdrawing alkoxide and stabilizing pyridine ligands; they show high activities in metathesis upon activation with $\text{B}(\text{C}_6\text{F}_5)_3$. We show by using a combined experimental and computational approach that the activation mechanism for initiating alkene metathesis and formation of alkylidene involves two key steps: i) the C–H bond activation of an allylic C–H group that must be present in the alkene reactant, and ii) a proton transfer process facilitated by pyridine and $\text{B}(\text{C}_6\text{F}_5)_3$.

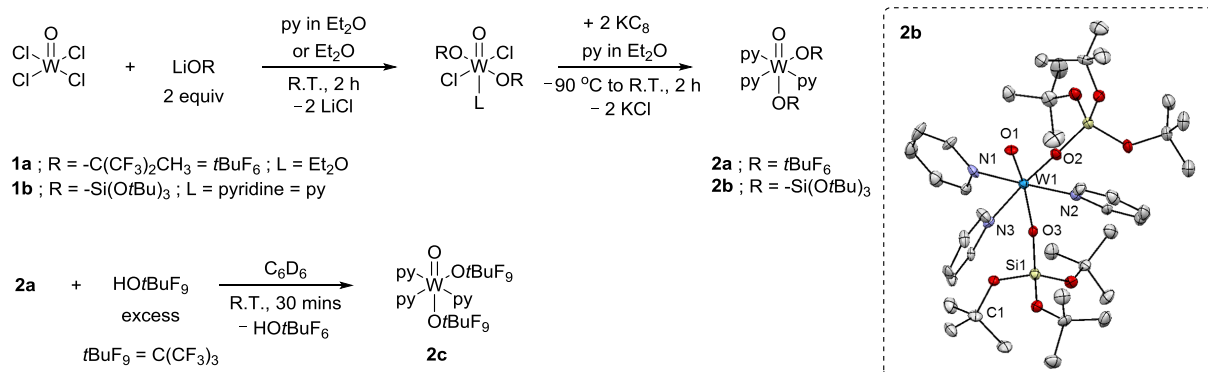
3.2 Result and Discussion

3.2.1 Synthesis of $\text{WO}(\text{OR})_2(\text{py})_3$

W(VI)–oxo complexes $\text{WOCl}_2(\text{OR})_2\text{L}$ (**1a**: $\text{R} = \text{CMe}(\text{CF}_3)_2 = t\text{BuF}_6$ and $\text{L} = \text{pyridine} = \text{py}$, **1b**: $\text{R} = \text{Si}(\text{O}t\text{Bu})_3$ and $\text{L} = \text{Et}_2\text{O}$) were synthesized by salt metathesis of WOCl_4 and 2 equiv of LiOR in diethyl ether (Scheme 3.2). The pure products were obtained as colorless crystals in ca. 70% yield upon recrystallization in pentane at $-40\text{ }^\circ\text{C}$. The alkoxide groups are *trans* to each other according to NMR spectroscopies and single crystal X-ray diffraction studies (see Appendix).

The subsequent reduction of these compounds with KC_8 at $-90\text{ }^\circ\text{C}$ in the presence of pyridine yields their W(IV) analogues $\text{WO}(\text{OR})_2\text{py}_3$ (**2a** and **2b**), which can be obtained as dark blue crystals after recrystallization in pentane at $-40\text{ }^\circ\text{C}$. Attempts of using the same synthetic route to synthesize $\text{WO}(\text{OC}(\text{CF}_3)_3)_2\text{py}_3$ (**2c**) resulted in a mixture of products. However, pure **2c** could be obtained as pure dark purple solid from protonolysis of **2b** with perfluoro-*tert*-butanol (Scheme 3.2), similar to the reaction of pyrrole complexes with various alcohols.⁹ We have so far not been able to prepare the corresponding *OtBu* or $\text{OC}(\text{CH}_3)_2(\text{CF}_3)$ complex by the approaches described above. The three six-coordinated octahedral $\text{WO}(\text{OR})_2\text{py}_3$ complexes described above are diamagnetic and share the same geometry with

one of the OR groups on the equatorial plane and the other one at the axial position *trans* to the oxo ligand (see Appendix, Figure A.3.2 – A.3.4). Attempts to use other weakly coordinating ligands instead of pyridine, such as THF or dimethoxyethane, did not yield any desirable product.



Scheme 3.2. Synthetic routes for complexes **1a-1b**, **2a-2c** and X-ray crystal structure of **2b**.

(Thermal ellipsoids plot at 50% probability; hydrogen atoms omitted.)

3.2.2 Catalytic Activity and Reactivity of WO(OR)₂(py)₃

Reaction of the complex **2a** with *cis*-4-nonene (300 equiv/[W]) shows no activity in metathesis at 70 °C, even after 24 h. This can be ascribed to the absence of an empty coordination site due to the relative strong binding of pyridine in these complexes.¹⁰ On the other hand, in the presence of a Lewis acid, such as ZnCl₂(dioxane) or B(C₆F₅)₃, metathesis activity is observed, presumably due to the removal of pyridine. While equilibrium conversion is not reached with ZnCl₂(dioxane) (3 equiv/[W]) after 24 h (Figure A.3.7), 3 equiv of B(C₆F₅)₃ leads to equilibrium conversion (51%) of *cis*-4-nonene (300 equiv/[W]) within 12 h at 70 °C. The catalytic activities of complexes **2a-2c** in the presence of B(C₆F₅)₃ are shown in Table 3.1.

Similar activities are observed for the hexafluoro-*tert*-butoxide (**2a**) and siloxide complexes (**2b**), but the perfluoro-*tert*-butoxide complex (**2c**) shows a significantly higher activity (time to equilibrium < 30 min). These activities are comparable to those reported for the corresponding pre-formed molecular W-oxo alkylidene complexes.¹¹⁻¹⁵ With the terminal alkene 1-nonene, the initial activity is similar to that of internal *cis*-4-nonene, but a significantly higher catalyst loading (1 mol% catalyst) is required to reach 83 % conversion. Increasing the amount of B(C₆F₅)₃ (4 equiv/[W]) further increases the catalytic activity of

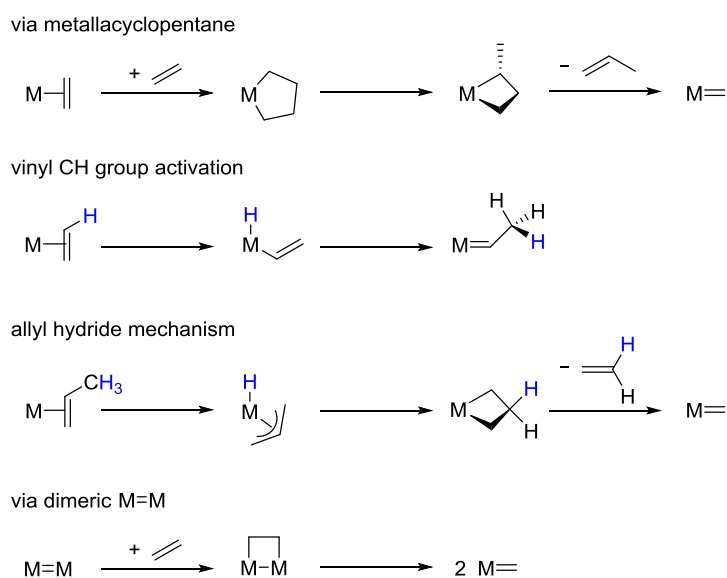
complex **2a** and reduces the time to reach equilibrium conversion from 12 h to 3 h, while this approach has little to no effect on **2c**.

Table 3.1. Catalytic activities of complexes **2a-2c**.^a

Catalyst precursor	Loading /mol %	$B(C_6F_5)_3$ /mol %	Substrate	TOF ^c /min ⁻¹	Equil. Time ^d
2a	0.3	1	4-nonene ^b	2	12 h
	0.3	1.3	4-nonene ^b	4	3 h
2b	0.3	1	4-nonene ^b	2	12 h
2c	0.3	1	4-nonene ^b	15	0.5 h
	0.3	1.3	4-nonene ^b	11	0.5 h
	1	3	1-nonene	7	83% ^{24 h}

^a1.0 M toluene solution, batch reactor, 70 °C; ^b*cis*-4-nonene; ^cTOF is expressed as initial TOF after 3 min of reaction; ^dTime to reach equilibrium conversion unless otherwise noted by giving the final conversion after 24 h.

Encouraged by the promising catalytic results, we further studied the activation mechanism involved in transforming these W(IV)–oxo species into W(VI)–oxo alkylidenes. Several activation mechanisms have been proposed for the formation of active M(VI) (M = Mo or W) alkylidenes from M(IV) pre-catalysts (Scheme 3.3).^{4, 16}

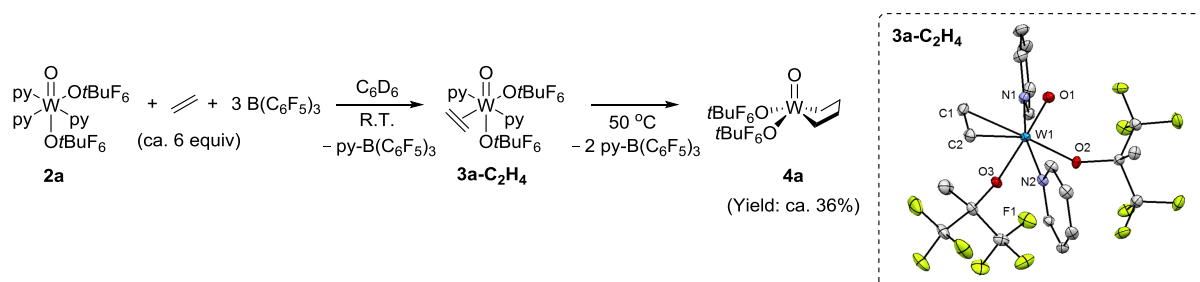


Scheme 3.3. Proposed oxidative initiation mechanisms.

The first possibility involves the formation of a metallacyclopentane, which can subsequently undergo ring contraction via β -H transfer followed by an insertion to yield a

metallacyclobutane that can participate in metathesis.¹⁷⁻¹⁸ Alternatively, the second and third pathways require a vinyl and an allylic C–H activation, respectively. The fourth pathway involves a dimeric species, which has been proposed to undergo [2+2] cycloaddition with reactive olefins (norbornene or diallylether).³ Since one of the mechanisms should be specific to alkene containing the allylic CH group, we first set to investigate the reactivity of complex **2a** towards alkenes with or without allylic CH groups.

Reaction of **2a** in C₆D₆ with ethylene leads to an immediate color change from dark blue to yellow at room temperature. By in-situ ¹H-NMR, free pyridine and new proton signals at δ 3.04 and 2.84 ppm are observed. In the ¹³C-NMR spectrum, a characteristic singlet peak is observed at δ 65.3 ppm ($J_{WC} = 22.9$ Hz) indicating the formation of ethylene π complex, **3a-C₂H₄** (Scheme 3.4).^{4, 19} **3a-C₂H₄** can be isolated by recrystallization in toluene at –40 °C and its structure is confirmed by single crystal X-ray diffraction studies. The C1=C2 bond distance of the coordinated ethylene molecule is 1.41 Å, indicating a significant back donation from the metal center to the π^* orbital of ethylene.²⁰ In the presence of 3 equiv of B(C₆F₅)₃, the reaction of **2a** and ¹³C-dilabeled ethylene yields the py-B(C₆F₅)₃ adduct, **3a-C₂H₄** along with a small amount of the metallacyclopentane **4a** (Scheme 3.4) at room temperature.

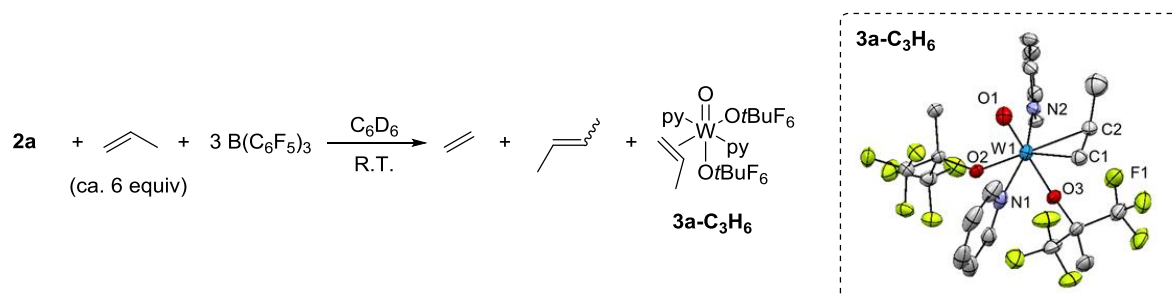


Scheme 3.4. Reaction of **2a** with ethylene in the presence of B(C₆F₅)₃ and X-ray crystal structure of **3a-C₂H₄**. (Thermal ellipsoids plot at 50% probability; hydrogen atoms omitted.)

Heating the reaction mixture to 50 °C leads to complete conversion of **3a-C₂H₄**, removal of most of the coordinated pyridine from W centers to give py-B(C₆F₅)₃ (ca. 3 equiv/[W]) and increases the amount of **4a**. The complex **4a** gives rise to two broad peaks at ca. δ 3.0 ppm and 2.8 ppm in the ¹H-NMR spectrum. These signals correlate with the carbon resonances at δ 74.8 (α -C) and 36.4 ppm (β -C), respectively, in the ¹³C-NMR spectrum according to ¹H-¹³C HSQC experiment (Figure A.3.10 – A.3.12). These resonances are similar to those reported for other metallacyclopentane complexes of Mo and W.^{4, 8, 19-22} No peak associated with the metallacyclobutane or alkylidene is observed in ¹H and ¹³C NMR, even upon further heating at 70 °C. While a small amount of 1-butene is observed, likely resulting from the

decomposition of **4a** after prolonged heating (Figure A.3.10), this process seems to be relatively slow. The rearrangement of metallacyclopentane to 1-butene has also been reported in several high valent metallacyclopentane complexes.^{4, 19, 21, 23} The complex **4a** slowly decomposes under high vacuum (10^{-5} mbar) or in the absence of ethylene making its isolation unsuccessful so far. The absence of metallacyclobutane may also suggest that **4a** does not undergo ring contraction readily (Scheme 3.3; first pathway).

Reaction of **2a** with propylene leads to the formation of the propylene π complex **3a-C₃H₆** at room temperature. Its structure is confirmed by X-ray diffraction (Scheme 3.5). The major isomer of **3a-C₃H₆** shows carbon resonances at δ 24.4 (–CH₃), 66.0 (=CH₂) and 72.4 (=CH–) ppm. In the presence of 3 equiv of B(C₆F₅)₃, the py-B(C₆F₅)₃ adduct and **3a-C₃H₆** are formed together with ethylene and 2-butene as shown by in-situ ¹H-NMR studies (Figure A.3.13). This result indicates that self-metathesis of propylene (ca. 6 equiv/[W]) occurs readily and reaches equilibrium in less than 15 min at room temperature.

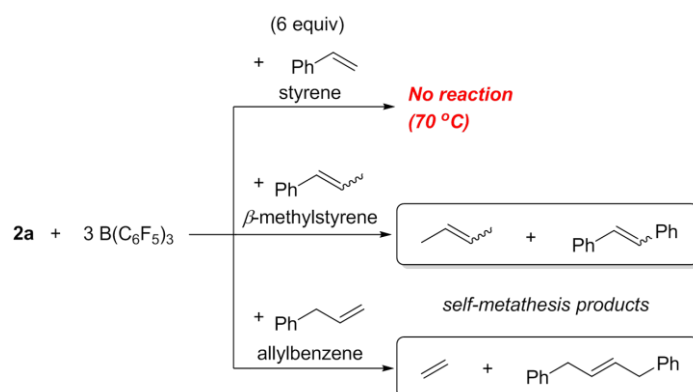


Scheme 3.5. Reaction of **2a** with propylene in the presence of B(C₆F₅)₃ and X-ray crystal structure of **3a-C₃H₆**. (Thermal ellipsoids plot at 50% probability; hydrogen atoms omitted.)

Notably, the reaction of **2a** with styrene in the presence of 3 equiv of B(C₆F₅)₃ does not lead to the formation of self-metathesis products, even upon heating at 70 °C for 13 h, as shown by in-situ ¹H-NMR and GC-MS. In contrast, reaction of **2a**, B(C₆F₅)₃ and β -methylstyrene results in the formation of 2-butene and stilbene under the same conditions. The complex **2a** also reacts with allylbenzene in the presence of B(C₆F₅)₃ to form ethylene and 1,4-diphenyl-2-butene PhCH₂(CH=CH)CH₂Ph, in less than 45 min at room temperature (Scheme 3.6).

All these results suggest that the presence of an allylic C–H group is probably crucial for the conversion of the W(IV)–oxo pre-catalyst into the active species. In order to gain more insights into the initiation mechanism, we decided to conduct a detailed investigation of the

reaction between **2a** and *trans*- β -methylstyrene, in particular by monitoring the organic products formed during the activation period.



Scheme 3.6. Reactions of **2a** with styrene, β -methylstyrene and allylbenzene in the presence of $B(C_6F_5)_3$

When monitoring the self-metathesis reaction of *trans*- β -methylstyrene (6 equiv/[W]) catalyzed by **2a** in the presence of $B(C_6F_5)_3$ (3 equiv/[W]), a small amount of styrene (0.05 equiv/[W]) is observed as a primary product according to GC-MS and no further formation is observed after ca. 30 min. In contrast, the formation of self-metathesis products is observed after a short induction period (Figure 3.1). These results support that styrene is an initiation product formed during the formation of the active alkylidene species.

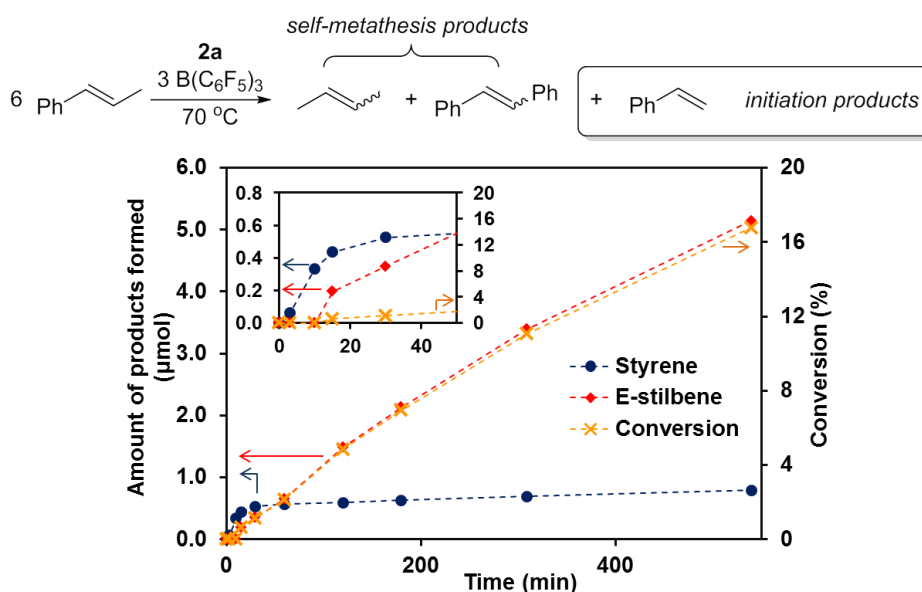


Figure 3.1. Formation of styrene (dark blue circle), *trans*-stilbene (red diamond) and conversion (orange cross) vs time plot at 70 °C.

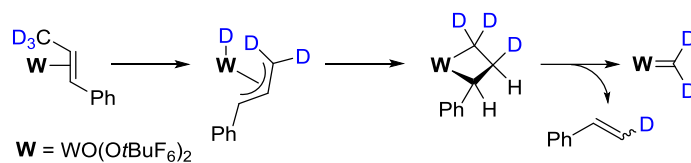
In addition, a small amount of propylene is observed in the gas phase by GC-FID implying the formation of a W-methylidene and its subsequent reaction with *trans*- β -methylstyrene or 2-butene. The observation of styrene as an initiation product points to the allyl hydride mechanism as the initiation step for alkylidene formation (Scheme 3.3). No other heavier organic product is observed suggesting that other initiation mechanisms are unlikely (Scheme A.3.1). The observation of only a substoichiometric amount of styrene (0.05 equiv/[W]) suggests that only small amounts of active species are formed upon activation.

3.2.3 Reactions of $\text{WO}(\text{OtBuF}_6)_2(\text{py})_3$ with *trans*- β -(methyl- d_3)styrene and Allylbenzene

In order to understand better how styrene is formed during the reaction and whether or not C–H activation is indeed an important elementary step in the initiation process, the reactivity of *trans*- β -(methyl- d_3)styrene with **2a** was also investigated. According to in-situ ^2H -NMR studies (Figure 3.2), β -deuteriostyrene is observed upon reaction of *trans*- β -(methyl- d_3)styrene and **2a** in the presence of 3 equiv of $\text{B}(\text{C}_6\text{F}_5)_3$. This observation further supports the proposed allyl hydride initiation mechanism (Eq. 3.1). The initial rates of formation of initiation products with *trans*- β -(methyl- d_3)styrene and *trans*- β -methylstyrene show a $k_{\text{H}}/k_{\text{D}}$ of 3.6 (Figure 3.2; see Appendix for details), a primary kinetic isotopic effect (KIE), which suggests the involvement of the allylic hydrogen atom in the rate-determining step.²⁴ Notably, the amount of styrene formed (0.01 equiv/[W]) upon using *trans*- β -(methyl- d_3)styrene is much lower than upon using *trans*- β -methylstyrene. The smaller amount of detected deuterated initiation product could be due to the slower rate of initiation for the deuterated alkene while decomposition could occur at similar rates for both deuterated and non-deuterated alkene during initiation. Such decomposition is likely one of the reasons for having intrinsically small amounts of active species. Even though the number of active species formed by using *trans*- β -(methyl- d_3)styrene is lower, the conversion of self-metathesis is slightly higher than that of *trans*- β -methylstyrene (Figure A.3.19). This may be due to the advantageous isotope effect that can reduce deactivation via β -H elimination of the metathesis active metallacyclobutane intermediates.^{19, 25-27}

Similarly, the reaction of **2a** with allylbenzene (6 equiv/[W]) in the presence of $\text{B}(\text{C}_6\text{F}_5)_3$ (3 equiv/[W]) also yields styrene which further supports the same allyl hydride intermediate. Meanwhile, isomerization of allylbenzene into the thermodynamically more stable *trans*- β -methylstyrene is also observed during this reaction. The observed double bond isomerization is known to possibly involve a π -allyl metal hydride intermediate.²⁸ Monitoring the reaction by in-situ ^1H -NMR indicates that the isomerization process occurs prior to

metathesis (Figure A.3.22). This result suggests that the formation of a metallacyclobutane from an allyl hydride is slower than the isomerization process.



Eq. 3.1. Proposed allyl hydride initiation mechanism

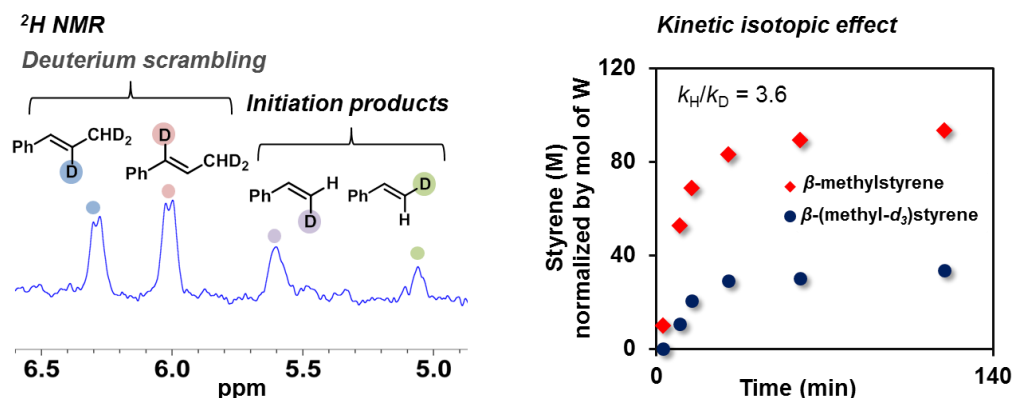


Figure 3.2. Left: ^2H -NMR spectrum at $=\text{CH}$ region (for full spectrum, see Figure A.3.17).

Right: Concentration of styrene (normalized by the no. of mole of $[\text{W}]$) vs time plot with *trans*- β -methylstyrene (red diamond) and *trans*- β -(methyl- d_3)styrene (dark blue circle) as substrates.

3.2.4 DFT Computational Studies of the Initiation Mechanisms

To further probe the allylic C–H activation mechanism, DFT calculations were performed using **2a** and *trans*- β -methylstyrene in light of the kinetic findings mentioned above. The calculations show that formation of the pyridine free π complex (**IM-1**) is thermodynamically favorable in the presence of $\text{B}(\text{C}_6\text{F}_5)_3$ (Figure A.3.23). The free energy barrier required for activating the allylic C–H bond (**TS-1**) to form $\text{W}(\text{VI})$ η^1 -allyl hydride intermediate (**IM-2**) from the π complex (**IM-1**) is 22.7 kcal/mol (Figure 3.3). **IM-2** further converts into its isomer **IM-3** ($\Delta G = -8.4$ kcal/mol). However, transferring the hydrogen atom to the β -carbon on the allyl group to form a metallacyclobutane requires a very high free energy barrier (**TS-3A**: $\Delta G^\ddagger = 36.0$ kcal/mol with an overall barrier of $\Delta G^\ddagger = 47.1$ kcal/mol), making this direct process unlikely. Since H-transfer is the most energy demanding step, we also consider additional factors that might play a role in facilitating this process. However, coordination of $\text{B}(\text{C}_6\text{F}_5)_3$ to the oxo ligand or $\text{B}(\text{C}_6\text{F}_5)_3$ assisted H-transfer are both high in energies (Figure A.3.24). In particular, the free energy required for abstracting the H by $\text{B}(\text{C}_6\text{F}_5)_3$ is $\Delta G^\ddagger = 30.2$ kcal/mol with an overall barrier of $\Delta G^\ddagger = 41.3$ kcal/mol (**TS-3D**;

Figure A.3.24), suggesting that the H atom may not have a strong hydridic character and the subsequent formation of cationic W center is unfavorable.

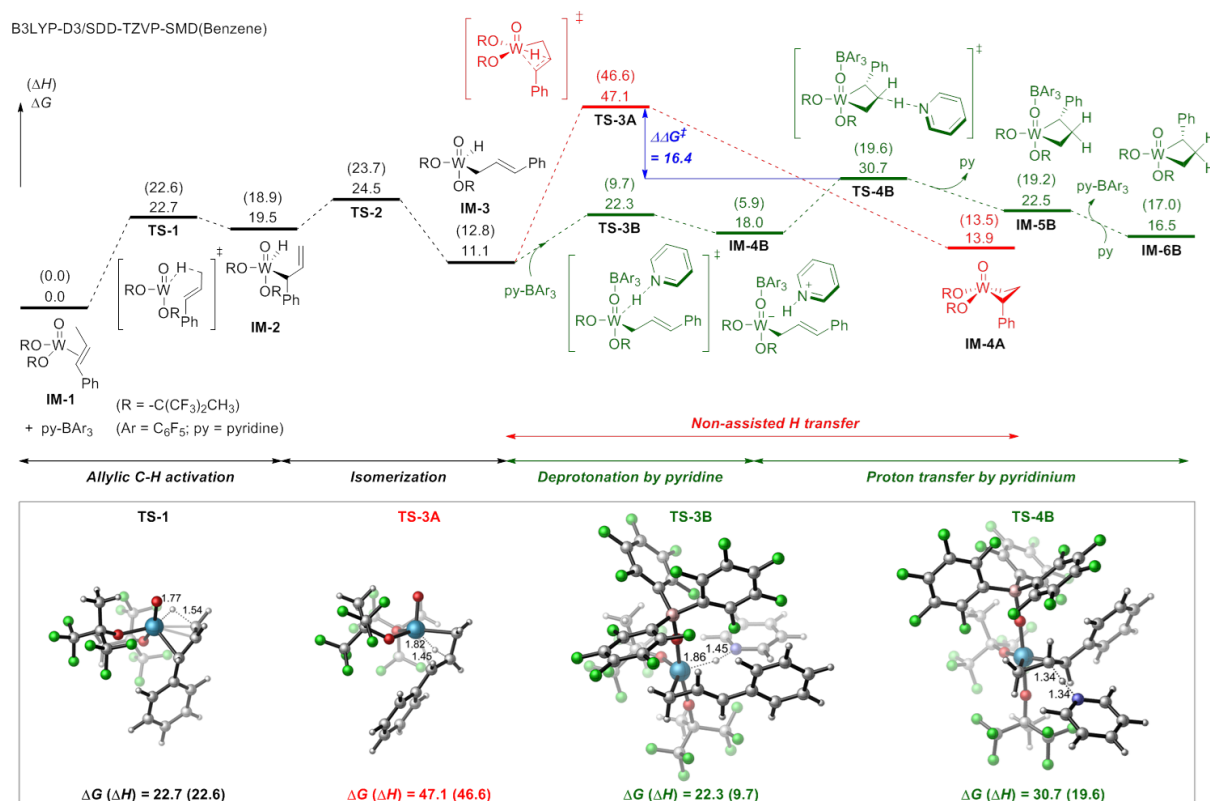
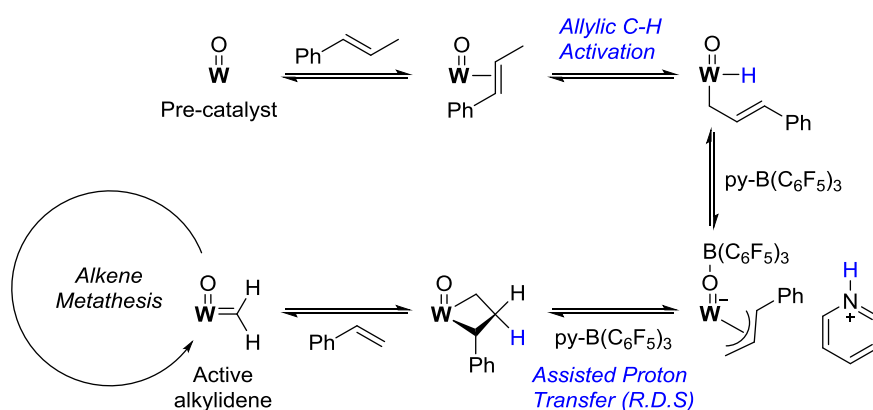


Figure 3.3. Computed Gibbs free energies and enthalpies in parentheses at 298.15 K (in kcal mol⁻¹) for initiation pathways via allyl hydride intermediates (Red: non-assisted; Green: assisted) involved in the reaction between **2a** and *trans*- β -methylstyrene (B3LYP-D3/SDD-TZVP-SMD(Benzene)).

Alternatively, pyridine can abstract the H from W to form an anionic π -allyl intermediate along with a pyridinium (PyH⁺), which can then transfer the proton to the β -carbon of the allyl group and thus generate a metallacyclobutane. While the energy required for abstracting H by pyridine to form a pyridinium (PyH⁺) intermediate is shown to be quite high ($\Delta G^\ddagger = 26.4$ kcal/mol) (TS-3E; Figure A.3.25), the energy barrier is significantly lowered (TS-3B: $\Delta G^\ddagger = 11.2$ kcal/mol) upon coordination of B(C₆F₅)₃ onto the oxo ligand (Figure 3.3). This is likely facilitated by the decrease in electron density at the W center, and hence increasing the acidity of the “hydride” ligand. Furthermore, coordination of B(C₆F₅)₃ can also stabilize the anionic W center formed after H abstraction (IM-4B lies 18.0 kcal/mol above the reference state IM-1). While protonation of the β -carbon by PyH⁺ (TS-4B) is the highest in energy for this pathway (overall energy barrier of $\Delta G^\ddagger = 30.7$ kcal/mol), it lies significantly lower ($\Delta\Delta G^\ddagger = -16.4$ kcal/mol) than TS-3A that corresponds to the non-assisted

formation of metallacyclobutane. Note that the entropy and resulting free energy of activation for **TS-4B** is likely overestimated since it involves the dissociation and reaction of py-B(C₆F₅)₃ in solution (for detailed discussion see Appendix),²⁹ making this proton transfer step accessible. In fact, this step is similar to the recently reported reverse elementary step involved in the decomposition pathway of ruthenium metallacyclobutane induced by base.³⁰ Such proton transfer reactions (protonation or deprotonation) on the β -carbon are consistent with its formally positively charged nature as recently evidenced by detailed solid-state NMR analysis of trigonal bipyramidal metallacyclobutane intermediates.¹⁰ In addition, the calculated KIE on this rate-determining proton transfer step (**TS-4B**) ($(k_H/k_D)_{\text{DFT}} = 3.7$) matches well with the experimentally observed KIE ($(k_H/k_D) = 3.6$). The thus-formed metallacyclobutane (**IM-6B**) can then undergo cycloreversion to give alkylidenes. The overall initiation process is endergonic by 10.8 and 13.6 kcal/mol with respect to the π complex **IM-1** (Figure A.3.28) which explains the observation of only a small amount of initiation product and the difficulty to detect the propagating – alkylidenes and metallacyclobutanes – species by NMR. The small amounts of alkylidenes formed will participate in the catalytic conversion of β -methylstyrene into stilbene and 2-butene.

All the data above point to an initiation mechanism involving an allylic C–H activation by the W(IV) pre-catalyst. The thus-formed allyl hydride intermediate generates the required metallacyclobutane for metathesis by a proton transfer which is assisted by both pyridine and B(C₆F₅)₃. From this metallacyclobutane, cycloreversion yields a putative W(VI) alkylidene, which is active in metathesis, along with the olefinic initiation product. Both the observed primary KIE and the calculated highest energy transition state indicate that proton transfer is the rate-determining step in the activation process yielding metallacyclobutanes and alkylidenes (Scheme 3.7).



Scheme 3.7. Proposed initiation mechanism (**W** = W containing organometallic fragment).

3.3 Conclusion

We have synthesized well-defined monomeric d^2 W(IV)–oxo bisalkoxide complexes that can initiate alkene metathesis and show comparable catalytic activities to W(VI)–oxo alkylidene complexes. Detailed studies of the initiation step including deuterium-labeling have shown that allylic C–H activation is involved during the activation of these W(IV) pre-catalysts. DFT computational studies reveal that both pyridine and $B(C_6F_5)_3$ are important for the formation of the metallacyclobutane, the initiation product and the metathesis activity. Our studies suggest that formation of the metallacyclobutane is the rate-determining initiation step, which involves a pyridine-assisted proton transfer to the β -carbon position of the allyl ligand and is consistent with the observed KIE. Based on the quantities of initiation products detected, the amounts of active intermediates (metallacyclobutane or alkylidene) formed are small, making direct spectroscopic observation of such intermediates a challenge. The small amounts of active intermediates are likely due to: i) the thermodynamically unfavorable initiation process and ii) competing decomposition of reactive intermediates during the initiation process. Nevertheless, the present work demonstrates the importance of assisted proton transfer pathways in generating alkylidene species and shows how a Lewis acid and Lewis base cooperate to generate the active species.³¹ One may thus wonder if a similar pathway could also take place in the classical heterogeneous catalysts, where basic surface O atoms in combination with Lewis acids and strained surface sites could play a similar role.

3.4 Experimental Details

3.4.1 General procedures

Unless otherwise noted, all experiments were carried out under dry and oxygen free argon atmosphere using either standard Schlenk or glove-box techniques. *n*-Pentane and toluene were purified using double MBRAUN SPS alumina column, and were degassed by 3 freeze-pump-thaw cycles before use. Pyridine was distilled from CaH₂. Diethyl ether, C₆H₆ and C₆D₆ were distilled from Na/benzophenone. LiOtBuF₆ (OtBuF₆ = OC(CH₃)(CF₃)₂) and LiOSi(OtBu)₃³² were prepared by treating the corresponding alcohols with *n*-BuLi in diethyl ether. LiOtBuF₆ was sublimed in *vacuo* before use. KC₈³³, *trans*- β -(methyl-*d*₃)styrene and *trans*- β -methylstyrene³⁴ were synthesized according to literature procedures. Tungsten(VI) oxychloride was purchased from Aldrich and sublimed prior to use. Perfluoro-*tert*-butyl alcohol was purchased from Apollo Scientific Ltd. Tris(pentafluorophenyl)borane was purchased from TCI and sublimed before use. Styrene and Allylbenzene was purchased from ABCR and distilled from CaH₂. All the alkene were treated with Selexsorb for 5 hours and passed through a pad of activated neutral Al₂O₃ before use. Solution NMR was recorded on Bruker 200, 300, 400 and 500 MHz at 298K.

3.4.2 Syntheses of 1a-1b, 2a-2c, 3a-C₂H₄, 3a-C₃H₆

trans-WOCl₂(OtBuF₆)₂(Et₂O) **1a**

A solution of LiOtBuF₆ (366 mg, 1.94 mmol, 2 equiv) in diethyl ether (5 mL) was added to a stirred suspension of WOCl₄ (333 mg, 0.973 mmol, 1 equiv) in diethyl ether (5 mL) at room temperature. The reaction mixture was stirred at room temperature for 2 h. The color changed from orange to light yellow and white precipitate was formed. The volatiles were removed in *vacuo*, the product was extracted with pentane (5 mL \times 3), and the combined extract was filtered to give a clear light yellow solution. Crystallization at -40 °C resulted in the formation of white crystals. Followed by the removal of supernatant, the crystals were dried in *vacuo*. Yield 463 mg (67.3 %). ¹H NMR (C₆D₆, 200 MHz): δ 3.86 (q, 4H, OCH₂CH₃, *J* = 7.0 Hz), 1.78 (s, 6H, OCCH₃(CF₃)₂), 0.86 (t, 6H, OCH₂CH₃, *J* = 7.0 Hz). ¹⁹F NMR (C₆D₆, 188 MHz): δ -75.4 (s, 12F, OCCH₃(CF₃)₂). ¹³C{¹H} NMR (C₆D₆, 50 MHz): δ 123.2 (q, *J*_{CF} = 287 Hz, CF₃), 86.9 (m, OCCH₃(CF₃)₂), 64.9 (OCH₂CH₃), 14.5 (OCCH₃(CF₃)₂), 12.1 (OCH₂CH₃). Anal. Found (Calcd, C₁₂H₁₆Cl₂F₁₂O₄W): C 20.45 % (20.39 %), H 2.24 % (2.28 %).

trans-WOCl₂(OSi(OtBu)₃)₂(py) **1b**

A solution of LiOSi(OtBu)₃ (223 mg, 0.82 mmol, 2 equiv) in diethyl ether (5 mL) was added to a stirred suspension of WOCl₄ (141 mg, 0.41 mmol, 1 equiv) in diethyl ether (5 mL)

and pyridine (36 mg, 0.46 mmol, 1.1 equiv) at room temperature. The reaction mixture was stirred at room temperature for 2 h. The color changed from orange to colorless and white precipitate was formed. The volatiles were removed in *vacuo*, the product was extracted with toluene (5 mL × 3), and the combined extract was filtered to give a clear solution. Crystallization at -40 °C resulted in the formation of white crystals. Followed by the removal of supernatant, the crystals were dried in *vacuo*. Yield 122 mg (33.9 %). ¹H NMR (C₆D₆, 200 MHz): δ 9.44 (br s, 2H, *o*-CH in NC₅H₅), 6.95 (m, 1H, *p*-CH in NC₅H₅), 6.81 (m, 2H, *m*-CH in NC₅H₅), 1.44 (s, 54H, OC(CH₃)₃). ¹³C{¹H} NMR (C₆D₆, 125 MHz): δ 151.8 (*o*-CH in NC₅H₅), 137.8 (*p*-CH in NC₅H₅), 123.4 (*m*-CH in NC₅H₅), 73.9 (OC(CH₃)₃), 31.7 (OC(CH₃)₃). Anal. Found (Calcd, C₂₉H₅₉Cl₂NO₉Si₂W): C 39.92 % (39.73 %), H 6.77 % (6.78 %), N 1.62 % (1.60 %).

mer-WO(O*t*BuF₆)₂py₃ **2a**

A solution of **1a** (295 mg, 0.42 mmol, 1 equiv) in diethyl ether (7 mL) was slowly added to a stirred suspension of KC₈ (130 mg, 0.96 mmol, 2.3 equiv) in diethyl ether (3 mL) and pyridine (100 mg, 1.26 mmol, 3 equiv) at -100 °C. The reaction mixture was stirred and slowly warmed up to room temperature over 2 h. The reaction mixture became dark blue and the volatiles were removed in *vacuo*. The residue was extracted with toluene (5 mL × 5), and the combined extract was filtered to give a dark blue solution. The volatiles were removed in *vacuo* to give dark blue solid (X-ray quality crystals can be obtained by recrystallizing in toluene at -40 °C). Yield 243 mg (72.4 %). ¹H NMR (C₆D₆, 300 MHz): δ 8.52 (m, 4 H, *o*-CH in NC₅H₅), 8.32 (m, 2 H, *o*-CH in NC₅H₅), 6.58 (m, 6H, *m*-CH in NC₅H₅), 5.99 (m, 2H, *p*-CH in NC₅H₅), 5.52 (m, 1H, *p*-CH in NC₅H₅), 1.56 (s, 3H, OCCH₃(CF₃)₂), 1.43 (s, 3H, OCCH₃(CF₃)₂). ¹⁹F NMR (C₆D₆, 282 MHz): δ -76.1 (s, 6F, OCCH₃(CF₃)₂), -76.5 (s, 6F, OCCH₃(CF₃)₂). ¹³C{¹H} NMR (C₆D₆, 100 MHz): δ 148.5 (*o*-CH in NC₅H₅), 146.8 (*o*-CH in NC₅H₅), 137.9 (*p*-CH in NC₅H₅), 137.3 (*p*-CH in NC₅H₅), 126.4 (q, *J*_{CF} = 290 Hz, CF₃, partially overlap with solvent peak), 125.2 (q, *J*_{CF} = 292 Hz, CF₃, partially overlap with pyridine peak), 122.4 (*m*-CH in NC₅H₅), 121.2 (*m*-CH in NC₅H₅), 84.4 (m, OCCH₃(CF₃)₂), 80.7 (m, OCCH₃(CF₃)₂), 18.1 (OCCH₃(CF₃)₂), 17.1 (OCCH₃(CF₃)₂). Anal. Found (Calcd, C₂₃H₂₁F₁₂N₃O₃W): C 34.54 % (34.56 %), H 2.72 % (2.65 %), N 5.27 % (5.26 %).

mer-WO(OSi(O*t*Bu)₃)₂py₃ **2b**

The compound **2b** was prepared as described for **2a**. A solution of **1b** (95 mg, 0.11 mmol, 1 equiv) in diethyl ether was slowly added to a stirred suspension of KC₈ (34 mg, 0.25 mmol, 2.3 equiv) in diethyl ether (3 mL) and pyridine (26 mg, 0.33 mmol, 3 equiv) at -100 °C. A dark blue solid was obtained. Yield 55 mg (52.3%). ¹H NMR (C₆D₆, 300 MHz): δ 8.74

(d, 2H, *o*-CH in NC₅H₅, *J* = 5.7 Hz), 8.54 (br s, 4H, *o*-CH in NC₅H₅), 6.81 (m, 4H, *m*-CH in NC₅H₅), 6.72 (m, 2H, *m*-CH in NC₅H₅), 5.91 (br s, 3H, overlapping of *p*-CH in NC₅H₅), 1.48 (s, 27H, OSi(OC(CH₃)₃)₃), 1.39 (s, 27H, OSi(OC(CH₃)₃)₃). ¹³C{¹H} NMR (C₆D₆, 100 MHz): δ 149.9 (*o*-CH in NC₅H₅), 148.2 (*o*-CH in NC₅H₅), 136.3 (*p*-CH in NC₅H₅), 135.6 (*p*-CH in NC₅H₅), 121.0 (*p*-CH in NC₅H₅), 120.8 (*p*-CH in NC₅H₅), 72.1 (OSi(OC(CH₃)₃)₃), 71.1 (OSi(OC(CH₃)₃)₃), 32.2 (OSi(OC(CH₃)₃)₃), 32.1 (OSi(OC(CH₃)₃)₃). Anal. Found (Calcd, C₃₉H₆₉N₃O₉Si₂W): C 48.31 % (48.59 %), H 7.17 % (7.21 %), N 4.38 % (4.36 %).

mer-WO(O*t*BuF₉)₂py₃ **2c**

To a solution of **2a** (66 mg, 83 μmol, 1 equiv) in benzene (1 mL), perfluoro-*tert*-butanol (0.23 mL, 1.65 mmol, 20 equiv) was added at room temperature. The reaction mixture changed from dark blue to dark purple immediately and was stirred at room temperature for 1 h. The volatiles were removed under high vacuum (10⁻⁵ mbar), and the residue was washed with cold pentane (1 mL × 3). Dark purple crystals were obtained by recrystallizing in toluene at -40 °C. Yield 10 mg (13.3 %). ¹H NMR (C₆D₆, 500 MHz): δ 8.47 (d, 4H, *o*-CH in NC₅H₅, *J* = 5.4 Hz), 8.02 (d, 2H, *o*-CH in NC₅H₅, *J* = 5.6 Hz), 6.65 (t, 4H, *m*-CH in NC₅H₅, *J* = 6.7 Hz), 6.52 (t, 2H, *m*-CH in NC₅H₅, *J* = 6.8 Hz), 6.15 (t, 2H, *p*-CH in NC₅H₅, *J* = 7.5 Hz), 5.59 (t, 1H, *p*-CH in NC₅H₅, *J* = 7.4 Hz). ¹⁹F NMR (C₆D₆, 282 MHz): δ -71.8 (s, 9F, OC(CF₃)₃), -72.4 (s, 9F, OC(CF₃)₃). ¹³C{¹H} NMR (C₆D₆, 125 MHz): δ 149.8 (*o*-CH in NC₅H₅), 149.6 (*o*-CH in NC₅H₅), 138.8 (*p*-CH in NC₅H₅), 138.6 (*p*-CH in NC₅H₅), 123.8 (q, *J*_{CF} = 294 Hz, CF₃, partially overlap with solvent peak), 122.4 (q, *J*_{CF} = 293 Hz, CF₃, partially overlap with solvent peak), 84.8 (m, OC(CF₃)₃, tertiary carbons from the two *Ot*BuF₉ groups are overlapping). Anal. Found (Calcd, C₂₃H₁₅F₁₈N₃O₃W): C 30.36 % (30.45 %), H 1.55 % (1.67 %), N 4.42 % (4.63 %).

WO(O*t*BuF₆)₂py₂(C₂H₄) **3a-C₂H₄**.

To a solution of **2a** (42 mg, 52 μmol, 1 equiv) in benzene (1 mL), ethylene (15 equiv) was added at room temperature. The reaction mixture immediately changed from dark blue to yellow. After stirring at room temperature for 1 h, the volatiles were removed under high vacuum (10⁻⁵ mbar) to afford a yellow solid. Recrystallization at -40 °C in toluene resulted in yellow crystals. Followed by the removal of supernatant, the crystals were dried in *vacuo*. Yield 27 mg (68.9 %). ¹H NMR (C₆D₆, 300 MHz): δ 9.06 (4H, d, *o*-CH in NC₅H₅, *J* = 5.3 Hz), 6.85 (2H, t, *p*-CH in NC₅H₅, *J* = 7.6 Hz), 6.62 (4H, t, *m*-CH in NC₅H₅, *J* = 7.1 Hz), 3.04 (2H, m, -CH=CH- overlapping), 2.85 (2H, m, -CH=CH- overlapping), 1.14 (s, 3H, OCCH₃(CF₃)₂), 1.09 (s, 3H, OCCH₃(CF₃)₂). ¹⁹F NMR (C₆D₆, 282 MHz): δ -76.6 (s, 6F, OCCH₃(CF₃)₂), -77.8 (s, 6F, OCCH₃(CF₃)₂). ¹³C{¹H} NMR (C₆D₆, 75 MHz): δ 151.8 (*o*-CH

in NC₅H₅), 138.4 (*p*-CH in NC₅H₅), 4 carbons from CF₃ are partially overlapping with the solvent peaks, 124.2 (*m*-CH in NC₅H₅), 80.8 (m, OCCH₃(CF₃)₂), 79.8 (m, OCCH₃(CF₃)₂), 65.3 (CH₂=CH₂, $J_{WC} = 22.9$ Hz), 17.8 (OCCH₃(CF₃)₂), 16.4 (OCCH₃(CF₃)₂). Anal. Found (Calcd, C₂₀H₂₀F₁₂N₂O₃W): C 32.15 % (32.11 %), H 2.74 % (2.69 %), N 3.87 % (3.74 %).

WO(*Ot*BuF₆)₂py₂(C₃H₆) **3a-C₃H₆**

To a solution of **2a** (38 mg, 48 μmol, 1 equiv) in benzene (1 mL), propylene (33 equiv) was added at room temperature. The reaction mixture changed from dark blue to yellow-brown immediately. After stirring for 1 h at room temperature, the volatiles were removed under high vacuum (10⁻⁵ mbar) to afford greenish yellow solid (X-ray quality crystals can be obtained by recrystallizing in toluene at -40 °C). Yield 20 mg (55.6 %). Major isomer; ¹H NMR (C₆D₆, 300 MHz): δ 9.06 (m, 2H, *o*-CH in NC₅H₅), 8.95 (m, 2H, *o*-CH in NC₅H₅), 6.87 (m, 2H, *p*-CH in NC₅H₅), 6.64 (m, 4H, *m*-CH in NC₅H₅), 3.14 (m, 2H, overlapping of =CH- and =CH₂), 2.73 (d, 3H, =CH-CH₃, $J = 5.5$ Hz), 2.55 (m, 1H, =CH₂), 1.15 (s, 3H, OCCH₃(CF₃)₂), 1.11 (s, 3H, OCCH₃(CF₃)₂). ¹⁹F NMR (C₆D₆, 282 MHz): δ -76.3 (q, 3F, OCCH₃(CF₃)₂, $J_{FF} = 9.3$ Hz), -76.5 (q, 3F, OCCH₃(CF₃)₂, $J_{FF} = 9.3$ Hz), -77.7 (q, 3F, OCCH₃(CF₃)₂, $J_{FF} = 10.3$ Hz), -78.3 (q, 3F, OCCH₃(CF₃)₂, $J_{FF} = 10.3$ Hz). ¹³C{¹H} NMR (C₆D₆, 75 MHz): δ 152.1 (*o*-CH in NC₅H₅), 151.2 (*o*-CH in NC₅H₅), 138.4 (*p*-CH in NC₅H₅), 138.4 (*p*-CH in NC₅H₅), 4 carbons from CF₃ are partially overlapping with the solvent peaks, 124.1 (*m*-CH in NC₅H₅), 124.1 (*m*-CH in NC₅H₅), 80.3 (m, overlapping of the 2 tertiary carbons from OCCH₃(CF₃)₂), 72.4 (=CH-CH₃), 66.0 (=CH₂), 24.4 (=CH-CH₃), 17.9 (OCCH₃(CF₃)₂), 16.6 (OCCH₃(CF₃)₂). Decomposition was observed in the solid state at -40 °C likely due to the loss of propylene, thus no elemental analysis could be performed.

3.4.3 Catalytic tests

Catalytic tests were performed inside a glove box. The calculated amount of olefin was added to the catalyst that was introduced and weighed in a conical base vial containing a wingshaped magnetic stirring bar. Then, the calculated amount of B(C₆F₅)₃ (or ZnCl₂(dioxane)) was added to the mixture of alkene and catalyst. At $t = 0$, the reaction mixture was started to stir at 600 rpm and kept at 70 °C using an aluminum heating block. 10 μL aliquots of the solution were sampled, diluted with pure toluene (100 μL), and quenched by the addition of 1 μL of wet ethyl acetate after exposing to air. The resulting solution was analyzed by GC/FID (Agilent Technologies 7890 A) equipped with an HP-5 (Agilent Technologies) column. Conversion was determined from metathesis product formation (without taking *cis/trans* isomerization of nonene into account). In that case, equilibrium

conversion for *cis*-4-nonene is ca. 51% and 1-nonene is ca. 100%, assuming the ethylene generated could escape from the liquid phase efficiently at 70 °C.

3.4.4. Reaction with olefins

Reactions with ethylene and propylene

Representative procedures for reactions of 2a and ethylene or propylene in the presence of B(C₆F₅)₃. **2a** (9-12 mg, 1 equiv) and B(C₆F₅)₃ (3 equiv) were loaded in a J-Young NMR tube and sealed. The NMR tube was attached onto high vacuum line, evacuated and contacted with olefin (ca. 6 equiv). The olefin was condensed with liquid nitrogen into the NMR tube and frozen (by liquid nitrogen). Then, C₆D₆ (ca. 0.5 mL) was vacuum transferred and condensed into the NMR tube. The frozen mixture was slowly warmed up.

Reactions with liquid alkenes: styrene, trans-β-methylstyrene and allylbenzene

Representative procedures for reactions of 2a and olefin (liquid substrate) in the presence of B(C₆F₅)₃ (monitored by NMR). **2a** (9-12 mg, 1 equiv) and B(C₆F₅)₃ (3 equiv) were loaded in a J-Young NMR tube. To the J-Young tube, a solution of olefin (6-7 equiv) in C₆D₆ (0.5 mL) was added. The reaction was monitored by ¹H NMR and the reaction mixture was analyzed by GC-MS at the end of the reaction.

3.4.5. Kinetic studies on the reaction of 2a and *trans*-β-methylstyrene in the presence of B(C₆F₅)₃

Similar procedures as catalytic test described above (**S13**) were used for these reaction. The complex **2a** (10.1 mg, 12.6 μmol, 1 equiv) was loaded in conical base vial containing a wingshaped magnetic stirring bar. A mixture of *trans*-β-methylstyrene (9.8 μL, 75.8 μmol, 6 equiv) and B(C₆F₅)₃ (19.4 mg, 37.8 μmol, 3 equiv) in toluene (421 μL) with decalin (as internal standard) was added to **2a** and the reaction was monitored via GC/FID (Agilent Technologies 7890 A) equipped with an HP-5ms (Agilent Technologies) column.

Determination of kinetic isotope effect.

The kinetic studies of reaction of **2a** and *trans*-β-methylstyrene in the presence of B(C₆F₅)₃ were carried out as described above. Two separate parallel experiments using *trans*-β-(methyl-*d*₃)styrene or *trans*-β-methylstyrene were performed under the same reaction conditions and these experiments were repeated three times. The initial rates were determined by plotting the concentration of styrene (normalized by the number of mole of **2a**) vs time for the first 20 minutes. k_H/k_D = slope of the plot for *trans*-β-methylstyrene/ slope of the plot for *trans*-β-(methyl-*d*₃)styrene. See Figure A.3.18 for more details.

3.4.6. Computational details

All DFT calculations were performed with the Gaussian 09 (d1) software package.³⁵ Ground state and transition state geometries were optimized using the B3LYP³⁶⁻³⁷ functional augmented with the D3 version of Grimme's empirical dispersion correction.³⁸ Solvent effects of benzene were taken into account using SMD solvation model.³⁹ The SDD⁴⁰ basis set was used for tungsten and the TZVP⁴¹⁻⁴² basis set for the other atoms. The frequency calculations were performed at the same level of theory. The Gibbs free energy and enthalpy were calculated at 298.15 K using the harmonic approximation for vibrational contributions. A standard-state correction ($RT \cdot \ln(24.46) = 1.89$ kcal/mol) was added to the calculated Gibbs free energy of each molecule to account for the change from 1 atm to 1 M.

3.5 References

1. Mougél, V.; Chan, K.-W.; Siddiqi, G.; Kawakita, K.; Nagae, H.; Tsurugi, H.; Mashima, K.; Safonova, O.; Copéret, C., Low Temperature Activation of Supported Metathesis Catalysts by Organosilicon Reducing Agents. *ACS Cent. Sci.* **2016**, *2*, 569-576.
2. Yamamoto, K.; Chan, K. W.; Mougél, V.; Nagae, H.; Tsurugi, H.; Safonova, O. V.; Mashima, K.; Coperet, C., Silica-supported isolated molybdenum di-oxo species: formation and activation with organosilicon agent for olefin metathesis. *Chem. Commun.* **2018**, *54*, 3989-3992.
3. Schrock, R. R.; Lopez, L. P. H.; Hafer, J.; Singh, R.; Sinha, A.; Müller, P., Olefin Metathesis Reactions Initiated by d² Molybdenum or Tungsten Complexes. *Organometallics* **2005**, *24*, 5211-5213.
4. Marinescu, S. C.; King, A. J.; Schrock, R. R.; Singh, R.; Müller, P.; Takase, M. K., Simple Molybdenum(IV) Olefin Complexes of the Type Mo(NR)(X)(Y)(olefin). *Organometallics* **2010**, *29*, 6816-6828.
5. Schrock, R. R., Recent Advances in High Oxidation State Mo and W Imido Alkylidene Chemistry. *Chem. Rev.* **2009**, *109*, 3211-3226.
6. Javier de la Mata, F. J.; Grubbs, R. H., Synthesis and Reactions of Tungsten Oxo Vinylalkylidene Complexes: Reactions of WCl₂(O)(PX₃) (X = OMe, R) Precursors with 3,3-Diphenylcyclopropene. *Organometallics* **1996**, *15*, 577-584.
7. Javier de la Mata, F., Synthesis and characterization of tungsten oxo alkylidene complexes via the reaction of WCl₂(O)[PX₃]₃ (PX₃ = P(OMe)₃, PMe₂Ph, PMePh₂) with 4,8-dioxaspiro[2,5]oct-1-ene (ketalcyclopropene). *J. Organomet. Chem.* **1996**, *525*, 183-189.
8. Peryshkov, D. V.; Forrest, W. P.; Schrock, R. R.; Smith, S. J.; Müller, P., B(C₆F₅)₃ Activation of Oxo Tungsten Complexes That Are Relevant to Olefin Metathesis. *Organometallics* **2013**, *32*, 5256-5259.
9. Hock, A. S.; Schrock, R. R.; Hoveyda, A. H., Dipyrrolyl Precursors to Bisalkoxide Molybdenum Olefin Metathesis Catalysts. *J. Am. Chem. Soc.* **2006**, *128*, 16373-16375.
10. Gordon, C. P.; Yamamoto, K.; Liao, W.-C.; Allouche, F.; Andersen, R. A.; Copéret, C.; Raynaud, C.; Eisenstein, O., Metathesis Activity Encoded in the Metallacyclobutane Carbon-13 NMR Chemical Shift Tensors. *ACS Cent. Sci.* **2017**, *3*, 759-768.
11. Peryshkov, D. V.; Schrock, R. R.; Takase, M. K.; Müller, P.; Hoveyda, A. H., Z-Selective Olefin Metathesis Reactions Promoted by Tungsten Oxo Alkylidene Complexes. *J. Am. Chem. Soc.* **2011**, *133*, 20754-20757.
12. Peryshkov, D. V.; Schrock, R. R., Synthesis of Tungsten Oxo Alkylidene Complexes. *Organometallics* **2012**, *31*, 7278-7286.
13. Conley, M. P.; Mougél, V.; Peryshkov, D. V.; Forrest, W. P.; Gajan, D.; Lesage, A.; Emsley, L.; Copéret, C.; Schrock, R. R., A Well-Defined Silica-Supported Tungsten Oxo Alkylidene Is a Highly Active Alkene Metathesis Catalyst. *J. Am. Chem. Soc.* **2013**, *135*, 19068-19070.
14. Mougél, V.; Copéret, C., Isostructural Molecular and Surface Mimics of the Active Sites of the Industrial WO₃/SiO₂ Metathesis Catalysts. *ACS Catal.* **2015**, *5*, 6436-6439.
15. Schowner, R.; Frey, W.; Buchmeiser, M. R., Cationic Tungsten-Oxo-Alkylidene-N-Heterocyclic Carbene Complexes: Highly Active Olefin Metathesis Catalysts. *J. Am. Chem. Soc.* **2015**, *137*, 6188-6191.
16. Schrock, R. R.; Copéret, C., Formation of High-Oxidation-State Metal–Carbon Double Bonds. *Organometallics* **2017**, *36*, 1884-1892.
17. Schrock, R. R.; Duval-Lungulescu, M.; Tsang, W. C. P.; Hoveyda, A. H., Catalytic Homologation of Vinyltributylstannane to Allyltributylstannane by Mo(IV) Complexes in the Presence of Ethylene. *J. Am. Chem. Soc.* **2004**, *126*, 1948-1949.
18. McLain, S. J.; Sancho, J.; Schrock, R. R., Metallacyclopentane to metallacyclobutane ring contraction. *J. Am. Chem. Soc.* **1979**, *101*, 5451-5453.
19. Tsang, W. C. P.; Hultsch, K. C.; Alexander, J. B.; Bonitatebus, P. J.; Schrock, R. R.; Hoveyda, A. H., Alkylidene and Metalacyclic Complexes of Tungsten that Contain a Chiral Biphenoxide Ligand. Synthesis, Asymmetric Ring-Closing Metathesis, and Mechanistic Investigations. *J. Am. Chem. Soc.* **2003**, *125*, 2652-2666.

20. Wang, S.-Y. S.; VanderLende, D. D.; Abboud, K. A.; Boncella, J. M., Metallacyclopentane Formation: A Deactivation Pathway for a Tungsten(VI) Alkylidene Complex in Olefin Metathesis Reactions. *Organometallics* **1998**, *17*, 2628-2635.
21. Tsang, W. C. P.; Jamieson, J. Y.; Aeilts, S. L.; Hultsch, K. C.; Schrock, R. R.; Hoveyda, A. H., Investigations of Reactions between Chiral Molybdenum Imido Alkylidene Complexes and Ethylene: Observation of Unsolvated Base-Free Methylene Complexes, Metalacyclobutane and Metalacyclopentane Complexes, and Molybdenum(IV) Olefin Complexes. *Organometallics* **2004**, *23*, 1997-2007.
22. Robbins, J.; Bazan, G. C.; Murdzek, J. S.; O'Regan, M. B.; Schrock, R. R., Reduction of molybdenum imido-alkylidene complexes in the presence of olefins to give molybdenum(IV) complexes. *Organometallics* **1991**, *10*, 2902-2907.
23. Fellmann, J. D.; Rupprecht, G. A.; Schrock, R. R., Rapid selective dimerization of ethylene to 1-butene by a tantalum catalyst and a new mechanism for ethylene oligomerization. *J. Am. Chem. Soc.* **1979**, *101*, 5099-5101.
24. Simmons, E. M.; Hartwig, J. F., On the Interpretation of Deuterium Kinetic Isotope Effects in C-H Bond Functionalizations by Transition-Metal Complexes. *Angew. Chem. Int. Ed.* **2012**, *51*, 3066-3072.
25. Arndt, S.; Schrock, R. R.; Müller, P., Synthesis and Reactions of Tungsten Alkylidene Complexes That Contain the 2,6-Dichlorophenylimido Ligand. *Organometallics* **2007**, *26*, 1279-1290.
26. Solans-Monfort, X.; Coperet, C.; Eisenstein, O., Shutting Down Secondary Reaction Pathways: The Essential Role of the Pyrrolyl Ligand in Improving Silica Supported d⁰-ML₄ Alkene Metathesis Catalysts from DFT Calculations. *J. Am. Chem. Soc.* **2010**, *132*, 7750-7757.
27. Solans-Monfort, X.; Copéret, C.; Eisenstein, O., Oxo vs Imido Alkylidene d⁰-Metal Species: How and Why Do They Differ in Structure, Activity, and Efficiency in Alkene Metathesis? *Organometallics* **2012**, *31*, 6812-6822.
28. Larionov, E.; Li, H.; Mazet, C., Well-defined transition metal hydrides in catalytic isomerizations. *Chem. Commun.* **2014**, *50*, 9816-9826.
29. For recent discussion on computing entropies see reference below: [a] Besora, M.; Vidossich, P.; Lledós, A.; Ujaque, G.; Maseras, F., Calculation of Reaction Free Energies in Solution: A Comparison of Current Approaches. *J. Phys. Chem. A* **2018**, *122*, 1392-1399.; [b] Falivene, L.; Barone, V.; Talarico, G., Unraveling the role of entropy in tuning unimolecular vs. bimolecular reaction rates: The case of olefin polymerization catalyzed by transition metals. *Mol. Catal.* **2018**, *452*, 138-144.
30. Bailey, G. A.; Lummiss, J. A. M.; Foscatto, M.; Occhipinti, G.; McDonald, R.; Jensen, V. R.; Fogg, D. E., Decomposition of Olefin Metathesis Catalysts by Brønsted Base: Metallacyclobutane Deprotonation as a Primary Deactivating Event. *J. Am. Chem. Soc.* **2017**, *139*, 16446-16449.
31. Stephan, D. W.; Erker, G., Frustrated Lewis Pair Chemistry: Development and Perspectives. *Angew. Chem. Int. Ed.* **2015**, *54*, 6400-6441.
32. Jarupatrakorn, J.; Coles, M. P.; Tilley, T. D., Synthesis and Characterization of MO[OSi(OtBu)₃]₄ and MO₂[OSi(OtBu)₃]₂ (M = Mo, W): Models for Isolated Oxo-Molybdenum and -Tungsten Sites on Silica and Precursors to Molybdena- and Tungsta-Silica Materials. *Chem. Mater.* **2005**, *17*, 1818-1828.
33. Bergbreiter, D. E.; Killough, J. M., Reactions of potassium-graphite. *J. Am. Chem. Soc.* **1978**, *100*, 2126-2134.
34. Arrowsmith, C. H.; Kresge, A. J., A correlation between .beta.-hydrogen isotope effects on carbon-13 NMR chemical shifts in unsaturated systems and the strength of hyperconjugative interactions. *J. Am. Chem. Soc.* **1986**, *108*, 7918-7920.
35. Frisch, M. J. T., G. W.; Schlegel, H. B.; Scuseria, G. E.; Robb, M. A.; Cheeseman, J. R.; Scalmani, G.; Barone, V.; Mennucci, B.; Petersson, G. A.; Nakatsuji, H.; Caricato, M.; Li, X.; Hratchian, H. P.; Izmaylov, A. F.; Bloino, J.; Zheng, G.; Sonnenberg, J. L.; Hada, M.; Ehara, M.; Toyota, K.; Fukuda, R.; Hasegawa, J.; Ishida, M.; Nakajima, T.; Honda, Y.; Kitao, O.; Nakai, H.; Vreven, T.; Montgomery, J. A.; Peralta, J. E.; Ogliaro, F.; Bearpark, M.; Heyd, J. J.; Brothers, E.; Kudin, K. N.; Staroverov, V. N.; Keith, T.; Kobayashi, R.; Normand, J.; Raghavachari, K.; Rendell, A.; Burant, J. C.; Iyengar, S. S.; Tomasi, J.; Cossi, M.; Rega, N.; Millam, J. M.; Klene, M.; Knox, J. E.; Cross, J. B.; Bakken, V.; Adamo, C.; Jaramillo, J.; Gomperts, R.; Stratmann, R. E.; Yazyev, O.;

- Austin, A. J.; Cammi, R.; Pomelli, C.; Ochterski, J. W.; Martin, R. L.; Morokuma, K.; Zakrzewski, V. G.; Voth, G. A.; Salvador, P.; Dannenberg, J. J.; Dapprich, S.; Daniels, A. D.; Farkas, O.; Foresman, J. B.; Ortiz, J. V.; Cioslowski, J.; Fox, D. J. *Gaussian 09, Revision D.01*, Gaussian, Inc.: Wallingford CT., 2013.
36. Becke, A. D., Density-functional thermochemistry. III. The role of exact exchange. *J. Chem. Phys.* **1993**, *98*, 5648-5652.
37. Stephens, P. J.; Devlin, F. J.; Chabalowski, C. F.; Frisch, M. J., Ab Initio Calculation of Vibrational Absorption and Circular Dichroism Spectra Using Density Functional Force Fields. *J. Phys. Chem.* **1994**, *98*, 11623-11627.
38. Grimme, S.; Antony, J.; Ehrlich, S.; Krieg, H., A consistent and accurate ab initio parametrization of density functional dispersion correction (DFT-D) for the 94 elements H-Pu. *J. Chem. Phys.* **2010**, *132*, 154104.
39. Marenich, A. V.; Cramer, C. J.; Truhlar, D. G., Universal Solvation Model Based on Solute Electron Density and on a Continuum Model of the Solvent Defined by the Bulk Dielectric Constant and Atomic Surface Tensions. *J. Phys. Chem. B* **2009**, *113*, 6378-6396.
40. Andrae, D.; Häußermann, U.; Dolg, M.; Stoll, H.; Preuß, H., Energy-adjusted ab initio pseudopotentials for the second and third row transition elements. *Theoretica chimica acta* **1990**, *77*, 123-141.
41. Schäfer, A.; Horn, H.; Ahlrichs, R., Fully optimized contracted Gaussian basis sets for atoms Li to Kr. *J. Chem. Phys.* **1992**, *97*, 2571-2577.
42. Schäfer, A.; Huber, C.; Ahlrichs, R., Fully optimized contracted Gaussian basis sets of triple zeta valence quality for atoms Li to Kr. *J. Chem. Phys.* **1994**, *100*, 5829-5835.
43. Liang, Y.; Liu, S.; Xia, Y.; Li, Y.; Yu, Z. X., Mechanism, Regioselectivity, and the Kinetics of Phosphine-Catalyzed [3+2] Cycloaddition Reactions of Allenes and Electron-Deficient Alkenes. *Chem.: Eur. J.* **2008**, *14*, 4361-4373.
44. Huang, F.; Lu, G.; Zhao, L.; Li, H.; Wang, Z.-X., The Catalytic Role of N-Heterocyclic Carbene in a Metal-Free Conversion of Carbon Dioxide into Methanol: A Computational Mechanism Study. *J. Am. Chem. Soc.* **2010**, *132*, 12388-12396.
45. Kua, J.; Krizner, H. E.; De Haan, D. O., Thermodynamics and Kinetics of Imidazole Formation from Glyoxal, Methylamine, and Formaldehyde: A Computational Study. *J. Phys. Chem. A* **2011**, *115*, 1667-1675.
46. Li, H.; Lu, G.; Jiang, J.; Huang, F.; Wang, Z.-X., Computational Mechanistic Study on Cp*Ir Complex-Mediated Acceptorless Alcohol Dehydrogenation: Bifunctional Hydrogen Transfer vs β -H Elimination. *Organometallics* **2011**, *30*, 2349-2363.

Chapter 4. Well-defined Silica-supported Tungsten(IV)-oxo Complex: Olefin Metathesis Activity, Initiation and Role of Brønsted Acid Sites

Adapted with permission from Chan, K. W.; Mance, D.; Safonova, O. V.; Copéret, C., Well-defined Silica-supported Well-Defined Silica-Supported Tungsten(IV)-Oxo Complex: Olefin Metathesis Activity, Initiation, and Role of Brønsted Acid Sites. *J. Am. Chem. Soc.* **2019**, in press. Copyright 2019 American Chemical Society.

4.1 Introduction

As shown previously in Chapter 3, molecular W(IV)-oxo complexes can initiate metathesis reaction with allylic C–H activation and proton transfers being the key initiation steps. Despite the comparable catalytic performances to well-defined alkylidene complexes, this initiation process only leads to the formation of a small amount of active species in solution (few percent of the total W species). The low initiation efficiency can be ascribed to the endergonic nature of this initiation process, as shown by DFT calculations, combined with the fast decomposition of the low coordinated W(IV) and W(VI) species generated in solution upon activation with *tris*(pentafluorophenyl)borane B(C₆F₅)₃. We thus reasoned that generating the corresponding well-defined silica-supported W(IV)-oxo complex could improve the catalytic performance by switching off some possible deactivation pathways in solution, such as bimolecular decomposition.^{1, 2-7} Furthermore, this will allow us to relate the reactivity of the W(IV)-oxo molecular species to its supported analogue and provide a supported model system containing selectively W(IV)-oxo species that can be used to understand the activity of low valent species generated upon reduction in silica-supported W(VI)-oxo materials (Chapter 2).

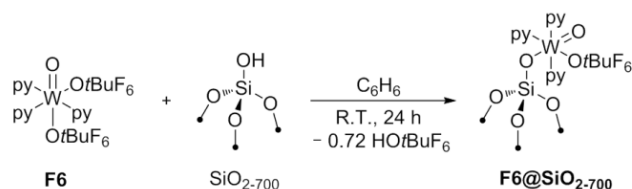
In this chapter, we synthesize and investigate the reactivity of well-defined silica-supported W(IV)-oxo species ($\equiv\text{SiO}$)WO(*O*tBuF₆)(py)₃ (*O*tBuF₆ = OC(CH₃)(CF₃)₂; py = pyridine) prepared via Surface Organometallic Chemistry (SOMC).⁸⁻¹¹ We demonstrate that the supported W(IV) precatalyst is active in olefin metathesis upon activation with B(C₆F₅)₃ or thermal treatment that removes the coordinated pyridine ligands. The activated surface species displays one order of magnitude higher catalytic activity than its molecular analogue, and, in contrast to the latter, it also catalyzes the self-metathesis of olefins without any allylic

C–H group, such as styrene. We demonstrate that metathesis activity of styrene is linked to the presence of surface OH groups that opens additional initiation pathways.

4.2 Result and Discussion

4.2.1 Synthesis and Characterization of $(\equiv\text{SiO})\text{WO}(\text{OtBuF}_6)(\text{py})_3$

Grafting of $\text{WO}(\text{OtBuF}_6)_2(\text{py})_3$ (**F6**) on silica partially dehydroxylated at 700 °C (SiO_{2-700}) in benzene for 24 h afforded a dark blue material **F6@SiO₂₋₇₀₀** (Scheme 4.1). Analysis of the combined supernatant and washings of the material by ^1H NMR spectroscopy revealed the consumption of **F6** and the release of HOtBuF_6 (0.72 equiv. per grafted W center) suggesting that grafting occurred via protonolysis. Furthermore, no free pyridine was observed in the washings.



Scheme 4.1. Preparation of well-defined silica-supported W(IV)-oxo species.

Comparison of the IR spectra of **F6@SiO₂₋₇₀₀** and SiO_{2-700} reveal the consumption of isolated silanol $\nu(\text{O–H})$ at 3747 cm^{-1} upon grafting (Figure A.4.1), while a broad red shifted band appear at 3700 cm^{-1} indicating the interactions between remaining surface silanols and the grafted species. Additional $\nu(\text{C–H})$ bands of the alkoxide and pyridine ligands are observed in the region of $3200\text{--}2800\text{ cm}^{-1}$ and $1630\text{--}1360\text{ cm}^{-1}$. The ν_{19b} and ν_{8a} ring-breathing vibrations modes of pyridine ligands also appear in the region of $1630\text{--}1440\text{ cm}^{-1}$ indicating the presence of pyridine on the surface. Elemental analysis of **F6@SiO₂₋₇₀₀** reveals 3.82 wt% of W (i.e. 0.6 Wnm^{-2}) and the composition of 19 C, 17 H, 4 N and 6 F per W center. These data are consistent with the formation of $(\equiv\text{SiO})\text{WO}(\text{OtBuF}_6)(\text{py})_3$ as shown in Scheme 4.1. Further analysis of **F6@SiO₂₋₇₀₀** by X-ray Absorption Near Edge Structure (XANES) spectroscopy at both W L_I and L_{III} edge (Figure A.4.2–A.4.3) show that **F6@SiO₂₋₇₀₀** share the same edge energy and spectroscopic features as **F6** indicating the retention of the oxidation state and geometry upon grafting. The lack of pre-edge feature in the W L_I edge XANES spectrum further supports that the grafted species remain in an octahedral geometry. Extended X-ray Absorption Fine Structure (EXAFS) fitting analysis of the first coordination

sphere of **F6@SiO₂₋₇₀₀** is also consistent with the structure ($\equiv\text{SiO}$)WO(*O*tBuF₆)(py)₃ (Table 4.1). ¹H Magic Angle Spinning (MAS) NMR spectrum of **F6@SiO₂₋₇₀₀** displays two signals at δ 1.95 and 1.69 ppm (Figure A.4.6) indicating the presence of $-\text{CH}_3(\text{CF}_3)_2$ groups in two different environments. Additional proton resonances at δ 8.88 and 7.71 ppm indicate the presence of pyridine. Similarly, ¹⁹F MAS NMR spectrum shows a broad signal at ca. δ -81 ppm corresponding to the $-\text{CF}_3$ groups (Figure A.4.7). These chemical shifts are similar to the reported **F6** molecular analogue.¹²

Table 4.1. EXAFS fit parameters for the W L_{III}-edge spectrum of **F6@SiO₂₋₇₀₀**.

<i>neighbor</i>	N^a	σ^2 (\AA^2) ^b	R (\AA) ^c
O	1*	0.002 (2)	1.73 (1)
O	2*	0.003 (2)	2.00 (3)
N	3*	0.005 (3)	2.16 (4)

^aNumber of specified neighbors. ^bDebye-Waller factor. ^cDistance between W metal center to the specified neighbors. *Fixed parameters in the fit.

4.2.2 Catalytic Activity

We then examined the catalytic activity of **F6@SiO₂₋₇₀₀** towards self-metathesis of *cis*-4-nonene at 70 °C. In the absence of activator, this material displays no metathesis activity, similarly to what is found with the **F6** molecular compound.¹² However, upon the addition of B(C₆F₅)₃ for removing the coordinated pyridine, **F6@SiO₂₋₇₀₀** catalyzes self-metathesis of *cis*-4-nonene (1000 equiv per W) at 70 °C to reach equilibrium conversion (51 %) within 3 h (Figure A.4.13). Alternatively, thermal treatment of **F6@SiO₂₋₇₀₀** at 400 °C under high vacuum also removes the pyridines and results in a metathesis active material **F6@SiO_{2-700-thermal}** without the need of any activator. Under the same reaction conditions with *cis*-4-nonene, while a short induction period of ca. 30 min is observed in the case of **F6@SiO_{2-700-thermal}**, the equilibrium conversion is reached within 2 h (Figure A.4.13). It is noteworthy that **F6@SiO₂₋₇₀₀** displays a significantly higher catalytic activity compared to its **F6** homogeneous analogue (Table 4.2). This difference in activity points to the advantage of site isolation in the supported **F6@SiO₂₋₇₀₀** that likely prevents bimolecular deactivation of low-coordinated reaction intermediates, thus improving catalyst stability.¹³

We then investigated the metathesis activity towards other substrates including 1-nonene, *trans*- β -methylstyrene and styrene. The results are summarized in Table 4.2. In the presence of B(C₆F₅)₃, self-metathesis of 1-nonene catalyzed by **F6@SiO₂₋₇₀₀** reaches 86%

conversion at 6 h (Figure A.4.14). The rate of self-metathesis of *trans*- β -methylstyrene catalyzed by **F6@SiO₂₋₇₀₀** is an order of magnitude higher compared to **F6** (Table 4.2; Figure A.4.15). Noteworthy, **F6@SiO₂₋₇₀₀** also catalyzes the self-metathesis of styrene while **F6** does not under similar reaction conditions (Figure A.4.16). These results indicate that immobilization of the precatalyst on silica enables efficient metathesis and allows initiation of substrate without allylic C–H group. The presence of surface OH groups, which are not present in the molecular system, may open new initiation reaction pathways for substrates that do not contain allylic C–H bond (vide infra).^{14, 15-16}

Table 4.2. Catalytic activities of supported and molecular species in olefin metathesis^a

<i>catalysts</i>	<i>mol %^c</i>	<i>substrate</i>	<i>rate (M.min⁻¹.g_W⁻¹)^f</i>	<i>conv. at 6 h^g</i>
F6@SiO₂₋₇₀₀	0.1	Cis-4-nonene	190 ^d	Equil.; 3 h
F6@SiO_{2-700-thermal}^b	0.1	Cis-4-nonene	390 ^{d,h}	Equil.; 2 h
F6	0.3	Cis-4-nonene	3.2 ^d	47%
F6@SiO₂₋₇₀₀	1	1-nonene	41 ^d	86%
F6@SiO₂₋₇₀₀	2	β -methylstyrene	3.8 ^e	59%
F6@SiO₂₋₇₀₀	2	Styrene	0.91 ^e	40%
F6	2	β -methylstyrene	0.09 ^{e,h}	12%

^a Batch reactor, 70 °C, in the presence of B(C₆F₅)₃ (3 equiv per W). ^b Without B(C₆F₅)₃. ^c Loading of the catalysts based on W mol%. ^d 1.0 M toluene solution. ^e 0.2 M toluene solution. ^f Rate of metathesis normalized per gram of W at conversion < 20%. ^g Conversion at 6 h unless otherwise noted by giving the time reaching equilibrium conversion. ^h Following an induction period (ca. 30 min), the metathesis starts and reaches a maximum rate after 60 min.

4.2.3 Effect of Surface OH Density

In order to investigate the possible involvement of surface OH groups in facilitating initiation, the molecular complex **F6** was thus grafted on silica having increasing initial surface OH densities, that can be achieved through decreasing the dehydroxylation temperature of the supports (SiO_{2-x}, x = dehydroxylation temperatures in °C), namely SiO₂₋₅₀₀ (0.46 mmol_{OH}/ g) and SiO₂₋₂₀₀ (0.84 mmol_{OH}/ g) yielding **F6@SiO₂₋₅₀₀** and **F6@SiO₂₋₂₀₀**, respectively. The catalytic activity of these materials was then compared to **F6@SiO₂₋₇₀₀** with an initial OH density of 0.31 mmol_{OH}/ g on SiO₂₋₇₀₀. In all materials, the weight loadings of W were kept the same, i.e. with a density of ca. 0.6 Wnm⁻², yielding materials with different densities of remaining silanols. IR spectra of the grafted materials (Figure 4.1) indicate that no

isolated silanol (3747 cm^{-1}) remains, while broad OH bands – associated with OH groups interacting with the grafted species – appear at $3690\text{--}3700\text{ cm}^{-1}$ whose intensity increases with the amounts of the initial OH groups: $\mathbf{F6@SiO}_{2-200} > \mathbf{F6@SiO}_{2-500} > \mathbf{F6@SiO}_{2-700}$.

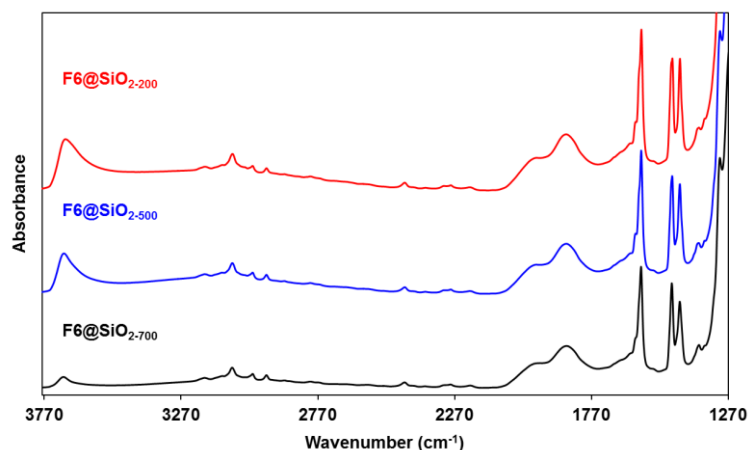


Figure 4.1. IR spectra of $\mathbf{F6@SiO}_{2-200}$ (red; top), $\mathbf{F6@SiO}_{2-500}$ (blue; middle) and $\mathbf{F6@SiO}_{2-700}$ (black; bottom).

The catalytic activities of $\mathbf{F6@SiO}_{2-700}$, $\mathbf{F6@SiO}_{2-500}$ and $\mathbf{F6@SiO}_{2-200}$ in the self-metathesis of *trans*- β -methylstyrene and styrene in the presence of $\text{B}(\text{C}_6\text{F}_5)_3$ were then investigated. The rates of self-metathesis of *trans*- β -methylstyrene are similar for all three materials, while the rate of self-metathesis of styrene parallels the increase OH density of the materials (Figure 4.2). The rate of styrene metathesis in $\mathbf{F6@SiO}_{2-200}$ is approximately 2.5 times higher than that in $\mathbf{F6@SiO}_{2-700}$. The increases in activities with increasing OH densities and the lack of styrene metathesis activity in $\mathbf{F6}$ molecular system suggest that OH groups could be involved in the initiation step with styrene as the olefinic substrate having no allylic C–H bond (vide infra).

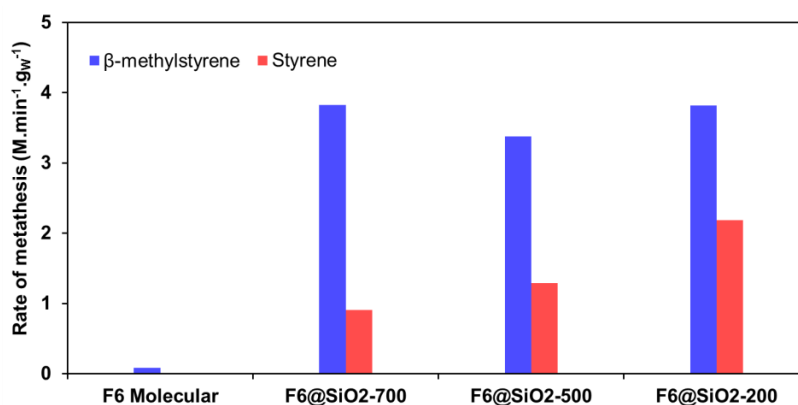


Figure 4.2. Rates of metathesis ($\text{M}\cdot\text{min}^{-1}\cdot\text{g}^{-1}$) normalized per gram of W (at conversion $< 20\%$) of $\mathbf{F6}$, $\mathbf{F6@SiO}_{2-700}$, $\mathbf{F6@SiO}_{2-500}$ and $\mathbf{F6@SiO}_{2-200}$ for *trans*- β -methylstyrene (blue) and styrene (red).

4.2.4 Investigation of Reaction Intermediates Formed Upon Reaction of F6@SiO₂₋₂₀₀ with Styrene

To investigate the reaction intermediates formed on the surface, **F6@SiO₂₋₂₀₀** was exposed to ¹³C-dilabeled styrene- α,β -¹³C₂ in the presence of B(C₆F₅)₃ in toluene at 70 °C for 1 h. The supernatant was then removed, and the solid was washed with toluene followed by drying under high vacuum. ¹³C solid-state NMR spectrum of the resulting solid reveals a major signal at ca. δ 65 ppm (Figure A.4.18), which indicates the presence of ethylene π complex formed from the ethylene released via styrene metathesis. This assignment is further confirmed by the ¹³C-¹³C single-quantum double-quantum SQ-DQ experiment (Figure 4.3), in which a strong self-correlating signal at δ 130 ppm in the DQ dimension and δ 65 ppm in the SQ dimension was observed. Noticeably, such self-correlating signal appears to be very broad, indicating a distribution of surface W ethylene π complexes likely associated with slightly different environments. In addition, two intense signals at δ 65 and 85 ppm that correlate with each other (Figure 4.3) are assigned to the β - and α -carbons of the styrene π complex, respectively. The signals at δ 75 ppm (α -C) and 36 ppm (β -C) that are also correlated in the SQ-DQ experiment can be attributed to the α - and β - carbons of the unsubstituted metallacyclopentane, respectively. The observation of both olefin π complexes and metallacyclopentane as the major species is in line with the reported **F6** molecular system.¹²

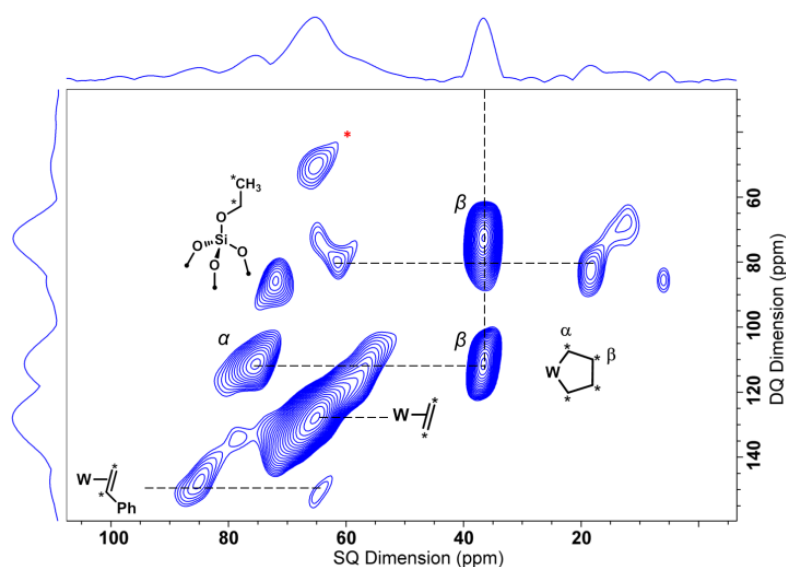


Figure 4.3. ¹³C-¹³C SQ-DQ MAS NMR experiment acquired on a 600 MHz spectrometer at 12kHz MAS of **F6@SiO₂₋₂₀₀** after contacting with styrene- α,β -¹³C₂ under reaction conditions. Asterisk (in red) indicates spinning sideband.

However, the absence of evidence for alkylidenes or metallacyclobutanes is noteworthy; it implies that the amount of active species formed is likely small, possibly pointing out the low efficiency of the initiation process due to the competing and favorable formation of olefin π complexes and metallacyclopentane.¹² Finally, two additional signals at δ 61 and 19 ppm are assigned to the presence of ethoxy group (EtO–) on the surface,¹⁷⁻¹⁸ which arises from the protonation of ethylene by surface OH groups. Such species are not observed on silica (see Appendix for details) suggesting the presence of highly Brønsted acidic OH groups in **F6@SiO₂₋₂₀₀** under reaction conditions.

We also attempted to quantify the amount of active alkylidenes formed by cross-metathesis reactions between styrene and *cis*-5-decene. However, the presence of off cycle species (e.g. olefin π complex and metallacyclopentane) that can serve as an olefin reservoir for subsequent cross-metathesis reactions have prevented us to obtain a reliable quantification of the active alkylidene (see Appendix for details).

4.2.5 Brønsted Acid Site in **F6@SiO₂₋₂₀₀** Probed by ¹⁵N-pyridine

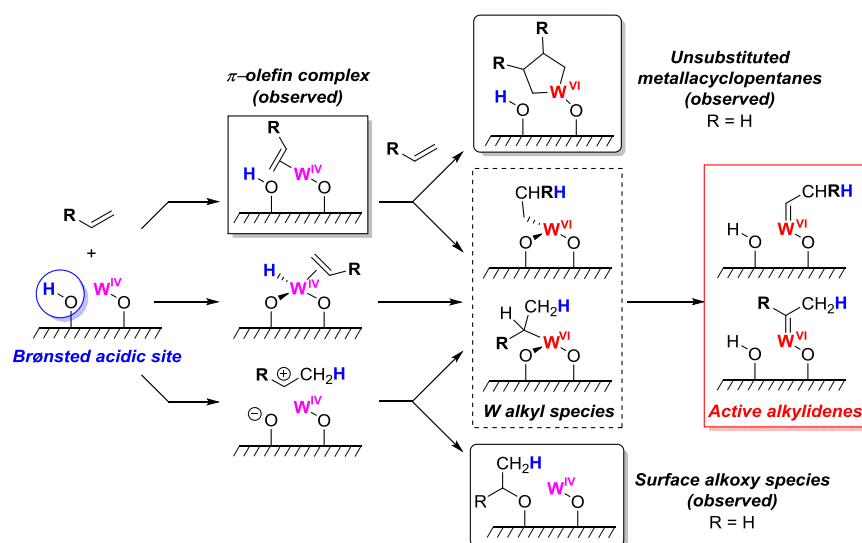
The observation of surface EtO– group (Figure 4.3) upon contacting **F6@SiO₂₋₂₀₀** with styrene- α,β -¹³C₂ under reaction conditions suggests the presence of strong Brønsted acidic site, which is further evidenced by using ¹⁵N-labeled pyridine (¹⁵N-py), a probe molecule. ¹⁵N-labeled **F6@SiO₂₋₂₀₀** (¹⁵N-**F6@SiO₂₋₂₀₀**) was synthesized and its ¹⁵N Cross-polarization (CP) MAS NMR spectrum shows similar ¹⁵N resonance signals compared to the ¹⁵N-labeled molecular precursor (¹⁵N-**F6**) (Figure A.4.19) along with a small peak at δ 293 ppm indicating a small amount of ¹⁵N-py, likely released upon grafting, that is H-bonded with the OH groups on the surface.¹⁹⁻²⁰ Upon activating the ¹⁵N-**F6@SiO₂₋₂₀₀** with 3 equiv of B(C₆F₅)₃ at 70 °C followed by the subsequent addition of extra ¹⁵N-py, a shift in the major ¹⁵N signals to lower chemical shifts, compared to ¹⁵N-**F6@SiO₂₋₂₀₀**, was observed. This result indicates that part of the changes in the coordination environment of the W centers after the removal of ¹⁵N-py ligands by B(C₆F₅)₃ are irreversible and that the surface remaining ¹⁵N-py-B(C₆F₅)₃ adducts that are formed likely contribute to the signal observed.²¹ Notably, a small peak at δ 207 ppm also appeared, which is attributed to pyridinium (¹⁵N-pyH⁺) (Figure A.4.19).¹⁹⁻²⁰ The presence of ¹⁵N-pyH⁺ is further supported by the peak observed at 1533 cm⁻¹ in the IR spectrum corresponding to a combination of vibration modes involving ¹⁵N⁺–H (Figure A.4.20).²²⁻²⁴ The formation of ¹⁵N-pyH⁺ by protonating the ¹⁵N-py indicates the presence of strong Brønsted acid site upon addition of B(C₆F₅)₃ to ¹⁵N-**F6@SiO₂₋₂₀₀**. Notably, such Brønsted acid site is absent on SiO₂₋₂₀₀ despite the presence of pyridine and B(C₆F₅)₃ (Figure A.4.20), indicating the low-coordinated W center is likely responsible for the

formation of the strong Brønsted acid site by interacting with the OH groups in close proximity.

4.2.6 Proposed Initiation Mechanism for the Formation of Alkylidenes

Based on the above observations: i) the increase activity in styrene metathesis parallels the increase in surface OH density (Figure 4.2), and ii) strong Brønsted acid sites in the supported system are present due to the presence of W centers as shown by the ^{15}N -py experiments, we propose that, for olefins having no allylic C–H group, e.g. styrene, surface OH groups can assist the initiation by protonating the olefins as shown in Scheme 4.2.^{14, 15-16} Protonation of the W-coordinated olefin by surface OH groups can directly lead to the formation of tungsten–carbon bond, a tungsten alkyl species. Alternatively, protonation of the free olefin can yield transient carbocations that can either generate surface alkoxy groups that are observed experimentally (Figure 4.3) or further react with the W(IV) centers forming the tungsten alkyl species. The tungsten alkyl species can then convert into an alkylidene via deprotonation by the silanolate ligand. The proposed carbocation intermediates could also lead to an indirect initiation pathway involving dimerization of styrene followed by the allylic C–H activation.²⁵⁻²⁶ However, the corresponding dimer does not initiate metathesis as shown in the molecular **F6** system (see Appendix for details), hence precluding the possibility of the latter initiation pathway. The feasibility of the proposed initiation mechanism in Scheme 4.2 is also supported by DFT calculations, which suggest that the initiation pathway, especially the formation of tungsten alkyl from W(IV) species is thermodynamically very favorable. The calculations also show that subsequent deprotonation of the alkyl ligand would be thermoneutral in specific environments, i.e. with a slightly elongated W–O silanolate bond, which is only possible for a small amount of surface strained sites. This likely contributes to the formation of only a small amount of active sites associated with low initiation efficiency (see Appendix for details). In order to obtain more insight into the initiation mechanism, we also tried to track the initiation product formed in the process. However, unlike the reported homogeneous **F6** system,¹² monitoring the metathesis of either β -methylstyrene or styrene by GC-MS does not reveal the formation of a specific initiation product, which may be due to strong adsorption on the surface accompanied by further reactions. Although there is no direct initiation product being observed in **F6@SiO_{2-x}** during the generation of alkylidene species, we propose that olefins with allylic C–H groups likely follow the allylic C–H activation mechanism and subsequent proton transfers to generate the metallacyclobutane intermediates, as reported in the molecular **F6** system.¹² Since increasing OH density does not lead to an

increase in the metathesis activity with the *trans*- β -methylstyrene (Figure 4.2), this suggests the presence of competing initiation mechanisms that depend on the olefinic substrates.



Scheme 4.2. Proposed initiation mechanism for olefin without allylic C–H group.

4.3 Conclusion

We have shown that well-defined W(IV) oxo species ($\equiv\text{SiO}$)WO(O*t*BuF₆)(py)₃ (**F6**@SiO₂₋₇₀₀) prepared via SOMC is active in olefin metathesis upon activation by B(C₆F₅)₃ or thermal treatment. **F6**@SiO₂₋₇₀₀ shows an order of magnitude higher catalytic activity compared to the **F6** molecular analogue, confirming the advantage of site isolation when reactive intermediates are formed. Furthermore, **F6**@SiO₂₋₇₀₀ also initiates the self-metathesis of styrene, which is in sharp contrast to the reported **F6**, suggesting that alternative initiation mechanisms are involved in supported species. The fact that increasing surface OH density of the supports further increases the initial rates of styrene metathesis suggests a surface proton assisted initiation mechanism for the olefin without allylic C–H group. This is also consistent with the generation of strong Brønsted acidic surface sites in the activated catalysts. For substrates with allylic C–H groups e.g. β -methylstyrene, initiation via allylic C–H activation is still likely involved, as evidenced by the lack of dependence of metathesis activity with OH density. This study suggests that the initiation mechanisms for generating W-based olefin metathesis catalysts from W(IV) oxo species depend on the olefin substrates. Furthermore, these findings reveal the participation of the surface functionalities of the oxide support, namely the surface Brønsted acid sites. It is noteworthy that initiation of metathesis catalysts (whether involving allylic C–H activation or not) involves a key proton transfer step. This also indicates that oxide supports in heterogeneous olefin metathesis catalysts might not

always be inert, even for a support like silica. Surface Brønsted acid sites, formed by the presence of W, can be responsible for metathesis activity by opening alternative initiation processes. This study helps to further understand the effects of Brønsted acidity in heterogeneous metathesis catalysts.

4.4 Experimental Details

4.4.1 General Procedures

Unless otherwise noted, all experiments were carried out under dry and oxygen free argon atmosphere using either standard Schlenk or glove-box techniques. Toluene was purified using double MBRAUN SPS alumina column, and was degassed by 3 freeze-pump-thaw cycles before use. C_6H_6 and C_6D_6 were distilled from Na/benzophenone. $WO(OtBuF_6)_2(py)_3$ (**F6**) (py = pyridine) was synthesized according to literature procedures.¹² Tris(pentafluorophenyl)borane was purchased from TCI and sublimed before use. styrene- α , β - $^{13}C_2$ was purchased from Aldrich and dried and distilled over CaH_2 followed by the purification procedure as styrene (details in S13) before used. Solution NMR was recorded in C_6D_6 on Bruker 200, 300, 400 and 500 MHz at 298K.

Silica (Aerosil Degussa, $200\text{ m}^2\cdot\text{g}^{-1}$) was compacted with distilled water, calcined at $500\text{ }^\circ\text{C}$ ($5\text{ }^\circ\text{C}/\text{min}$) under air for 10 h and treated under vacuum (10^{-5} mbar) at $500\text{ }^\circ\text{C}$ ($1\text{ }^\circ\text{C}/\text{min}$) $^\circ\text{C}$ for 10 h and then at $700\text{ }^\circ\text{C}$ ($1\text{ }^\circ\text{C}/\text{min}$) for 20 h (support referred to as SiO_{2-700}). SiO_{2-500} was prepared similarly by treatment under vacuum (10^{-5} mbar) at $500\text{ }^\circ\text{C}$ ($1\text{ }^\circ\text{C}/\text{min}$) for 30 h after calcination under air. SiO_{2-200} was prepared by calcination of the silica under air at $500\text{ }^\circ\text{C}$ ($5\text{ }^\circ\text{C}/\text{min}$) for 10 h, followed by evacuation and cool down to room temperature under vacuum (10^{-5} mbar). Then, the silica was heated up to $200\text{ }^\circ\text{C}$ ($5\text{ }^\circ\text{C}/\text{min}$), contacted with pure degassed water for 45 min at $200\text{ }^\circ\text{C}$ and further dehydroxylated at $200\text{ }^\circ\text{C}$ for 30 h under vacuum (10^{-5} mbar). The amounts of OH per g were measured by titration with $PhCH_2MgCl$.

All infrared (IR) spectra were recorded using a Bruker α -T spectrometer placed in an Ar glovebox, equipped with OPUS software. A typical experiment consisted in the measurement of transmission in 32 scans in the region from 4000 to 400 cm^{-1} . Solid-state NMR spectra were obtained on a Bruker Avance III 400, 600 or 700 MHz spectrometer, using a 3.2 or 1.3 mm probe; the spectra were externally referenced by setting the downfield ^{13}C signal of adamantane to 38.52 ppm . Samples were loaded in a 3.2 or 1.3 mm zirconia rotor inside the glovebox. Cross polarization magic angle spinning (CP-MAS) type experiments were employed in order to acquire ^{13}C and ^{15}N spectra at 12 or 16 kHz MAS on the 400 and 600 MHz spectrometer. 1H decoupling was performed using the SPINAL64 sequence at 100kHz .²⁷ For the CP-MAS measurements, the CP condition was optimized experimentally to match the Hartmann-Hahn condition using an 80 to 100 % Ramp. The ^{13}C - ^{13}C DQ-SQ spectrum was recorded by applying the SPC5 homonuclear recoupling sequence during the excitation and reconversion periods.²⁸ The 1H and ^{19}F were acquired by making using of the Hahn-echo sequence at 50kHz MAS at the 700 MHz spectrometer. XAS measurements were

carried out at the W L_I and L_{III} edge at the SuperXAS beamline at SLS (PSI, Villigen, Switzerland). The storage ring was operated at 2.4 GeV in top-up mode with a ring current of around 400 mA. The incident photon beam provided by a 2.9 T super bend magnet source was selected by a Si (111) quick-EXAFS monochromator and the rejection of higher harmonics and focusing were achieved by a rhodium-coated collimating mirror at 2.8 mrad and a rhodium-coated torroidal mirror at 2.8 mrad. The beam size on the sample was 100 x 100 μm. During measurements the monochromators was rotating with 10 Hz frequency in 2 deg angular range and X-ray absorption spectra were collected in transmission mode using ionization chambers specially developed for quick data collection with 1 MHz frequency.²⁹ The spectra were collected for 2 min and averaged. Calibration of the beamline energy was performed using W reference foil (W L_I and L_{III}-edge position at 12100 and 10207 eV, respectively). To avoid contact with air, all samples were sealed in a glovebox. For ex situ samples, pressed pellets (with optimized thickness for transmission detection) were placed in two aluminized plastic bags (Polyaniline (15 μm), polyethylene (15 μm), Al (12 μm), polyethylene (75 μm) from Gruber-Folien GmbH & Co. KG, Straubing, Germany) using an impulse sealer inside a glovebox; one sealing layer was removed immediately before the measurements. Data were analyzed by standard procedures³⁰ using Ifeffit program package³¹⁻³². S₀² values were obtained by fitting W foil for W L_{III} edge. Elemental analyses were performed by the “Mikroanalytisches Labor Pascher” in Remagen, Germany.

4.4.2 Syntheses and characterizations of Supported Species (F6@SiO_{2-x})

Synthesis of F6@SiO₂₋₇₀₀. A solution of 127 mg of WO(O*t*BuF₆)₂(py)₃ (0.16 mmol, 0.84 equiv) in benzene (5 mL) was added to a suspension of SiO₂₋₇₀₀ (610 mg, 0.19 mmol, 1 equiv) in benzene (1 mL) at room temperature. The suspension was slowly stirred at room temperature for 24 h. The supernatant was removed by decantation and the dark blue solid was washed by five suspension/decantation cycles in benzene (5 x 2 mL). The resulting solid was dried thoroughly under high vacuum (10⁻⁵ mbar) at room temperature for 3 h to afford 600 mg of the title compound. All the supernatants were collected and analyzed by ¹H NMR spectroscopy in C₆D₆ using ferrocene as internal standard, indicating that 0.11 mmol of HO*t*BuF₆ (i.e. 0.72 equiv per grafted W) was released upon grafting.

Elemental Analysis: W 3.82%, F 2.43% (6.1 F/W), N 1.02% (3.5 N/W), H 0.35% (16.7 H/W), C 4.61% (18.5 C/W). Expected for (≡SiO)WO(O*t*BuF₆)(py)₃: 6 F/W, 3 N/W, 18 H/W, 19 C/W.

IR, XANES and solid state NMR spectra of the material are given in Figure A.4.1-A.4.3 and Figure A.4.6-A.4.7, respectively.

EXAFS fitting analysis is given in Figure A.4.4 and Table A.4.1.

Syntheses of F6@SiO_{2-x} (x = 500 or 200). Both materials were synthesized by using the same procedure as F6@SiO₂₋₇₀₀ by replacing SiO₂₋₇₀₀ with either SiO₂₋₅₀₀ or SiO₂₋₂₀₀. The weight of WO(O*t*BuF₆)₂(py)₃ used per gram of SiO_{2-x} were maintained the same in all materials to achieve the same W loading.

F6@SiO₂₋₅₀₀. 0.88 equiv of HO*t*BuF₆ per grafted W was released upon grafting. Elemental Analysis: W 3.70%, F 2.40% (6.3 F/W), N 1.03% (3.6 N/W), H 0.39% (19.2 H/W), C 4.44% (18.4 C/W).

IR spectra of the material are given in Figure A.4.8.

F6@SiO₂₋₂₀₀. 1.18 equiv of HO*t*BuF₆ per grafted W was released upon grafting. Elemental Analysis: W 3.67%, F 1.65% (4.4 F/W), N 1.01% (3.6 N/W), H 0.38% (19.0 H/W), C 4.41% (18.4 C/W).

IR and solid state NMR spectra of the material are given in Figure A.4.9 and Figure A.4.10-A.4.11, respectively.

Synthesis of F6@SiO_{2-700-thermal}. F6@SiO₂₋₇₀₀ (150 mg) was loaded into a reactor and placed under high vacuum (10⁻⁵ mbar) and heated to 200 °C (1 °C/min) and held at this temperature for 3 h then heated at 400 °C (1 °C/min) and held at this temperature for 6 h. The reactor was cooled to ambient temperature under static vacuum, and F6@SiO_{2-700-thermal} was stored in an Ar filled glovebox.

Elemental Analysis: W 4.15%.

IR spectra of the material are given in Figure A.4.12.

4.4.3 Catalytic activity measurements

Starting materials. *Cis*-4-nonene (> 97%) and 1-nonene (> 99.5%) were purchased from TCI Chemicals. Styrene (99.5%) was purchased from ABCR. *trans*- β -methylstyrene were synthesized according to literature procedures.³³ HPLC grade toluene, heptane and decalin were distilled from Na/benzophenone, degassed by 3 freeze-pump-thaw cycles, and stored in a glove-box over Selexsorb. Al₂O₃ was dried at 250 °C in high vacuum overnight. Molecular sieves were activated at 300 °C in high vacuum overnight. BASF Selexsorb® CD 1/8'' was calcined at 550 °C in air for 12 h and heated in high vacuum at 500 °C for 2 h.

Preparation of olefin stock solutions. *Cis*-4-nonene was stirred overnight with Na at room temperature, distilled in vacuo, degassed by 3 freeze-pump-thaw cycles, and stored in the glovebox over 3 Å MS. Before the preparation of stock solution, neat *cis*-4-nonene was treated with Selexsorb (~20–30% w/w) for 5 hours. After removal of Selexsorb, the solution was passed through a pad of activated neutral Al₂O₃ (~3 mL per 10 mL of *cis*-4-nonene)

inside a glove-box. The as-prepared *cis*-4-nonene was used for the preparation of stock solution (~1.0 M) in toluene, using *n*-heptane (~0.1 M) as an internal standard. The solution was stored in a glove-box in an ampoule with a Teflon stopcock.

1-nonene solutions (~1.0 M) were prepared according to the same procedure.

trans- β -methylstyrene and styrene were dried and distilled over CaH₂ (styrene was freshly distilled before use). The neat olefins were further treated according to the procedures above and the *trans*- β -methylstyrene and styrene solutions (~0.2 M) in toluene were prepared with decalin as the internal standard.

Catalytic tests. Catalytic tests were performed inside a glove box. The calculated amount of olefin stock solution was added to the catalyst that was introduced and weighed in a conical base vial containing a wing-shaped magnetic stirring bar. Then, the calculated amount of B(C₆F₅)₃ was added to the mixture of alkene and catalyst (if needed). At $t = 0$, the reaction mixture was started to stir at 600 rpm and kept at 70 °C using an aluminum heating block. 5 μ L aliquots of the solution were sampled, diluted with pure toluene (100 μ L), and quenched by the addition of 1 μ L of wet ethyl acetate after exposing to air. The resulting solution was analyzed by GC/FID (Agilent Technologies 7890 A) equipped with an HP-5 (Agilent Technologies) column. Conversion of *cis*-4-nonene was determined from metathesis products formation, as follows:

$$\text{Conversion of } cis - 4 - nonene = \frac{\sum[\text{metathesis products}]_t}{[\text{substrate}]_{initial}}$$

Conversions of 1-nonene, *trans*- β -methylstyrene or styrene were determined by substrate consumption. In all cases, *cis/trans* isomerizations of nonene and β -methylstyrene were not taken into account. Equilibrium conversion for *cis*-4-nonene is ca. 51% and 1-nonene, *trans*- β -methylstyrene or styrene is ca. 100%, assuming the gas phase products (ethylene or 2-butene) generated could escape from the liquid phase efficiently at 70 °C.

Rates (Mmin⁻¹g⁻¹) of metathesis were determined by:

$$\text{Initial rate of metathesis} = \frac{\Delta c / \Delta t}{m}$$

Δc = product concentration (M) corresponding to Δt

Δt = the time ranges where conversions are below 20 %. i.e. from 3 to 10 min for nonene; from 10 to 30 min for β -methylstyrene and styrene. (If induction period is present, Δt is taken after the induction period at a maximum rate).

m = mass of W (gram) in the catalysts

4.4.4 Reactions of **F6@SiO₂₋₂₀₀** with styrene- α , β -¹³C₂

F6@SiO₂₋₂₀₀ (44 mg, 8.8 μ mol) and B(C₆F₅)₃ (13.5 mg, 26 μ mol, 3 equiv) was loaded in a 10 mL Schlenk followed by the addition of styrene- α , β -¹³C₂ (10 μ L, 88 μ mol, 10 equiv) in toluene. The reaction mixture was heated at 70 °C for 1 h. The supernatant was then removed and the solid residue was rinsed by toluene (2 mL x 5) at 70 °C. Subsequently, the resulting solid was dried under high vacuum (10⁻⁵ mbar).

¹H and ¹³C solid state NMR spectra of the material are given in Figure A.4.17-A.4.18.

4.4.5 Reaction of ¹⁵N-F6@SiO₂₋₂₀₀ with ¹⁵N-py/B(C₆F₅)₃

¹⁵N-F6 and ¹⁵N-F6@SiO₂₋₂₀₀ was synthesized with the same procedures as **F6** and **F6@SiO₂₋₂₀₀**, respectively, using ¹⁵N-labeled pyridine in the synthesis in place of pyridine. ¹⁵N-F6@SiO₂₋₂₀₀ (48.6 mg, 1 equiv) and B(C₆F₅)₃ (14.9 mg, 29 μ mol, 3 equiv) were loaded in a 10 mL Schlenk followed by the addition of toluene (3 mL). The reaction mixture was heated at 70 °C for 15 min followed by the addition of extra ¹⁵N-labeled pyridine (10 μ L, 124 μ mol). The reaction mixture was further heated at 70 °C for 45 min. The supernatant was removed and the residue was washed by toluene (2 mL x 5) at 70 °C. The resulting solid was dried under high vacuum (10⁻⁵ mbar) at room temperature for 5 h.

¹⁵N CP-MAS NMR and IR spectra of the resulting solid are shown in Figure A.4.19 and Figure A.4.20, respectively.

4.5 References

1. Schrock, R. R., Recent Advances in High Oxidation State Mo and W Imido Alkylidene Chemistry. *Chem. Rev.* **2009**, *109*, 3211-3226.
2. Schrock, R. R.; DePue, R. T.; Feldman, J.; Yap, K. B.; Yang, D. C.; Davis, W. M.; Park, L.; DiMare, M.; Schofield, M., Further studies of imido alkylidene complexes of tungsten, well-characterized olefin metathesis catalysts with controllable activity. *Organometallics* **1990**, *9*, 2262-2275.
3. Tsang, W. C. P.; Hultsch, K. C.; Alexander, J. B.; Bonitatebus, P. J.; Schrock, R. R.; Hoveyda, A. H., Alkylidene and Metalacyclic Complexes of Tungsten that Contain a Chiral Biphenoxide Ligand. Synthesis, Asymmetric Ring-Closing Metathesis, and Mechanistic Investigations. *J. Am. Chem. Soc.* **2003**, *125*, 2652-2666.
4. Lopez, L. P. H.; Schrock, R. R., Formation of Dimers That Contain Unbridged W(IV)/W(IV) Double Bonds. *J. Am. Chem. Soc.* **2004**, *126*, 9526-9527.
5. Lopez, L. P. H.; Schrock, R. R.; Müller, P., Dimers that Contain Unbridged W(IV)/W(IV) Double Bonds. *Organometallics* **2006**, *25*, 1978-1986.
6. Arndt, S.; Schrock, R. R.; Müller, P., Synthesis and Reactions of Tungsten Alkylidene Complexes That Contain the 2,6-Dichlorophenylimido Ligand. *Organometallics* **2007**, *26*, 1279-1290.
7. Solans-Monfort, X.; Coperet, C.; Eisenstein, O., Shutting Down Secondary Reaction Pathways: The Essential Role of the Pyrrolyl Ligand in Improving Silica Supported d^0 -ML₄ Alkene Metathesis Catalysts from DFT Calculations. *J. Am. Chem. Soc.* **2010**, *132*, 7750-7757.
8. Coperet, C.; Allouche, F.; Chan, K. W.; Conley, M. P.; Delley, M. F.; Fedorov, A.; Moroz, I. B.; Mougel, V.; Pucino, M.; Searles, K.; Yamamoto, K.; Zhizhko, P. A., Bridging the Gap between Industrial and Well-Defined Supported Catalysts. *Angew. Chem. Int. Ed.* **2018**, *57*, 6398-6440.
9. Copéret, C.; Chabanas, M.; Petroff Saint-Arroman, R.; Basset, J.-M., Homogeneous and Heterogeneous Catalysis: Bridging the Gap through Surface Organometallic Chemistry. *Angew. Chem. Int. Ed.* **2003**, *42*, 156-181.
10. Copéret, C.; Comas-Vives, A.; Conley, M. P.; Estes, D. P.; Fedorov, A.; Mougel, V.; Nagae, H.; Núñez-Zarur, F.; Zhizhko, P. A., Surface Organometallic and Coordination Chemistry toward Single-Site Heterogeneous Catalysts: Strategies, Methods, Structures, and Activities. *Chem. Rev.* **2016**, *116*, 323-421.
11. Copéret, C., Single-Sites and Nanoparticles at Tailored Interfaces Prepared via Surface Organometallic Chemistry from Thermolytic Molecular Precursors. *Acc. Chem. Res.* **2019**, *52*, 1697-1708.
12. Chan, K. W.; Lam, E.; D'Anna, V.; Allouche, F.; Michel, C.; Safonova, O. V.; Sautet, P.; Copéret, C., C-H Activation and Proton Transfer Initiate Alkene Metathesis Activity of the Tungsten(IV)-Oxo Complex. *J. Am. Chem. Soc.* **2018**, *140*, 11395-11401.
13. Blanc, F.; Copéret, C.; Thivolle-Cazat, J.; Basset, J.-M.; Lesage, A.; Emsley, L.; Sinha, A.; Schrock, R. R., Surface versus Molecular Siloxy Ligands in Well-Defined Olefin Metathesis Catalysts: $[(\text{RO})_3\text{SiO}]\text{Mo}(=\text{NAr})(=\text{CH}t\text{Bu})(\text{CH}_2t\text{Bu})$. *Angew. Chem. Int. Ed.* **2006**, *45*, 1216-1220.
14. Lwin, S.; Wachs, I. E., Olefin Metathesis by Supported Metal Oxide Catalysts. *ACS Catal.* **2014**, *4*, 2505-2520.
15. Lavery, D. T.; Rooney, J. J.; Stewart, A., Possible role of hydrido-metal complexes in metathesis, isomerization, dimerization, and polymerization of alkenes. *J. Catal.* **1976**, *45*, 110-113.
16. Amakawa, K.; Wrabetz, S.; Kröhnert, J.; Tzolova-Müller, G.; Schlögl, R.; Trunschke, A., In Situ Generation of Active Sites in Olefin Metathesis. *J. Am. Chem. Soc.* **2012**, *134*, 11462-11473.
17. Bluemel, J., Reactions of Ethoxysilanes with Silica: A Solid-State NMR Study. *J. Am. Chem. Soc.* **1995**, *117*, 2112-2113.
18. Malfait, W. J.; Verel, R.; Koebel, M. M., Hydrophobization of Silica Aerogels: Insights from Quantitative Solid-State NMR Spectroscopy. *J. Phys. Chem. C* **2014**, *118*, 25545-25554.
19. Gunther, W. R.; Michaelis, V. K.; Griffin, R. G.; Román-Leshkov, Y., Interrogating the Lewis Acidity of Metal Sites in Beta Zeolites with ¹⁵N Pyridine Adsorption Coupled with MAS NMR Spectroscopy. *J. Phys. Chem. C* **2016**, *120*, 28533-28544.
20. Moroz, I. B.; Larmier, K.; Liao, W.-C.; Copéret, C., Discerning γ -Alumina Surface Sites with Nitrogen-15 Dynamic Nuclear Polarization Surface Enhanced NMR Spectroscopy of Adsorbed Pyridine. *J. Phys. Chem. C* **2018**, *122*, 10871-10882.

21. ^{15}N chemical shift of py-B(C₆F₅)₃ adduct in C₆D₆ solution is at 233 ppm (see Figure A.4.21), which is lower than that of $^{15}\text{N-F6}$.
22. Parry, E. P., An infrared study of pyridine adsorbed on acidic solids. Characterization of surface acidity. *J. Catal.* **1963**, *2*, 371-379.
23. Busca, G., Spectroscopic characterization of the acid properties of metal oxide catalysts. *Catal. Today* **1998**, *41*, 191-206.
24. Zaki, M. I.; Hasan, M. A.; Al-Sagheer, F. A.; Pasupulety, L., In situ FTIR spectra of pyridine adsorbed on SiO₂-Al₂O₃, TiO₂, ZrO₂ and CeO₂: general considerations for the identification of acid sites on surfaces of finely divided metal oxides. *Colloids Surf. A Physicochem. Eng. Asp.* **2001**, *190*, 261-274.
25. Mayo, F. R., The dimerization of styrene. *J. Am. Chem. Soc.* **1968**, *90*, 1289-1295.
26. Kuroki, T.; Ogawa, T.; Sekiguchi, Y.; Ikemura, T., Vapor-phase dimerization of styrene in the presence of silica-alumina catalyst. *Ind. Eng. Chem. Prod. Res. Dev.* **1983**, *22*, 234-237.
27. Fung, B. M.; Khitrin, A. K.; Ermolaev, K., An Improved Broadband Decoupling Sequence for Liquid Crystals and Solids. *Journal of Magnetic Resonance* **2000**, *142*, 97-101.
28. Hohwy, M.; Rienstra, C. M.; Jaroniec, C. P.; Griffin, R. G., Fivefold symmetric homonuclear dipolar recoupling in rotating solids: Application to double quantum spectroscopy. *J. Chem. Phys.* **1999**, *110*, 7983-7992.
29. Müller, O.; Stötzel, J.; Lützenkirchen-Hecht, D.; Frahm, R., Gridded Ionization Chambers for Time Resolved X-Ray Absorption Spectroscopy. *Journal of Physics: Conference Series* **2013**, *425*, 092010.
30. Koningsberger, D. C.; Prins, R., *X-ray absorption : principles, applications, techniques of EXAFS, SEXAFS, and XANES*. New York : Wiley: 1988.
31. Newville, M., IFEFFIT : interactive XAFS analysis and FEFF fitting. *Journal of Synchrotron Radiation* **2001**, *8*, 322-324.
32. Ravel, B.; Newville, M., ATHENA and ARTEMIS: interactive graphical data analysis using IFEFFIT. *Phys. Scripta* **2005**, *2005*, 1007.
33. Arrowsmith, C. H.; Kresge, A. J., A correlation between .beta.-hydrogen isotope effects on carbon-13 NMR chemical shifts in unsaturated systems and the strength of hyperconjugative interactions. *J. Am. Chem. Soc.* **1986**, *108*, 7918-7920.

Chapter 5. Effects of Preparation Methods and Organosilicon Reductants on the Olefin Metathesis Activity of Silica-supported W(VI)-oxo Species

5.1 Introduction

W(IV) species has been shown to be an active precatalyst for olefin metathesis. Its activity and proposed initiation mechanism have been shown to differ significantly between the homogeneous (as discussed in Chapter 3) and supported systems due to the presence of surface OH groups (as discussed in Chapter 4). These new findings together with a better understanding in the initiation mechanism lead us to further investigate the silica-supported W(VI)-oxo species generated by Surface Organometallic Chemistry (SOMC) approach and extend our studies to classical heterogeneous WO_3/SiO_2 catalyst prepared by incipient wetness impregnation (IWI).

One limitation in the synthesis of the molecularly-defined silica-supported W(VI)-oxo species, by grafting well-defined $\text{WO}_2(\text{OSi}(\text{O}t\text{Bu})_3)_2(\text{DME})$ onto SiO_{2-700} followed by a thermal treatment, is the formation of a 1:1 mixture of surface $(\equiv\text{SiO})_2\text{W}(=\text{O})_2$ and $(\equiv\text{SiO})_4\text{W}(=\text{O})$ species (as discussed in Chapter 2).¹ In addition, the use of organosilicon reductant 2,3,5,6-tetramethyl-1,4-bis(trimethylsilyl)-1,4-diaza-2,5-cyclohexadiene (**Red4**) as the activator leads to the formation of undesirable by-product that can poison the catalyst, despite the promising low-temperature (70 °C) olefin metathesis activity observed.

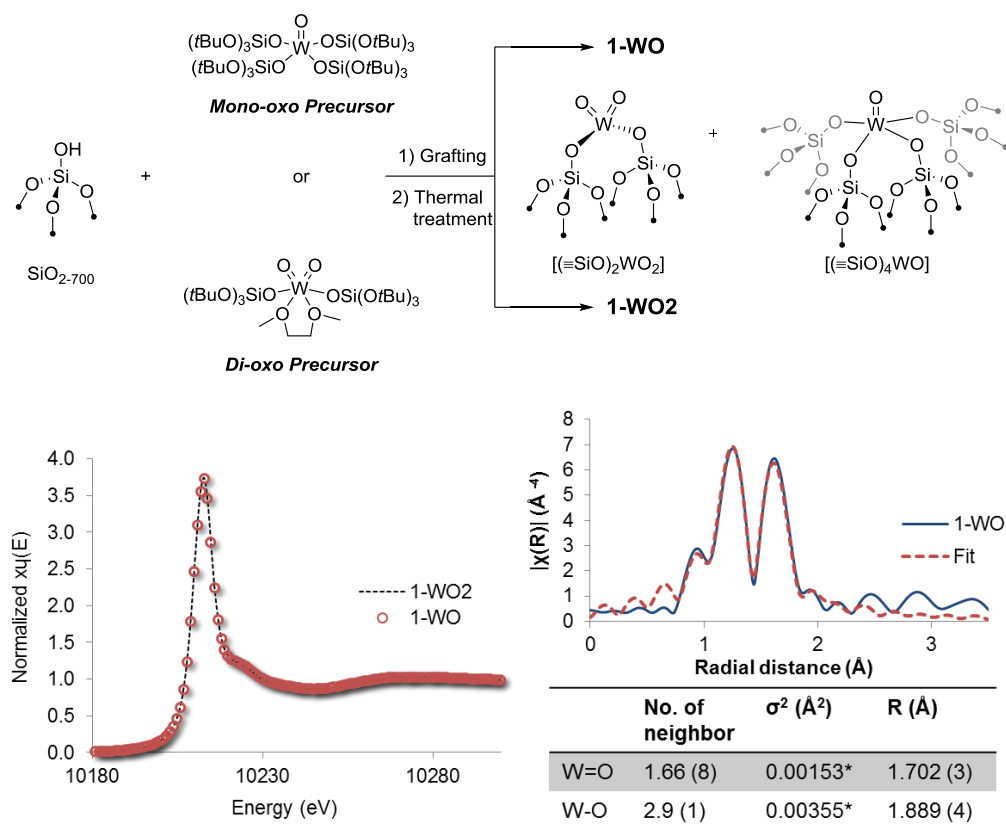
In this chapter, we investigate how different factors including i) the choice of molecular precursors for grafting, ii) the synthetic methods (SOMC vs. IWI) and iii) the organosilicon reductants affect the structures, reactivities and the amounts of active sites in different supported W(VI)-oxo materials.

5.2 Result and Discussion

5.2.1 Effects of Precursors and Preparation Methods on the Structure of Supported W-oxo Species

Tungsten mono-oxo complex $\text{WO}(\text{OSi}(\text{O}t\text{Bu})_3)_4$, which was reported to be a precursor for generating well-dispersed tungsten oxo sites on SBA-15,² was grafted on partially dehydroxylated silica SiO_{2-700} followed by thermal treatment under high vacuum to afford material **1-WO**. W L_{III} edge X-ray absorption near edge structure (XANES) spectroscopy

shows that **1-WO** and **1-WO2**, synthesized from $\text{WO}_2(\text{OSi}(\text{OtBu})_3)_2(\text{DME})$ molecular precursor using the same approach, share identical white line energies and similar spectroscopic features. In addition, extended X-ray absorption fine structure (EXAFS) fitting analysis suggests that **1-WO** also contains ca. 1:1 mixture of $[(\equiv\text{SiO})_2\text{WO}_2]$ and $[(\equiv\text{SiO})_4\text{WO}]$, as previously found for **1-WO2** (Scheme 5.1). In both cases, no W–W scattering path (typically at ca. 3.7 Å for bulk WO_3) is found, confirming the formation of isolated W(VI) oxo species independently of the molecular precursor. The formation of both mono- and di-oxo surface species, starting from either the mono- or di-oxo molecular precursors, clearly indicates that the surface species re-structures under thermal treatment condition with the presence of H_2O produced during the thermolysis of the $(t\text{BuO})_3\text{SiO}$ ligands.



Scheme 5.1. Characterization of surface species in **1-WO** and **1-WO2** by W L_{III} edge X-ray Absorption Spectroscopy.

In addition, WO_3/SiO_2 (**2**) was prepared through incipient wetness impregnation of ammonium tungstate solution on SiO_2 with similar W loading (3.26 wt%) as in **1-WO** and **1-WO2**. Powder XRD (Figure A.5.4) shows the absence of crystalline tungsten oxide on the surface of **2**. W L_{III} edge XANES of **2** is very similar to that of **1-WO** or **1-WO2** while the

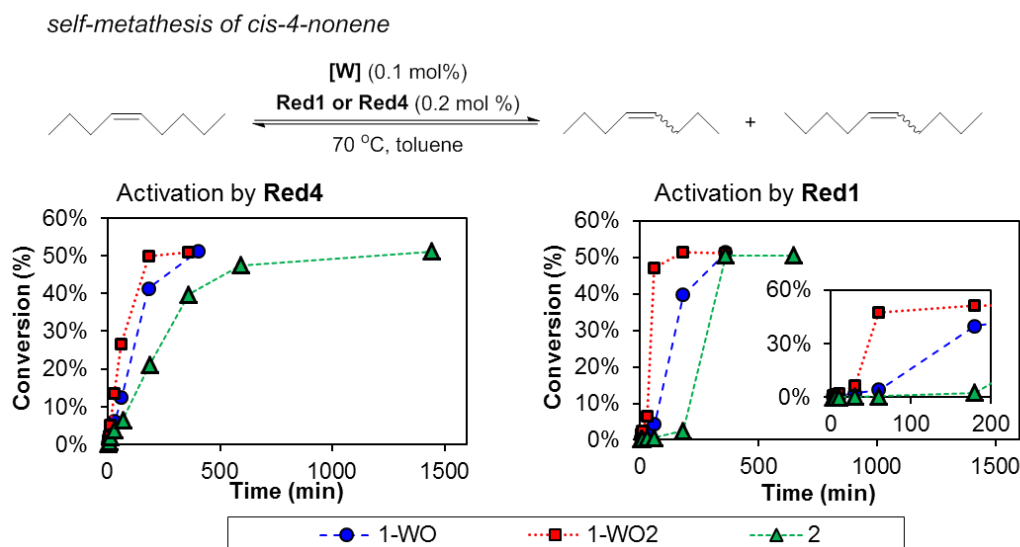
white line energy of **2** is 0.1 eV higher in energy. EXAFS fitting analysis suggests the absence of W–W scattering path in **2** as well (Figure A.5.3), consistent with the presence of isolated W centers in **2** as previously reported.³ The isolated nature of W sites is further supported by UV-vis diffuse reflectance spectra (UV-DRS) of **2**, which reveals an electronic edge energy (E_g) of 4.0 eV (Figure A.5.6) consistent with distorted isolated tungstate species.⁴ Based on the no. of W=O and W–O neighbors obtained from EXAFS fitting (Table A.5.2), **2** also consists of ca. 1:1 mixture of $[(\equiv\text{SiO})_2\text{WO}_2]$ and $[(\equiv\text{SiO})_4\text{WO}]$, similar to the material prepared via SOMC approach.

5.2.2 Effects of Reductants on the Catalytic Activities of W-oxo Species Prepared by Different Approaches

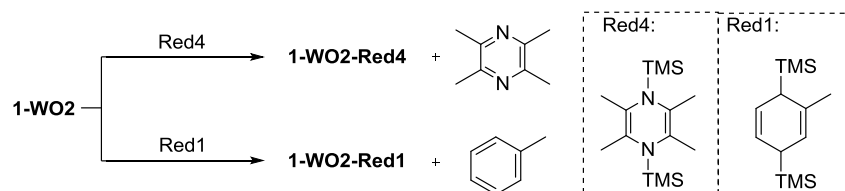
Self-metathesis of *cis*-4-nonene catalyzed by in-situ activated **1-WO** and **2** was investigated (Scheme 5.2). Two equivalents of organosilicon reagents per [W] were added to the catalysts in the presence of *cis*-4-nonene (1.0 M toluene solution; 1000 equiv per [W]) solution at 70 °C. In the case of the in-situ activated **1-WO** by 2,3,5,6-tetramethyl-1,4-bis(trimethylsilyl)-1,4-diaza-2,5-cyclohexadiene (**Red4**), equilibrium conversion of *cis*-4-nonene (51 %) was reached within ca. 6.5 h, which is longer than what was found for **1-WO2** (3 h). When **2** is used as a catalyst precursor, a much longer time (24 h) is required for reaching equilibrium conversion under the same reaction conditions. These results indicate that **2** is notably less “active” than the materials prepared by SOMC when comparing the time required to reach equilibrium, despite their similarity in XAS signature and EXAFS fitting analysis. Since 2,3,5,6-tetramethylpyrazine, released upon activation with **Red4**, can reversibly or irreversibly poison some of the active sites by coordinating to the unsaturated metal centers, we investigated the use of an alternative activator, i.e. 1-methyl-3,6-bis(trimethylsilyl)-1,4-cyclohexadiene (**Red1**) (Scheme 5.3), that only releases toluene-based by-products.

1-WO2 in-situ activated with **Red1** leads to 47 % conversion of the *cis*-4-nonene within 1 h (vs. 27 % in the case of **Red4**), while the overall activity (time to equilibrium) is similar for **1-WO** with both reductants (Scheme 5.2; Table 5.1). Notably, short induction periods were observed during the activation by **Red1** for both **1-WO2** and **1-WO**. Although in-situ activation of **2** with **Red1** reduces the time to equilibrium conversion for *cis*-4-nonene metathesis from 24 to 6 h, a long induction period (ca. 3 h) was observed. Such induction periods were not observed when **Red4** was used as the activator for the reaction described above. This may be related to the fact that **Red4** is a stronger reductant than **Red1**.⁵⁻⁶ However, despite the observed induction period for **Red1**, the in-situ activated materials

allow a faster conversion to equilibrium at 0.1 mol% catalyst loading compared to **Red4**. It is consistent with the poisoning of active sites in the presence of 2,3,5,6-tetramethylpyrazine, a side product from **Red4**. The particularly long induction period observed for **2** indicates that **2** is significantly less reducible than **1-WO** or **1-WO2**.



Scheme 5.2. Catalytic activities of **1-WO**, **1-WO2** and **2** in self-metathesis of *cis*-4-nonene via in-situ activation.



Scheme 5.3. Preparation of activated catalysts with **Red1** and **Red4**.

In order to better understand the difference between the activated species generated upon using **Red1** versus **Red4**, we investigated the (ex-situ) activated systems **1-WO2-Red1** and **1-WO2-Red4** (Scheme 5.3) that were prepared by treating **1-WO2** at 70 °C for 12 h in benzene with 2 equiv of **Red1** and **Red4**, respectively.

With these pre-reduced species, the self-metathesis of *cis*-4-nonene (1000 equiv per [W]) reaches equilibrium conversion within 3 h at 70 °C with **1-WO2-Red1** (Figure A.5.7), while 12 h is required for **1-WO2-Red4** under the same reaction conditions (Table 5.1). In addition, no induction period is observed with **1-WO2-Red1** in contrast to what is observed with **1-WO2-Red4**. This result further supports that the 2,3,5,6-tetramethylpyrazine, formed as a by-product from **Red4** in **1-WO2-Red4**, competes with the coordination of *cis*-4-nonene

leading to the induction period. Increasing the amount of *cis*-4-nonene to 5000 equiv per W leads to equilibrium conversion in 28 h with **1-WO2-Red1** (Figure A.5.8) while no activity is observed for **1-WO2-Red4**.

Table 5.1. Catalytic activities of the in-situ activated catalysts and (ex-situ) activated **1-WO2** by both **Red1** and **Red4**^a

Materials	Substrate	TOF _{5min} ^b /min	Time to equil. ^c /h
<i>in-situ activation with Red4</i>			
1-WO	4-nonene ^d	3.0	6.5
1-WO2	4-nonene ^{d,h}	4.6	3
2	4-nonene ^d	1.4	24
<i>in-situ activation with Red1</i>			
1-WO	4-nonene ^d	1.0	4 % ^{1h} ; 6
1-WO2	4-nonene ^d	3.1	47 % ^{1h} ; 3
2	4-nonene ^d	0 ^f	1 % ^{1h} ; 6
<i>ex-situ activation of 1-WO2</i>			
1-WO2-Red4	4-nonene ^{d,h}	0 ^f	12
	1-nonene ^{e,h}	2.0	59 % ^{24h}
	Styrene ^g	0 ^f	2% ^{1h}
1-WO2-Red1	4-nonene ^d	16.5	3
	1-nonene ^e	4.0	88 % ^{24h}
	Styrene ^g	0.3	40% ^{1h}

^a1.0 M toluene solution (0.2 M toluene solution for styrene), batch reactor, 70 °C; ^bTOF is expressed as initial TOF in min⁻¹ after 5 min of reaction; ^cTime for reaching equilibrium conversion unless otherwise noted by giving the conversion after 1 or 24 h; ^d*cis*-4-nonene 1000 equiv per [W]; ^e100 equiv per [W]; ^fInduction period was present; ^g50 equiv per [W]; ^hvalues reported in ref 1.

The metathesis conversion of terminal alkene, 1-nonene and styrene, by **1-WO2-Red1** is also higher than that found with **1-WO2-Red4** (Table 5.1, Figure A.5.9-A.5.10). A similar behavior is also observed for propylene metathesis under flow condition at 70 °C, in which **1-WO2-Red1** leads to a much higher conversion compared to **1-WO2-Red4** (Figure A.5.11). The significant difference in metathesis observed in these activated systems supports the poisoning effect of 2,3,5,6-tetramethylpyrazine. In fact, adding 0.5 equiv of 2,3,5,6-

tetramethylpyrazine per W centers to **1-WO2-Red1**, which mimic the composition in **1-WO2-Red4**, induces a short induction period prior to metathesis conversion of *cis*-4-nonene (Figure A.5.12).

5.2.3 Origins of the Difference in Activities between Various Systems

Apart from the effects of reductants, materials prepared by IWI (**2**) and SOMC (**1-WO** or **1-WO2**) also demonstrated significant difference in their metathesis activities. To investigate the origins of their difference, we decided to i) study and compare the activated **2** and **1-WO2** by W L_{III} edge XANES, ii) investigate the effects of thermal treatments and iii) quantify the amount of metathesis active alkylidenes formed in different materials.

As shown in Figure 5.1, the white line energies in W L_{III} edge XANES of all the activated materials are lower than their corresponding as-synthesized materials **1-WO2** or **2** indicating the reduction of W centers upon activation. Both **2** and its activated materials (by **Red4** and **Red1**, namely **2-Red4** and **2-Red1**, respectively) show higher white line energies than the corresponding **1-WO2** and its activated version indicating that the materials prepared by IWI are less reduced under the same conditions. This is consistent with the long induction period observed for **2** during its in-situ activation by **Red1** implying its lower reducibility (Scheme 5.2). This result also suggests that in **2-Red4** and **2-Red1**, the overall oxidation state of W centers are higher and the amounts of reduced species are less than that in **1-WO2-Red4** and **1-WO2-Red1**, respectively. It is worth noting that comparison of the white line energies between materials activated by **Red1** and **Red4** does not provide a direct correlation to the amount of reduced species in these materials since the coordination of 2,3,5,6-tetramethylpyrazine to the W centers in the **Red4** activated materials would also affect the white line energies.⁷⁻⁸

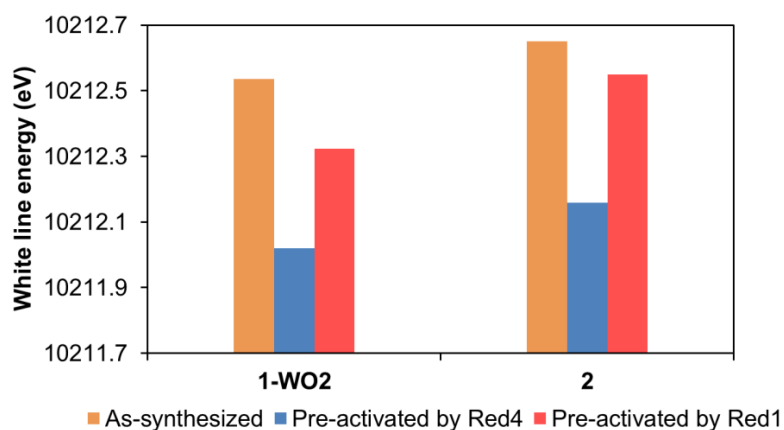


Figure 5.1. White line energies of the different materials in W L_{III} edge.

We wonder whether the difference in reducibility between **2** and **1-WO2** could only be due to the difference in thermal treatment steps between the two preparation methods. The preparation of **2** involves calcination under synthetic air at 500 °C, while **1-WO2** involves thermolysis under high vacuum at 400 °C. Therefore, we prepared **1-WO2-SA500** by grafting $\text{WO}_2(\text{OSi}(\text{OtBu})_3)_2(\text{DME})$ on SiO_{2-700} followed by calcination under synthetic air at 500 °C and investigated its activity towards self-metathesis of *cis*-4-nonene via in-situ activation with **Red1** and **Red4**. In-situ activation of **1-WO2-SA500** by **Red1** has an induction period of ca. 3 h, which is much longer than **1-WO2** and similar to that of **2** (Figure 5.2), indicating that calcination under synthetic air results in less reducible catalysts. Besides, **1-WO2-SA500** in-situ activated by **Red4** also shows a lower activity with a longer time to reach equilibrium conversion compared to that of **1-WO2** suggesting that calcination under synthetic air leads to less active catalyst (or catalyst that is harder to be activated), thus explaining the significantly lower activity observed for **2** vs. **1-WO2** or **1-WO**.

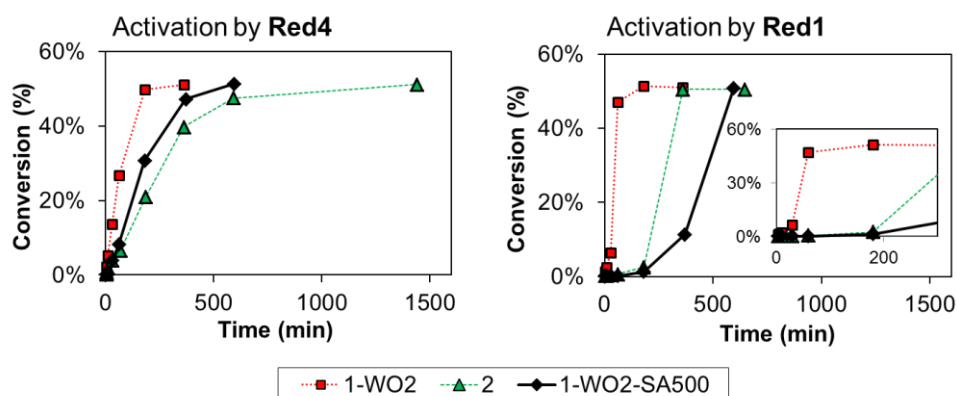
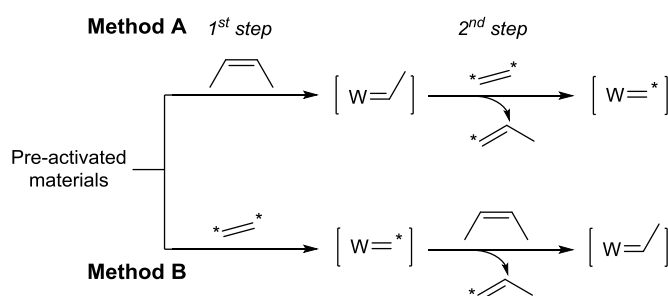


Figure 5.2. Catalytic activities of **1-WO2**, **2** and **1-WO2-SA500** in self-metathesis of *cis*-4-nonene via in-situ activation by **Red4** (left) and **Red1** (right).

While the types of reductants and the preparation methods clearly affect the overall catalytic behavior, i.e. the presence or absence of induction period and the time to reach equilibrium conversion, it is not clear how these parameters influence the amounts of metathesis active alkylidenes formed in these different materials. We thus evaluated the amounts of alkylidenes generated in the activated materials by cross-metathesis using two different methods (Scheme 5.4 and the results are summarized in Table 5.2). Method A consists of contacting the material with *cis*-2-butene at 70 °C for 12 h in a 1st step, followed by the removal of gaseous products and reaction of the solid in a 2nd step with ¹³C-dilabeled ethene at 70 °C for 12 h. Method B consists of contacting the material with ¹³C-dilabeled

ethene at 70 °C for 12 h in a 1st step, followed by the removal of gaseous products and reaction of the solid in a 2nd step with *cis*-2-butene at 70 °C for 12 h. These stepwise cross-metathesis reactions were monitored by GC/MS with the gas phase collected after the 1st and 2nd steps. Under these conditions, the amounts of ¹³C-mono-labeled propene formed via cross-metathesis allow evaluating the amount of alkylidenes, while the other products can provide information related to the initiation and deactivation pathways, as well as possible resting states species.



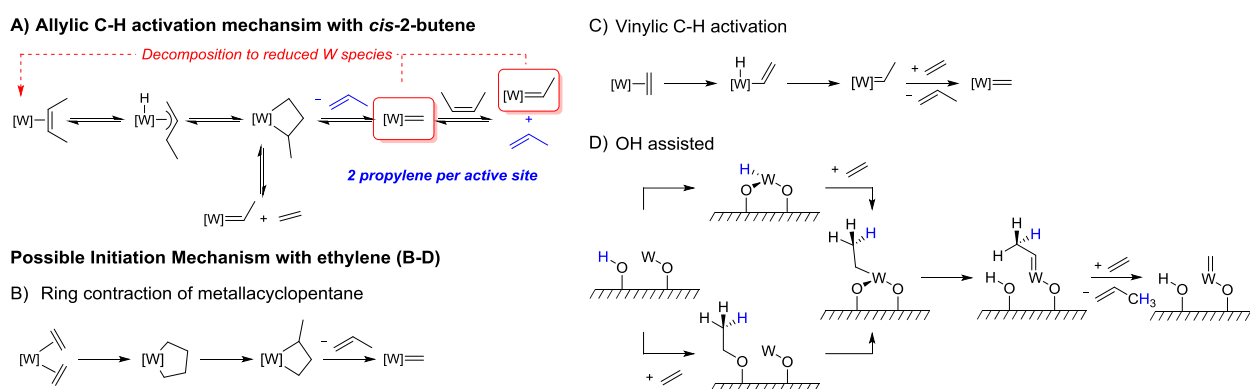
Scheme 5.4. Two different titration methods used for quantifying the amounts of alkylidenes formed by the activated materials (Method A and Method B).

Table 5.2. Amounts of various gaseous products observed in the titration of different activated materials.^a

Activated materials	Olefin formed in 1 st step: Amount	Olefin formed in 2 nd step: Amount	¹³ C isotope labeling distribution of propene ^b
<i>Method A</i>			
1-WO2-Red1	C3: 4.3 C5: 1.4	C3: 0.3	^{un} C3: 0.033 ^{mono} C3: 0.084 ^{di} C3: 0.18
<i>Method B</i>			
1-WO2-Red1	C3: 0.95	C3: 0.67 C5: 0.26	^{un} C3: 0.63 ^{mono} C3: 0.029
1-WO2-Red4	C3: 0.24	C3: 0.36 C5: 0.16	^{un} C3: 0.33 ^{mono} C3: 0.023
2-Red1	C3: 0.24	C3: 0.87 C5: 0.12	^{un} C3: 0.85 ^{mono} C3: 0.019
2-Red4	C3: 0.047	C3: 0.33 C5: 0.17	^{un} C3: 0.31 ^{mono} C3: 0.017

^aQuantification is performed by GC-FID; C_x refers to olefin with x number of carbons; all the values are reported in equivalent per W center. ^bAnalyzed by GC-MS; ^{un}C₃, ^{mono}C₃ and ^{di}C₃ refers to un-, ¹³C-mono- and ¹³C-di-labeled propene, respectively.

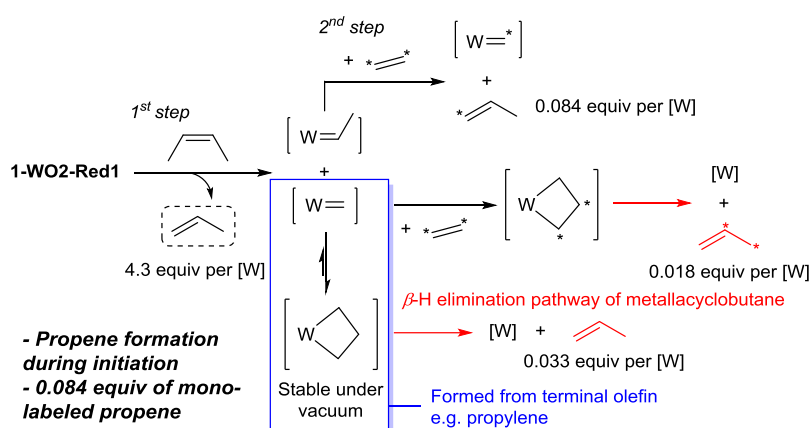
Titration of **1-WO2-Red1** were performed with Methods A and B. With Method A, analysis of the gas phase after the 1st step indicates the formation of 4.3 equiv of propene (per W) along with a small amount of C5 olefins (Table 5.2). The latter is likely formed via secondary reactions such as cross-metathesis of 2-butenes and 1-butenes. The formation of propene from *cis*-2-butene is consistent with the initiation involving an allylic C–H activation mechanism (Scheme 5.5.A), as proposed in the molecular (Chapter 3) or supported W(IV) systems (Chapter 4).



Scheme 5.5.A. Allylic C–H activation mechanism with *cis*-2-butene. **5.5.B.** Ring contraction of metallacyclopentane. **5.5.C.** Vinylic C–H activation mechanism. **5.5.D.** OH assisted initiation mechanism.

However, the large amount of observed propene, exceeding 2 equiv per W, indicates that other (catalytic) processes took place. For instance, alkylidene or metallacyclobutane complexes can transform back into olefin complexes,⁹⁻¹³ which can in turn be a source of alkylidene and metallacyclobutane intermediates again as shown in Scheme 5.5.A. Such process would lead to a catalytic production of propene and infer that the measured quantity of propene formed correspond to a “cumulated” number of alkylidene species rather than a defined number of alkylidene per total W! In the 2nd titration step (cross-metathesis with ¹³C-di-labeled ethene), 0.3 equiv of propene was observed (per W) that consists of 0.033 equiv of un-labeled, 0.084 equiv of ¹³C-mono-labeled and 0.18 equiv of ¹³C-di-labeled propene, while other olefins are formed in negligible amount (< 1 % of the gas phase products). The ¹³C-mono-labeled propene likely results from the cross-metathesis between ¹³C-di-labeled ethene and W=CHMe, while the un-labeled and ¹³C-di-labeled propene likely result from the decomposition of unsubstituted unlabeled and ¹³C-di-labeled metallacyclobutane, respectively (Scheme 5.6). The former likely arises from the presence of residual metallacyclobutane

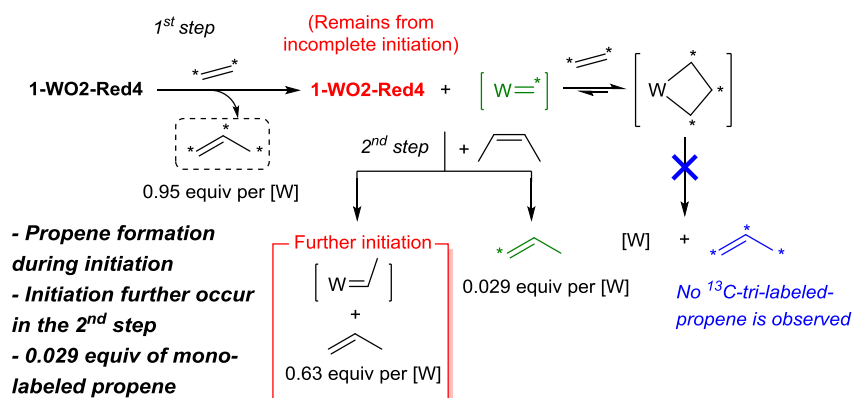
formed in the 1st step because of its high stability, while the latter formed from the reaction of un-labeled surface methyldiene with ¹³C-di-labeled ethylene. These metallacyclobutane species can be converted into propene and a reduced W(IV) species directly via a well-known β -H elimination pathway.¹³⁻¹⁴ These results suggest that the amount of metathesis active intermediates formed can be as much as 0.3 equiv per W based on the proposed reaction pathways; the lowest amount based on counting solely ¹³C-mono-labeled propene being 0.084 equiv per W.



Scheme 5.6. Titration results of **1-WO2-Red1** by Method A and the putative intermediates involved.

As shown in Table 5.2, titration of alkylidene species in **1-WO2-Red1** with Method B (reaction with ¹³C-dilabeled ethene first) leads to the formation of 0.95 equiv propene per W center in the 1st step. The formation of propene from ethene can be a result of initiation involving the following mechanisms: the ring contraction of unsubstituted metallacyclopentane (Scheme 5.5.B), the vinylic C–H activation of ethylene (Scheme 5.5.C) or the OH assisted mechanism (Scheme 5.5.D). However, DFT studies on molecular analogues have shown that ring contraction of metallacyclopentane to metallacyclobutane and vinylic C–H activation have very high energy barriers (see Appendix for details), while OH-assisted mechanism is favored based on a recent experimental study on the supported W(IV) catalyst (see Chapter 4 for more details). Therefore, it is likely that propene is formed from cross-metathesis of ethylene and W=CHMe, which is generated via OH assisted mechanism from ethylene (Scheme 5.5.D). Apart from the initiation step, propene can also be produced once the methyldiene W=CH₂ is formed. Reaction of W=CH₂ with ethene yields unsubstituted metallacyclobutane, which can directly convert into propene and reduced W(IV) as discussed above and Scheme 5.6. Initiation and decomposition of metallacyclobutanes could take place consecutively leading to the catalytic production of propene. After the 2nd

step (cross-metathesis of surface species with 2-butene), propene is formed along with a small amount of C5 olefins (Table 5.2). The propene is mostly un-labeled (95 %) with only 0.029 equiv of ^{13}C -mono-labeled propene per W! The large amount of un-labeled propene is likely a result of the initiation of W centers with *cis*-2-butene via allylic C–H activation mechanism, as discussed above (Scheme 5.5.A). This result implies that additional alkylidenes are generated upon contacting with 2-butene because some of the W sites were not activated by ethene in the 1st step (Scheme 5.7). The ^{13}C -mono-labeled propene likely results from the cross-metathesis between *cis*-2-butene and the ^{13}C -labeled $\text{W}=\text{CH}_2$ generated via the 1st step, indicating the formation of 0.029 equiv of propagating alkylidenes upon contact with ^{13}C -dilabeled ethene. However, we cannot exclude that ^{13}C -mono-labeled propene also arise from the cross-metathesis of *cis*-2-butene and ^{13}C -di-labeled ethylene, released from the stable metallacyclopentane formed at the 1st step.¹



Scheme 5.7. Titration results of **1-WO2-Red1** by Method B and the putative intermediates involved

In short, the quantities of alkylidenes in **1-WO2-Red1** obtained by Method A range between 8.4 % and 30 % of the W centers, illustrating the complexity of initiation on reduced W(IV) species. Method B gives a significantly smaller amount of alkylidene sites (2.9 %); it shows in particular that initiation via an allylic C–H activation (probed by Method A) is more efficient than via the OH assisted mechanism (probed by Method B) that take places for substrate without allylic CH group. Lastly, while the quantity of alkylidenes is related to the number of active sites, these two values are likely not identical since the active sites are constantly generated (W(IV) to W(VI) alkylidene) and decomposed (W(VI) alkylidene to W(IV)) as suggested by the data above.

Titrations of the other activated materials by using Method B show similar observations as in **1-WO2-Red1**. Formation of propene was observed in the 1st step and most

of the propene detected in the 2nd step upon contacting *cis*-2-butene was non-labeled (Table 5.2) indicating the formation of additional active species via the allylic C–H activation of 2-butene as discussed above. The amounts of alkylidenes obtained by counting ¹³C-mono-labeled propene correspond to ca. 2 – 3 % of W centers under these conditions. Comparing the amounts of ¹³C-mono-labeled propene (Table 5.2) in different activated materials using the same titration method indicates that the amounts of alkylidenes vary as follows **1-WO2-Red1** > **1-WO2-Red4** > **2-Red1** > **2-Red4**. This trend is consistent with the catalytic behavior observed in the in-situ activation experiments.

5.3 Conclusion

In summary, we have shown that the use of WO(OSi(*O*tBu)₃)₄ molecular precursor for generating silica-supported W-oxo species via grafting and thermal treatment under high vacuum leads to the same surface species generated by using WO₂(OSi(*O*tBu)₃)₂(DME) indicating surface species re-structures under thermal treatment condition that leads to the formation of water. In addition, isolated surface W-oxo species with similar structures can be obtained by IWI according to EXAFS. All of these materials can be activated by tailored organosilicon reductants **Red1** at 70 °C and they demonstrate a better catalytic performance compared to those activated by **Red4**. Notably, the catalyst prepared by IWI shows a longer induction period with a lower activity compared to those prepared by SOMC approach, which is attributed to its lower reducibility as indicated by the white line energies in the W L_{III} edge XANES. Calcination under synthetic air results in W(VI)-oxo species with lower reducibility compared to thermal treatment under high vacuum. Quantification of the active alkylidenes generated in different materials further supports that the amounts of active catalysts in the material prepared by impregnation is smaller than that by SOMC, which is in line with their reducibility. However, it is clear that various competitive reaction pathways including initiation and decomposition occurred simultaneously during the titration experiments, which lead to a strong dependence of the titration results on the experimental conditions, such as the olefins used and their order of addition. Therefore, it should be noted that comparison of the titration results is only possible when they are obtained under exactly the same titration condition, and more importantly, with isotopic labeling, which is the only way to track and differentiate the formation pathways of different olefin products. This study demonstrates the effects of preparation methods, conditions and organosilicon reductants on the catalytic performance of silica-supported W(VI)-oxo species. In addition, the reaction pathways

involved and the complexity in cross-metathesis titration methods for quantifying the amounts of active alkylidenes in supported metal-oxo systems have been investigated in detail.

5.4 Experimental Details

5.4.1 General procedures

All experiments were carried out under dry and oxygen free argon atmosphere using either standard Schlenk or glove-box techniques for organometallic synthesis. For the syntheses, reactions were carried out using high vacuum lines (10^{-5} mbar) and glove-box techniques. Pentane, toluene and diethyl ether were purified using double MBraun SPS alumina column, and were degassed using three freeze-pump-thaw cycles before being used. DME and THF were distilled from Na/Benzophenone. Silica (Aerosil Degussa, $200 \text{ m}^2 \cdot \text{g}^{-1}$) was compacted with distilled water, calcined at $500 \text{ }^\circ\text{C}$ ($5 \text{ }^\circ\text{C}/\text{min}$) under air for 10 h and treated under vacuum (10^{-5} mbar) at $500 \text{ }^\circ\text{C}$ ($1 \text{ }^\circ\text{C}/\text{min}$) for 10 h and then at $700 \text{ }^\circ\text{C}$ ($1 \text{ }^\circ\text{C}/\text{min}$) for 20 h. The amounts of OH per g were measured by titration with PhCH_2MgCl . All infrared (IR) spectra were recorded using a Bruker α -T spectrometer placed in an Ar glovebox, equipped with OPUS software. A typical experiment consisted in the measurement of transmission in 32 scans in the region from 4000 to 400 cm^{-1} . The solution spectra were recorded in C_6D_6 at room temperature. The electronic structures of the catalysts were obtained with a Varian Cary UV-vis spectrophotometer employing a Praying Mantis integration sphere. The UV-vis spectra were processed with Microsoft Excel software, consisting of calculation of the Kubelka-Munk function, $F(R_\infty)$, which was extracted from the UV-vis DRS absorbance. The edge energy (E_g) for allowed transitions was determined by finding the intercept of the straight line in the low-energy rise of a plot of $[F(R_\infty)h\nu]^2$.⁴ Powder XRD experiments were performed on a STOE Padi Diffractometer in Debye-Scherrer Mode (2θ) with a Dectris Mythen 1K area detector using $\text{Cu K}\alpha 1$ radiation. The sample was prepared and measured in a sealed quartz capillary. XAS measurements were carried out at the W L_{III} edge at the SuperXAS beamline at SLS (PSI, Villigen, Switzerland). The storage ring was operated at 2.4 GeV in top-up mode with a ring current of around 400 mA . The incident photon beam provided by a 2.9 T super bend magnet source was selected by a Si (111) quick-EXAFS monochromator and the rejection of higher harmonics and focusing were achieved by a rhodium-coated collimating mirror at 2.8 mrad and a rhodium-coated torroidal mirror at 2.8 mrad . The beam size on the sample was $100 \times 100 \text{ }\mu\text{m}$. During measurements the monochromators was rotating with 10 Hz frequency in 2 deg angular range and X-ray absorption spectra were collected in transmission mode using ionization chambers specially developed for quick data collection with 1 MHz frequency.¹⁵ The spectra were collected for 2 min and averaged. Calibration of the beamline energy was performed using W reference foil (W L_{III} -edge position at 10207 eV , respectively). To avoid contact with air, all samples were

sealed in a glovebox. For ex situ samples, pressed pellets (with optimized thickness for transmission detection) were placed in two aluminized plastic bags (Polyaniline (15 μm), polyethylene (15 μm), Al (12 μm), polyethylene (75 μm) from Gruber-Folien GmbH & Co. KG, Straubing, Germany) using an impulse sealer inside a glovebox; one sealing layer was removed immediately before the measurements. Data were analyzed by standard procedures¹⁶ using Ifeffit program package¹⁷⁻¹⁸. S_0^2 values were obtained by fitting W foil for W L_{III} edge. Elemental analyses were performed by the “Mikroanalytisches Labor Pascher” in Remagen, Germany.

$[\text{W}(\text{O})(\text{OSi}(\text{OtBu})_3)_4]$,² **1-WO2**,¹ **1-WO2-Red4**,¹ WO_3/SiO_2 (2),³ 1-methyl-3,6-bis(trimethylsilyl)-1,4-cyclohexadiene (**Red1**)¹⁹ and 2,3,5,6-tetramethyl-1,4-bis(trimethylsilyl)-1,4-diaza-2,5-cyclohexadiene (**Red4**)⁵ were synthesized according to literature procedures.

5.4.2 Synthesis of 1-WO

A solution of 0.17 g of $\text{W}(\text{O})(\text{OSi}(\text{OtBu})_3)_4$ (0.14 mmol, 1 equiv.) in benzene (3 mL) was added to a suspension of SiO_{2-700} (0.52 g, 0.14 mmol, 1 equiv.) in benzene (1 mL) at room temperature. The suspension was slowly stirred at room temperature for 6 h. The white solid was collected by filtration, and was washed by five suspension/filtration cycles in benzene (5 x 2 mL). The resulting solid was dried thoroughly under high vacuum (10^{-5} mbar) at room temperature for 3 h and loaded into a reactor, which then placed under high vacuum (10^{-5} mbar) and heated to 200 °C (1 °C/min) and held at this temperature for 3 h followed by increasing to 400 °C (1 °C/min) and held at this temperature for 6 h. The reactor was cooled to ambient temperature under vacuum, and **1-WO** was stored in an Ar filled glovebox.

Elemental analysis: W 2.16 %.

IR spectrum and EXAFS fitting analysis of the material are given in Figure A.5.1, A.5.2 and Table A.5.1., respectively.

5.4.3 Synthesis of 1-WO2-Red1

1-WO2-Red1 was synthesized according to the reported procedures¹ by using 2 equiv (per W center) of **Red1**.

Elemental analysis: W 2.93 %, C 0.69 %, H 0.36 % corresponding to 3.6 C/W and 22.6 H/W.

IR spectrum of the material is given in Figure A.5.1.

5.4.4 Synthesis of 1-WO2-SA500

500 mg of **1-WO2** was loaded into a flow reactor, which then heated to 500 °C (1 °C/min) for 340 min under flow of synthetic air on the high vacuum line. Then, the reactor

was cooled to ambient temperature under vacuum, and **1-WO2-SA500** was stored in an Ar filled glovebox.

5.4.5 Catalytic activity measurements

Starting materials. *Cis*-4-nonene (> 97%) and 1-nonene (> 99.5%) were purchased from TCI Chemicals. Styrene (99.5%) was purchased from ABCR. HPLC grade toluene, heptane and decalin were distilled from Na/benzophenone, degassed by 3 freeze-pump-thaw cycles, and stored in a glove-box over Selexsorb. Al₂O₃ was dried at 250 °C in high vacuum overnight. Molecular sieves were activated at 300 °C in high vacuum overnight. BASF Selexsorb® CD 1/8'' was calcined at 550 °C in air for 12 h and heated in high vacuum at 500 °C for 2 h.

Preparation of olefin stock solutions. *Cis*-4-nonene was stirred at room temperature with Na overnight, distilled in vacuo, degassed by 3 freeze-pump-thaw cycles, and stored in the glovebox over 3 Å MS. Before the preparation of stock solution, neat *cis*-4-nonene was treated with Selexsorb (~20–30% w/w) for 5 hours, followed by the removal of Selexsorb and then passed through a pad of activated neutral Al₂O₃ (~3 mL per 10 mL of *cis*-4-nonene) inside a glove-box. The as-prepared *cis*-4-nonene was used for the preparation of stock solution (~1.0 M) in toluene, using *n*-heptane (~0.1 M) as an internal standard. The solution was stored in a glove-box in an ampoule with a Teflon stopcock.

1-nonene solutions (~1.0 M) were prepared according to the same procedure.

Styrene were dried and distilled over CaH₂ (styrene was freshly distilled before use). The neat olefins were further treated according to the procedures above and styrene solutions (~0.2 M) in toluene were prepared with decalin as the internal standard.

Catalytic tests. Catalytic tests were performed inside a glove box. The calculated amount of olefin stock solution was added to the catalyst that was introduced and weighed in a conical base vial containing a wingshaped magnetic stirring bar. Then, the calculated amount of organosilicon reductant was added to the mixture of alkene and catalyst (if needed). At $t = 0$, the reaction mixture was started to stir at 600 rpm and kept at 70 °C using an aluminum heating block. 5 µL aliquots of the solution were sampled, diluted with pure toluene (100 µL), and quenched by the addition of 1 µL of wet ethyl acetate after exposing to air. The resulting solution was analyzed by GC/FID (Agilent Technologies 7890 A) equipped with an HP-5 (Agilent Technologies) column. Conversion of *cis*-4-nonene was determined from metathesis products formation, as follows:

$$\text{Conversion of } cis - 4 - nonene = \frac{\sum[\text{metathesis products}]_t}{[\text{substrate}]_{\text{initial}}}$$

Conversions of 1-nonene and styrene were determined by substrate consumption. In all cases, *cis/trans* isomerizations of nonene was not taken into account. Equilibrium conversion for *cis*-4-nonene is ca. 51% and 1-nonene or styrene is ca. 100%, assuming the gas phase products (ethylene) generated could escape from the liquid phase efficiently at 70 °C.

Propene metathesis at 70 °C. 20 mg of the selected catalyst (**1-WO2-Red1** or **1-WO2-Red4**) was loaded into a quartz capillary flow cell in the glove box. The quartz flow reactor was then connected to a MFC setup, and the connections were flushed with N₂:propene 2.6:1 mixture (in mLmin⁻¹) for 30 min. The flow rate of the N₂:propene 2.6:1 mixture was then set to 16 mL.min⁻¹, 1 bar (66.9 mol propene/mol W/min⁻¹) and the temperature was set to 70 °C. The opening of the valve connecting the reactor to the gas line corresponds to the beginning of the catalytic test. The reaction was monitored by on-line micro GC. TONs (calculated by assuming all the W sites are active) are presented in Figure A.5.11.

5.4.6 Titration experiments with ethene and 2-butene

Representative procedures for titration. Method A. The activated material (ca. 50 mg) was loaded in a 26 mL glass reactor and contacted with butene (10 equiv. per W metal center). After 12 h at 70 °C, the gas phase was analyzed by GC-FID. The material was then evacuated under high vacuum (10⁻⁵ mbar) for 3 h followed by contacting with ¹³C-dilabeled ethene (1 equiv. per W metal center). The reaction mixture was heated at 70 °C for 12 h and the gas phase was analyzed by GC-FID and GC-MS. *Method B* was carried out with similar procedures, but inverted order of contacting butene and ¹³C-dilabeled ethene.

5.5 References

1. Mougel, V.; Chan, K.-W.; Siddiqi, G.; Kawakita, K.; Nagae, H.; Tsurugi, H.; Mashima, K.; Safonova, O.; Copéret, C., Low Temperature Activation of Supported Metathesis Catalysts by Organosilicon Reducing Agents. *ACS Cent. Sci.* **2016**, *2*, 569-576.
2. Jarupatrakorn, J.; Coles, M. P.; Tilley, T. D., Synthesis and Characterization of $\text{MO}[\text{OSi}(\text{OtBu})_3]_4$ and $\text{MO}_2[\text{OSi}(\text{OtBu})_3]_2$ (M = Mo, W): Models for Isolated Oxo-Molybdenum and -Tungsten Sites on Silica and Precursors to Molybdena- and Tungsta-Silica Materials. *Chem. Mater.* **2005**, *17*, 1818-1828.
3. Lwin, S.; Li, Y.; Frenkel, A. I.; Wachs, I. E., Nature of WO_x Sites on SiO_2 and Their Molecular Structure-Reactivity/Selectivity Relationships for Propylene Metathesis. *ACS Catal.* **2016**, *6*, 3061-3071.
4. Ross-Medgaarden, E. I.; Wachs, I. E., Structural Determination of Bulk and Surface Tungsten Oxides with UV-vis Diffuse Reflectance Spectroscopy and Raman Spectroscopy. *J. Phys. Chem. C* **2007**, *111*, 15089-15099.
5. Saito, T.; Nishiyama, H.; Tanahashi, H.; Kawakita, K.; Tsurugi, H.; Mashima, K., 1,4-Bis(trimethylsilyl)-1,4-diaza-2,5-cyclohexadienes as Strong Salt-Free Reductants for Generating Low-Valent Early Transition Metals with Electron-Donating Ligands. *J. Am. Chem. Soc.* **2014**, *136*, 5161-5170.
6. Tsurugi, H.; Mashima, K., Salt-Free Reduction of Transition Metal Complexes by Bis(trimethylsilyl)cyclohexadiene, -dihydropyrazine, and -4,4'-bipyridinylidene Derivatives. *Acc. Chem. Res.* **2019**, *52*, 769-779.
7. Penner-Hahn, J. E., 2.13 - X-ray Absorption Spectroscopy. In *Comprehensive Coordination Chemistry II*, McCleverty, J. A.; Meyer, T. J., Eds. Pergamon: Oxford, 2003; pp 159-186.
8. Sarangi, R., X-ray absorption near-edge spectroscopy in bioinorganic chemistry: Application to M-O₂ systems. *Coord. Chem. Rev.* **2013**, *257*, 459-472.
9. Robbins, J.; Bazan, G. C.; Murdzek, J. S.; O'Regan, M. B.; Schrock, R. R., Reduction of molybdenum imido-alkylidene complexes in the presence of olefins to give molybdenum(IV) complexes. *Organometallics* **1991**, *10*, 2902-2907.
10. Tsang, W. C. P.; Hultsch, K. C.; Alexander, J. B.; Bonitatebus, P. J.; Schrock, R. R.; Hoveyda, A. H., Alkylidene and Metalacyclic Complexes of Tungsten that Contain a Chiral Biphenoxide Ligand. Synthesis, Asymmetric Ring-Closing Metathesis, and Mechanistic Investigations. *J. Am. Chem. Soc.* **2003**, *125*, 2652-2666.
11. Arndt, S.; Schrock, R. R.; Müller, P., Synthesis and Reactions of Tungsten Alkylidene Complexes That Contain the 2,6-Dichlorophenylimido Ligand. *Organometallics* **2007**, *26*, 1279-1290.
12. Marinescu, S. C.; King, A. J.; Schrock, R. R.; Singh, R.; Müller, P.; Takase, M. K., Simple Molybdenum(IV) Olefin Complexes of the Type $\text{Mo}(\text{NR})(\text{X})(\text{Y})(\text{olefin})$. *Organometallics* **2010**, *29*, 6816-6828.
13. Solans-Monfort, X.; Copéret, C.; Eisenstein, O., Shutting Down Secondary Reaction Pathways: The Essential Role of the Pyrrolyl Ligand in Improving Silica Supported $\text{d}^0\text{-ML}_4$ Alkene Metathesis Catalysts from DFT Calculations. *J. Am. Chem. Soc.* **2010**, *132*, 7750-7757.
14. Solans-Monfort, X.; Copéret, C.; Eisenstein, O., Oxo vs Imido Alkylidene $\text{d}^0\text{-Metal}$ Species: How and Why Do They Differ in Structure, Activity, and Efficiency in Alkene Metathesis? *Organometallics* **2012**, *31*, 6812-6822.
15. Müller, O.; Stötzel, J.; Lützenkirchen-Hecht, D.; Frahm, R., Gridded Ionization Chambers for Time Resolved X-Ray Absorption Spectroscopy. *Journal of Physics: Conference Series* **2013**, *425*, 092010.
16. Koningsberger, D. C.; Prins, R., *X-ray absorption : principles, applications, techniques of EXAFS, SEXAFS, and XANES*. New York : Wiley: 1988.
17. Newville, M., IFEFFIT : interactive XAFS analysis and FEFF fitting. *Journal of Synchrotron Radiation* **2001**, *8*, 322-324.
18. Ravel, B.; Newville, M., ATHENA and ARTEMIS Interactive Graphical Data Analysis using IFEFFIT. *Physica Scripta* **2005**, 1007.

19. Laguerre, M.; Dunogues, J.; Calas, R.; Duffaut, N., Silylation reductrice de derives monoaromatiques fonctionnels. *J. Organomet. Chem.* **1975**, *93*, C17-C19.

Chapter 6. Conclusion and Perspective

The goal of this PhD is to understand the nature of active sites and their initiation mechanisms in silica-supported W(VI)-oxo (WO_3/SiO_2) olefin metathesis catalysts. This is achieved by detailed investigations in well-defined molecular and supported model systems, prepared by SOMC.

We show that molecularly-defined silica-supported W(VI)-oxo species can be generated by a combination of SOMC and TMP approach in **Chapter 2**. By activating these W(VI)-oxo species with organosilicon reducing agents at low temperature (70 °C), a highly active catalyst that can catalyze metathesis at 70 °C can be generated. This study demonstrates that organosilicon reductants are highly efficient activators, compared to the classical activation methods that require temperatures above 400 °C. The combination of molecularly-defined W(VI)-oxo sites and their activation with organosilicon reductants provided a system with large amounts of “activated” species that enable identification of their structures using various spectroscopic techniques. In particular, this study indicates that reduction of W(VI)-oxo to W(IV) species is a key step in generating highly active olefin metathesis catalyst and establishes the importance and potential of W(IV)-oxo species as precatalysts for olefin metathesis.

This led us to further study the initiation mechanism in **Chapter 3** by developing well-defined W(IV)-oxo molecular complexes as precursors for generating the metathesis active W(VI) alkylidene species. We established the syntheses of well-defined W(IV)-oxo bisalkoxide complexes that are stabilized by pyridine ligands. These complexes were shown to be highly active olefin metathesis precatalysts upon the removal of pyridine ligands by $\text{B}(\text{C}_6\text{F}_5)_3$ and subsequent generation of presumably W(VI)-oxo alkylidenes. Such systems display activities similar to the well-defined W(VI)-oxo alkylidenes, despite the small amount of active sites generated. By combining detailed experimental and DFT computational studies to examine the initiation mechanism, we reveal that C–H activation of the allylic C–H group and that proton transfers assisted by pyridine in this specific case are the key steps for initiating the W(IV) precatalysts.

The initiation mechanism of supported W(IV)-oxo species was then examined in **Chapter 4**. We first show that well-defined silica-supported W(IV)-oxo species can be generated by SOMC. By investigating the metathesis activity of the supported W(IV)-oxo species towards olefins with and without allylic C–H group, namely β -methylstyrene and

styrene, respectively, we demonstrate the role of surface OH groups in tuning the metathesis activity of styrene, as evidenced by the strong correlation between surface OH density and activity. The presence of Brønsted acidic surface sites in the catalyst was probed by ^{15}N -labeled pyridine. All the data suggests that the OH assisted mechanism is involved in initiating the metathesis of olefins without allylic C–H group (e.g. styrene), while allylic C–H activation mechanism is likely involved in initiating the olefins with allylic C–H group (e.g. β -methylstyrene). This study indicates that initiation mechanisms depend on the olefinic substrates, but always involve proton transfers. It also shows that the participation of oxide support in the initiation mechanism revealing the role of Brønsted acidic surface sites.

In **Chapter 5**, we show that the organosilicon reducing agents can be used as low temperature activators in different silica-supported W(VI)-oxo systems that are prepared via different synthetic approaches including the classical incipient wetness impregnation (IWI). By investigating the effects of using different organosilicon reducing agents as activators, we show that 1-methyl-3,6-bis(trimethylsilyl)-1,4-cyclohexadiene (**Red1**) results in improved metathesis activity compared to 1,4-bis(trimethylsilyl)-1,4-diaza-2,5-cyclohexadiene (**Red4**). We also demonstrate that the metathesis activity is affected by the thermal treatment conditions used for synthesizing the W(VI)-oxo surface species. Calcination under synthetic air generates less reducible W centers than the corresponding thermal treatment under vacuum; the former displays lower activity than the latter. The metathesis activities observed in different systems are also consistent with their amounts of active alkylidenes quantified by titrations via cross-metathesis even though the results of titration experiments should be interpreted with care, due to the very complex and interconnected initiation and deactivation pathways, as well as the presence of many olefin reservoirs.

Following these studies, two major directions are worth further pursuing. Firstly, finding methods to generate well-defined W(IV) species that is free of coordinating ligand and thereby no additional activator will be need. Reducing the complexity of the system will clearly facilitate the understanding of initiation step. One possibility is to use a Lewis acidic support, which can help to remove coordinating ligand from the W center during grafting. Alternatively, the development of novel low-coordinated W(IV) precursor complex, likely with very bulky –OR ligands, will be needed to avoid the needs of extra stabilizing ligands. Secondly, there is still a need to develop a robust titration method that will enable accurate quantifications of the amounts of active sites and will be generally applicable for different systems. The major challenges in active site titrations via cross-metathesis in these reduced W(IV) precatalyst systems are the presence of side reactions and olefin-containing surface

intermediates, which have been discussed in **Chapter 5**, complicating the quantification and interpretation of the titration results. Therefore, alternative titration method other than the commonly used cross-metathesis is needed. One possibility is to perform the titration by controlled poisoning of the active sites. For instance, addition of strongly coordinating ligands in various quantities to poison the active sites, and hence the quantity of the poison required for eliminating the catalytic activity should reflect the amounts of active sites in the materials.

Based on the fundamental understanding achieved in this PhD study, we also reveal that the key parameters in affecting the metathesis activities of supported W-oxo catalysts are as follows:

- (i) The reducibility of the W(VI)-oxo species in generating W(IV)-oxo site, which is the precatalyst for olefin metathesis.
- (ii) The efficiency of transforming the W(IV)-oxo precatalysts to the active alkylidenes during the initiation, in which proton transfers play an important role independent of the olefins used.

In view of these findings, novel strategy in tuning the reducibility of surface W(VI)-oxo species could be explored in order to favor the formation of W(IV)-oxo sites. More research efforts will be needed to discover novel ways that are simple and efficient in reducing the W(VI)-oxo species into W(IV)-oxo. In addition, optimizing the efficiency in initiating the W(IV)-oxo sites will be important. In this regard, facilitating the proton transfers on surfaces by tuning the electronic properties of the proton shuttles will be one possibility. Another option will be directly adding alkylidene- or proton- transfer reagents to the W(IV)-oxo materials. The findings in this PhD study may also be applicable in the other heterogeneous metal oxide (e.g. Mo- and Re-) based olefin metathesis catalysts providing a new direction for further investigations.

APPENDIXES

Appendix to Chapter 2

Passivation of SiO₂₋₇₀₀ with Red4

A solution of 3.7 mg of **Red4** (13 μmol , 1 equiv.) in benzene (0.5 mL) was added to a suspension of SiO₂₋₇₀₀ (50 mg, 19 μmol) in benzene (0.5 mL) at room temperature. The suspension was slowly stirred at 70 °C for 12 h. The solid was collected by filtration, and was washed by four suspension/filtration cycles in benzene (4 x 1 mL). The resulting solid was dried thoroughly under high vacuum (10^{-5} mbar) at room temperature for 3 h. All the filtrate solutions were collected and analyzed by ¹H NMR spectroscopy in C₆D₆ using ferrocene as internal standard, indicating consumption of 0.8 equiv. of **Red4** and that 0.5 equiv. 2,3,5,6-tetramethylpyrazine was released upon reacting (together with other unidentified products). IR spectrum of the material is given in Figure A.2.5.

Reaction of 1 with HMDSO

Hexamethyldisiloxane (7.6 μL , 35 μmol , 4 equiv) was added to a suspension of 1 (55 mg, 9 μmol) in 1 mL C₆D₆. The suspension was slowly stirred at 70 °C for 12 h. The solid was collected by filtration, and washed by three suspension/filtration cycles in C₆D₆ (3 x 0.5 mL). The resulting solid was dried thoroughly under high vacuum (10^{-5} mbar) at room temperature for 2 h. All the filtrate solutions were collected and analyzed by ¹H NMR spectroscopy in C₆D₆ using ferrocene as internal standard, indicating consumption of 41% (14 μmol) of HMDSO. The intensity of isolated SiOH in the IR decreased by 22% and a broad peak is observed ca. 3600 cm⁻¹. IR spectrum of the material is given in Figure A.2.6.

CCDC 1479019 and 1479020 contains the supplementary crystallographic data

Figure A.2.1. Thermal ellipsoid plot at the 50% probability of [WO₂(OSi(OtBu)₃)₂(DME)]. Hydrogen atoms have been omitted and only one of the three independent molecules in the asymmetric unit have been represented for clarity.

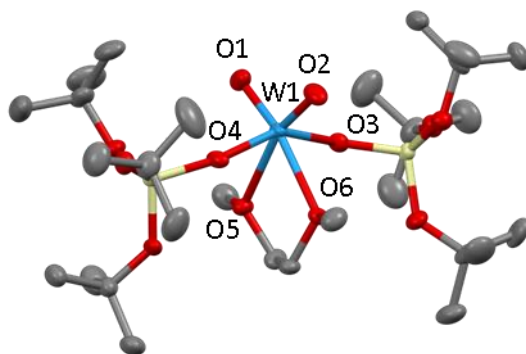


Table A.2.1. Selected bonds for [WO₂(OSi(OtBu)₃)₂(DME)] (distances are given in Å)

Structural parameters	[WO ₂ (OSi(OtBu) ₃) ₂ (DME)]
W1 – O1	1.719(5)
W1 – O2	1.716(5)
W1 – O3	1.924(4)
W1 – O4	1.928(4)
W1 – O5	2.332(4)
W1 – O6	2.344(4)

Table A.2.2. Crystallographic data for [WO₂(OSi(OtBu)₃)₂(DME)]

Formula	C ₁₁₉ H ₂₆₄ O ₄₈ Si ₈ W ₄
Crystal size (mm)	0.7 × 0.2 × 0.2
cryst syst	Tetragonal
space group	<i>I</i> 41
volume (Å ³)	16779.5(4)
<i>a</i> (Å)	23.6586(3)
<i>b</i> (Å)	23.6586(3)
<i>c</i> (Å)	29.9778(5)
<i>α</i> (deg)	90
<i>β</i> (deg)	90
<i>γ</i> (deg)	90
<i>Z</i>	4
formula weight (g/mol)	3423.44
density (g cm ⁻³)	1.355
F(000)	7075.3
temp (K)	150.0(3)

total no. reflections	30830
unique reflections [R(int)]	23689 [0.1046]
Final R indices [$I > 2\sigma(I)$]	$R_1 = 0.0641$, $wR_2 = 0.1208$
Largest diff. peak and hole ($e \cdot \text{\AA}^{-3}$)	2.62/-3.91
GOF	1.050

Figure A.2.2. Thermal ellipsoid plot at the 50% probability of $[\text{WO}(\text{OSi}(\text{OtBu})_3)_4]$. Hydrogen atoms have been omitted for clarity.

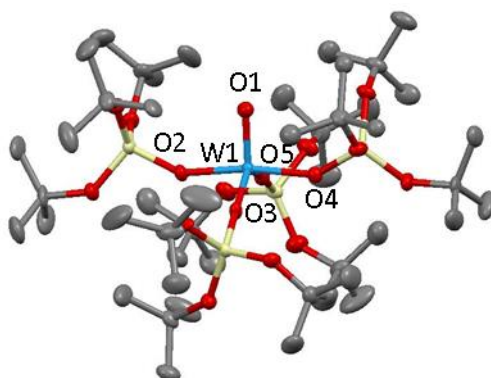


Table A.2.3. Selected bonds for $[\text{WO}(\text{OSi}(\text{OtBu})_3)_4]$ (distances are given in \AA)

Structural parameters	$[\text{WO}(\text{OSi}(\text{OtBu})_3)_4]$
W1 – O1	1.682(4)
W1 – O2	1.897(4)
W1 – O3	1.857(5)
W1 – O4	1.905(4)
W1 – O5	1.856(4)

Table A.2.4. Crystallographic data for $[\text{WO}(\text{OSi}(\text{OtBu})_3)_4]$

Formula	$\text{C}_{48}\text{H}_{108}\text{O}_{17}\text{Si}_4\text{W}$
Crystal size (mm)	$0.4 \times 0.33 \times 0.21$
cryst syst	Monoclinic
space group	$C2/c$
volume (\AA^3)	16779.5(4)
a (\AA)	26.1638(10)
b (\AA)	13.7832(5)

c (Å)	36.0594(14)
α (deg)	90
β (deg)	91.306(4)
γ (deg)	90
Z	8
formula weight (g/mol)	1253.55
density (g cm ⁻³)	1.281
F(000)	5296.0
temp (K)	150.0(3)
total no. reflections	88239
unique reflections [R(int)]	13807[R(int) = 0.1303]
Final R indices [$I > 2\sigma(I)$]	$R_1 = 0.0766$, $wR_2 = 0.1187$
Largest diff. peak and hole (e.Å ⁻³)	3.10/-2.92
GOF	1.273

Figure A.2.3. FTIR transmission spectra of **1** (red line) compared with the parent $[(\equiv\text{SiO})\text{WO}_2(\text{OSi}(\text{OtBu})_3)]$ complex (pink line) and SiO_{2-700} (blue line).

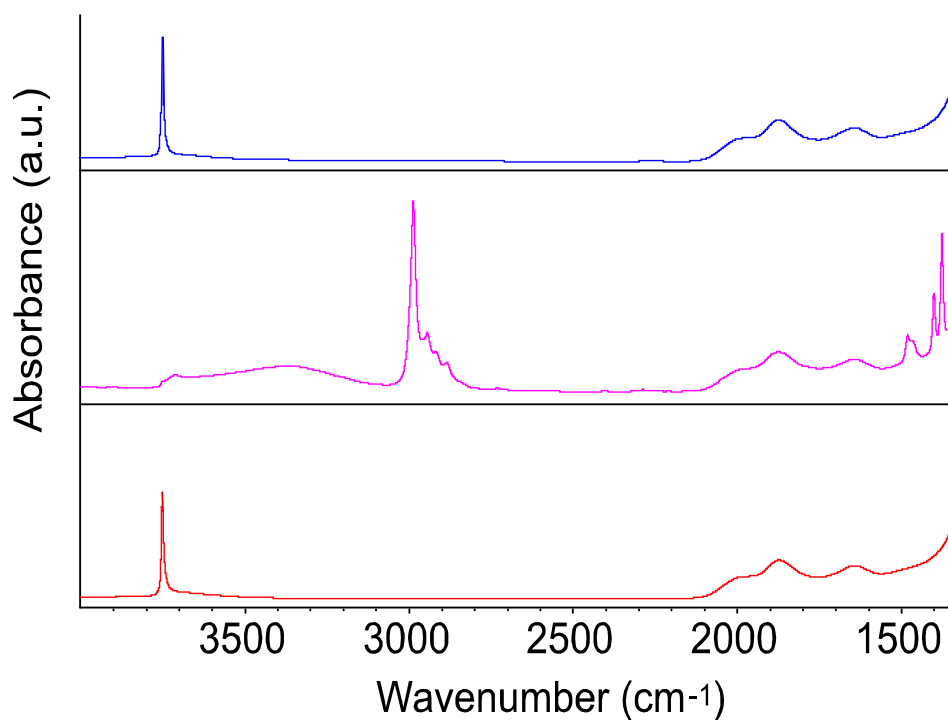


Figure A.2.4. FTIR of the materials **1-(Red)_{0.5}**, (blue line), **1-(Red)₁**, (light green line), **1-(Red)₂**, (red line), and **1-(Red)₃**, (dark green line).

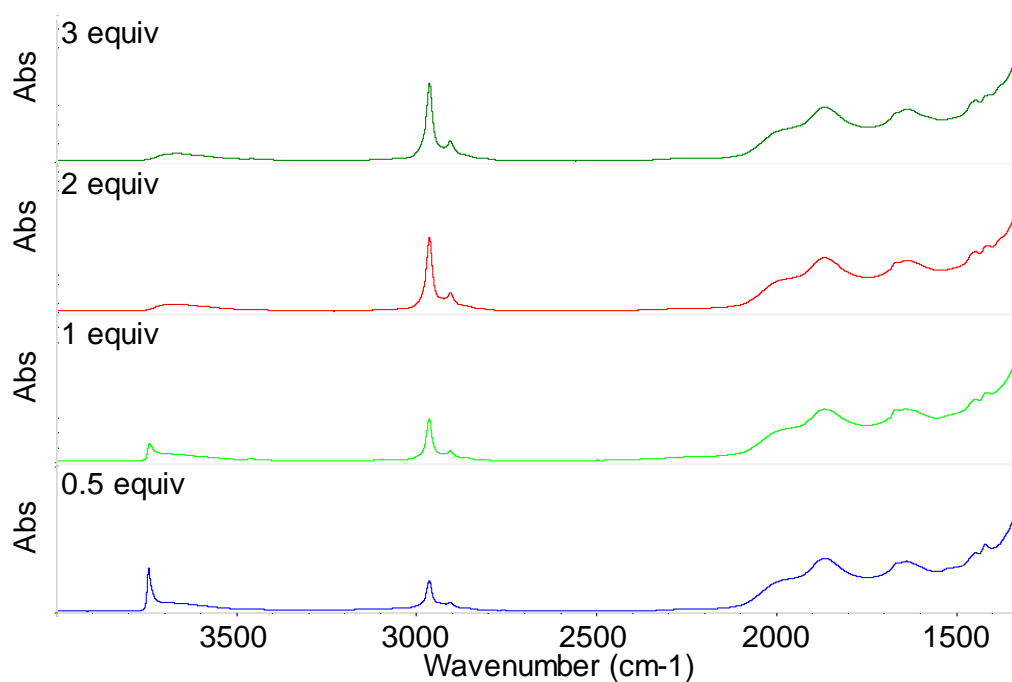


Figure A.2.5. FTIR of the $\text{SiO}_2\text{-700}$ before (red line) and after (blue line) passivation with one equiv. of **Red4** (procedure described above).

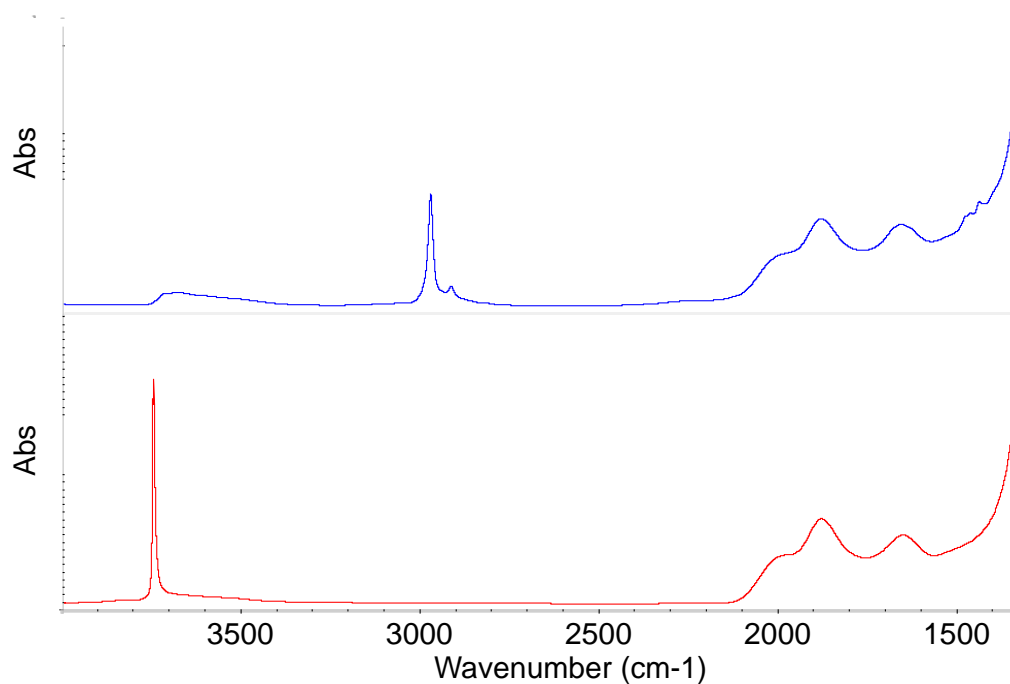


Figure A.2.6. FTIR of **1** before (red line) and after (blue line) reaction with 4 equiv. HMDSO (procedure described above).

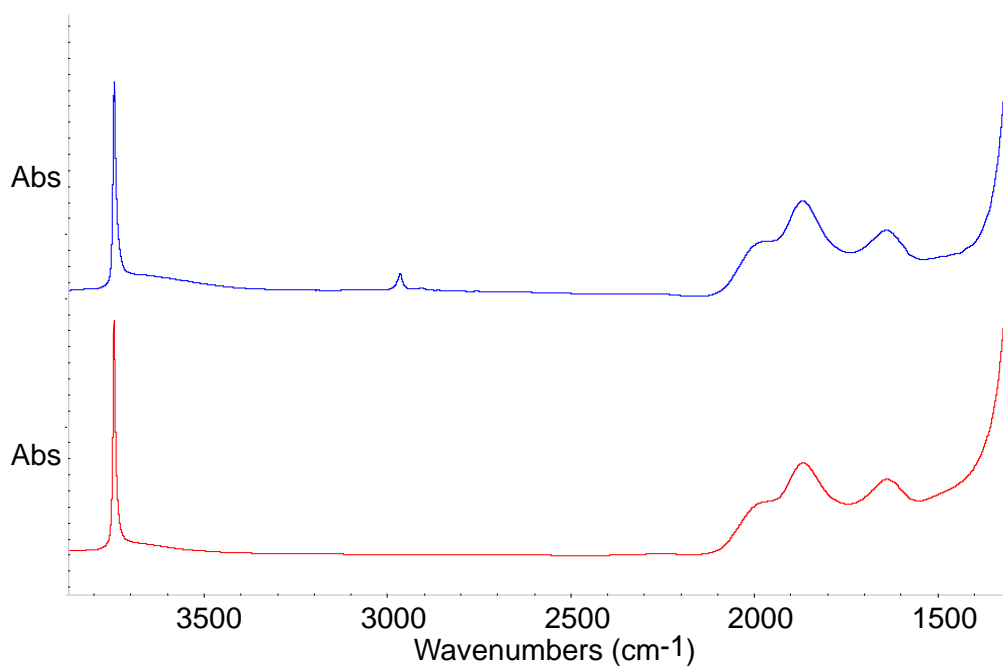


Figure A.2.7. ^1H NMR spectrum (400 MHz, spinning rate 10 kHz, 4 mm rotor) of $[(\equiv\text{SiO})\text{WO}_2(\text{OSi}(\text{OtBu})_3)]$.

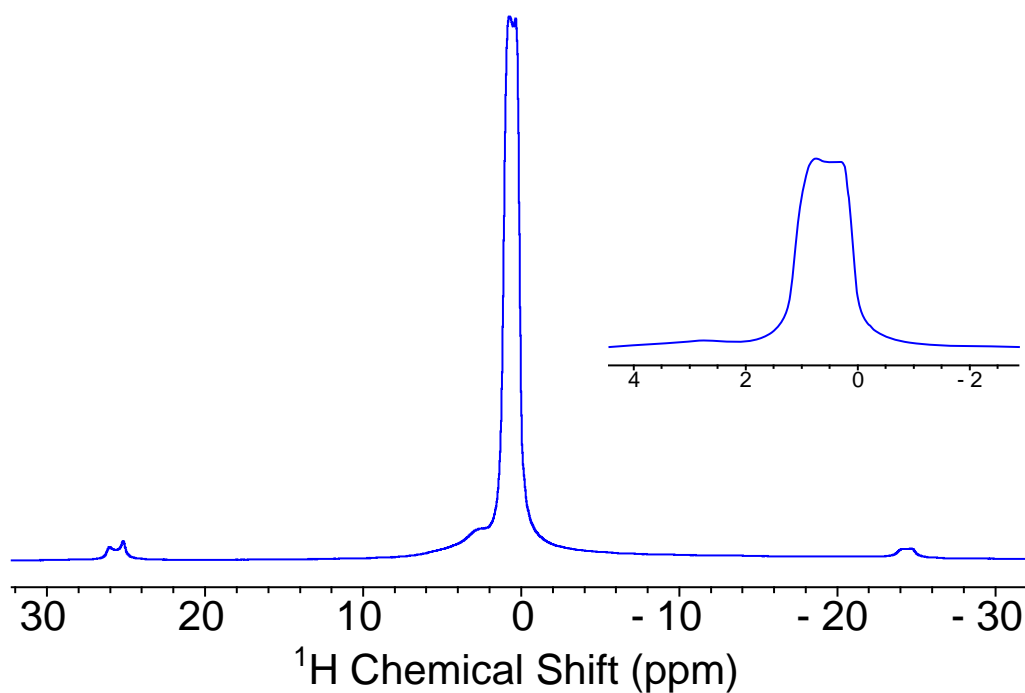


Figure A.2.8. ^{13}C CP-MAS NMR spectrum (400 MHz, spinning rate 10 kHz, 4 mm rotor) of $[(\equiv\text{SiO})\text{WO}_2(\text{OSi}(\text{OtBu})_3)]$ ($d_1 = 2$ s, contact time = 2 ms).

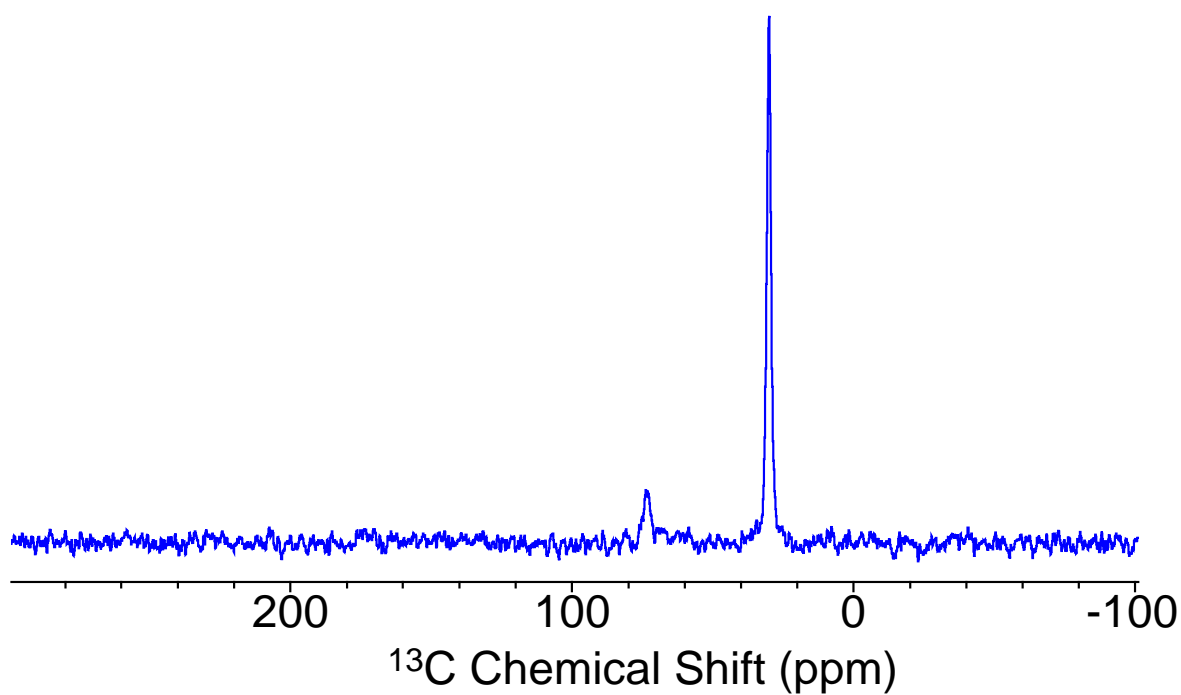


Figure A.2.9. ^1H NMR spectrum (400 MHz, spinning rate 10 kHz, 4 mm rotor) of **1-(Red)₂**.

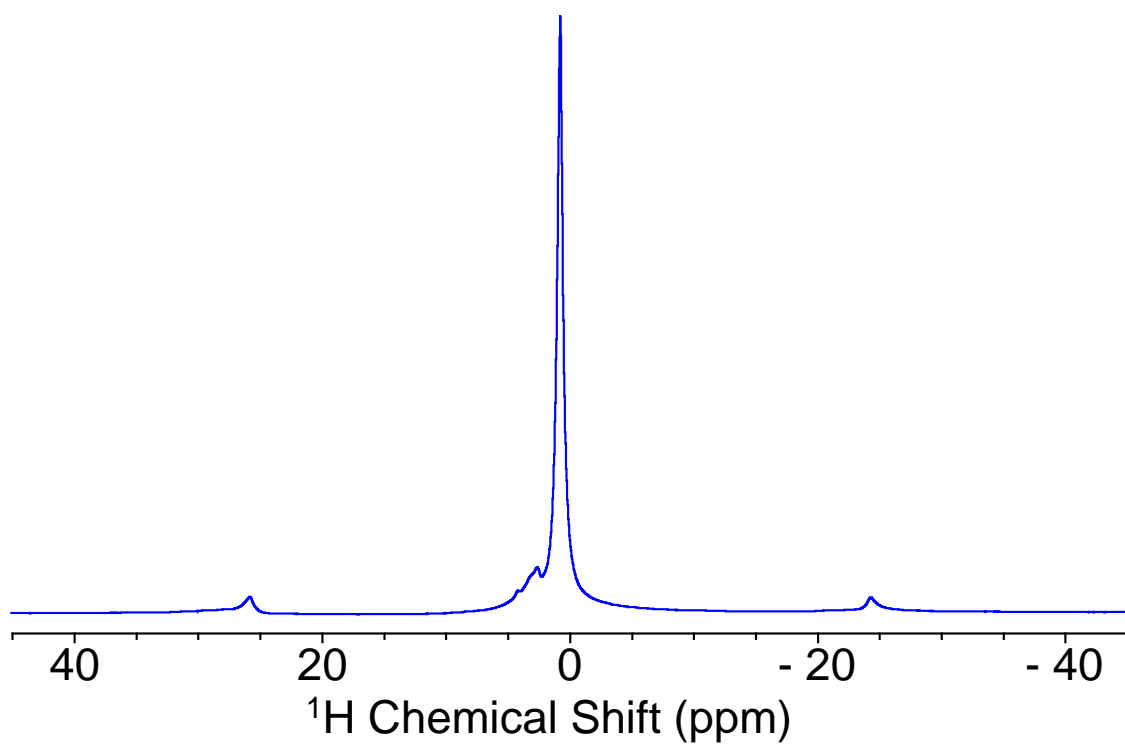


Figure A.2.10. ^{13}C CP-MAS NMR spectrum (400 MHz, spinning rate 10 kHz, 4 mm rotor) of **1-(Red)₂** (d1 = 2 s, contact time = 2 ms).

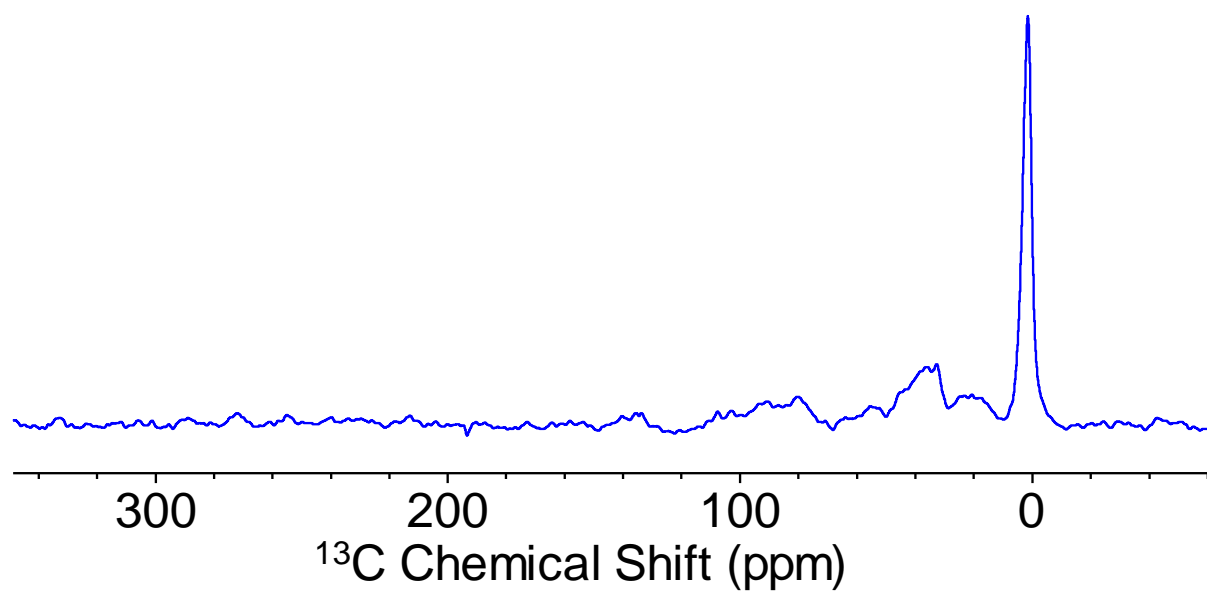


Figure A.2.11. ^1H NMR spectrum (400 MHz, spinning rate 10 kHz, 4 mm rotor) of **1-(Red)₂** after exposure to ^{13}C dilabeled ethylene (see details in part “N”).

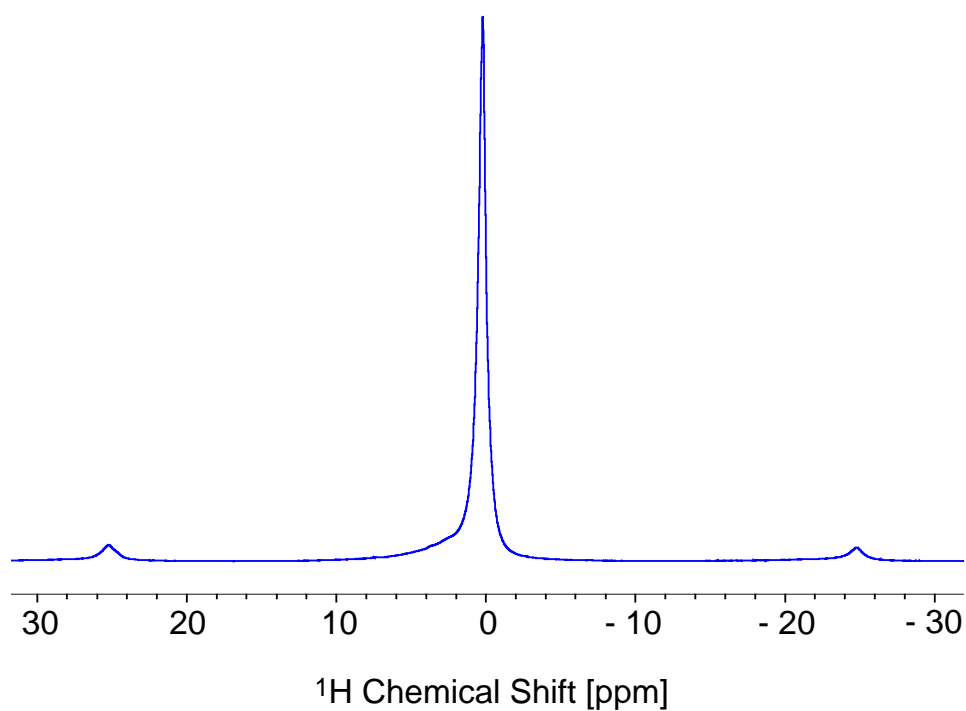


Figure A.2.12. ^{13}C CP-MAS NMR spectrum (400 MHz, spinning rate 10 kHz, 4 mm rotor) of **1-(Red)₂** after exposure to ^{13}C dilabeled ethylene (d1 = 2 s, contact time = 2 ms).

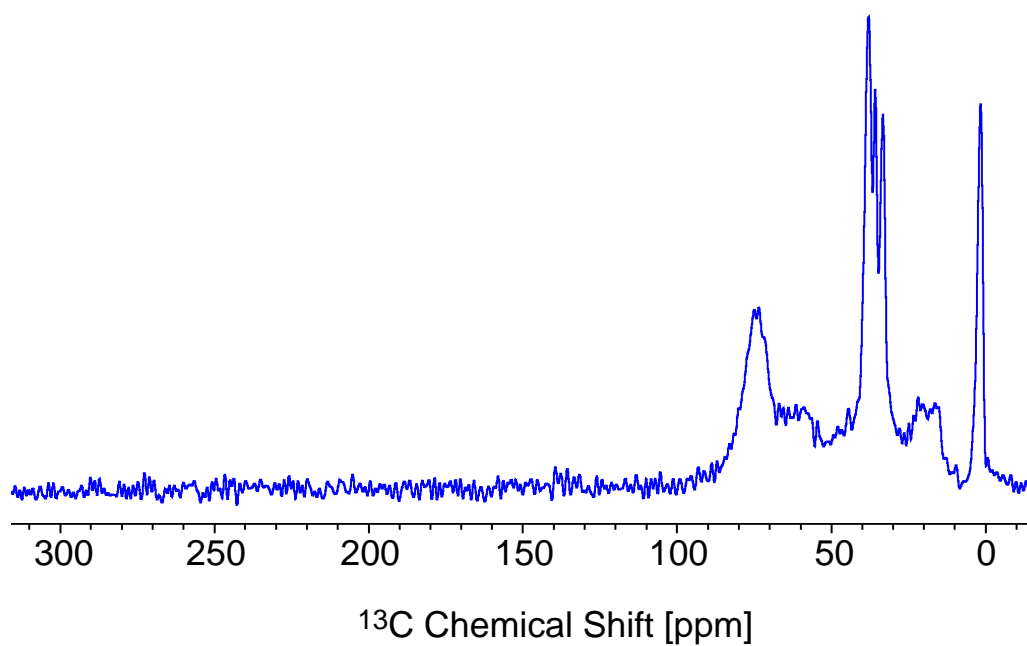


Figure A.2.13. HETCOR spectrum (400 MHz, spinning rate 10 kHz, 4 mm rotor) of **1-(Red)₂** of **1-(Red)₂** after exposure to ¹³C dilabeled ethylene.

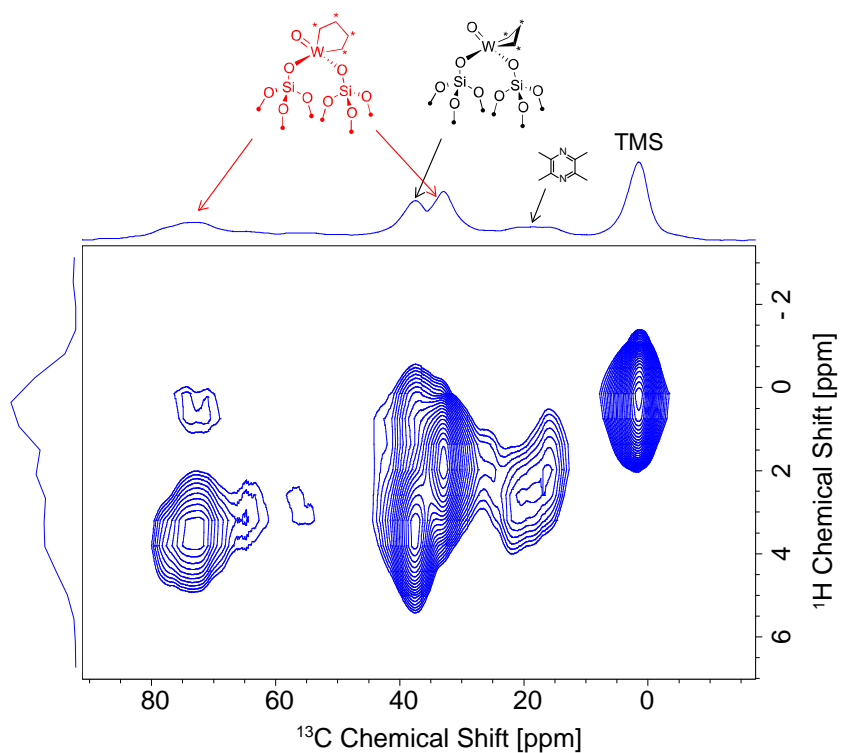


Figure A.2.14. UV-vis DRS spectra and E_g values of **1**

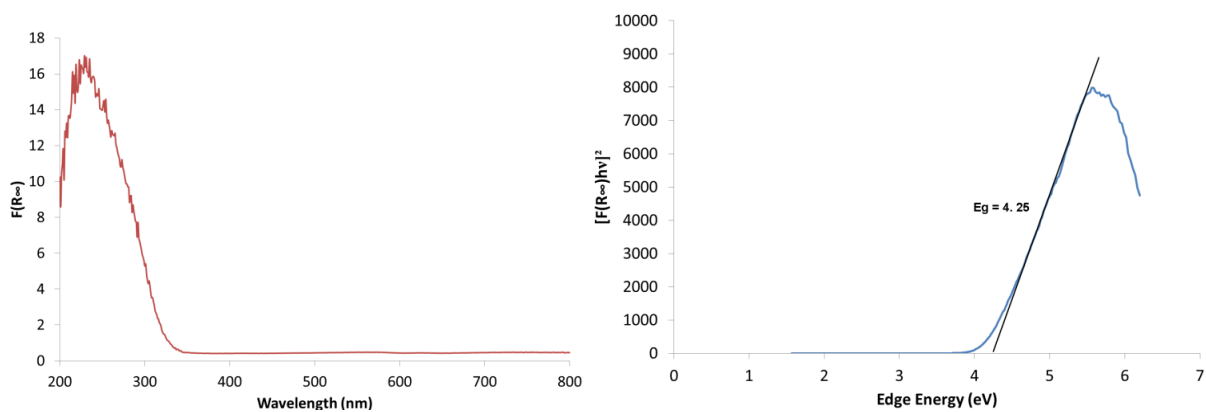


Figure A.2.15. UV-vis DRS spectrum of **1-(Red)₂**

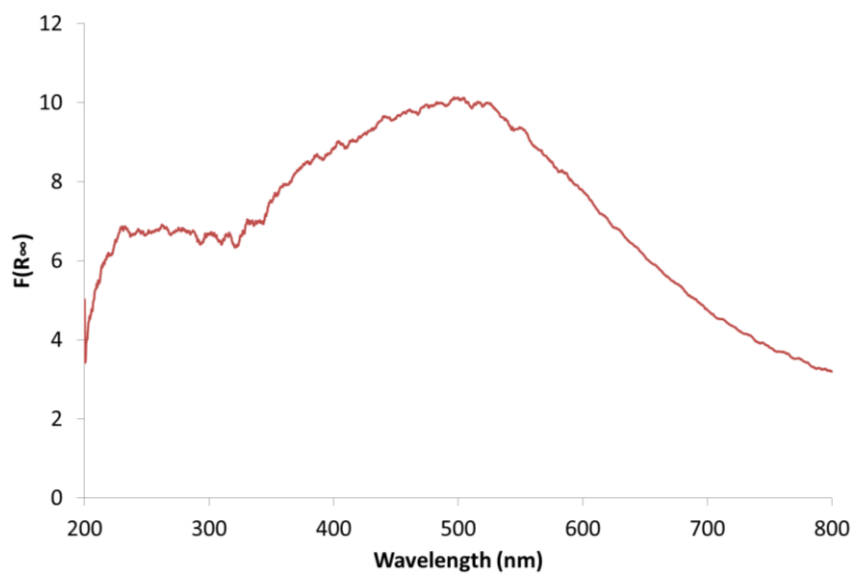
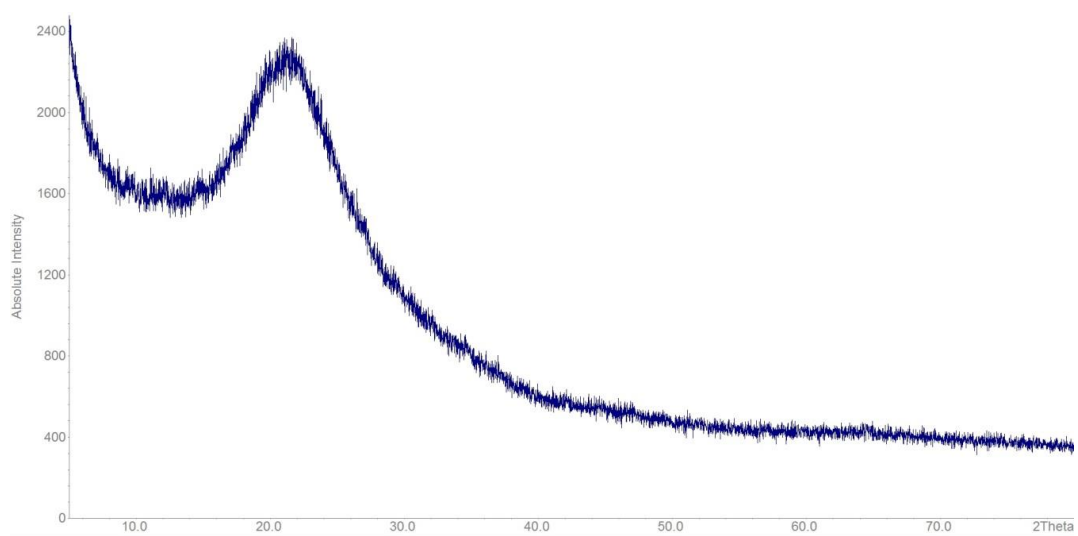


Figure A.2.16. Powder XRD pattern of **1**.



XAS characterisation of **1**

Figure A.2.17. Fit of **1** in k-space (top plot) and R-space (bottom plot).

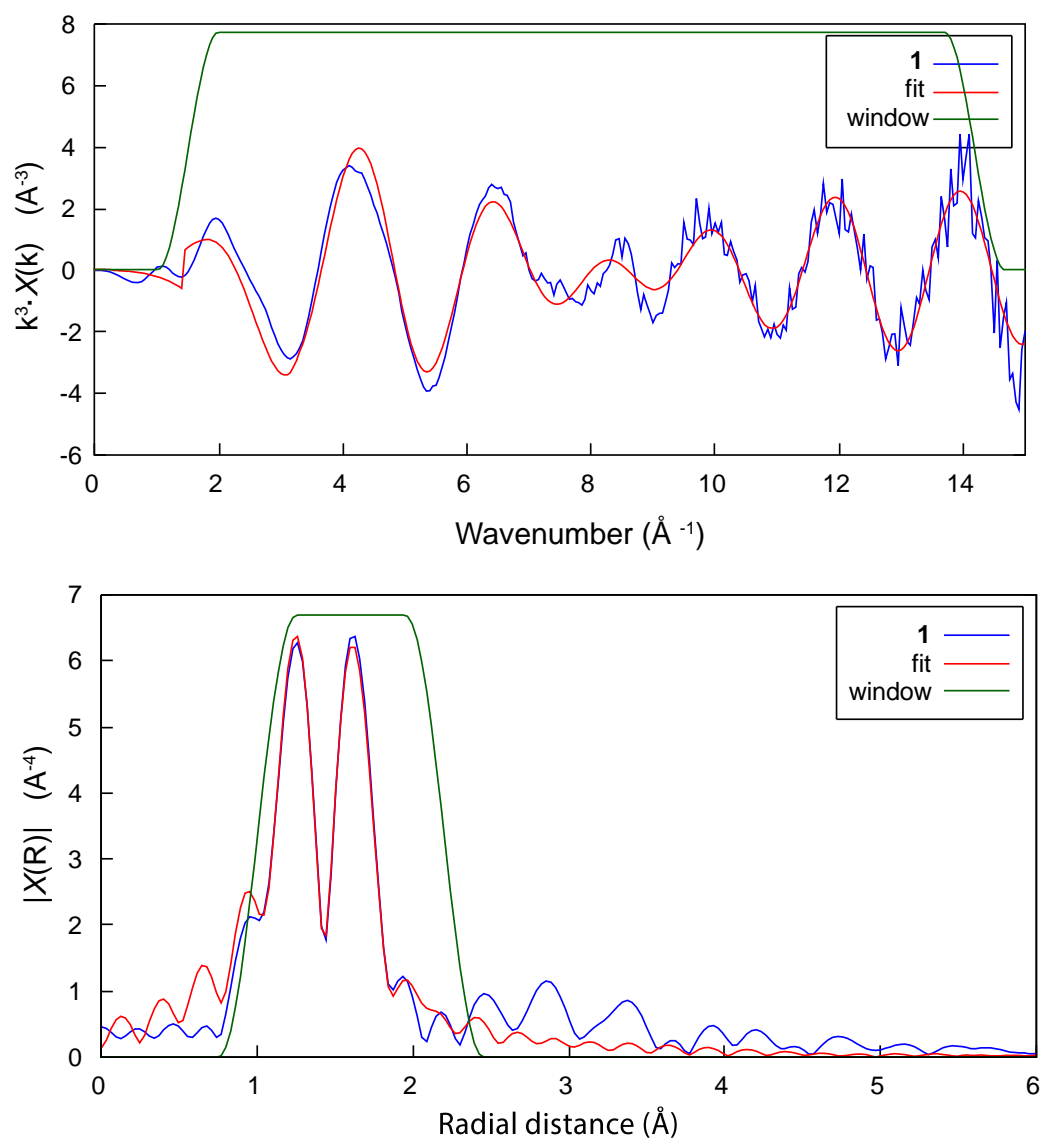


Table A.2.5. Scattering paths for **1**.

Scatterer	N	σ^2 (\AA^2)	Delr	Reff (\AA)	R (\AA)
O (W=O)	1.52 +/- 0.09	0.00153*	-0.013 +/- 0.002	1.71730	1.704 +/- 0.002
O (W-O)	2.9 +/- 0.1	0.00355*	-0.034 +/- 0.002	1.92630	1.892 +/- 0.002

*Values fixed in the fit. **S02** = 0.94; ΔE_0 = 7.598

XAS characterisation of WO_3

Figure A.2.18. W L_{III} -edge EXAFS k-space (top plot) and R-space (bottom plot) of WO_3 .

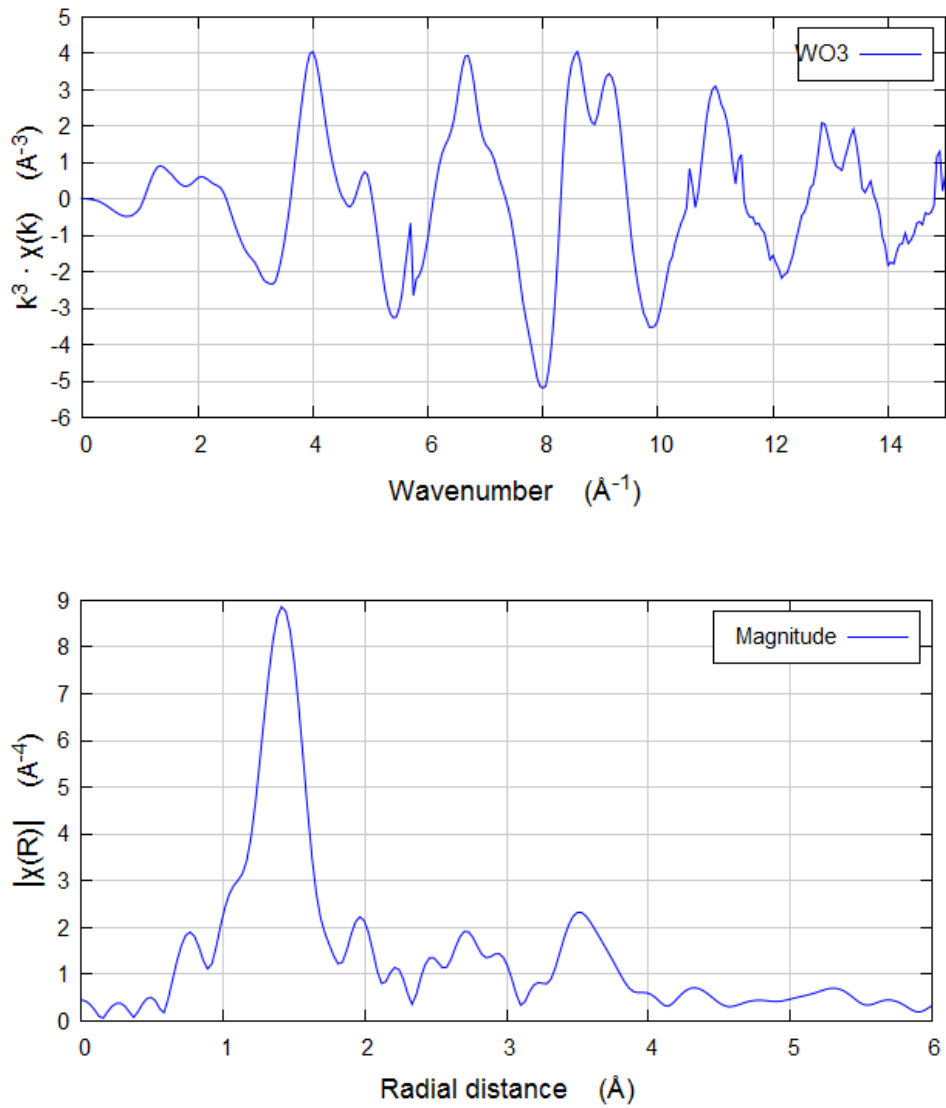
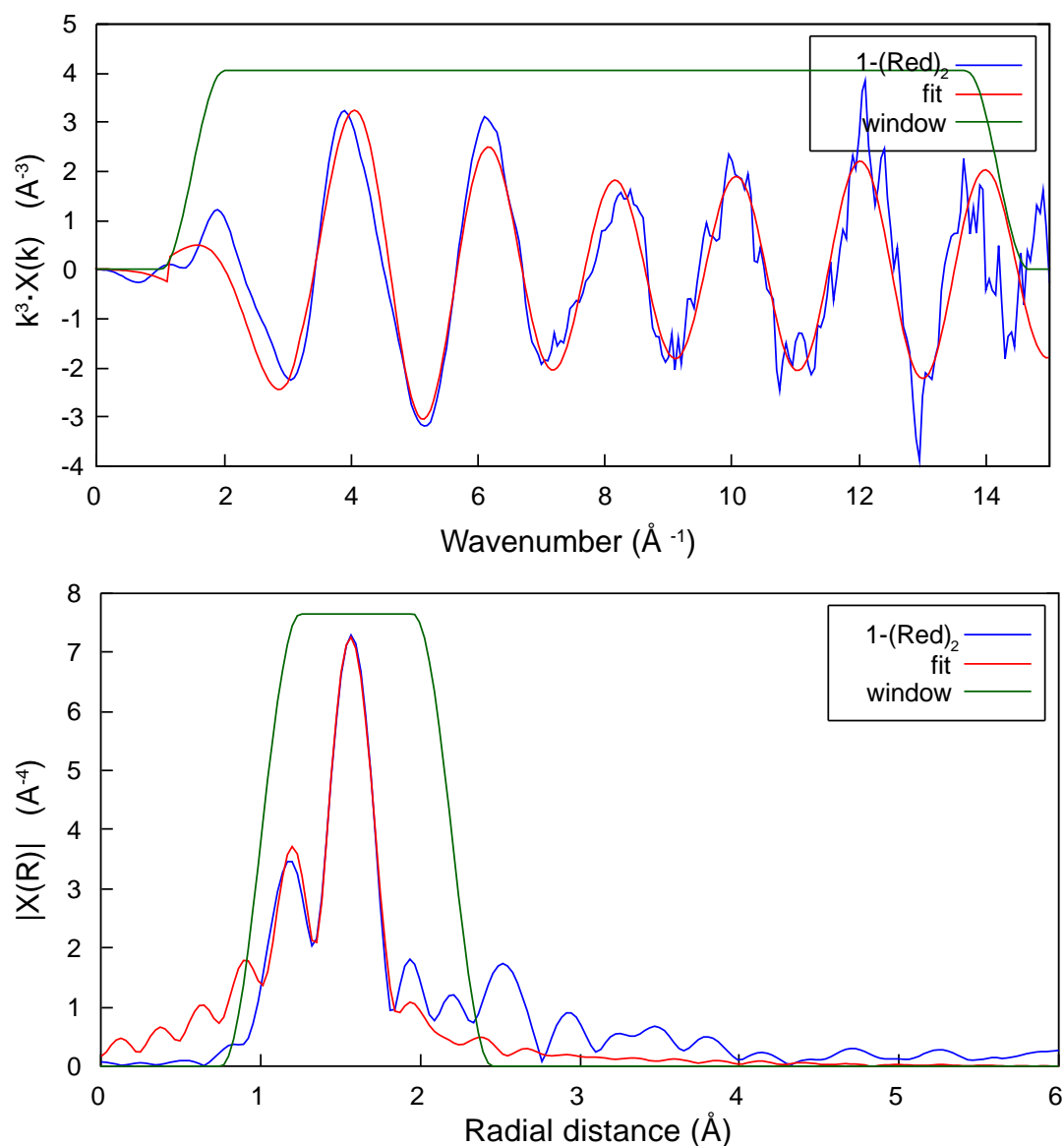


Table A.2.6. XANES whiteline energy of reference samples and **1**, before and after reduction with various amounts **Red4**.

Sample	Whiteline energy (eV)	Reference (synthesis)
1	10210,93	This work
1-(Red)_{0,5}	10209,61	This work
1-(Red)₁	10209,15	This work
1-(Red)₂	10209,13	This work
1-(Red)₃	10209,13	This work
[WO(OSi(OtBu)₃)₄]	10210,97	17
[WO₂(OSi(OtBu)₃)₂(DME)]	10210,87	This work
[(≡SiO)WO₂(OSi(OtBu)₃)]	10210,90	This work
W(OEt)₅/SiO₂	10209,53	25

Figure A.2.19. Fit of **1-(Red)₂** in k-space (top plot) and R-space (bottom plot).**Table A.2.7.** Scattering paths for **1-(Red)₂**.

Scatterer	N	σ^2 (\AA^2)	Delr	Reff (\AA)	R (\AA)
O (W=O)	0.8 +/- 0.2	0.00153*	-0.021 +/- 0.009	1.71730	1.696 +/- 0.009
O (W-O)	3.1 +/- 0.2	0.00355*	-0.029 +/- 0.008	1.92630	1.898 +/- 0.008

*Values fixed in the fit. **S02** = 0.94; ΔE_0 = 4.708 eV

XANES spectra

Figure A.2.20. W L₃ XANES spectra of **1** (blue line), [WO(OSi(OtBu)₃)₄] (red line) and [WO₂(OSi(OtBu)₃)₂(DME)] (green line) reference materials

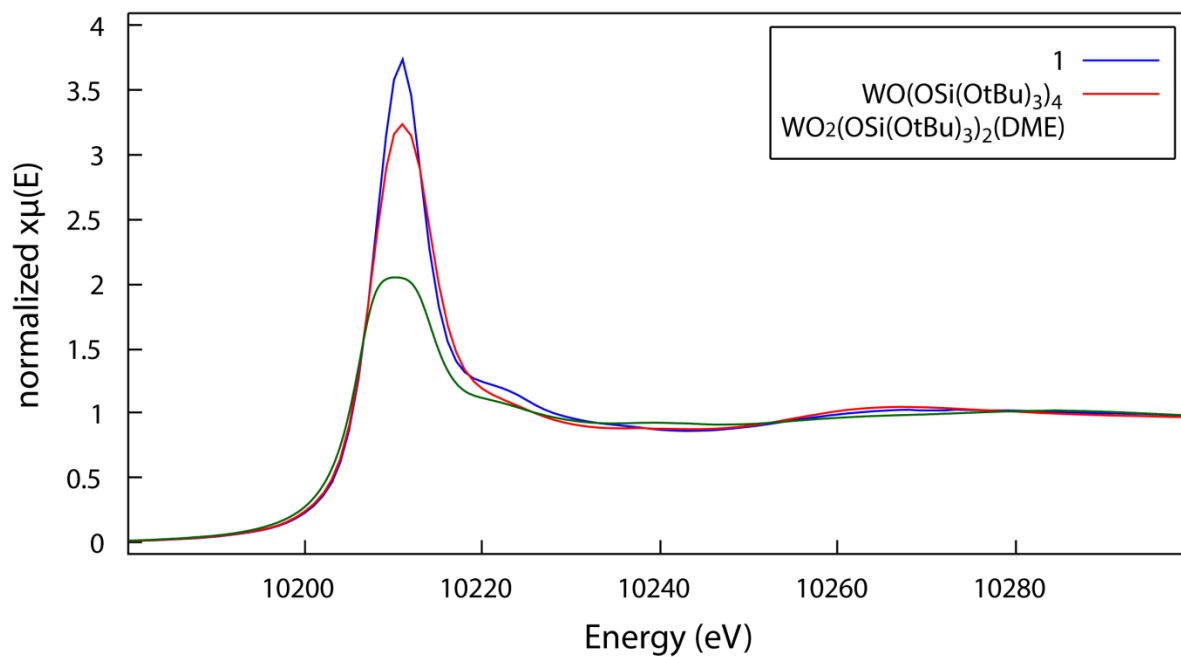
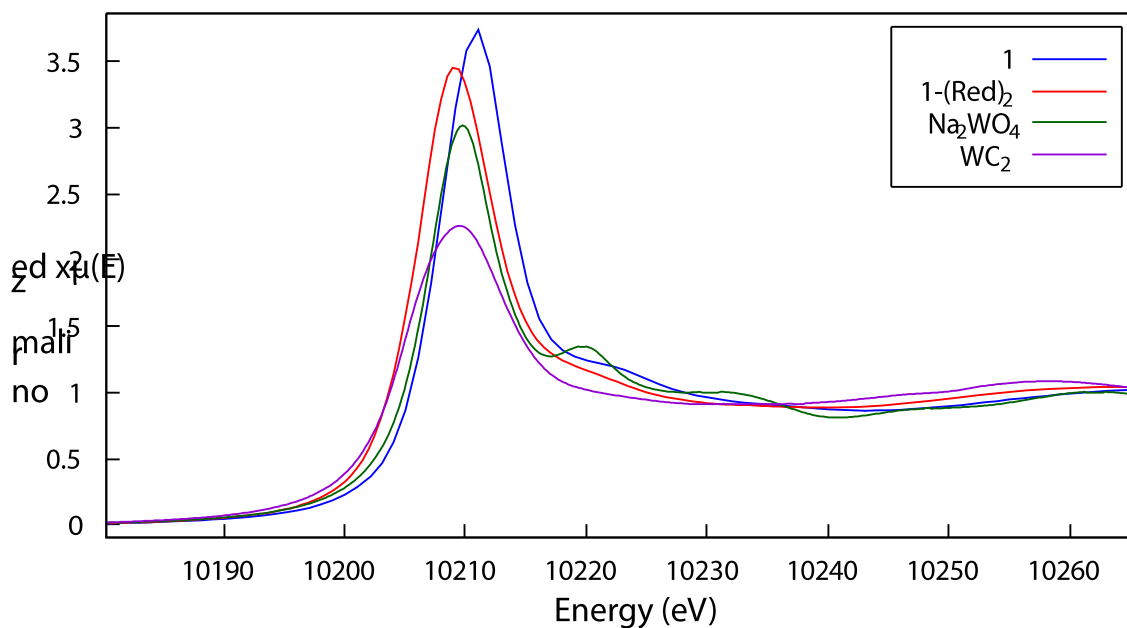


Figure A.2.21. W L₃ XANES spectra of **1** (blue line), **1**-(Red)₂ (red line), Na₂WO₄ (green line), and WO₂ (purple line) reference materials



EPR of 1-(Red)₂

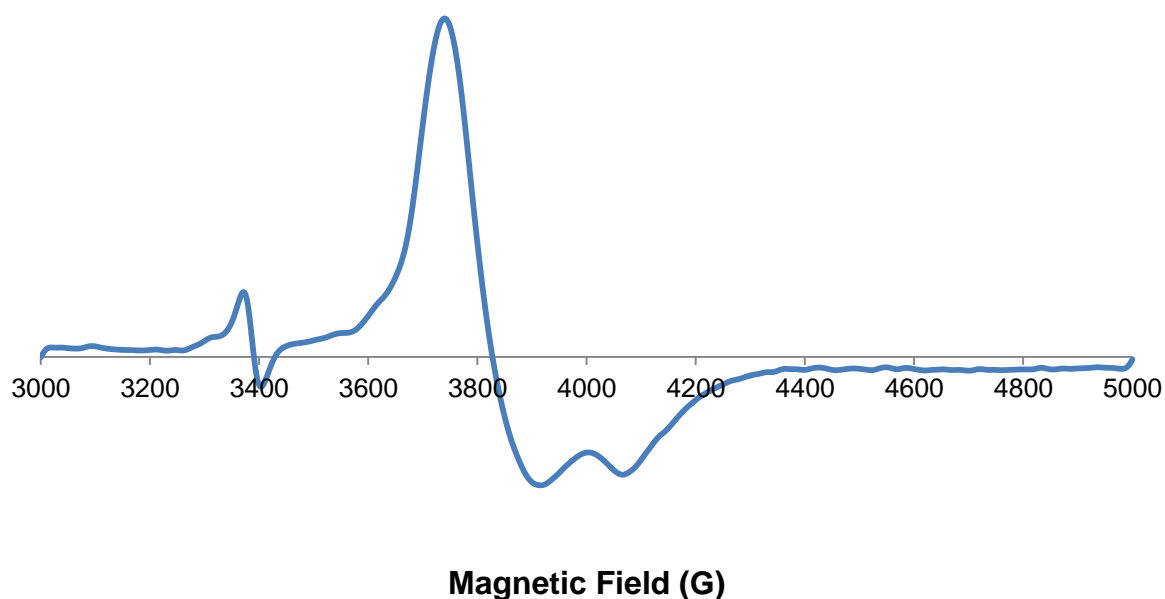
All measurements were conducted at X band (9.5-GHz electron paramagnetic resonance (EPR) frequency) at 110 K. Attenuation was varied between 14-20 dB such that no saturation was observed.

Spin counting

12.1 mg of the material **1-(Red)₂** was introduced in a Suprasil Quartz EPR tube fitted with a J. Young valve under argon. This amount was chosen to ensure that the total sample height is about 1 cm. The amount of W(V) in the material was determined by double integration of the continuous wave EPR spectrum between 3451 and 4282 Gauss and referencing to a calibration curve of obtained using the W(V) standard $\text{WOCl}_3(\text{bpy})$ (concentration range used for the calibration curve between 0.72 and 4.32 mM, in acetonitrile/ 2-methyltetrahydrofuran = 4:1). Additional correction of the difference in the incident microwave power was taken into account. Using this method, 0.33 μmol of W(V) centers were determined to be present in the sample, indicating the presence of ca 15% of W(V) sites among all W centers in **1-(Red)₂** (determined by elemental analysis).

This value was found constant among 2 measurements with different samples of **1-(Red)₂**.

Figure A.2.22. EPR spectra of **1-(Red)₂**



EPR of 1-(Red)₂ before and after exposure to 10 equiv. of cis-4-nonene

12.1 mg of **1-(Red)₂** was loaded into a Suprasil quartz EPR tube fitted with a J. Young valve. EPR spectrum was initially measured, followed by the addition of 22 μL of a 0.97 M solution of *cis*-4-nonene in toluene. The reaction mixture was heated at 70 °C for 6 h. The volatiles were removed under vacuum after reaction and EPR spectrum was measured again in same conditions (See Figure A.2.23).

Figure A.2.23. EPR spectra of **1-(Red)₂** before and after exposure to 10 equiv. of *cis*-4-nonene (Procedure described above) Note: Similar small sharp peak with g value 2.01 was reported to be O_2^- radical in the $\text{WO}_3/\text{Al}_2\text{O}_3$ system)

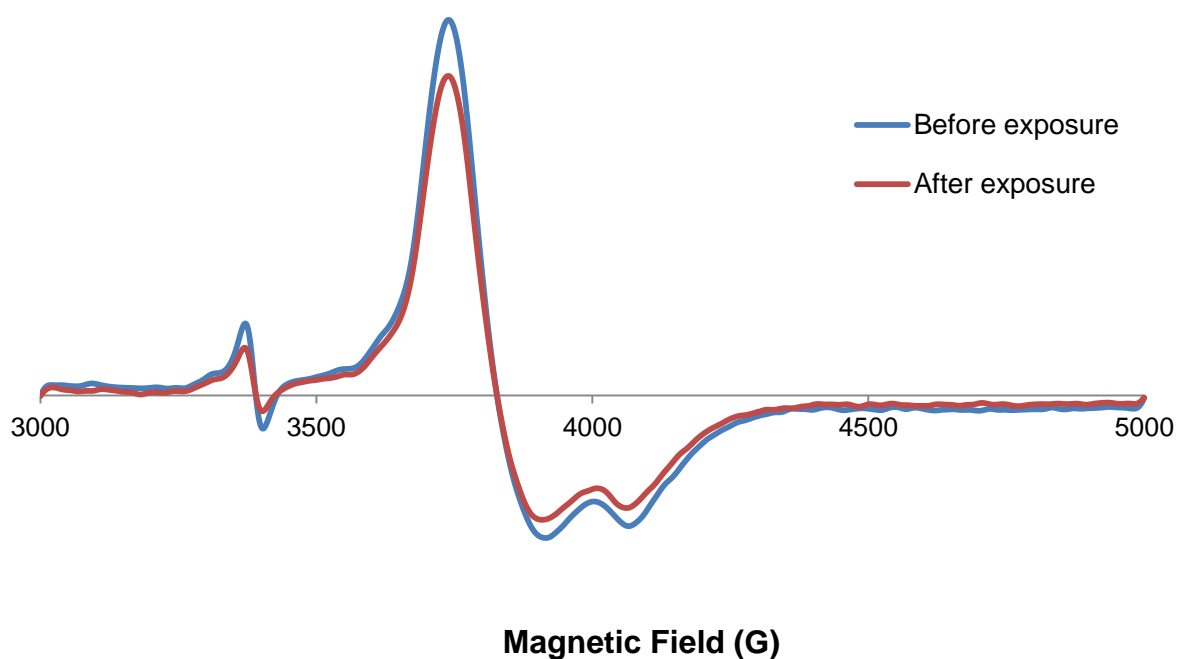


Table A.2.8. g-values of the material before and after exposure to 10 equiv. of *cis*-4-nonene.

	g1	g2	g3
Before exposure	2.014	1.777	1.674
After exposure	2.012	1.777	1.681

OH content of 1 and 1-(Red)₂

In an Ar filled glovebox, 30 mg of the supported catalyst were weighed into a Schlenk tube. A stock solution containing both ferrocene (internal standard, 0.075 mmol, 14 mg) and benzyl magnesium bromide (190 μ l, 0.19 mmol, 1 M solution in Et₂O) in 3 ml of d₆-benzene was prepared. 1 mL of this stock solution (0.063 mmol PhCH₂MgBr) was added dropwise into the Schlenk tube containing the catalyst. The reaction mixture was stirred at 200 rpm for 2 h at room temperature. After transferring the supernatant to a J. Young NMR tube, the amount of toluene formed was evaluated by ¹H NMR (d1=30 s). The results are shown in Table A.2.9.

Table A.2.9. OH content of **1** and **1-(Red)₂**.

Catalyst	Amount of OH sites (mmol/g)	No. of OH site per W (OH/W)
1	0.4	2.33
1-(Red)₂	0.15	0.94

Reaction with ferrocenium hexafluorophosphate

A solution of ferrocenium hexafluorophosphate (2.3 mg, 0.0063 mmol, 2.5 equiv) in d₈-THF (0.5 mL) was added at room temperature to 13 mg of **1-(Red)₂** and the reaction mixture was stirred at 70 °C for 12 h. The filtrate was then separated and analyzed by ¹H NMR using DME (10 μ l, 0.080 mmol) as internal standard for quantification. Results of the titration are given in Table A.2.10.

Table A.2.10. Amount of different products observed by ¹H-NMR after reaction of **1-(Red)₂** with FcPF₆.

Products observed	Amount (equiv/ W)
Ferrocene	1.66
Tetramethylpyrazine	0.1
TMS moieties	0.8

Molecular precursors

Catalytic activity of toluene solution of molecular precursors in presence of 2 equiv. of **Red4** was investigated. For all these precursors, no activity was observed in the absence of reductant. Conversion, TON and TOF at 70 °C are given in Table A.2.11.

Table A.2.11. Catalytic activity of the molecular precursors (*cis*-4-nonene, 1 mol% W, 2 mol% **Red4**, 70 °C).

Catalyst (0.1 mol % W)	TOF _{3min} (min ⁻¹)	TOF _{max} (min ⁻¹) ^a	Conversion at 24 h
WO(OSi(OtBu) ₃) ₄	<0.1	<0.1	< 1 %
WO ₂ (OSi(OtBu) ₃) ₂ (DME)	<0.1	<0.1	< 1 %

^a Maximum TOF determined during the test.

Heterogeneous catalysts

Catalytic activity of heterogeneous precursors in presence of 2 equiv. of **Red4** was investigated. For all these precursors, no activity was observed in absence of reductant. Conversion, TON and TOF at 70 °C are given in Table A.2.12.

Table A.2.12. Catalytic activity of the heterogeneous catalysts (*cis*-4-nonene, 1 mol% W, 2 mol% **Red4**, 70 °C).

Catalyst (0.1 mol % W)	TOF _{3min} (min ⁻¹)	TOF _{max} (min ⁻¹) ^a	Time to conversion
[(≡SiO)W(O)(OSi(OtBu) ₃) ₃]	<0.1	<0.1	< 1 % after 24h
[(≡SiO)W(O) ₂ (OSi(OtBu) ₃) ₃]	<0.1	<0.1	< 1 % after 24h
1	3	8 (10 min)	3 h
WO ₃ /SiO ₂	1	2 (320 min)	24 h
MoO ₃ /SiO ₂	0.5	0.6 (60 min)	24 h

^a Maximum TOF determined during the test.

Table A.2.13. Catalytic activity of the heterogeneous catalysts (*cis*-4-nonene, 1 mol% W, 70 °C).

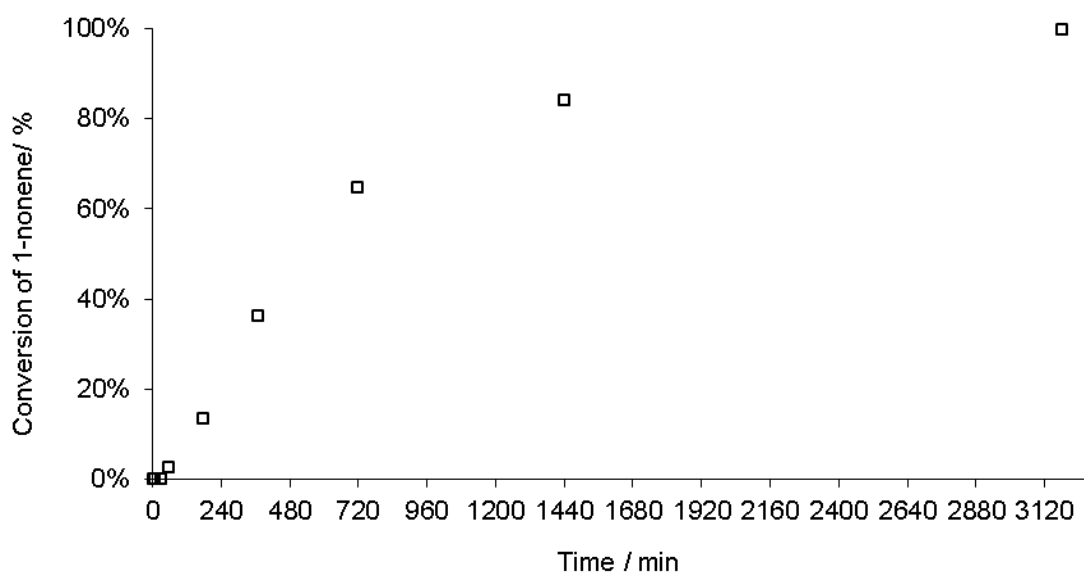
Catalyst (0.1 mol % W)	TOF _{3min} (min ⁻¹) 1)	TOF _{max} (min ⁻¹) 1) ^a	Time to final conversion
1-(Red)_{0.5}	5	8 (10 min)	3 h
1-(Red)₁	2	3 (10 min)	6 h
1-(Red)₂	<1	2 (540 min)	12 h

^a Maximum TOF determined during the test. Values in bracket the time for which maximum TOF was observed.

Metathesis of 1-nonene by 1 in presence of 2 equiv. of Red4.

At t=0 a 0.79 M solution of 1-nonene in toluene containing heptane as internal standard (0.08 M) and 2 equiv. of **Red4** (with respect to W centers) was added to the catalyst introduced in a conical base vial containing a wing shaped magnetic stirring bar. The reaction mixture was stirred at 600 rpm and kept at 70 °C using an aluminum heating block. 5 µL aliquots of the solution were sampled (by opening the vial), diluted with pure toluene (100 µL) and quenched by the addition of 1 µL of wet ethyl acetate. The resulting solution was analyzed by GC/FID (Agilent Technologies 7890 A) equipped with an HP-5 (Agilent Technologies) column.

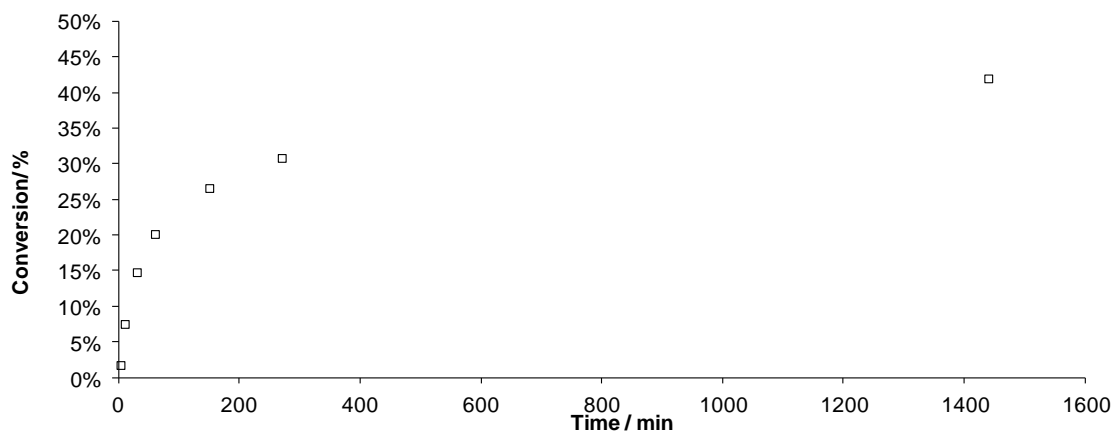
Figure A.2.24. Conversion vs time, 1-nonene homometathesis, 1 mol% W, 2 mol% **Red4**, 70 °C.



*Metathesis of ethyl oleate by **1** in presence of 2 equiv. of **Red4**.*

At $t=0$, a 0.53 M solution of ethyl oleate in toluene containing octadecane as internal standard (0.10 M) and 2 equiv. of **Red4** (with respect to **W** centers) was added to the catalyst introduced in a conical base vial containing a wing shaped magnetic stirring bar. The reaction mixture was stirred at 600 rpm and kept at 70 °C using an aluminum heating block. 5 μL aliquots of the solution were sampled (by opening the vial), diluted with pure toluene (100 μL) and quenched by the addition of 1 μL of wet ethyl acetate. The resulting solution was analyzed by GC/FID (Agilent Technologies 7890 A) equipped with an HP-88 (Agilent Technologies) column. Conversion is shown by eq.1. Equilibrium conversion is reached at ca. 50%.

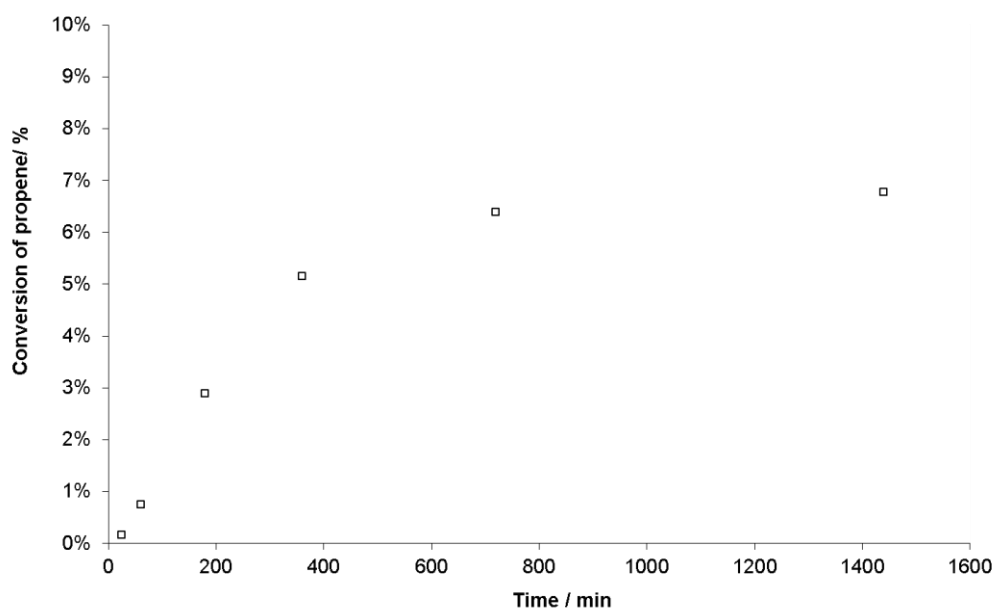
Figure A.2.25. Conversion vs time, ethyl oleate homometathesis, 1 mol% **W**, 2 mol% **Red4**, 70 °C.



Propene metathesis with 1 at 500 °C

Catalyst **1** (10 mg, 1.9 μmol) was loaded in a 400 mL reactor flask at 25 °C. The reactor was evacuated under high vacuum (10^{-5} mbar), and warmed to 500 °C (10 °C/min). Propene (305 mbar, 1.9 mmol, 1000 equiv.) was added. 250 μL aliquots were analysed by GC over time to follow the conversion and the product selectivities.

Figure A.2.26. Conversion vs time, propene metathesis, 0.1 mol% W, 500 °C for **1**

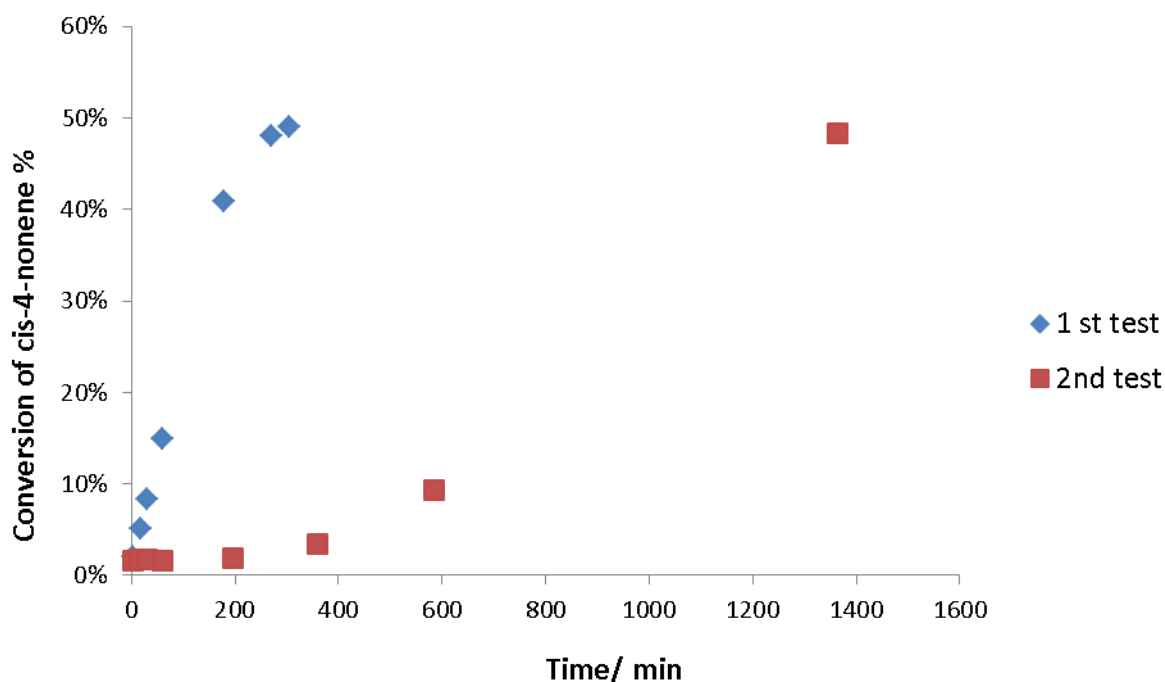


Recycling

Experimental procedure for recycling test: second addition of pure *cis*-4-nonene

At $t=0$ a 0.97 M solution of *cis*-4-nonene (1000 equiv.) in toluene containing heptane as internal standard (0.11 M) and 2 equiv. of **Red4** (with respect to W centers) was added to the catalyst introduced in a conical base vial containing a wing shaped magnetic stirring bar. The reaction mixture was stirred at 600 rpm and kept at 70 °C using an aluminum heating block. 5 μL aliquots of the solution were sampled, diluted with pure toluene (100 μL) and quenched by the addition of 1 μL of wet ethyl acetate. The resulting solution was analyzed by GC/FID (Agilent Technologies 7890 A) equipped with an HP-5 (Agilent Technologies) column. After reaching equilibrium conversion, the liquid phase of the reaction mixture was removed, and a fresh aliquot of *cis*-4-nonene (1000 equiv.) was added to the catalyst, following catalytic activity as described before.

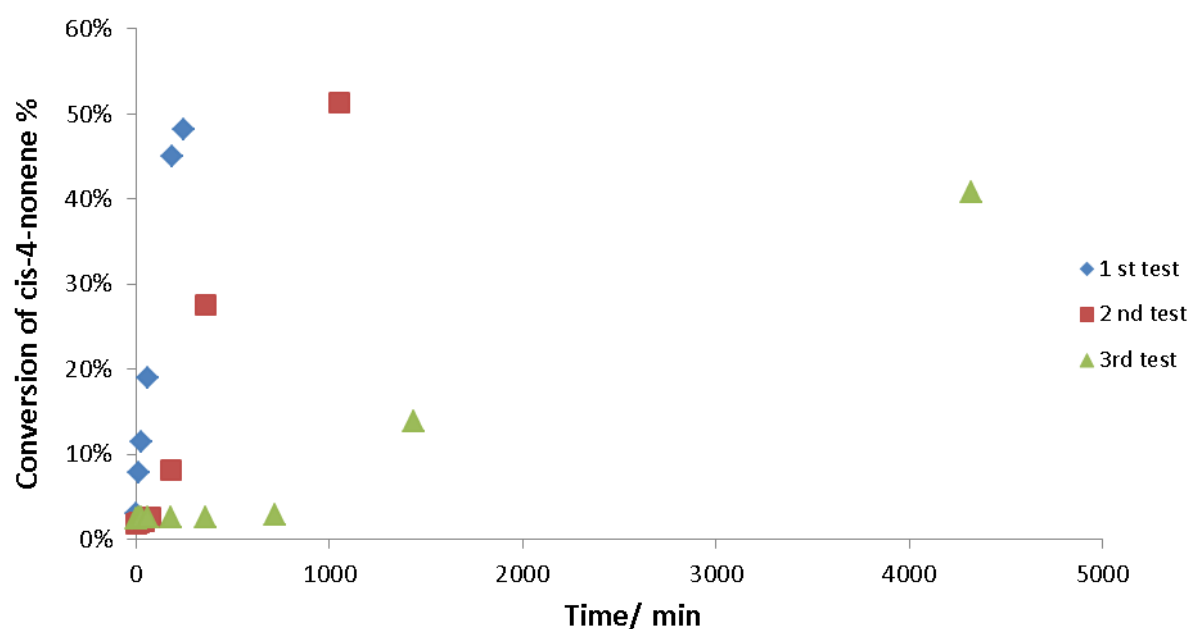
Figure A.2.27. Conversion vs time, *cis*-4-nonene homometathesis, 70 °C, 1000 equiv. of *cis*-4-nonene, 2 equiv. of **Red4** (Blue diamonds) and after removal of solution and addition of a fresh aliquot of 1000 equiv. of *cis*-4-nonene in absence of **Red4** (red squares, see procedure above for details).



Experimental procedure for recycling test: recycling in presence of Red4

At $t=0$ a 0.97 M solution of *cis*-4-nonene (1000 equiv.) in toluene containing heptane as internal standard (0.11 M) and 2 equiv. of **Red4** (with respect to W centers) was added to the catalyst introduced in a conical base vial containing a wing shaped magnetic stirring bar. The reaction mixture was stirred at 600 rpm and kept at 70 °C using an aluminum heating block. 5 μ L aliquots of the solution were sampled, diluted with pure toluene (100 μ L) and quenched by the addition of 1 μ L of wet ethyl acetate. The resulting solution was analyzed by GC/FID (Agilent Technologies 7890 A) equipped with an HP-5 (Agilent Technologies) column. After reaching equilibrium conversion, the liquid phase of the reaction mixture was removed, and a fresh aliquot of *cis*-4-nonene (1000 equiv.) and **Red4** (1 equiv.) was added to the catalyst for the 2nd and 3rd test, following catalytic activity as before.

Figure A.2.28. Conversion vs time, *cis*-4-nonene homometathesis, 70 °C, 1000 equiv. of *cis*-4-nonene, 2 equiv. of **Red4** (Blue diamonds) and after removal of solution and addition of a fresh aliquot of 1000 equiv. of *cis*-4-nonene and 1 equiv. of **Red4** (red squares. Conversion for the same process repeated a second time is given in green triangles (see procedure above for details). The 2nd test has similar induction period than [1-(Red)₂].



Poisoning and reactivation

General procedure: A 0.97 M solution of *cis*-4-nonene (1000 equiv.) in toluene containing heptane as internal standard (0.11 M) was added to the catalysts introduced in a conical base vial containing a wing shaped magnetic stirring bar. The reaction mixture was stirred at 600 rpm and kept at 70 °C using an aluminum heating block for 1.5 h. Catalytic activity of the material was ensured by following activity by GC (5 μ L aliquots, procedure described above). The catalyst was then contacted with H₂O (1 equiv., in toluene), O₂ (excess) or EtOH (1 equiv., in toluene) and stirred for 1.5 h. No further conversion was observed with respect to the conversion measured at the introduction of the H₂O, O₂ or EtOH respectively. The solution was then removed by filtration and a new batch of *cis*-4-nonene solution (1000 equiv.) was added. No catalytic activity at 24 h was observed in all cases confirming the complete deactivation of the catalyst after poisoning. At t=0, 2 equivalents of **Red4** (with respect to W centers) were added to the reaction mixture. Conversion vs. time after H₂O, O₂ and EtOH poisoning and addition of 2 equiv. of **Red4** are shown in Figure A.2.29, Figure A.2.30 and Figure A.2.31, respectively.

Figure A.2.29. Conversion vs time, *cis*-4-nonene (1000 equiv.) homometathesis at 70 °C after reactivation by additional 2 equiv. of **Red4** after H₂O poisoning

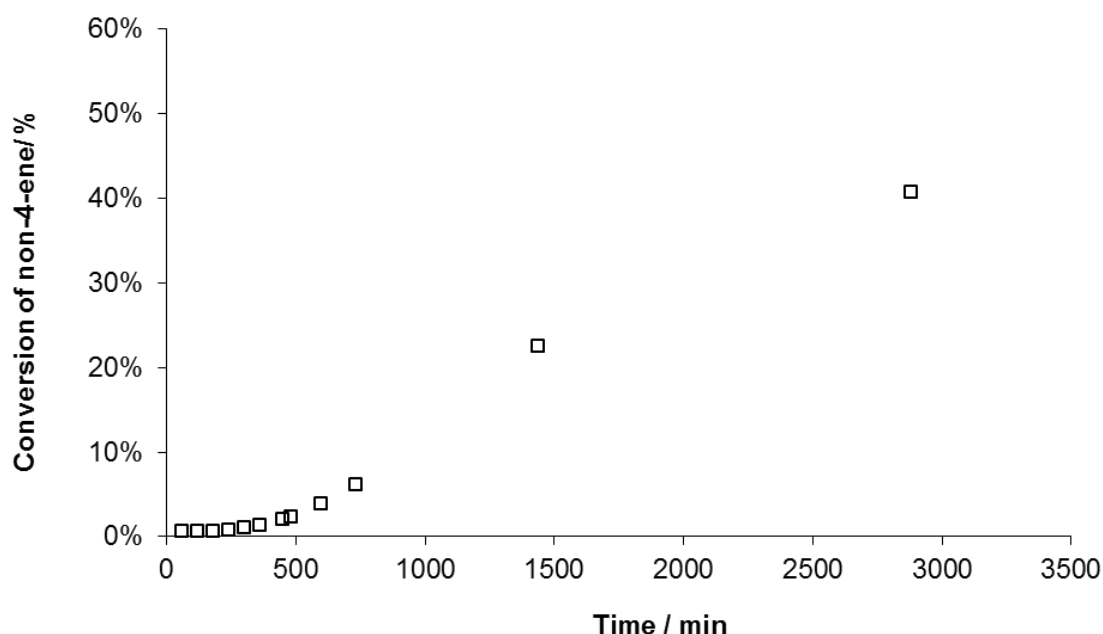


Figure A.2.30. Conversion vs time, *cis*-4-nonene (1000 equiv) homometathesis at 70 °C after reactivation by additional 2 equiv. of **Red4** after O₂ poisoning

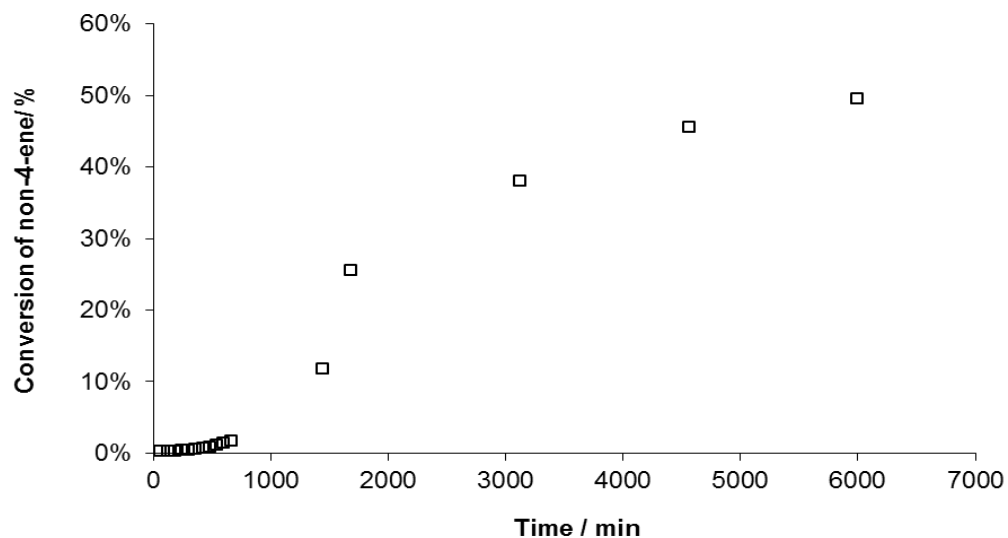


Figure A.2.31. Conversion vs time, *cis*-4-nonene (1000 equiv) homometathesis at 70 °C after reactivation by additional 2 equiv. of **Red4** after EtOH poisoning

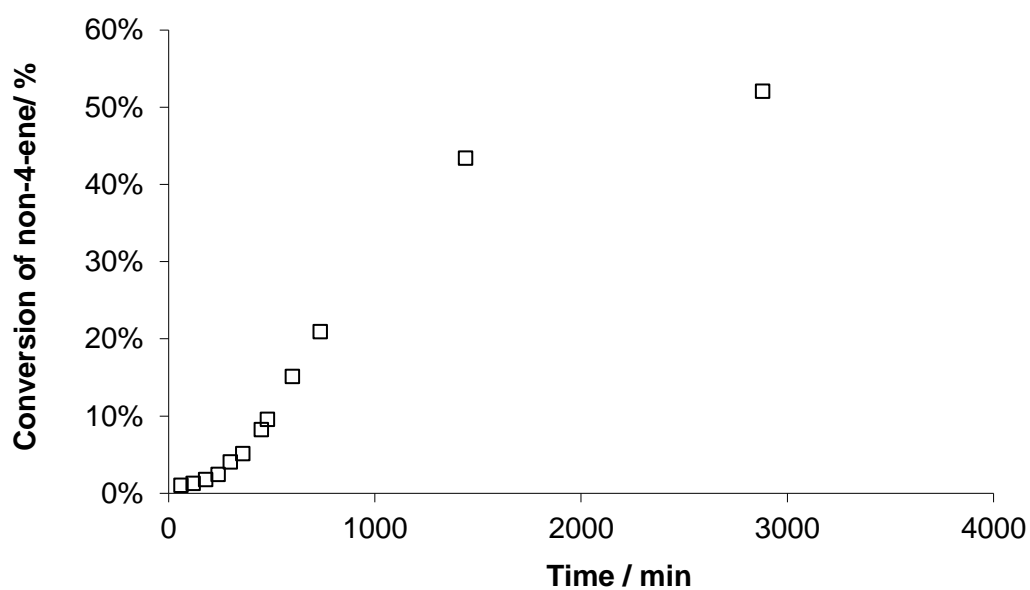


Table A.2.14. Analysis of the gas phase after exposing reduced **1-(Red)₂** to ethylene (12 h, 100 °C).

ethylene added (equiv.)	propene released (equiv.)	C4 products released (equiv.)
9.4	0.50	0.03

Br₂ exposure

1-(Red)₂ was first exposed to ethylene with the procedure described in experimental details **2.4.5**. The sample was then evacuated under high vacuum (10^{-5} mbar) for 1 h followed by the addition of a bromine solution (4 equiv., 0.19 M) in dibromomethane at -78 °C. The reaction mixture was stirred at room temperature for 2 h and quenched with a concentrated sodium thiosulphate solution. The organic layer was extracted by ethyl acetate (1 mL x 3) and dried over anhydrous magnesium sulfate. The organic layer was then analyzed by GC-MS showing the presence of 1,4-dibromobutane.

Figure A.2.32. GC-MS chromatogram of the reaction mixture after Br₂ exposure (procedure described above).

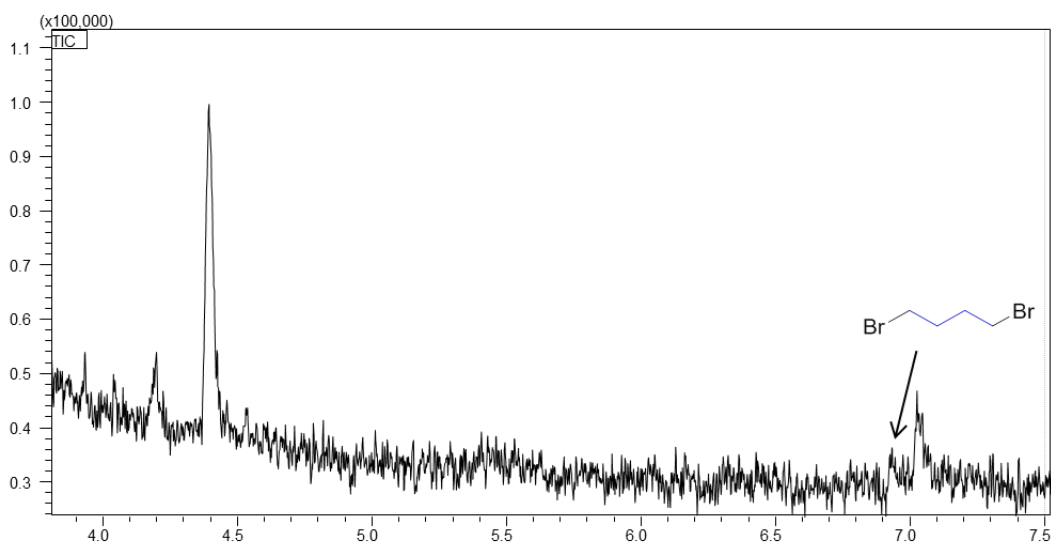


Figure A.2.33. Experimental MS spectrum of 1,4-dibromobutane (peak from 6.9 to 7 min retention time).

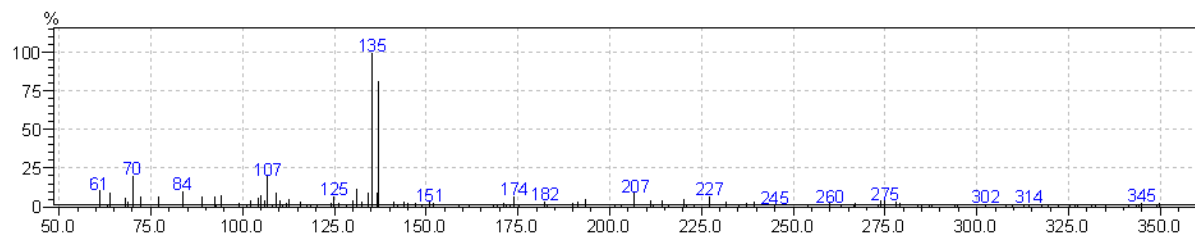
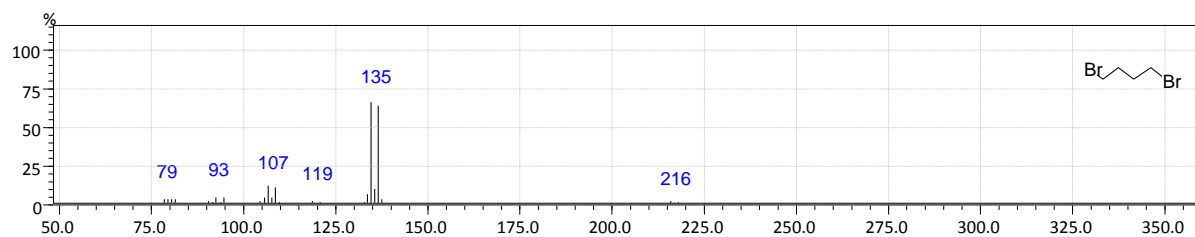


Figure A.2.34. Reference MS spectrum of 1,4-dibromobutane from NIST database



Appendix to Chapter 3

Single Crystals XRD Structures

Figure A.3.1. Thermal ellipsoid plot at 50% probability of $\text{WOCl}_2(\text{OSi}(\text{O}t\text{Bu})_3)_2(\text{py})$ **1b**. Hydrogen atoms have been omitted.

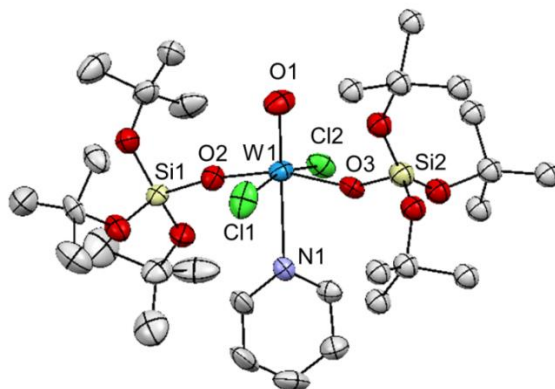


Table A.3.1. Crystal data and structure refinement for **1b**.

Identification code	1b
Empirical formula	$\text{C}_{29}\text{H}_{59}\text{Cl}_2\text{NO}_9\text{Si}_2\text{W}$
Formula weight	876.70
Temperature/K	111.92(15)
Crystal system	monoclinic
Space group	$P2_1$
$a/\text{\AA}$	9.45008(18)
$b/\text{\AA}$	14.9417(4)
$c/\text{\AA}$	14.5852(3)
$\alpha/^\circ$	90
$\beta/^\circ$	99.0652(19)
$\gamma/^\circ$	90
Volume/ \AA^3	2033.72(8)
Z	2
$\rho_{\text{calc}}/\text{g cm}^{-3}$	1.432
μ/mm^{-1}	3.074
F(000)	896.0
Crystal size/ mm^3	$0.5285 \times 0.3008 \times 0.2052$
Radiation	MoK α ($\lambda = 0.71073$)
2θ range for data collection/ $^\circ$	5.656 to 52.744
Index ranges	$-11 \leq h \leq 11, -18 \leq k \leq 18, -17 \leq l \leq 18$
Reflections collected	17559
Independent reflections	8276 [$R_{\text{int}} = 0.0316, R_{\text{sigma}} = 0.0474$]
Data/restraints/parameters	8276/7/350
Goodness-of-fit on F^2	1.045
Final R indexes [$I \geq 2\sigma(I)$]	$R_1 = 0.0534, wR_2 = 0.1201$
Final R indexes [all data]	$R_1 = 0.0569, wR_2 = 0.1226$
Largest diff. peak/hole / $e \text{\AA}^{-3}$	2.90/-1.96
Flack parameter	0.070(6)

Figure A.3.2. Thermal ellipsoid plot at 50% probability of $\text{WO}(\text{OtBuF}_6)_2\text{py}_3$ **2a**. Hydrogen atoms have been omitted.

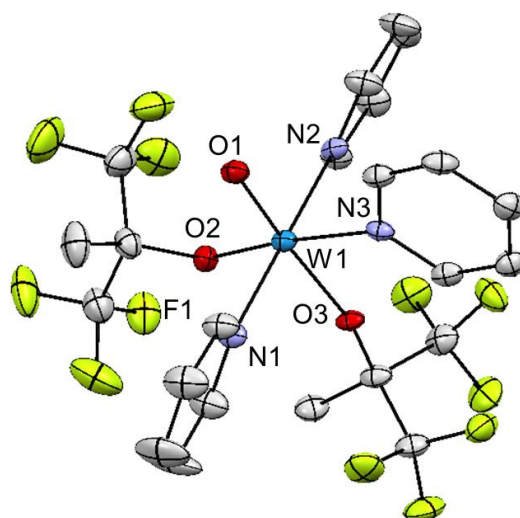


Table A.3.2. Crystal data and structure refinement for **2a**.

Identification code	2a
Empirical formula	$\text{C}_{23}\text{H}_{21}\text{F}_{12}\text{N}_3\text{O}_3\text{W}$
Formula weight	799.28
Temperature/K	100(4)
Crystal system	monoclinic
Space group	$P2_1/c$
$a/\text{\AA}$	14.62240(10)
$b/\text{\AA}$	15.53380(10)
$c/\text{\AA}$	24.4917(3)
$\alpha/^\circ$	90
$\beta/^\circ$	92.1230(10)
$\gamma/^\circ$	90
Volume/ \AA^3	5559.26(9)
Z	8
$\rho_{\text{calc}}/\text{g/cm}^3$	1.910
μ/mm^{-1}	4.267
F(000)	3088.0
Crystal size/ mm^3	$0.2269 \times 0.1714 \times 0.0587$
Radiation	$\text{MoK}\alpha$ ($\lambda = 0.71073$)
2Θ range for data collection/ $^\circ$	5.94 to 56.564
Index ranges	$-19 \leq h \leq 18, -20 \leq k \leq 20, -30 \leq l \leq 32$
Reflections collected	48961
Independent reflections	13786 [$R_{\text{int}} = 0.0492, R_{\text{sigma}} = 0.0531$]
Data/restraints/parameters	13786/0/761
Goodness-of-fit on F^2	1.004
Final R indexes [$I \geq 2\sigma(I)$]	$R_1 = 0.0335, wR_2 = 0.0677$
Final R indexes [all data]	$R_1 = 0.0458, wR_2 = 0.0725$
Largest diff. peak/hole / $e \text{\AA}^{-3}$	1.67/-1.57

Figure A.3.3. Thermal ellipsoid plot at 50% probability of $\text{WO}(\text{OSi}(\text{OtBu})_3)_2\text{py}_3$ **2b**. Hydrogen atoms have been omitted.

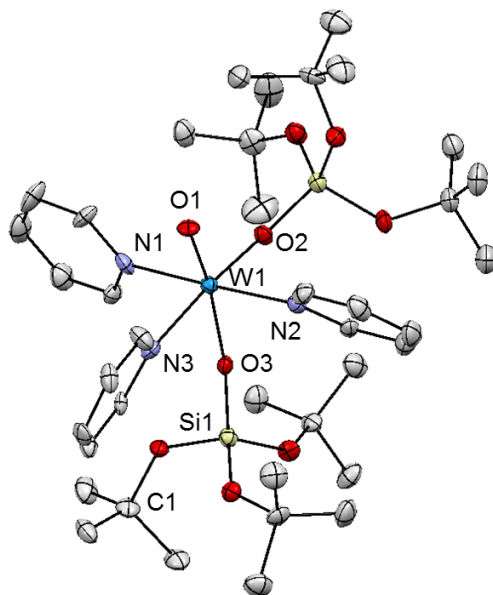


Table A.3.3. Crystal data and structure refinement for **2b**.

Identification code	2b
Empirical formula	$\text{C}_{39}\text{H}_{69}\text{N}_3\text{O}_9\text{Si}_2\text{W}$
Formula weight	964.00
Temperature/K	100(2)
Crystal system	orthorhombic
Space group	Pccn
a/Å	19.9297(10)
b/Å	28.0370(14)
c/Å	16.5710(9)
$\alpha/^\circ$	90
$\beta/^\circ$	90
$\gamma/^\circ$	90
Volume/Å ³	9259.4(8)
Z	8
$\rho_{\text{calc}}/\text{cm}^3$	1.383
μ/mm^{-1}	2.597
F(000)	3984.0
Crystal size/mm ³	0.18 × 0.13 × 0.12
Radiation	MoK α ($\lambda = 0.71073$)
2 Θ range for data collection/ $^\circ$	4.814 to 50.23
Index ranges	-22 ≤ h ≤ 23, -33 ≤ k ≤ 33, -19 ≤ l ≤ 19
Reflections collected	72144
Independent reflections	8153 [$R_{\text{int}} = 0.1287$, $R_{\text{sigma}} = 0.0735$]
Data/restraints/parameters	8153/0/505
Goodness-of-fit on F^2	1.058
Final R indexes [$I \geq 2\sigma(I)$]	$R_1 = 0.0380$, $wR_2 = 0.0668$
Final R indexes [all data]	$R_1 = 0.0945$, $wR_2 = 0.0831$
Largest diff. peak/hole / $e \text{ \AA}^{-3}$	1.89/-1.12

Figure A.3.4. Thermal ellipsoid plot at 50% probability of $\text{WO}(\text{OtBuF}_9)_2\text{py}_3$ **2c**. Hydrogen atoms have been omitted.

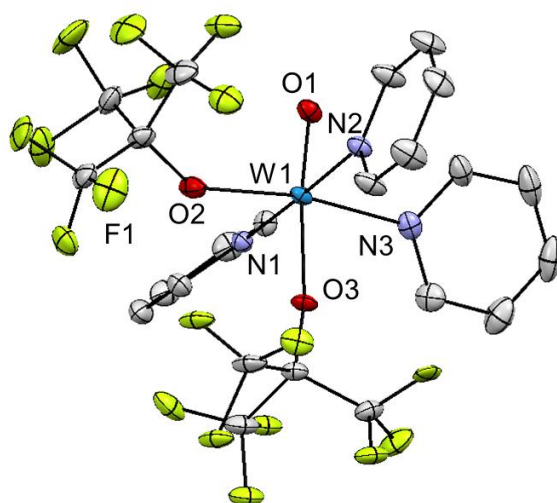


Table A.3.4. Crystal data and structure refinement for **2c**.

Identification code	2c
Empirical formula	$\text{C}_{23}\text{H}_{15}\text{F}_{18}\text{N}_3\text{O}_3\text{W}$
Formula weight	907.23
Temperature/K	100(2)
Crystal system	triclinic
Space group	P-1
a/Å	9.8228(6)
b/Å	9.9086(6)
c/Å	14.9056(8)
$\alpha/^\circ$	89.146(2)
$\beta/^\circ$	75.888(2)
$\gamma/^\circ$	78.116(2)
Volume/Å ³	1375.87(14)
Z	2
$\rho_{\text{calc}}/\text{g}/\text{cm}^3$	2.190
μ/mm^{-1}	4.355
F(000)	868.0
Crystal size/mm ³	0.29 × 0.21 × 0.12
Radiation	MoK α ($\lambda = 0.71073$)
2 θ range for data collection/ $^\circ$	4.974 to 56.614
Index ranges	-13 ≤ h ≤ 13, -13 ≤ k ≤ 13, -19 ≤ l ≤ 19
Reflections collected	71189
Independent reflections	6834 [$R_{\text{int}} = 0.0597$, $R_{\text{sigma}} = 0.0289$]
Data/restraints/parameters	6834/18/591
Goodness-of-fit on F ²	1.068
Final R indexes [$I \geq 2\sigma(I)$]	$R_1 = 0.0205$, $wR_2 = 0.0385$
Final R indexes [all data]	$R_1 = 0.0263$, $wR_2 = 0.0400$
Largest diff. peak/hole / e Å ⁻³	0.76/-0.83

Figure A.3.5. Thermal ellipsoid plot at 50% probability of $\text{WO}(\text{OtBuF}_6)_2\text{py}_2(\text{C}_2\text{H}_4)$ **3a-C₂H₄**. Hydrogen atoms have been omitted.

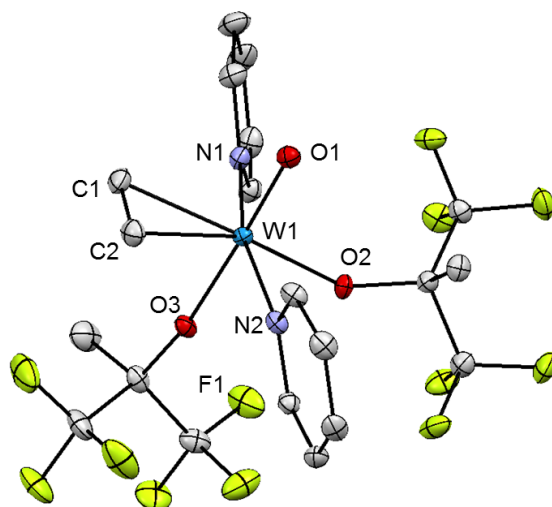


Table A.3.5. Crystal data and structure refinement for **3a-C₂H₄**.

Identification code	3a-C₂H₄
Empirical formula	$\text{C}_{20}\text{H}_{20}\text{F}_{12}\text{N}_2\text{O}_3\text{W}$
Formula weight	748.23
Temperature/K	100(2)
Crystal system	monoclinic
Space group	$P2_1/n$
$a/\text{\AA}$	9.9222(6)
$b/\text{\AA}$	15.4195(10)
$c/\text{\AA}$	15.5790(10)
$\alpha/^\circ$	90
$\beta/^\circ$	93.7910(10)
$\gamma/^\circ$	90
Volume/ \AA^3	2378.3(3)
Z	4
$\rho_{\text{calc}}/\text{g cm}^{-3}$	2.090
μ/mm^{-1}	4.978
F(000)	1440.0
Crystal size/ mm^3	$0.55 \times 0.34 \times 0.24$
Radiation	MoK α ($\lambda = 0.71073$)
2θ range for data collection/ $^\circ$	3.72 to 56.68
Index ranges	$-13 \leq h \leq 13, -20 \leq k \leq 20, -20 \leq l \leq 20$
Reflections collected	33303
Independent reflections	5945 [$R_{\text{int}} = 0.0487, R_{\text{sigma}} = 0.0342$]
Data/restraints/parameters	5945/0/423
Goodness-of-fit on F^2	1.029
Final R indexes [$I \geq 2\sigma(I)$]	$R_1 = 0.0217, wR_2 = 0.0440$
Final R indexes [all data]	$R_1 = 0.0286, wR_2 = 0.0462$
Largest diff. peak/hole / $e \text{\AA}^{-3}$	0.85/-0.46

Figure A.3.6. Thermal ellipsoid plot at 50% probability of $\text{WO}(\text{OtBuF}_6)_2\text{py}_2(\text{C}_3\text{H}_6)$ **3a-C₃H₆**. Hydrogen atoms have been omitted.

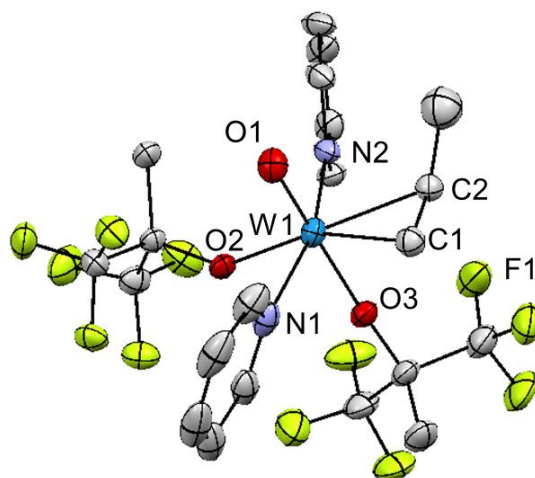


Table A.3.6. Crystal data and structure refinement for **3a-C₃H₆**.

Identification code	3a-C₃H₆
Empirical formula	$\text{C}_{21}\text{H}_{22}\text{F}_{12}\text{N}_2\text{O}_3\text{W}$
Formula weight	762.25
Temperature/K	100(10)
Crystal system	monoclinic
Space group	$P2_1/n$
$a/\text{\AA}$	9.16344(15)
$b/\text{\AA}$	15.7018(3)
$c/\text{\AA}$	17.4999(3)
$\alpha/^\circ$	90
$\beta/^\circ$	95.5026(16)
$\gamma/^\circ$	90
Volume/ \AA^3	2506.32(7)
Z	4
$\rho_{\text{calc}}/\text{cm}^3$	2.020
μ/mm^{-1}	4.726
F(000)	1472.0
Crystal size/ mm^3	$0.4036 \times 0.3301 \times 0.1644$
Radiation	$\text{MoK}\alpha$ ($\lambda = 0.71073$)
2θ range for data collection/ $^\circ$	5.692 to 56.558
Index ranges	$-12 \leq h \leq 12, -20 \leq k \leq 20, -23 \leq l \leq 23$
Reflections collected	49281
Independent reflections	6215 [$R_{\text{int}} = 0.0620, R_{\text{sigma}} = 0.0382$]
Data/restraints/parameters	6215/36/354
Goodness-of-fit on F^2	1.050
Final R indexes [$I \geq 2\sigma(I)$]	$R_1 = 0.0300, wR_2 = 0.0554$
Final R indexes [all data]	$R_1 = 0.0409, wR_2 = 0.0589$
Largest diff. peak/hole / $e \text{\AA}^{-3}$	0.88/-0.78

Catalytic Activity Measurements

Starting materials. *Cis*-4-nonene (> 97%) and 1-nonene (> 99.5%) were purchased from TCI Chemicals. HPLC grade toluene and heptane were distilled from Na/benzophenone, degassed by 3 freeze-pump-thaw cycles, and stored in a glove-box over Selexsorb. Al₂O₃ was dried at 250 °C in high vacuum overnight. Molecular sieves were activated at 300 °C in high vacuum overnight. BASF Selexsorb® CD 1/8” was calcined at 550 °C in air for 12 h and heated in high vacuum at 500 °C for 2 h.

Preparation of olefin stock solutions. *Cis*-4-nonene was stirred at room temperature with Na overnight, distilled in vacuo, degassed by 3 freeze-pump-thaw cycles, and stored in the glovebox over 3 Å MS. Before the preparation of stock solution, neat *cis*-4-nonene was passed through a pad of activated neutral Al₂O₃ (~3 mL per 10 mL of *cis*-4-nonene) inside a glove-box and then treated with Selexsorb (~20–30% w/w) for 5 hours. Selexsorb was filtered off and the as-prepared *cis*-4-nonene was used for the preparation of stock solution (~1.0 M) in toluene, using *n*-heptane (~0.1 M) as an internal standard. The solution was stored in a glove-box in an ampoule with a Teflon stopcock. 1-nonene solutions (~1.0 M) were prepared according to the same procedure.

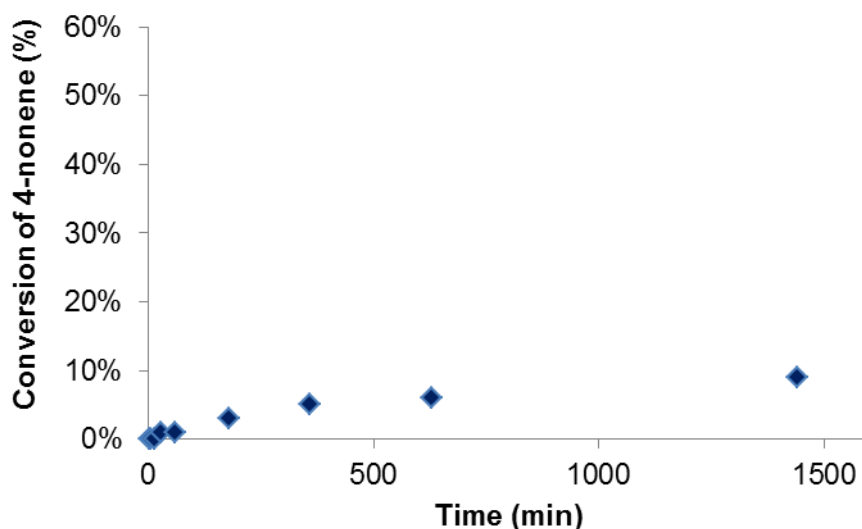


Figure A.3.7. Self-metathesis of *cis*-4-nonene (300 equiv) catalyzed by **2a** in the presence of ZnCl₂(dioxane) (1 mol%) at 70 °C.

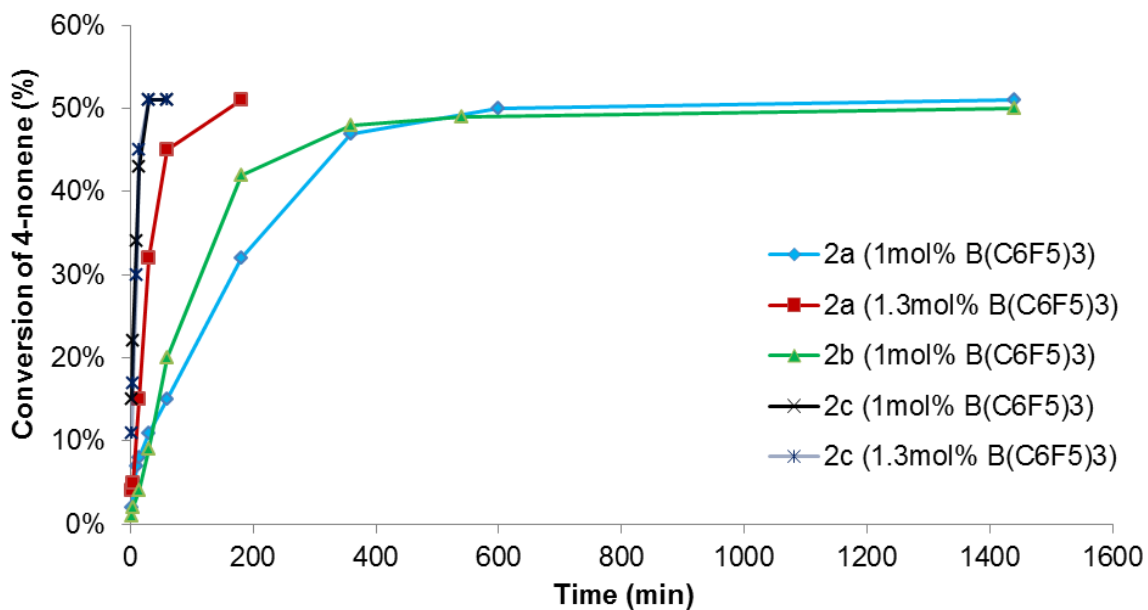


Figure A.3.8. Self-metathesis of *cis*-4-nonenene (300 equiv) catalyzed by **2a-2c** in the presence of B(C₆F₅)₃ at 70 °C.

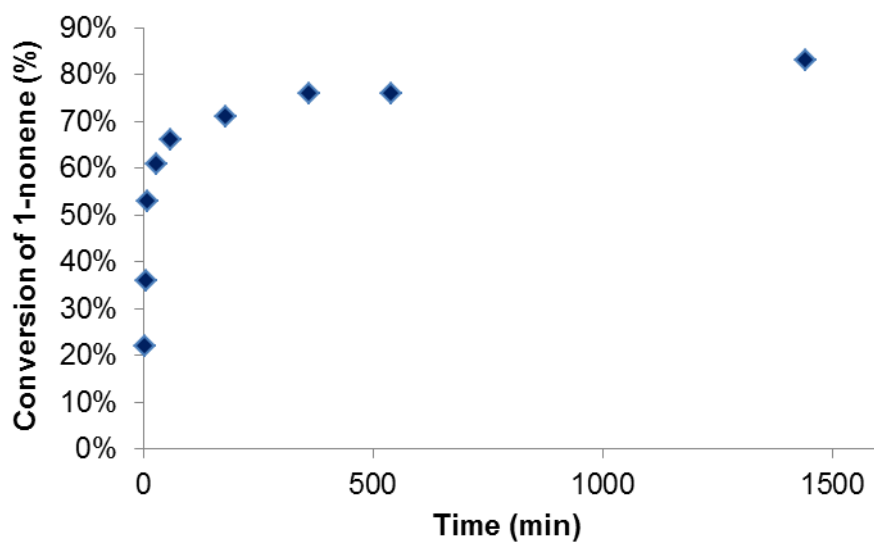


Figure A.3.9. Self-metathesis of 1-nonenene (100 equiv) catalyzed by **2c** in the presence of B(C₆F₅)₃ (3 mol%) at 70 °C.

Procedure for observation of 4a. **2a** (10 mg, 12.5 μmol , 1 equiv) and $\text{B}(\text{C}_6\text{F}_5)_3$ (19 mg, 37.5 μmol , 3 equiv) were loaded in a J-Young NMR tube and sealed. The NMR tube was attached onto high vacuum line, evacuated and contacted with ^{13}C -dilabled ethylene (ca. 6 equiv). The olefin was condensed with liquid nitrogen into the NMR tube and frozen (by liquid nitrogen). Then, C_6D_6 (ca. 0.5 mL) was vacuum transferred and condensed into the NMR tube. The frozen mixture was slowly warmed up to room temperature. The light brown reaction mixture was heated at 50 $^\circ\text{C}$ for 16 h (further heating at 70 $^\circ\text{C}$ or 50 $^\circ\text{C}$ for 36 h lead to the formation of 1-butene). The reaction was monitored by in-situ ^1H and ^{13}C NMR spectroscopy

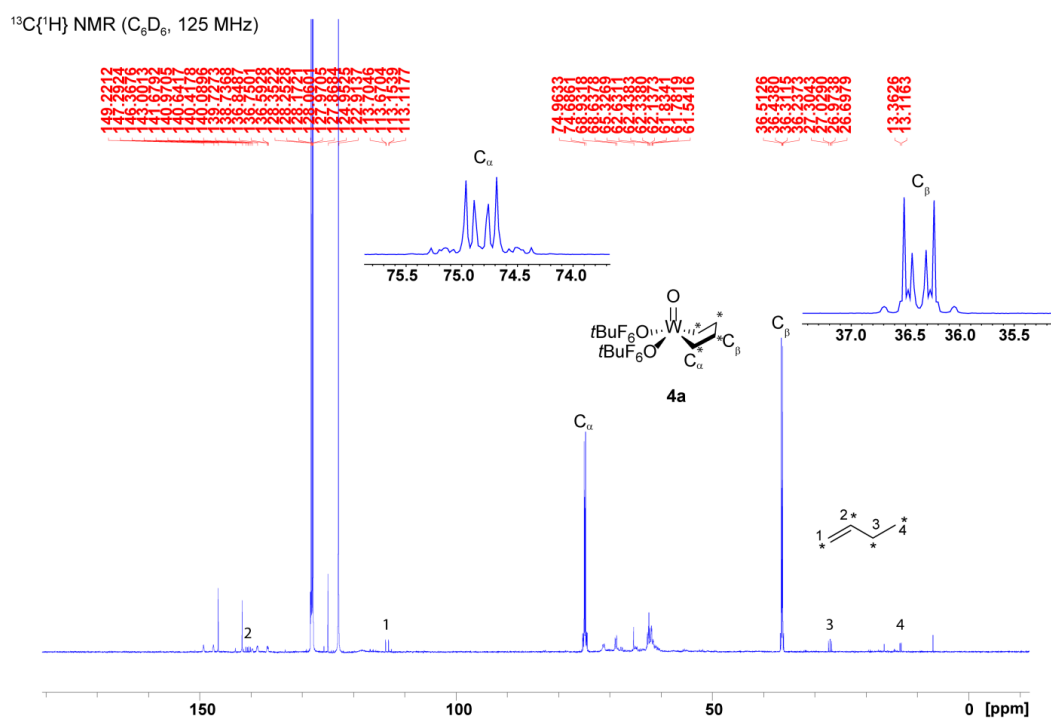


Figure A.3.10. In situ $^{13}\text{C}\{^1\text{H}\}$ NMR spectrum of the reaction of **2a**, $\text{B}(\text{C}_6\text{F}_5)_3$ and $^{13}\text{C}_2\text{H}_4$ after heating at 50 $^\circ\text{C}$ for 36 h.

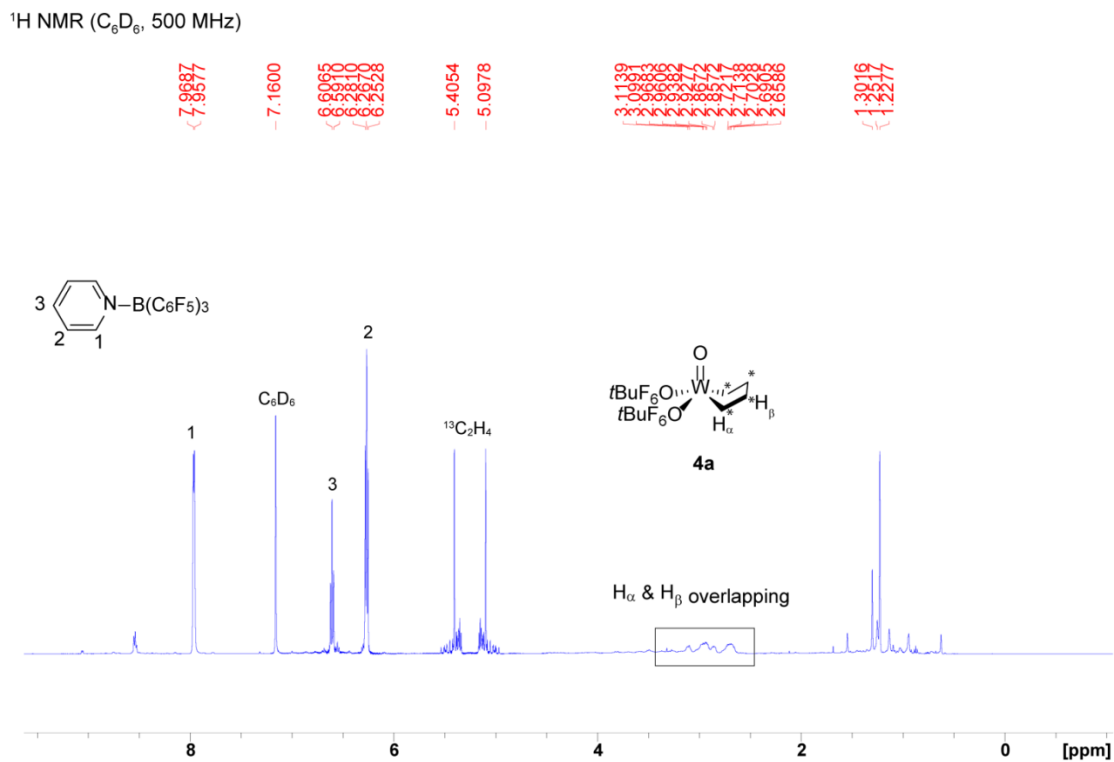


Figure A.3.11. In situ ^1H NMR spectrum of the reaction of **2a**, $\text{B}(\text{C}_6\text{F}_5)_3$ and $^{13}\text{C}_2\text{H}_4$ after heating at $50\text{ }^\circ\text{C}$ for 36 h.

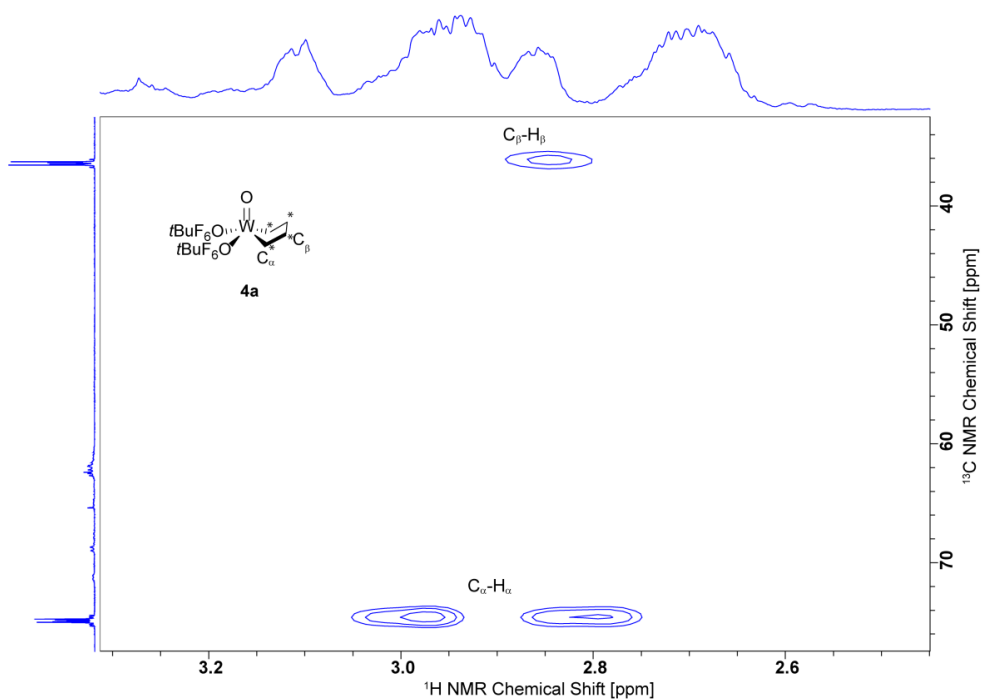


Figure A.3.12. In situ ^1H - ^{13}C HSQC NMR spectrum of the reaction of **2a**, $\text{B}(\text{C}_6\text{F}_5)_3$ and $^{13}\text{C}_2\text{H}_4$ after heating at $50\text{ }^\circ\text{C}$ for 36 h.

Reaction with propylene

$^1\text{H NMR}$ (C_6D_6 , 300 MHz)

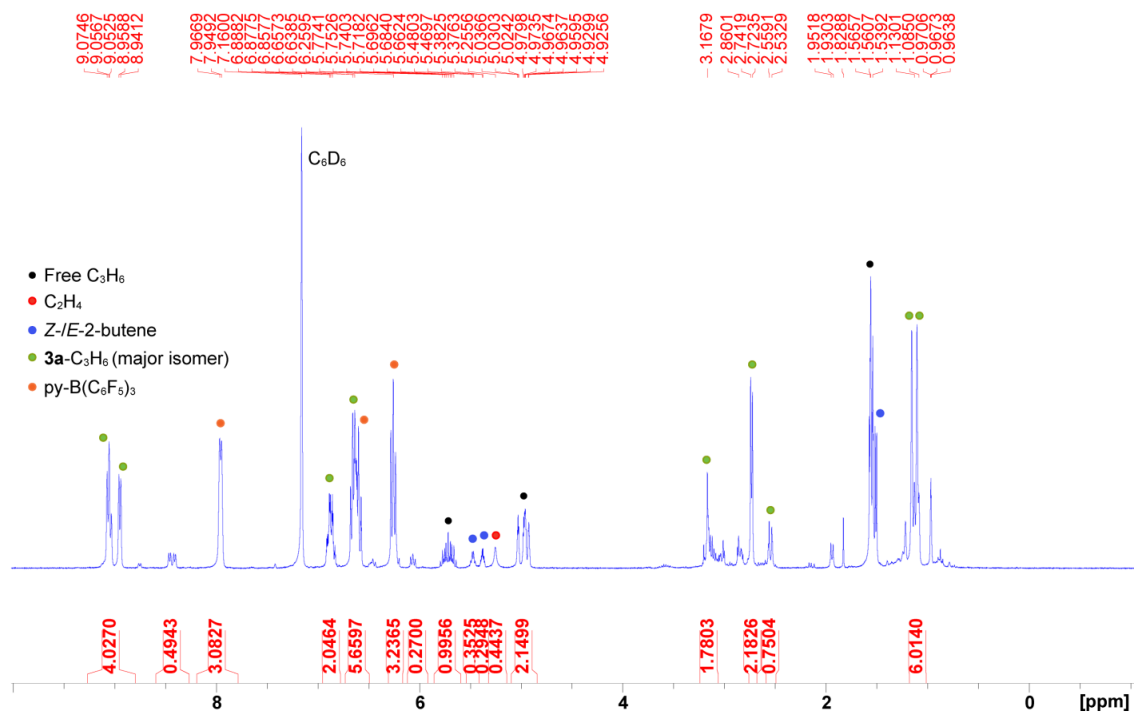


Figure A.3.13. In situ $^1\text{H NMR}$ spectrum of the reaction of **2a**, $\text{B}(\text{C}_6\text{F}_5)_3$ and C_3H_6 at room temperature for 15 min.

Reaction with styrene

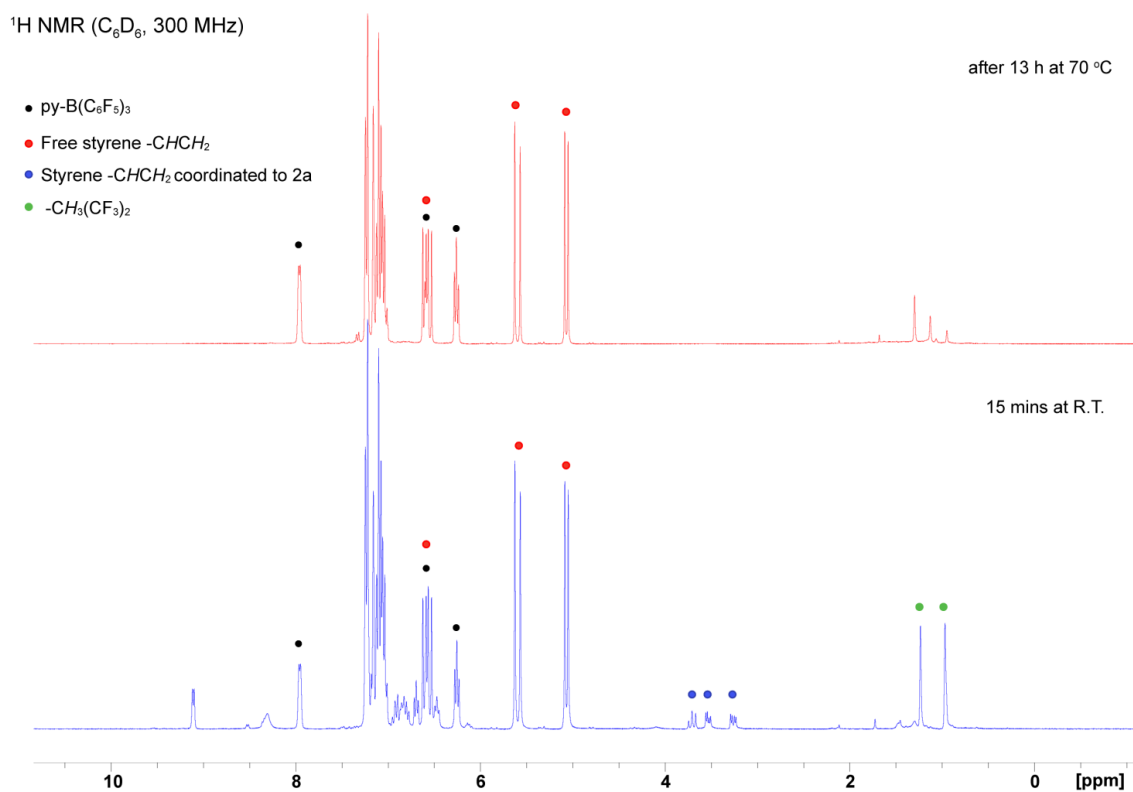


Figure A.3.14. In situ ^1H NMR spectra of the reaction of **2a**, $\text{B}(\text{C}_6\text{F}_5)_3$ and styrene at room temperature for 15 min (blue; bottom) and after heating at 70 °C for 13 h (red; top) (no self-metathesis product was observed).

Reaction with *trans*- β -methylstyrene

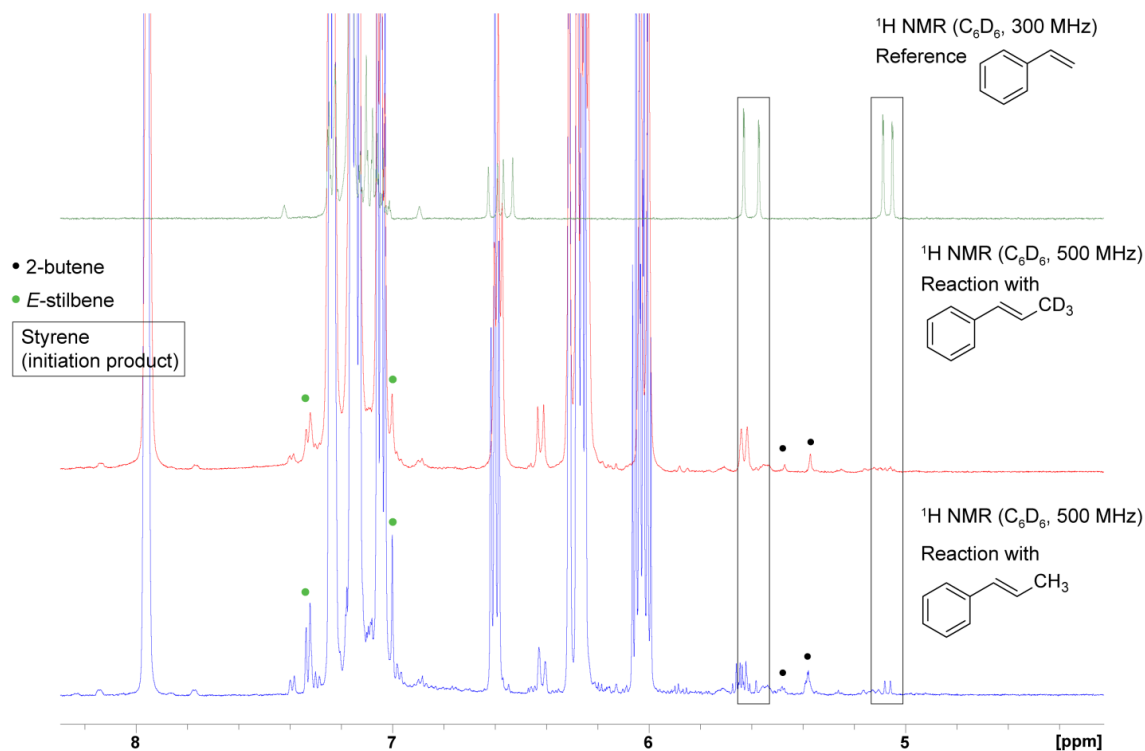


Figure A.3.15. In situ $^1\text{H NMR}$ spectra of the reaction of **2a**, $\text{B}(\text{C}_6\text{F}_5)_3$ and *trans*- β -methylstyrene (blue; bottom) or *trans*- β -(methyl- d_3)styrene (red; middle) at 70°C for 3.5 h; $^1\text{H NMR}$ spectrum of pure styrene as reference (green; top).

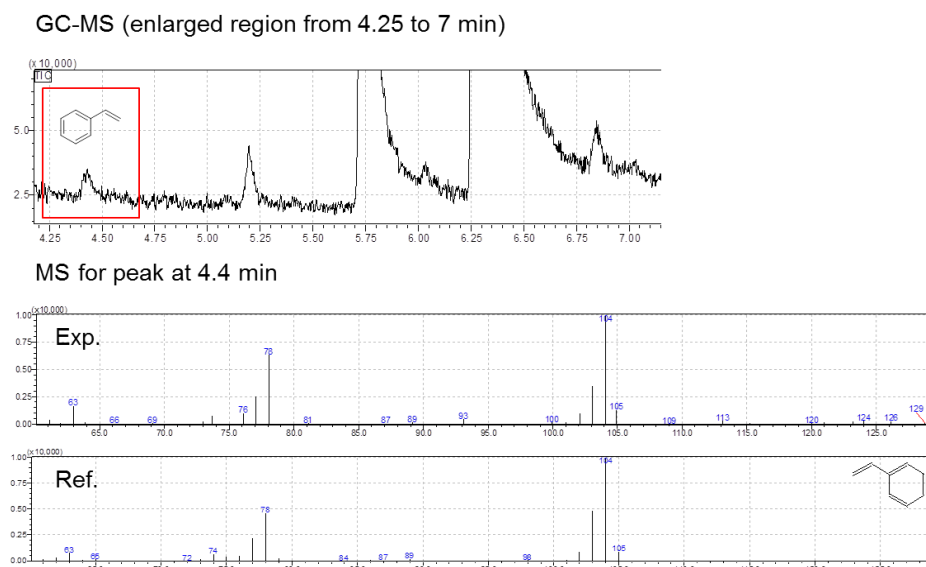
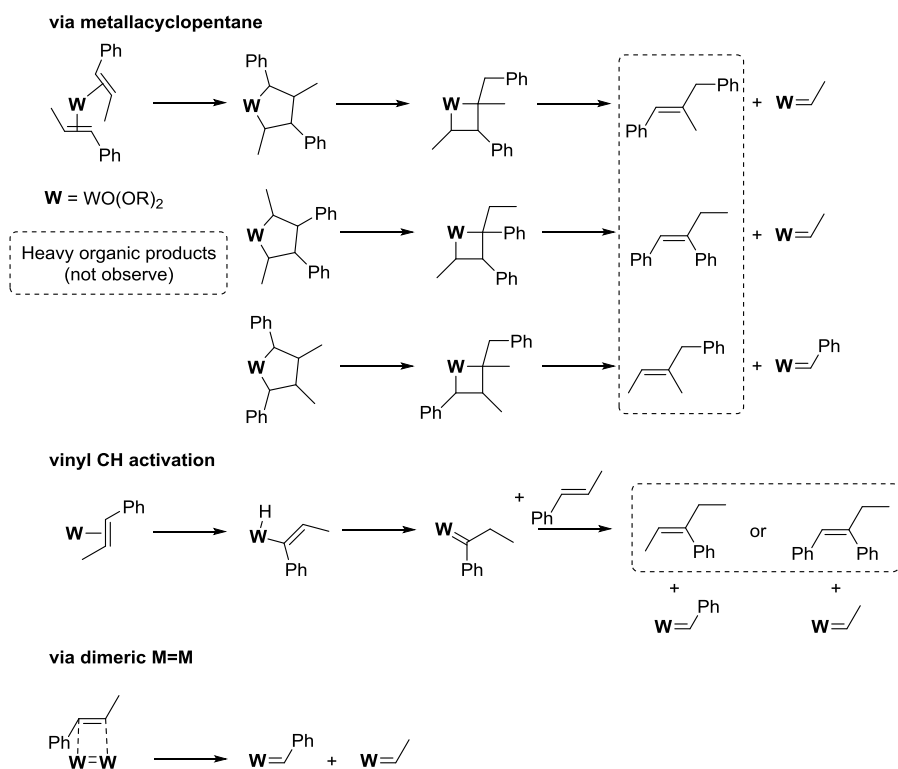


Figure A.3.16. GC-MS chromatogram (top), experimental MS spectrum (middle) and reference MS spectrum (bottom) of the reaction mixture of **2a**, $\text{B}(\text{C}_6\text{F}_5)_3$ and *trans*- β -methylstyrene after heating at 70°C for 3.5 h.



Scheme A.3.1. Possible initiation products (which were not observed experimentally by GC-MS) that would be formed from others initiation mechanisms.

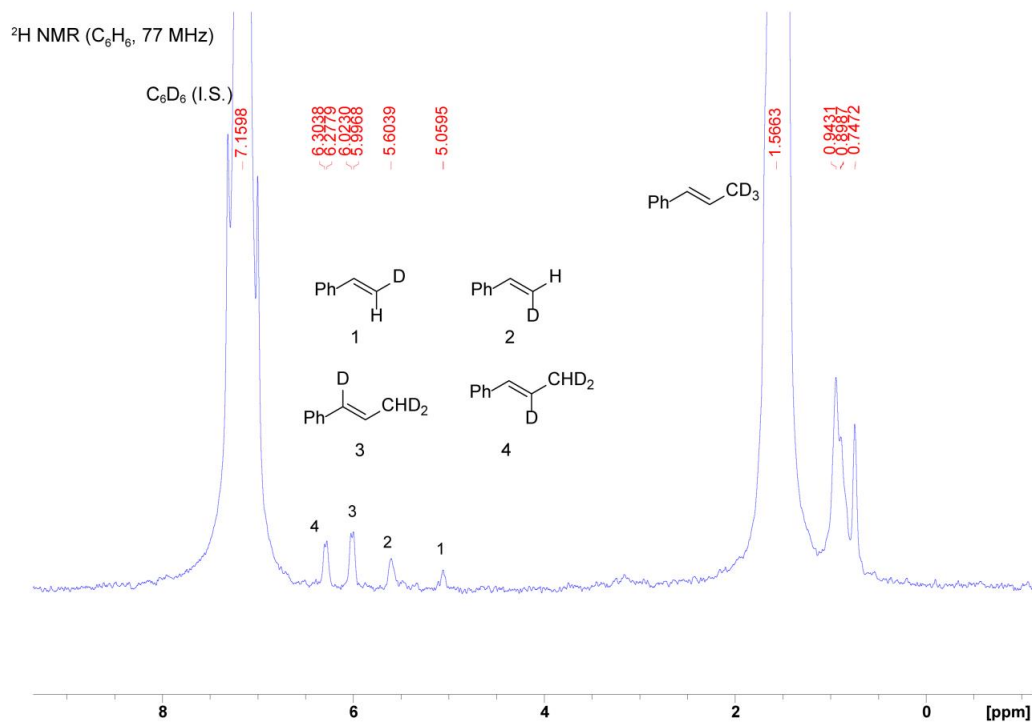


Figure A.3.17. In situ 2H NMR spectrum of the reaction of **2a**, $B(C_6F_5)_3$ and *trans*- β -(methyl- d_3)styrene at 70 °C for 3.5 h; C_6D_6 was used as internal standard.

Determination of kinetic isotope effect

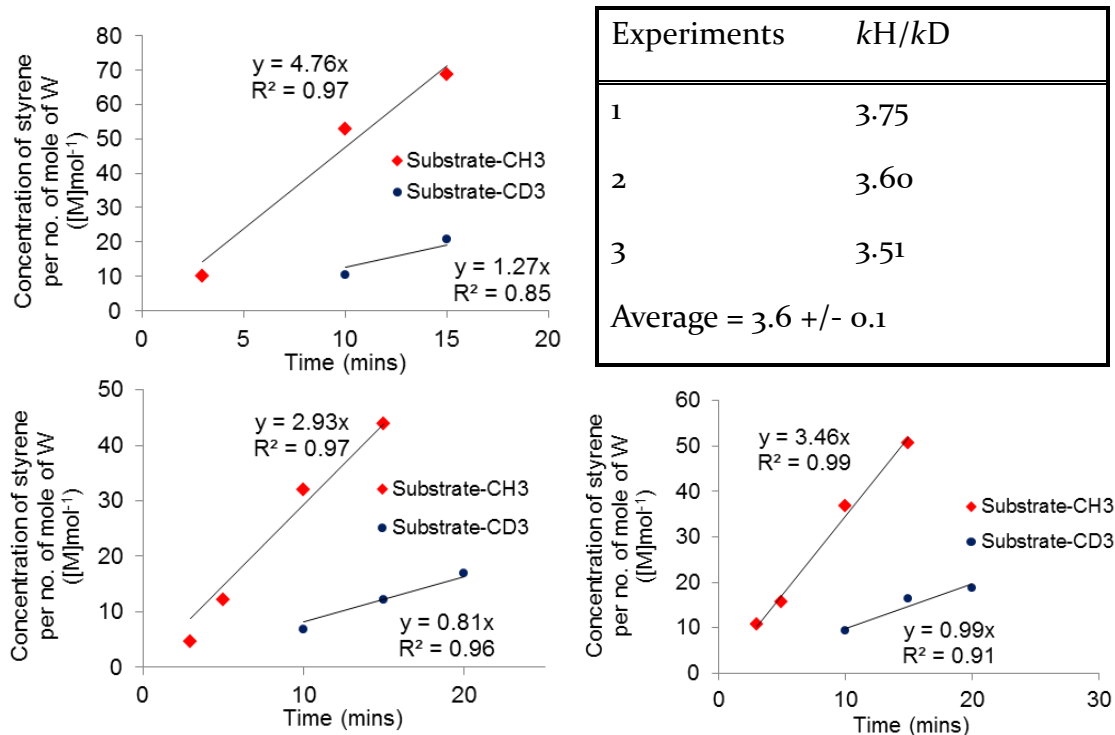


Figure A.3.18. Plots of the concentration of styrene vs time in three separate experiments with *trans*- β -methylstyrene (red diamond) and *trans*- β -(methyl- d_3)styrene (dark blue circle) as substrates.

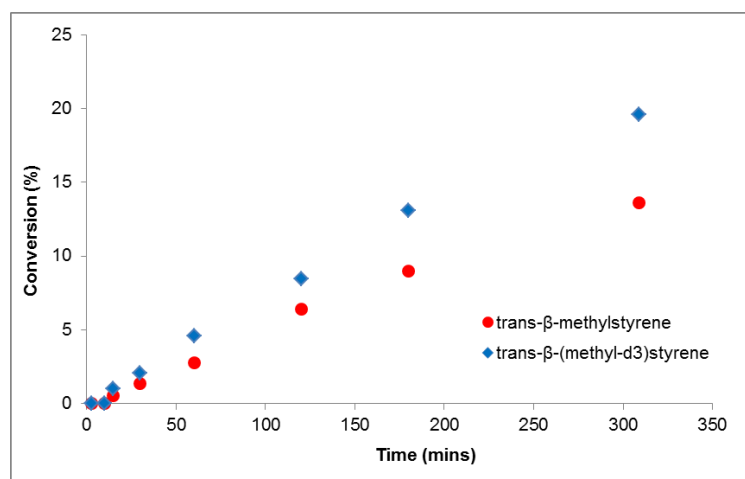
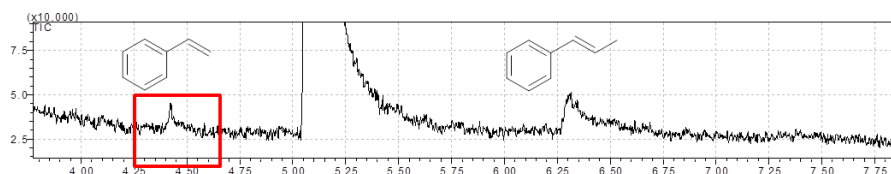


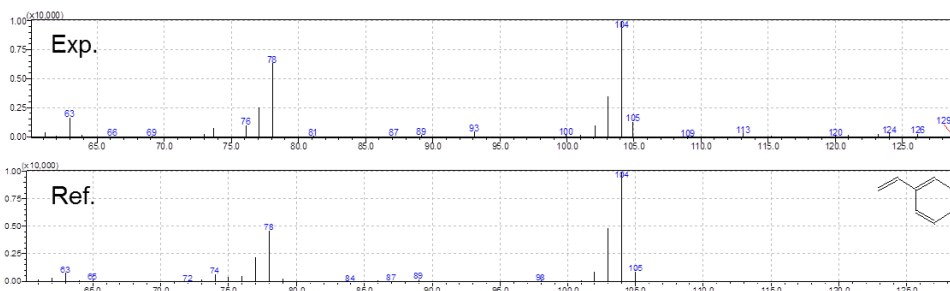
Figure A.3.19. Self-metathesis conversion of *trans*- β -methylstyrene (red circle) and *trans*- β -(methyl- d_3)styrene (blue diamond).

Reaction with allylbenzene

GC-MS (enlarged region from 4 to 7.75 min)



MS for peak at 4.4 min



MS for peak at 6.3 min

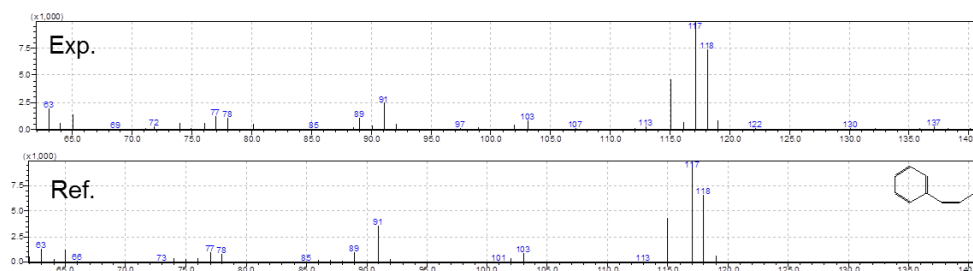


Figure A.3.20. Identification of styrene and β -methylstyrene in the reaction mixture of **2a**, $B(C_6F_5)_3$ and allylbenzene at R.T by GC-MS chromatogram (top), experimental (Exp.) MS and reference (Ref.) MS spectrum for the peaks at 4.4 min and 6.3 min.

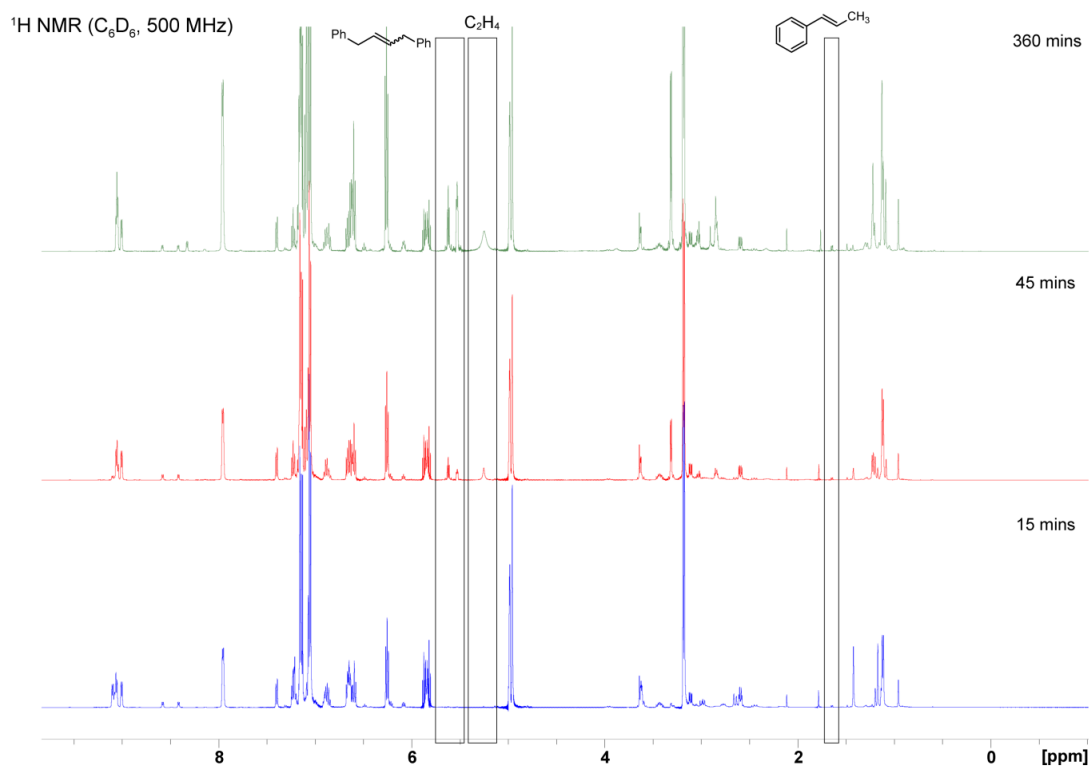


Figure A.3.21. In situ ¹H NMR spectra of the reaction of **2a**, B(C₆F₅)₃ and allylbenzene at R.T. for 15 min (blue; bottom), 45 min (red; middle) and 360 min (green; top).

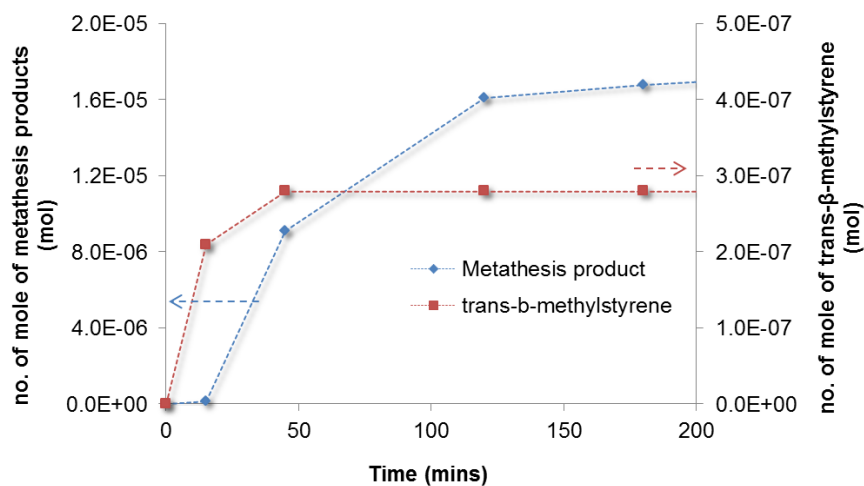


Figure A.3.22. Formation of metathesis products (blue; left axis) and *trans*- β -methylstyrene (isomerization products) (red; right axis) of the reaction of **2a**, B(C₆F₅)₃ and allylbenzene at R.T. monitored by ¹H-NMR.

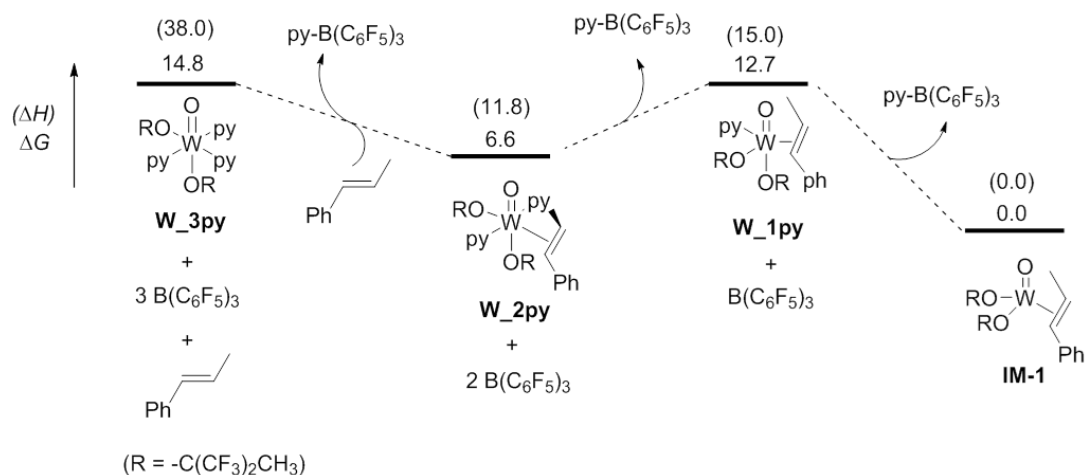


Figure A.3.23. Computed Gibbs free energies and Enthalpies in parentheses (in kcal mol⁻¹) for the formation of **IM-1** from **W_3py** (complex **2a**).

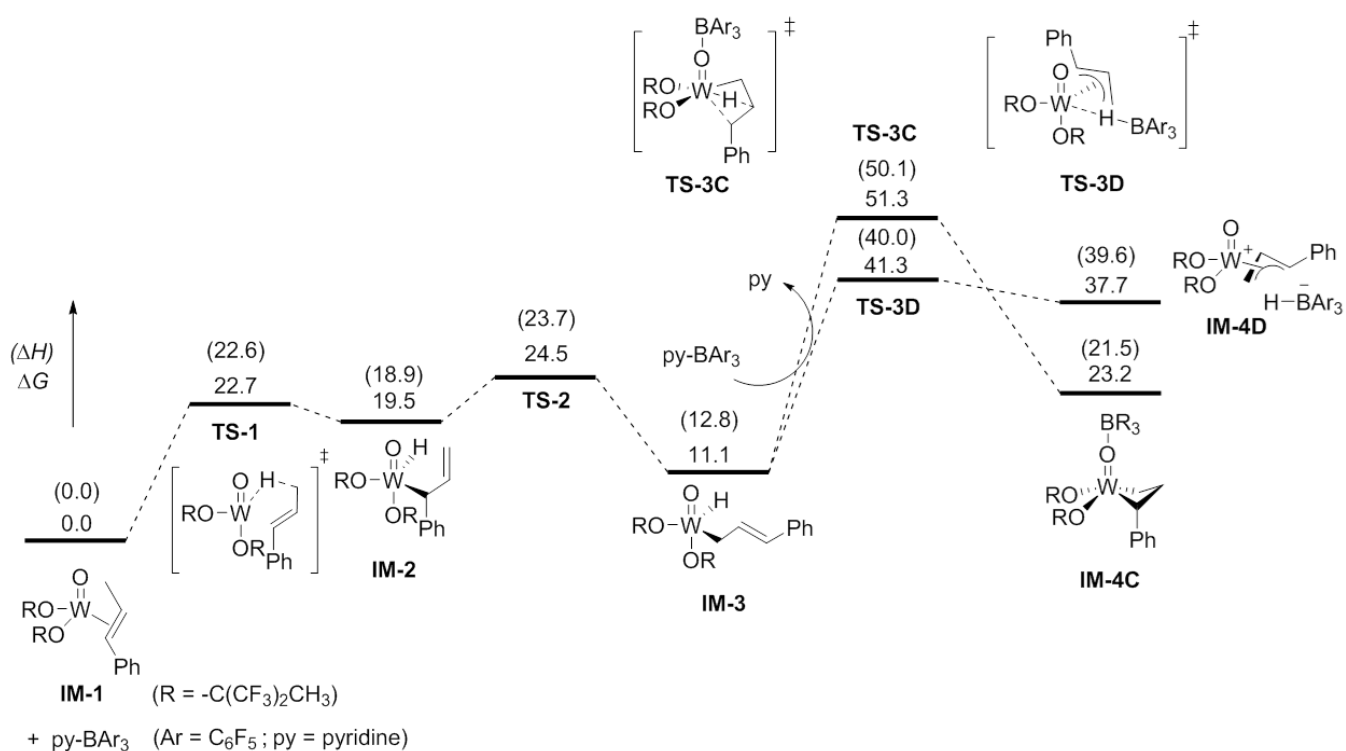


Figure A.3.24. Computed Gibbs free energies and Enthalpies in parentheses (in kcal mol⁻¹) for H-transfer pathways involving coordination of B(C₆F₅)₃ to oxo ligand (**TS-3C**) or abstraction of H by B(C₆F₅)₃ (**TS-3D**).

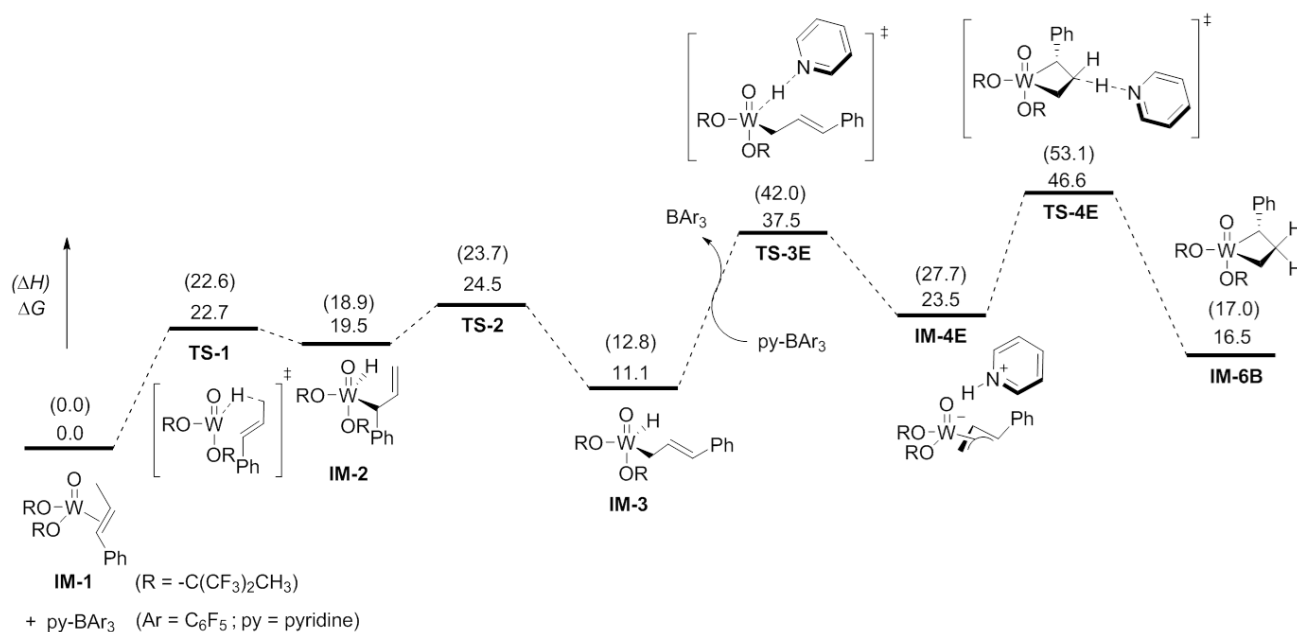


Figure A.3.25. Computed Gibbs free energies and Enthalpies in parentheses (in kcal mol⁻¹) for pyridine assisted H-transfer pathways without involving B(C₆F₅)₃.

Effect of entropic contribution on Gibbs free energy

While ΔH and ΔG are similar for most of the intermediates and transition states, they are significantly different for transition states **TS-3B** and **TS-4B** as well as the ground state **IM-4B** (Figure A.3.26). This difference is due to the bimolecular nature of the reaction of $\text{py-B}(\text{C}_6\text{F}_5)_3$ with the **W** complex leading to a significant entropic contribution. However, entropic contributions obtained by DFT for bimolecular reaction in solution is known to be typically overestimated. Applying a scaling factor of 0.5 to the entropy (S) term is often used to avoid such overestimation.⁴³⁻⁴⁶ The corresponding free energies $\Delta G_{50\%S}$ are shown in Figure A.3.26 showing that these steps are accessible. However, since it is difficult to determine what is the appropriate scaling factor for a better evaluation of the entropic contribution, we prefer to discuss this effect in a qualitative manner, instead of applying an arbitrary correction factor. Reducing the entropic contribution will not lead to a change in the preferred reaction pathway, but only further reduces its overall activation free energy.

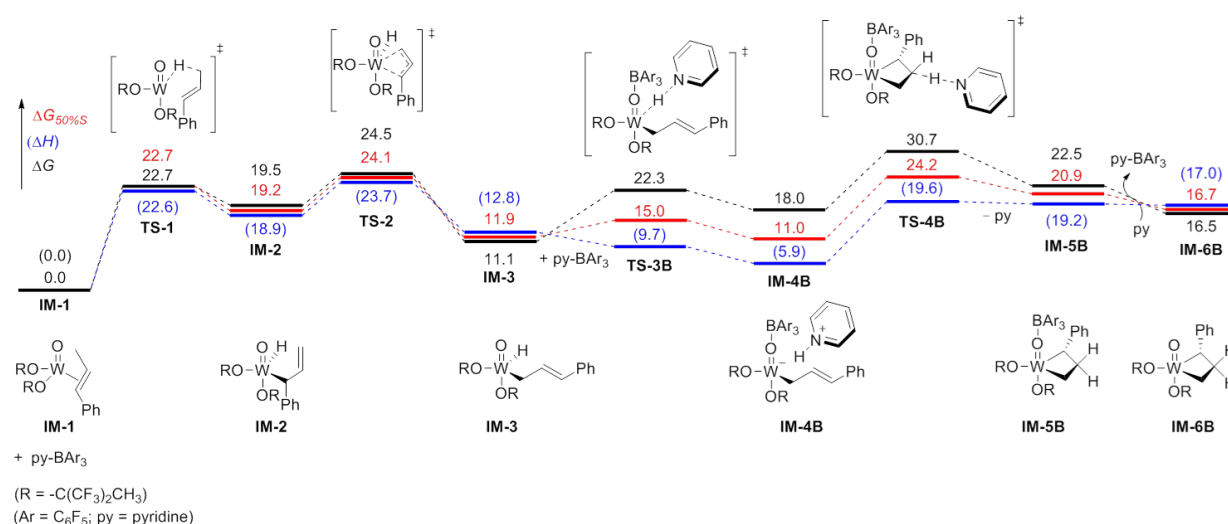


Figure A.3.26. Computed Gibbs free energies (black), Enthalpies (blue; in parentheses) and Gibbs free energies with 50 % correction on entropy (red) (in kcal mol^{-1}) as an example for illustrating the effect of entropy correction.

Calculated KIE. k_H/k_D is calculated from ΔG^\ddagger_H (**TS-4B**) and ΔG^\ddagger_D (**TS-4B-d3**) using the Eyring equation (simplified in **Figure A.3.27**, where $T = 343$ K; $R =$ gas constant).

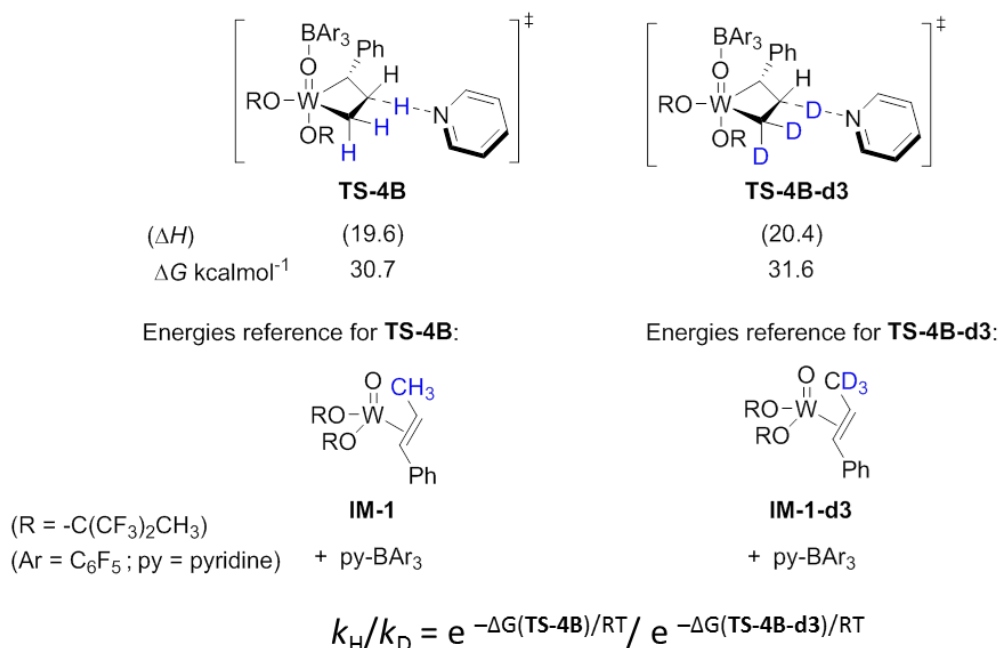


Figure A.3.27. Computed Gibbs free energies and Enthalpies in parentheses (in kcal mol⁻¹) for **TS-4B** and **TS-4B-d3**. Equation (bottom) for calculating the KIE based on computed Gibbs free energies.

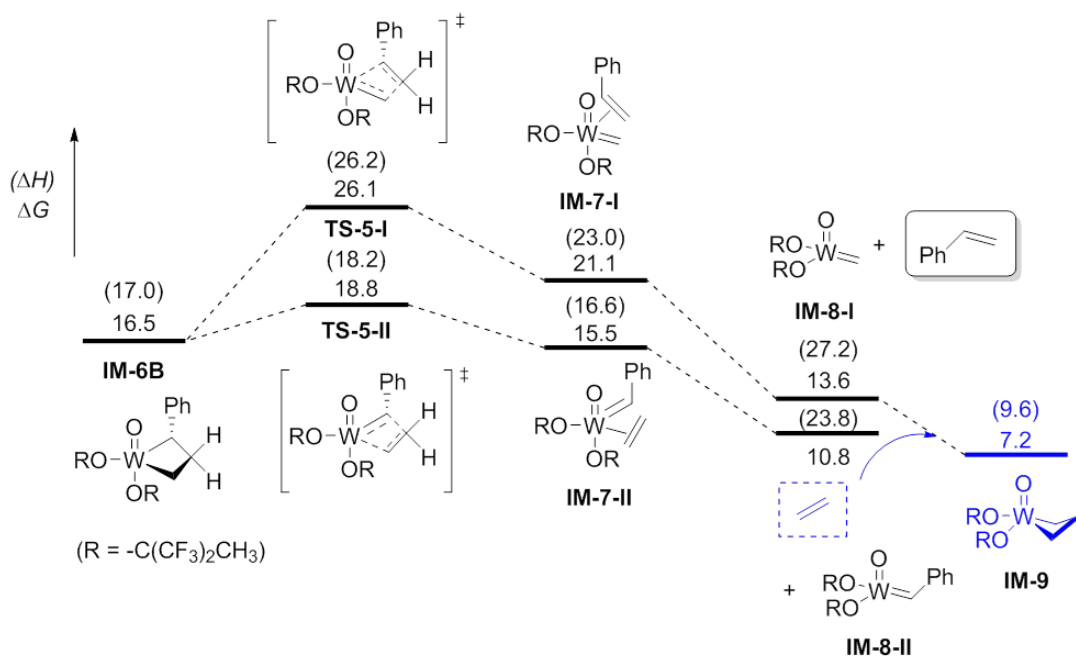


Figure A.3.28. Computed Gibbs free energies and Enthalpies in parentheses (in kcal mol⁻¹) for the formation of alkylidenes from metallacyclobutane (**IM-6B**) (energies are referenced to **IM-1**).

Table A.3.7. Computed Enthalpies and Gibbs free energies (in Hartrees or kcal/mol) for all the optimized structures and initiation pathways (**IM-1** as reference, except for **TS-4B-d3**).

label	Enthalpies (H) (a.u.)	Gibbs Free Energies (G) (a.u.)	ΔH		ΔG		ΔG corrected to 1 M kcal/mol
			a.u.	kcal/mol	a.u.	kcal/mol	
C ₂ H ₄	-78.568904	-78.595057					
Styrene	-309.630878	-309.670186					
<i>trans</i> - β - methylstyrene	-348.937248	-348.979988					
B(C ₆ F ₅) ₃	-2208.974463	-2209.066837					
py-B(C ₆ F ₅) ₃	-2457.305236	-2457.404391					
pyridine	-248.286255	-248.318868					
W_3py	-2545.002509	-2545.121281	0.060587	38.0	0.020558	12.9	14.8
W_2py	-2645.650748	-2645.773721	0.018823	11.8	0.010552	6.6	6.6
W_1py	-2397.314932	-2397.426494	0.023866	15.0	0.020225	12.7	12.7
IM-1	-2149.008025	-2149.109165	0	0	0	0	0
TS-1	-2148.971936	-2149.072933	0.036089	22.6	0.036232	22.7	22.7
IM-2	-2148.977853	-2149.07811	0.030172	19.0	0.031055	19.5	19.5
TS-2	-2148.970277	-2149.07013	0.037748	23.7	0.039035	24.5	24.5
IM-3	-2148.987568	-2149.091497	0.020457	12.8	0.017668	11.1	11.1
TS-3A	-2148.933823	-2149.034062	0.074202	46.6	0.075103	47.1	47.1
IM-4A	-2148.986553	-2149.086974	0.021472	13.5	0.022191	13.9	13.9
TS-3B	-4606.297828	-4606.474991	0.015433	9.7	0.038565	24.2	22.3
IM-4B	-4606.303871	-4606.481776	0.00939	5.9	0.03178	20.0	18.0
TS-4B	-4606.282008	-4606.461668	0.031253	19.6	0.051888	32.6	30.7
IM-5B	-4357.996412	-4358.158799	0.030594	19.2	0.035889	22.5	22.5
IM-6B	-2148.981011	-2149.082887	0.027014	17.0	0.026278	16.5	16.5
TS-3C	-4357.947376	-4358.112985	0.07963	50.0	0.081703	51.3	51.3
IM-4C	-4357.992739	-4358.157674	0.034267	21.5	0.037014	23.2	23.2
TS-3D	-4357.963316	-4358.128927	0.06369	40.0	0.065761	41.3	41.3
IM-4D	-4357.963825	-4358.134624	0.063181	39.6	0.060064	37.7	37.7
TS-3E	-2397.271814	-2397.386983	0.066984	42.0	0.059736	37.5	37.5
IM-4E	-2397.294698	-2397.409298	0.0441	27.7	0.037421	23.5	23.5
TS-4E	-2397.254117	-2397.37242	0.084681	53.1	0.074299	46.6	46.6
TS-5-I	-2148.966314	-2149.067544	0.041711	26.2	0.041621	26.1	26.1
TS-5-II	-2148.979081	-2149.079226	0.028944	18.2	0.029939	18.8	18.8
IM-7-I	-2148.971391	-2149.075584	0.036634	23.0	0.033581	21.1	21.1
IM-7-II	-2148.981517	-2149.084541	0.026508	16.6	0.024624	15.5	15.5
IM-8-I	-1839.333766	-1839.420324	0.043381	27.2	0.018655	11.7	13.6
IM-8-II	-2070.401232	-2070.499918	0.037889	23.8	0.01419	8.9	10.8
IM-9	-1917.930776	-1918.0226	0.015275	9.6	0.011436	7.2	7.2
IM-1-d3	-2149.017348	-2149.119319					
TS-4B-d3	-4606.290072	-4606.470352	0.032512	20.4	0.053358	33.5	31.6

Appendix to Chapter 4

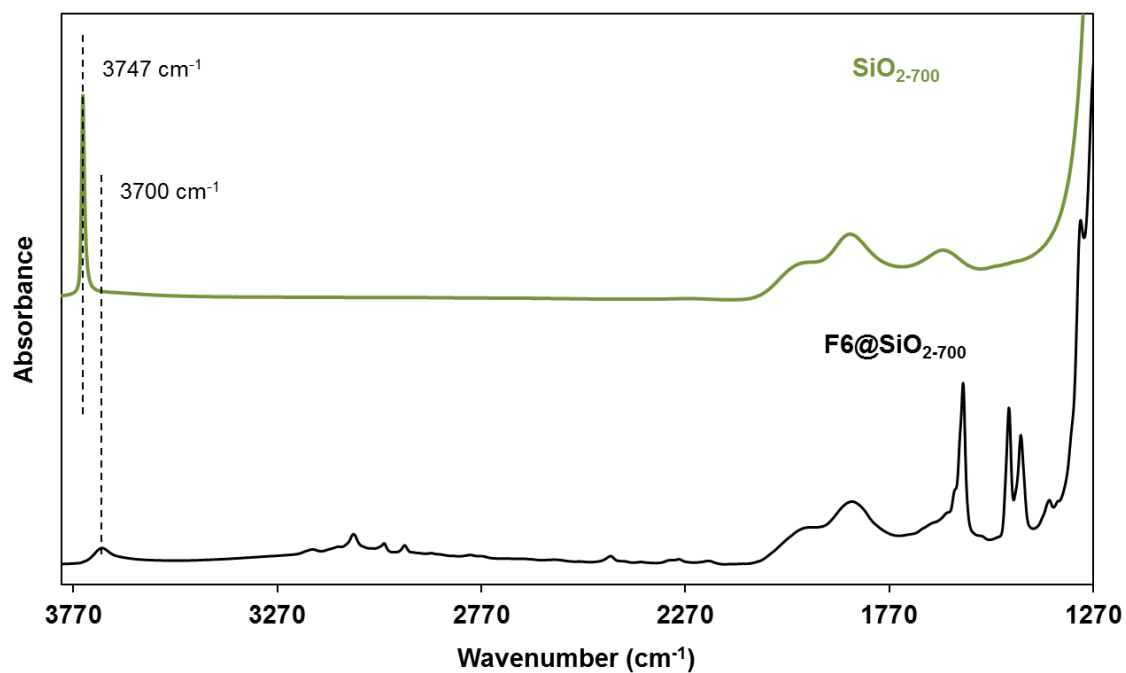


Figure A.4.1. IR spectra of SiO₂₋₇₀₀ (upper) and F6@SiO₂₋₇₀₀ (bottom)

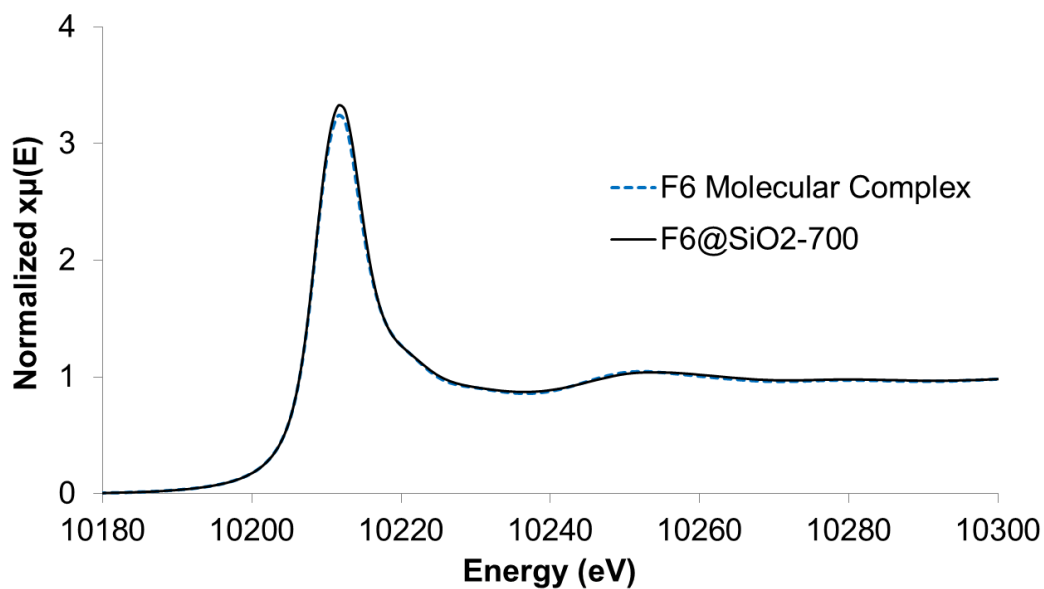


Figure A.4.2. W L_{III} edge XANES spectra of F6 molecular complex (light blue dotted line) and F6@SiO₂₋₇₀₀ (blue solid line)

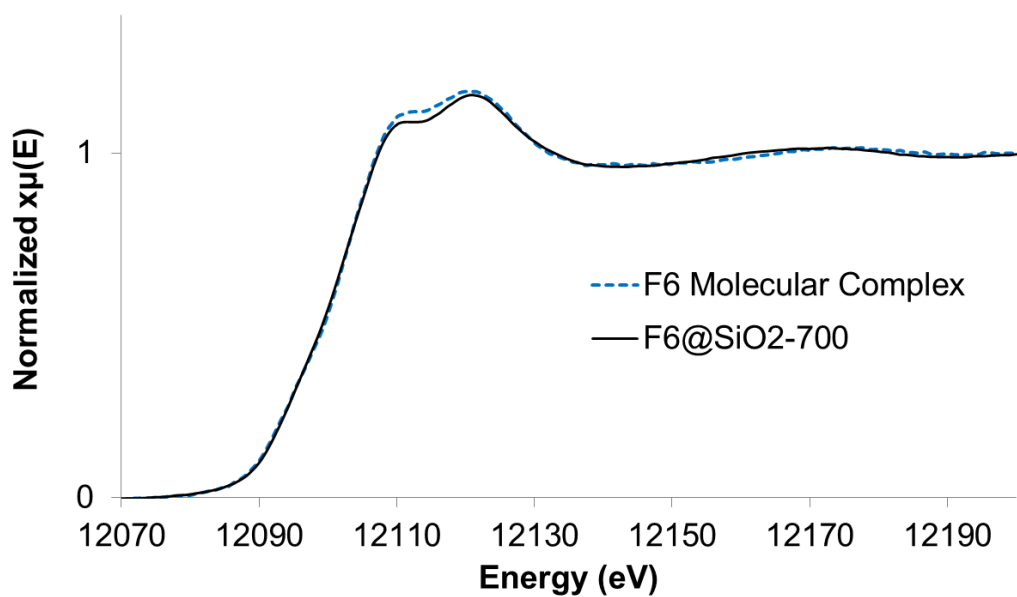


Figure A.4.3. W L_I edge XANES spectra of **F6** molecular complex (light blue dotted line) and **F6@SiO₂-700** (blue solid line)

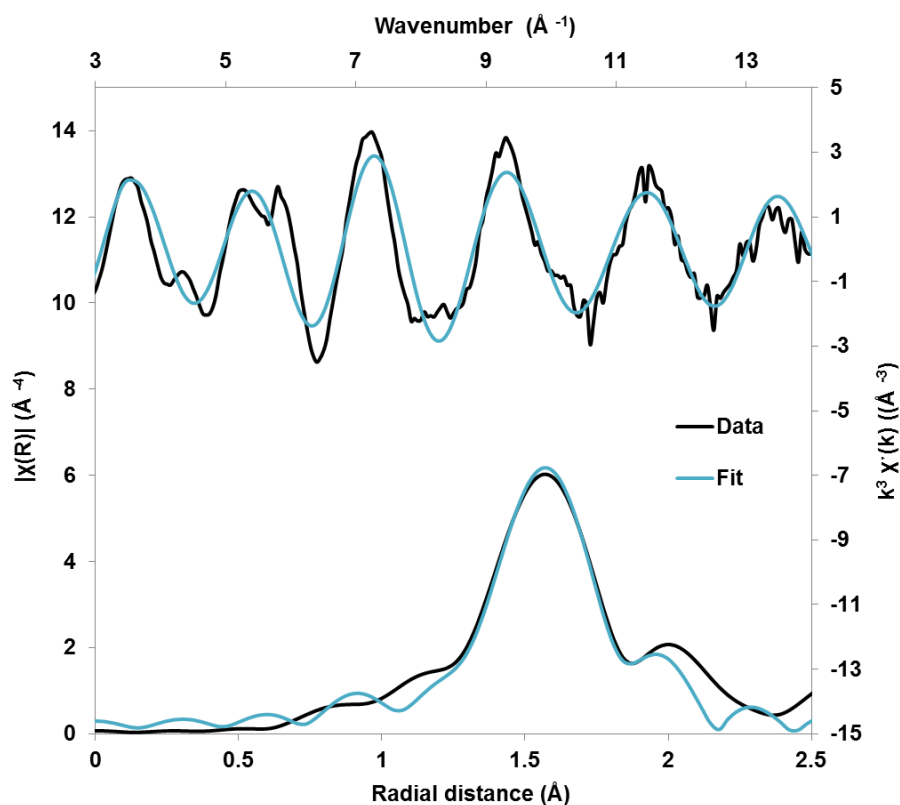


Figure A.4.4. EXAFS data (Black) and fits (Blue) in k-space (Upper; top and right axes) and R-space (Lower; bottom and left axes) of **F6@SiO₂₋₇₀₀** in W L_{III} edge.

	No. of neighbor	R (Å)	σ^2 (Å ²)
O	1*	1.73 (1)	0.002 (2)
O	2*	2.00 (3)	0.003 (2)
N	3*	2.16 (4)	0.005 (3)

Table A.4.1. EXAFS fit parameters for **F6@SiO₂₋₇₀₀**. $S0^2 = 0.92$; ΔE_0 (eV) = 9 (6); k range 3-14 Å⁻¹; R range 1-2.5 Å; k weight 3. *Fixed parameters in the fit.

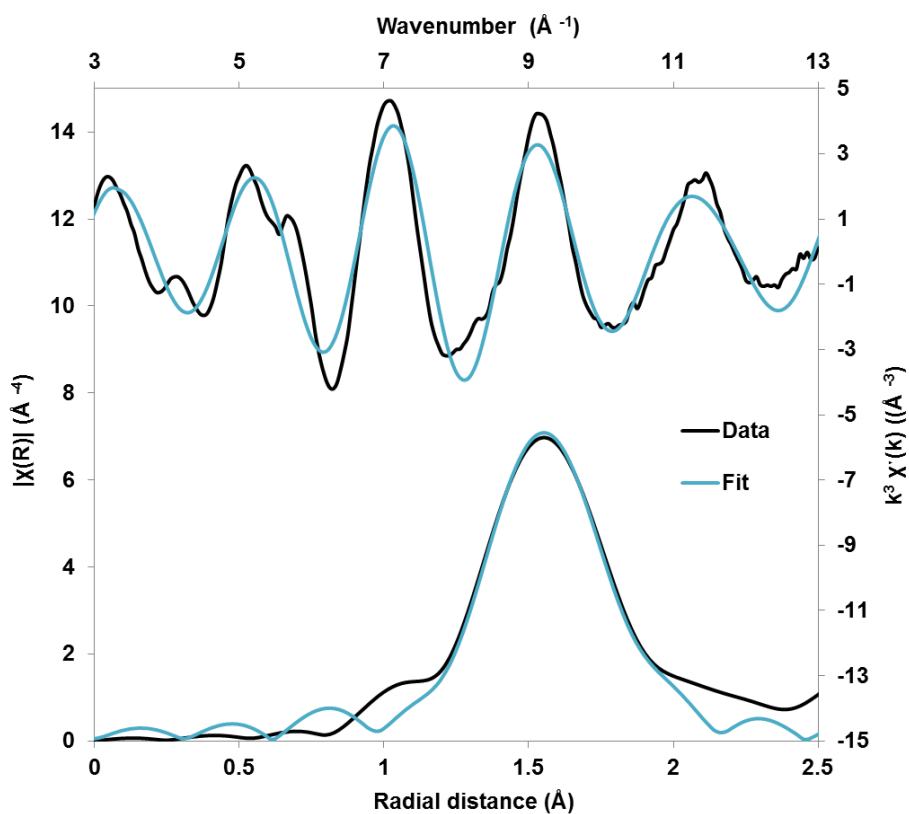


Figure A.4.5. EXAFS data (Black) and fits (Blue) in k-space (Upper; top and right axes) and R-space (Lower; bottom and left axes) of **F6** in W L_{III} edge.

	No. of neighbor	R (Å)	σ^2 (Å ²)
O	1*	1.73 (1)	0.0012 (8)
O	2*	2.02 (3)	0.0012 (8)
N	3*	2.16 (4)	0.002 (2)

Table A.4.2. EXAFS fit parameters for **F6**. $S_0^2 = 0.92$; ΔE_0 (eV) = 3 (6); k range 3-13 Å⁻¹; R range 1-2.5 Å; k weight 3. *Fixed parameters in the fit.

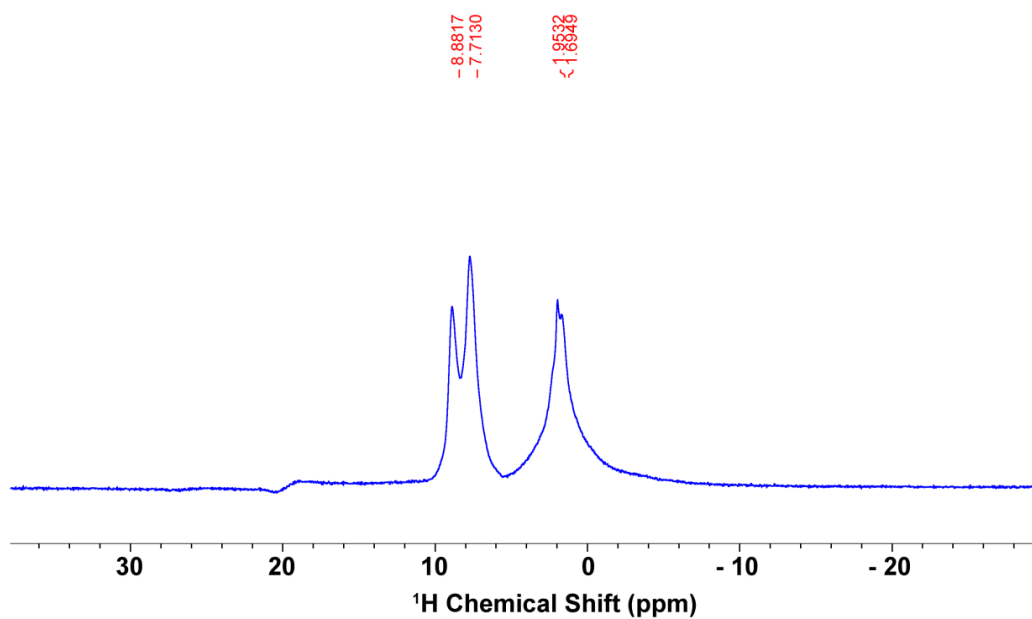


Figure A.4.6. ^1H -NMR (700 MHz, spinning rate 50kHz, 1.3 mm rotor) spectrum of **F6@SiO₂₋₇₀₀**.

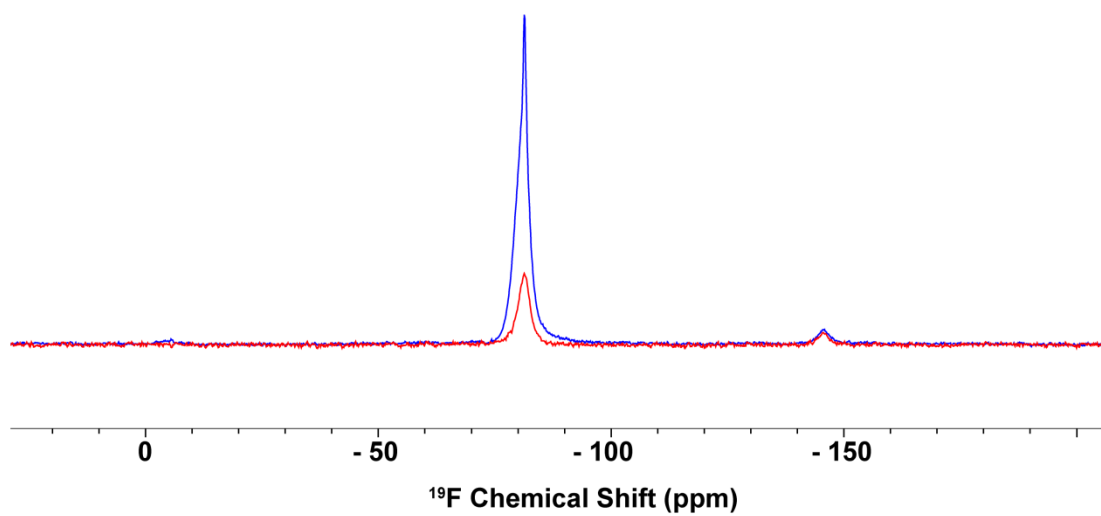


Figure A.4.7. ^{19}F -NMR (700 MHz, spinning rate 50kHz, 1.3 mm rotor) spectra of **F6@SiO₂₋₇₀₀** (blue) and the background signal (red).

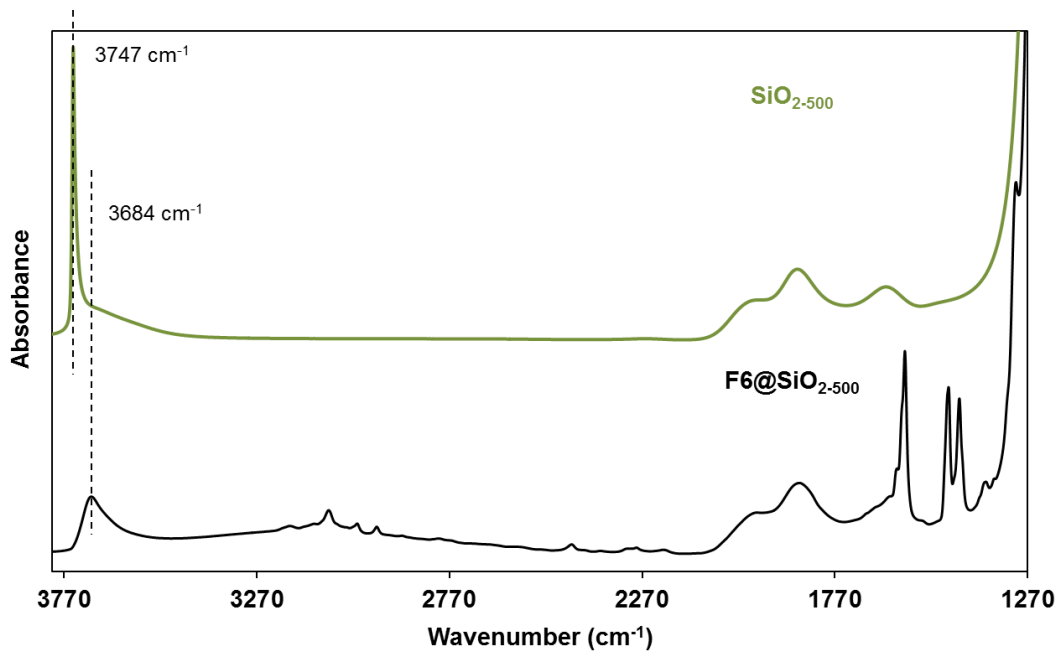


Figure A.4.8. IR spectra of SiO₂₋₅₀₀ (upper) and F6@SiO₂₋₅₀₀ (bottom).

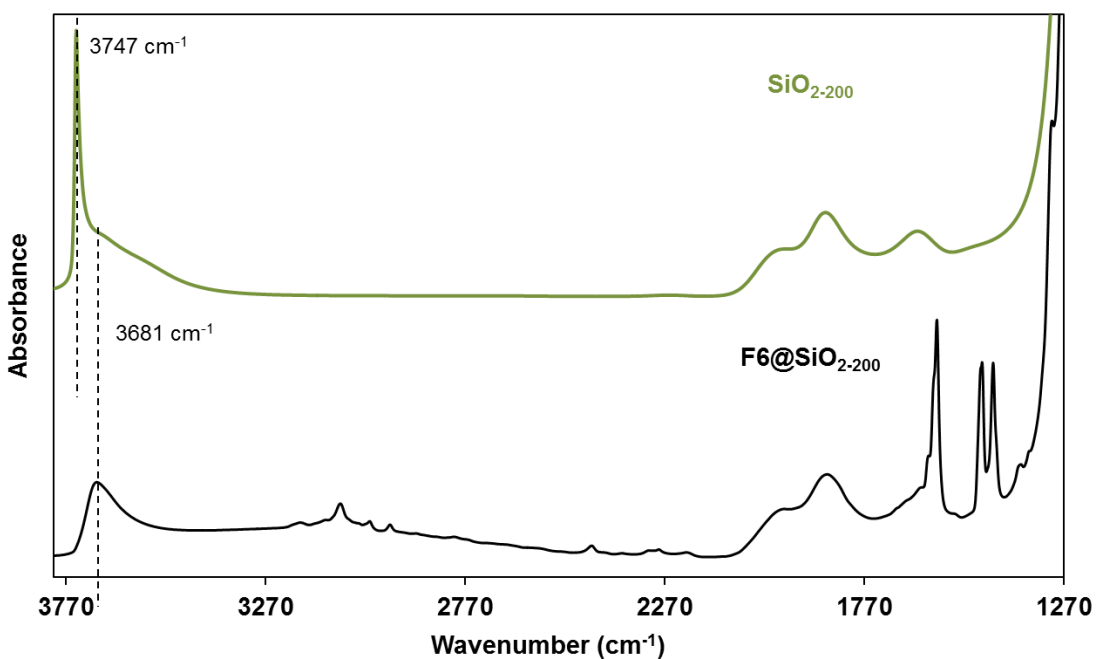


Figure A.4.9. IR spectra of SiO₂₋₂₀₀ (upper) and F6@SiO₂₋₂₀₀ (bottom).

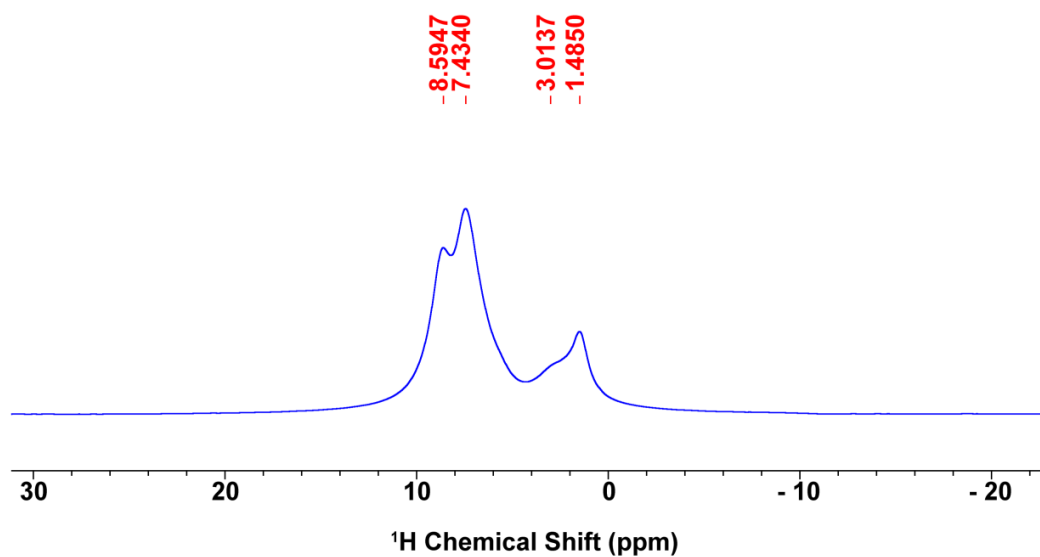


Figure A.4.10. ^1H -NMR (400 MHz, spinning rate 16kHz, 3.2 mm rotor) spectrum of **F6@SiO₂₋₂₀₀**.

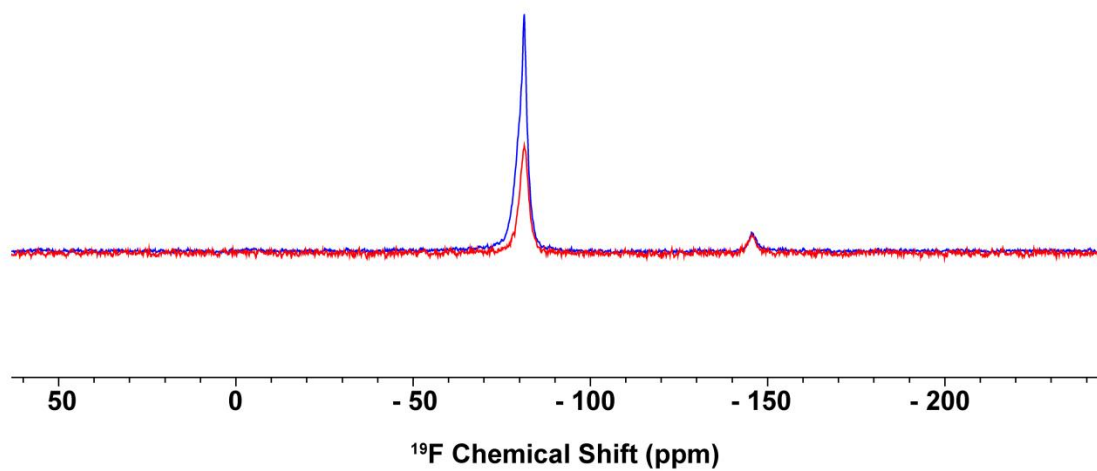


Figure A.4.11. ^{19}F -NMR (700 MHz, spinning rate 50kHz, 1.3 mm rotor) spectra of **F6@SiO₂₋₂₀₀** (blue) and the background signal (red).

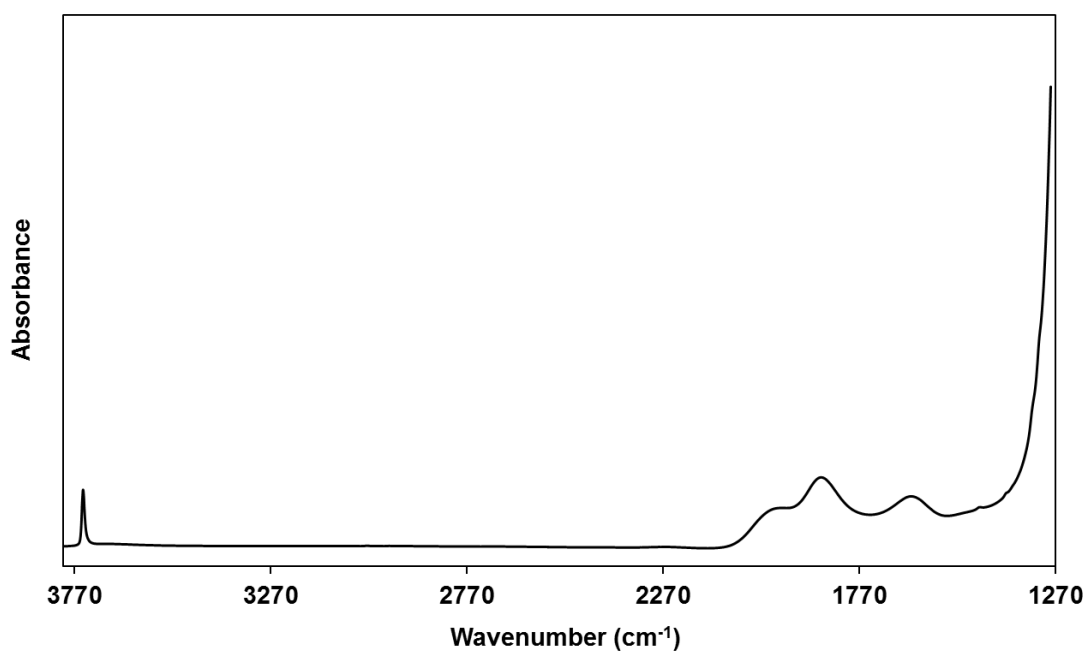


Figure A.4.12. IR spectrum of **F6@SiO₂-700-thermal**.

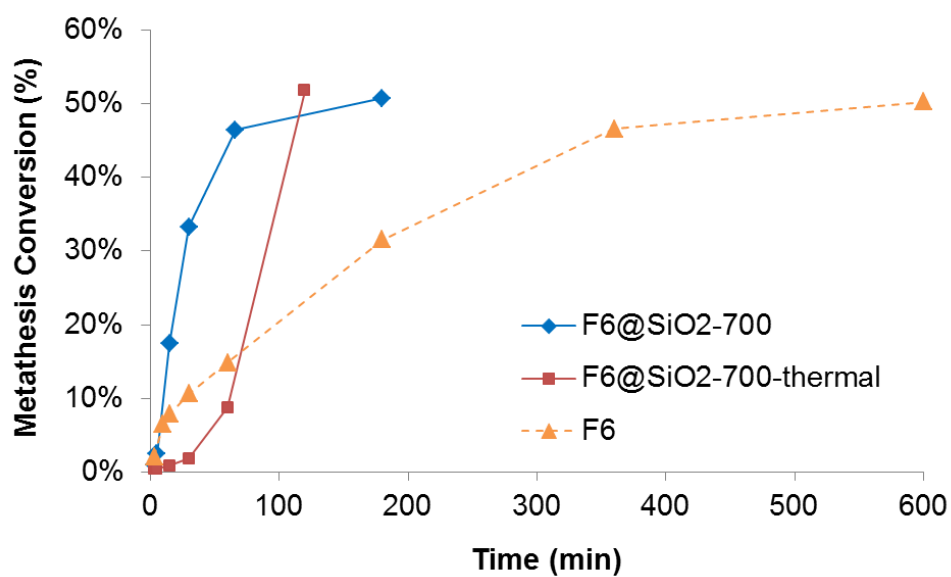


Figure A.4.13. Self-metathesis of *cis*-4-nonene catalyzed by **F6@SiO₂-700** (0.1 mol%; in the presence of 0.3 mol% B(C₆F₅)₃), **F6@SiO₂-700-thermal** (0.1 mol%; without B(C₆F₅)₃) and **F6** (0.3 mol%; in the presence of 0.9 mol% B(C₆F₅)₃) at 70 °C.

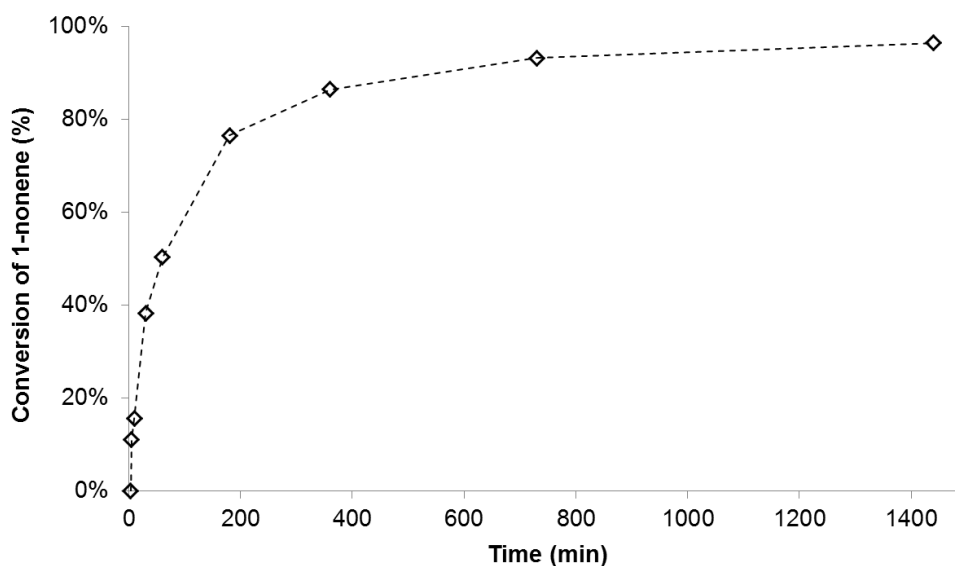


Figure A.4.14. Self-metathesis of 1-nonene catalyzed by **F6@SiO₂₋₇₀₀** (1 mol%); in the presence of 3 mol% B(C₆F₅)₃ at 70 °C.

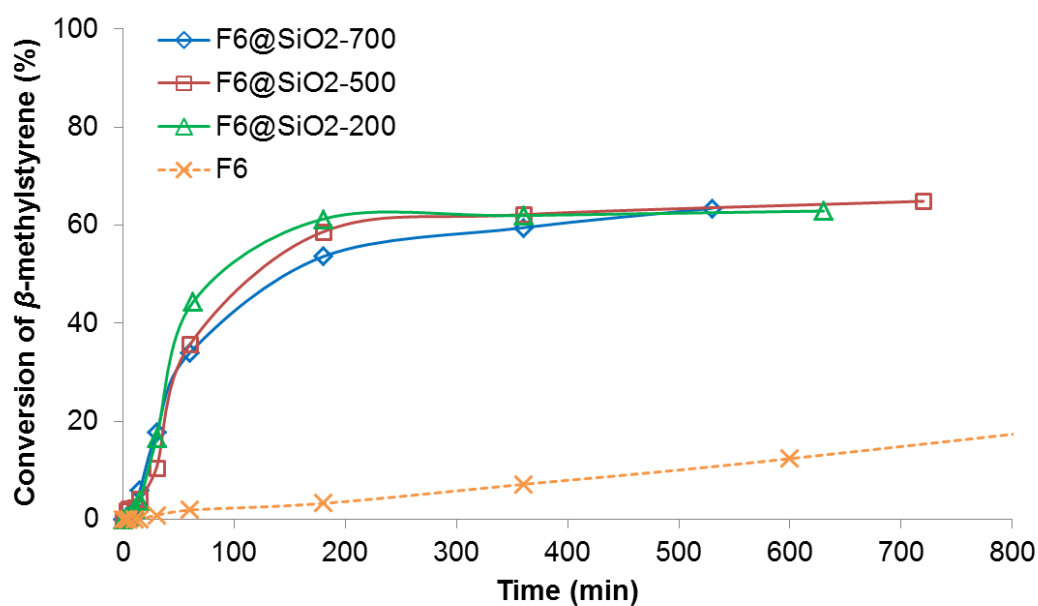


Figure A.4.15. Self-metathesis of *trans*- β -methylstyrene catalyzed by **F6@SiO_{2-x}** (x = 700, 500 or 200) and **F6** (2 mol% in the presence of 6 mol% B(C₆F₅)₃) at 70 °C.

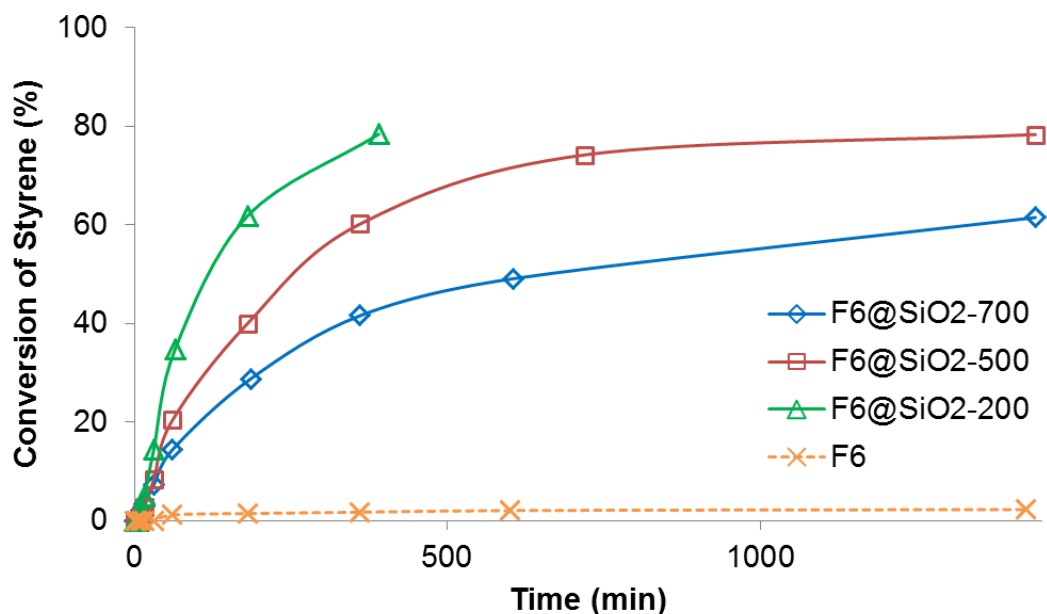


Figure A.4.16. Self-metathesis of styrene catalyzed by **F6@SiO_{2-x}** ($x = 700, 500$ or 200) and **F6** (2 mol% in the presence of 6 mol% $B(C_6F_5)_3$) at $70\text{ }^\circ\text{C}$.

Reaction of SiO_{2-200} with ^{13}C -dilabeled ethylene

SiO_{2-200} (58.5 mg) and $B(C_6F_5)_3$ (17.9 mg, 35 μmol) was loaded in a 10 mL Schlenk followed by the addition of ^{13}C -dilabeled ethylene (110 μmol) and then toluene (3 mL) by vacuum transfer. The reaction mixture was heated at $70\text{ }^\circ\text{C}$ for 1 h following by drying under high vacuum (10^{-5} mbar). The residue was washed by toluene (2 mL x 5) and the resulting solid was dried under high vacuum (10^{-5} mbar).

^{13}C ssNMR measurement of the resulting solid does not show any signal indicating the absence of EtO- group.

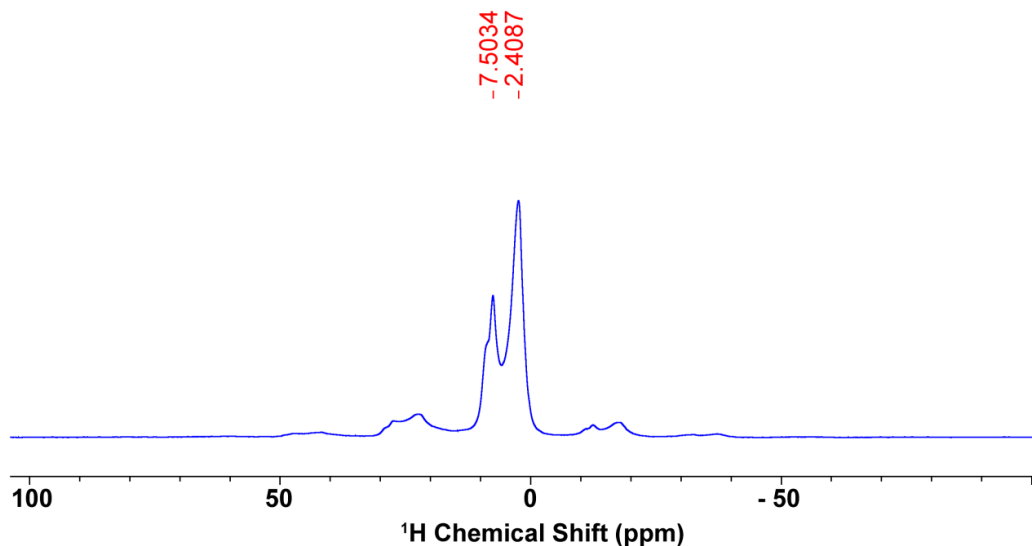


Figure A.4.17. ^1H -NMR (600 MHz, spinning rate 12kHz, 3.2 mm rotor) spectrum of **F6@SiO₂₋₂₀₀** after reacting with styrene- α , β - $^{13}\text{C}_2$ in the presence of $\text{B}(\text{C}_6\text{F}_5)_3$.

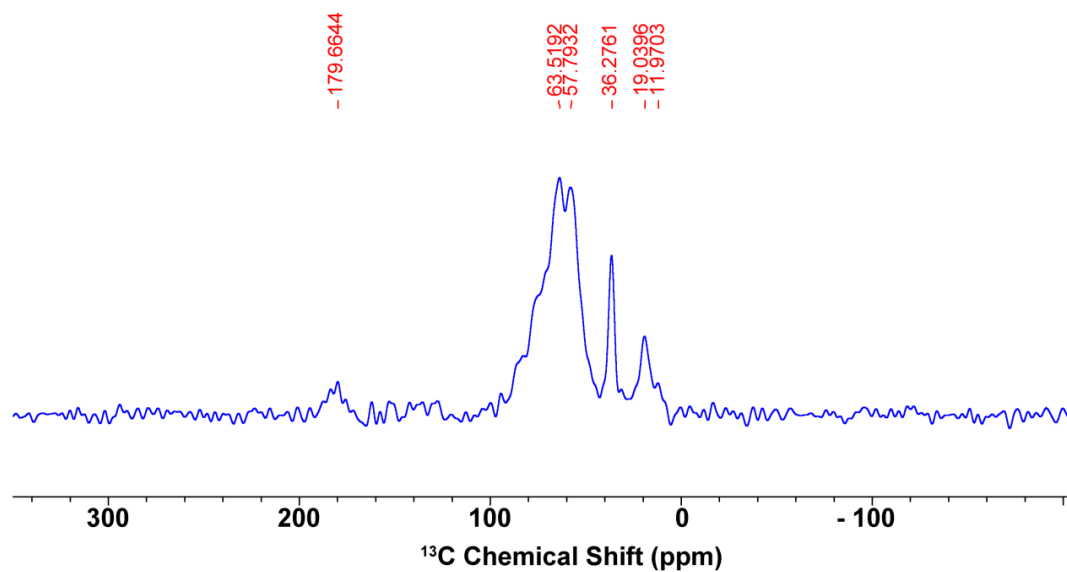


Figure A.4.18. ^{13}C CP-MAS NMR (600 MHz, spinning rate 12kHz, 3.2 mm rotor) spectrum of **F6@SiO₂₋₂₀₀** after reacting with styrene- α , β - $^{13}\text{C}_2$ in the presence of $\text{B}(\text{C}_6\text{F}_5)_3$.

Titration of surface intermediates formed upon exposure to styrene

Representative procedures for the titration of **F6@SiO_{2-x}** ($x = 700, 500$ or 200). **F6@SiO_{2-x}** (ca. 40 mg, 1 equiv) and $B(C_6F_5)_3$ (3 equiv) was loaded in a 10 mL Schlenk followed by the addition of styrene (10 equiv) in toluene. The reaction mixture was heated at 70 °C for y min ($y = 5$ or 60). The supernatant was then removed and the solid residue was rinsed by toluene (2 mL x 5) at 70 °C. Subsequently, the resulting solid was dried under high vacuum (10^{-5} mbar) for 2 h. The dried solid was then contact with *cis*-5-decene (3 equiv) in C_6D_6 at 70 °C for 6 h (ca. 0.5 mL). The supernatant was then removed and the solid residue was rinsed by C_6D_6 . All the filtrate solutions were collected and analyzed by 1H NMR spectroscopy using ferrocene as internal standard. 1H -NMR reveals the formation of 1-hexene and 1-hexenylbenzene (further confirmed by GC-MS), as cross-metathesis products between styrene and *cis*-5-decene. The quantities of cross-metathesis products in different system are summarized in Table A.4.3.

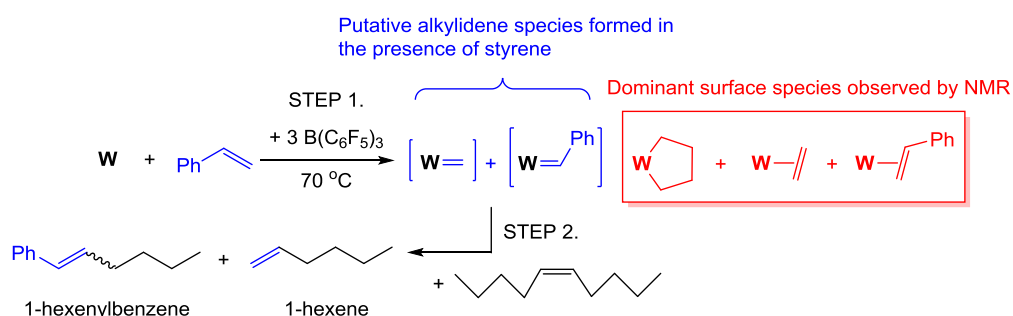
	Total amounts of cross-metathesis products (equiv per W)		
System	F6@SiO₂₋₇₀₀	F6@SiO₂₋₅₀₀	F6@SiO₂₋₂₀₀
Time (min)			
60	0.25	0.25	0.20
5	0.42	N/A	0.42

Table A.4.3. Amounts of cross-metathesis products detected in **F6@SiO_{2-x}** ($x = 700, 500$ or 200) after contacting with styrene for 60 or 5 min at 70 °C.

As shown in table A.4.3, in all **F6@SiO_{2-x}**, the quantities of cross-metathesis products are ca. 0.2 equiv per W (after 60 min). Assuming the same distribution of surface intermediates in all **F6@SiO_{2-x}**, this would suggest a similar amount of surface intermediates present in all catalysts after 60 min of reaction with styrene. Reducing the reaction time with styrene to 5 min for **F6@SiO₂₋₇₀₀** and **F6@SiO₂₋₂₀₀** result in higher amounts of cross-metathesis products (ca. 0.4 equiv per W) in both materials. The observed decreasing amount of cross-metathesis products with increasing reaction times suggests that deactivation takes place. Notably, the amounts of intermediates and decomposition are similar between different systems.

It is worth noting that the quantities of cross-metathesis products are likely contributed by all the surface species formed upon contacting with styrene including the putative alkylidene species and the others (dominant) species that are observed by ssNMR (Scheme A.4.1). Although those dominant species are not metathesis active catalysts, they might release

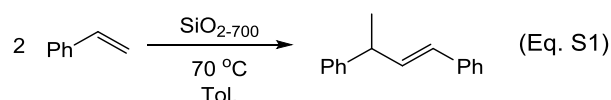
olefins or converted into metathesis active sites during the STEP 2 of titration (with *cis*-5-decene), and thus, contribute to the quantities of cross-metathesis products. Therefore, titration by cross-metathesis may not be a reliable way to evaluate the number of active sites (solely the alkylidene species) as the olefins-containing intermediates can contaminate the subsequent cross-metathesis experiment.



Scheme A.4.1. Titration of surface intermediates formed upon exposure to styrene by *cis*-5-decene

Reaction of SiO₂₋₇₀₀ with styrene

SiO₂₋₇₀₀ (41.5 mg) in a 10 mL Schlenk followed by the addition of styrene (0.2 M solution in toluene, 2 mL, 0.4 mmol) in toluene. The reaction mixture was heated at 70 °C for 24 h. Analysis of the supernatant by GC-MS indicates 70% conversion of styrene and formation of styrene dimers after 24 h (Eq. S1).



Reaction of F6 molecular complex with styrene in the presence of styrene dimers and B(C₆F₅)₃

500 μL of the supernatant (from the reaction of SiO₂₋₇₀₀ with styrene) was added to a mixture of F6 molecular complex (9.8 mg, 12 μmol, 1 equiv) and B(C₆F₅)₃ (18.8 mg, 36 μmol, 3 equiv). The reaction mixture was heated at 70 °C for 24 h. No consumption of styrene dimers or self-metathesis products from styrene was observed.

Reaction SiO₂₋₂₀₀ with B(C₆F₅)₃ in the presence of excess ¹⁵N-labeled pyridine

SiO₂₋₂₀₀ (52.7 mg) and B(C₆F₅)₃ (18.0 mg, 35 μmol) were loaded in a 10 mL Schlenk followed by the addition of toluene (3 mL) with ¹⁵N-labeled pyridine (20 μL, 247 μmol). The reaction mixture was heated at 70 °C for 1 h. The supernatant was removed and the residue

was washed by toluene (2 mL x 5) at 70 °C. The resulting solid was dried under high vacuum (10^{-5} mbar) at room temperature for 5 h.

^{15}N CP-MAS NMR spectrum of the resulting solid does not show any signal and its IR spectrum is shown in Figure A.4.20.

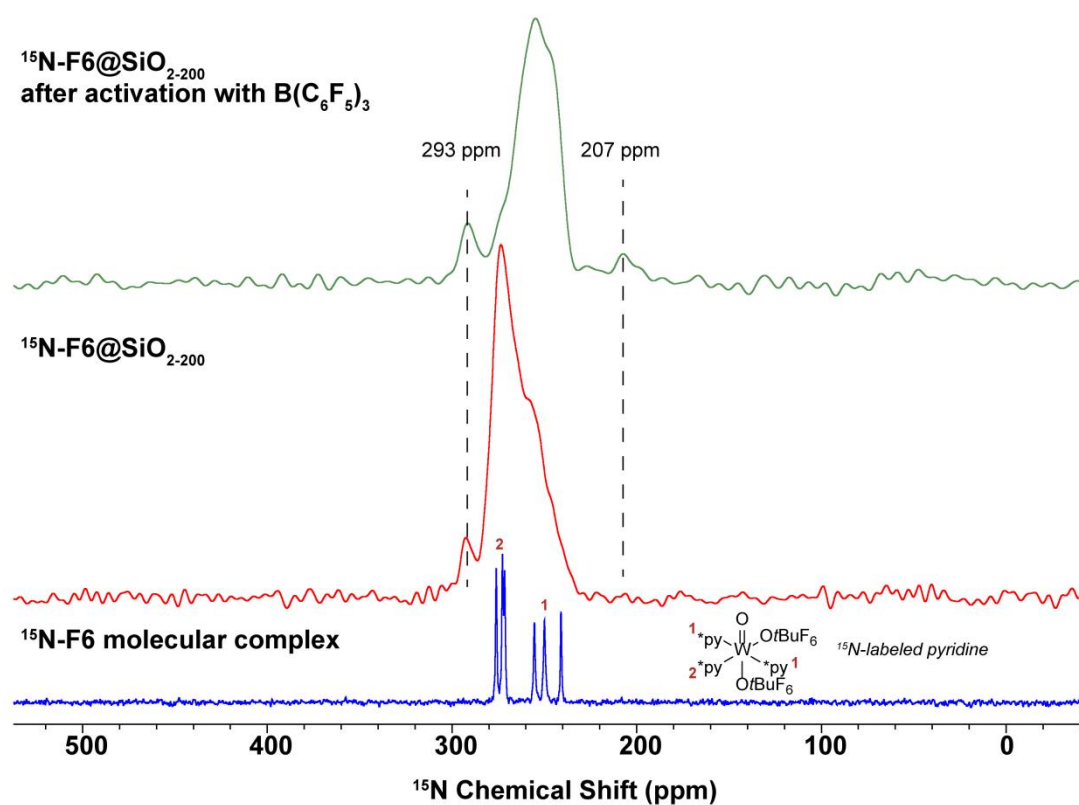


Figure A.4.19. ^{15}N CP-MAS NMR (400 MHz, spinning rate 16kHz, 3.2 mm rotor) spectra of $^{15}\text{N-F6}$ (blue; bottom spectrum), $^{15}\text{N-F6@SiO}_{2-200}$ (red; middle spectrum) and $^{15}\text{N-F6@SiO}_{2-200}$ after activation with $\text{B}(\text{C}_6\text{F}_5)_3$ in the presence of excess ^{15}N -labeled pyridine (green; top spectrum).

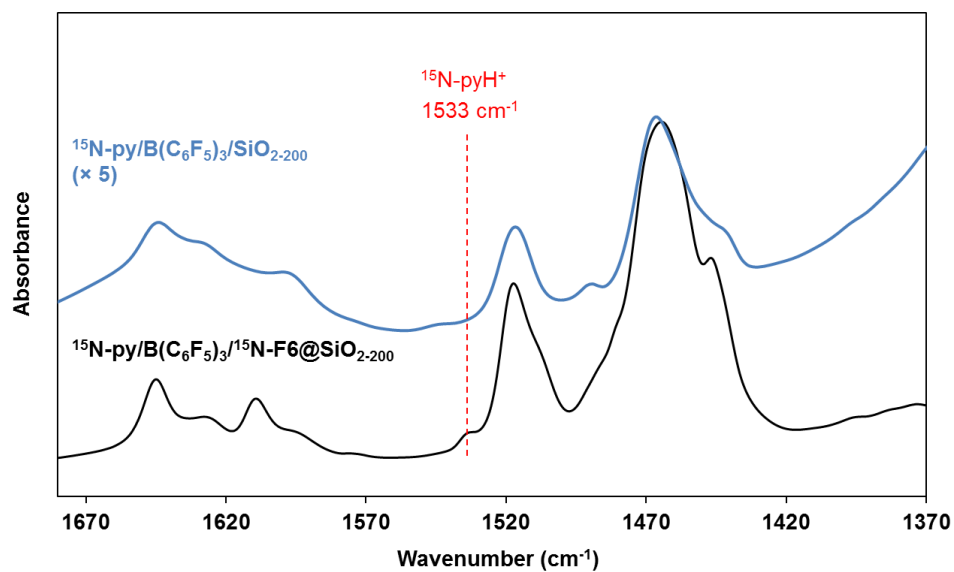


Figure A.4.20. IR spectra of $^{15}\text{N-F6@SiO}_{2-200}$ (black; bottom spectrum) and SiO_{2-200} (blue; upper spectrum) after reaction with $\text{B(C}_6\text{F}_5)_3$ in the presence of excess ^{15}N -labeled pyridine. The peak indicated at 1533 cm^{-1} is attributed to pyridinium ($^{15}\text{N-pyH}^+$).

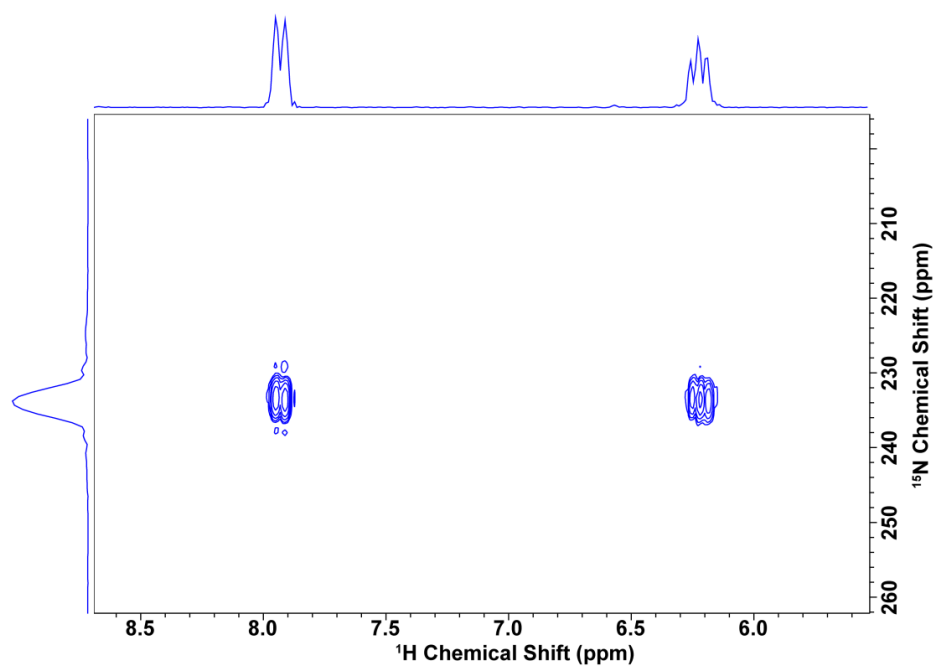


Figure A.4.21. 2D $^1\text{H-}^{15}\text{N}$ HMBC solution NMR spectrum of ^{15}N -labeled pyridine- $\text{B(C}_6\text{F}_5)_3$ ($^{15}\text{N-py-B(C}_6\text{F}_5)_3$) adduct in C_6D_6 .

DFT Computational Studies

Computational details. All DFT calculations were performed with the Gaussian 09 (d1) software package.¹ Ground state and transition state geometries were optimized using the B3LYP²⁻³ functional augmented with the D3 version of Grimme's empirical dispersion correction.⁴ Solvent effects of benzene were taken into account using SMD solvation model.⁵ The SDD⁶ basis set was used for tungsten and the TZVP⁷⁻⁸ basis set for the other atoms. The frequency calculations were performed at the same level of theory. The Gibbs free energy and enthalpy were calculated at 298.15 K using the harmonic approximation for vibrational contributions.

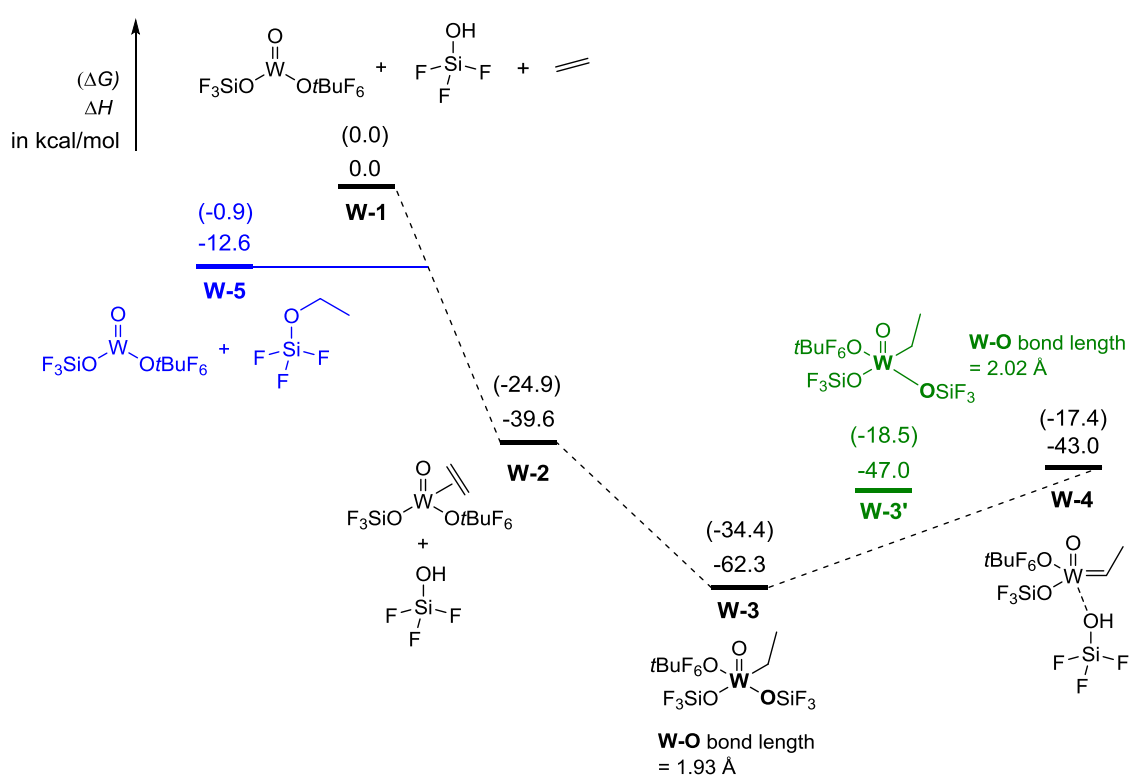


Figure A.4.22. Computed Enthalpies and Gibbs free energies in parentheses (in kcal mol⁻¹).

DFT calculations on the thermodynamics of various proposed intermediates indicates that the protonation of ethylene by $\equiv\text{SiOH}$ to form surface $-\text{OEt}$ ethoxy group (**W-5**) is energetically favorable. The formation of W ethylene π complex (**W-2**) from W(IV) species **W-1** is also thermodynamically favorable ($\Delta H = -39.6$ kcal/mol). Subsequent proton transfer from the $\equiv\text{SiOH}$ group to the coordinated ethylene (**W-2**) leads to the formation W-alkyl species (**W-3**) ($\Delta H = -22.7$ kcal/mol), which can then undergo α -H abstraction forming the W alkylidene species (**W-4**) ($\Delta H = 19.3$ kcal/mol).

It is worth noting that by slightly elongating the W–O bond length of **W-3** from 1.93 to 2.02 Å (**W-3'**), the enthalpy increases to a value that is very close to **W-4**. This result suggests that the transformation of **W-3** to **W-4** maybe thermodynamically more favorable or become thermoneutral on the surface, where strained site with slightly distorted bond length can exist.

XYZ Coordinates of Computed Structures

C₂H₄

C	-0.663021	0	-0.0000017
C	0.663021	0	-0.0000007
H	-1.233604	0.922679	0.0000013
H	-1.233604	-0.922679	0.0000003
H	1.233604	0.922679	0.0000003
H	1.233604	-0.922679	0.0000003

(OH)SiF₃

Si	-0.01038	0.00605	0
O	-1.63067	0.07947	0
F	0.58164	-0.74999	-1.28099
F	0.58164	-0.74997	1.281
F	0.54153	1.50113	-0.00001
H	-2.15261	-0.73094	0.00001

(CH₃CH₂O)SiF₃; (W-5)

Si	1.429496	1.212983	-0.03059
O	-0.15391	0.994011	-0.22381
F	2.327473	0.055267	-0.68423
F	1.859663	1.282022	1.513788
F	1.84536	2.587419	-0.72884
C	-1.01261	-0.01479	0.36899
C	-0.89123	-1.34208	-0.34929
H	-2.02259	0.385456	0.284014
H	-0.77635	-0.11352	1.431887
H	-1.10717	-1.22709	-1.4128
H	-1.60698	-2.05194	0.072825
H	0.108849	-1.76774	-0.24195

W-1

W	1.526756	-0.81448	0.231101
O	2.452843	-0.33576	1.572291
O	2.27022	-2.31264	-0.65873
O	-0.0136	0.21254	0.045012
C	-1.04184	1.118465	0.314974
C	-0.47336	2.540278	0.028443
C	-2.20417	0.758301	-0.65499
C	-1.49792	1.009167	1.764079
H	-0.6553	1.219836	2.420557
H	-1.84508	-0.00515	1.951611
H	-2.30328	1.711994	1.972398
F	-1.39902	3.486167	0.253071
F	-0.03722	2.671544	-1.23139
F	0.567968	2.775521	0.845389
F	-1.82537	0.789864	-1.94013
F	-3.24338	1.594731	-0.50253
F	-2.63453	-0.48903	-0.3913
Si	2.922493	-3.63854	-1.32873
F	1.805857	-4.75579	-1.55117
F	3.567218	-3.28503	-2.74321
F	4.060709	-4.25199	-0.39675

W-2

W	-1.07664	-1.33726	0.020603
O	-1.41428	-2.95191	0.460115
O	-2.42816	-0.03022	0.57663
O	0.519704	-0.61054	0.807018
C	1.598917	0.273835	0.805711
C	2.781559	-0.40773	0.056411
C	1.159907	1.587858	0.095784
C	2.005696	0.568243	2.247136
H	2.308802	-0.36183	2.724816
H	1.147016	0.971102	2.780103
H	2.827195	1.282173	2.29197
F	3.903104	0.329248	0.131236
F	2.516345	-0.61658	-1.24496
F	3.036606	-1.60302	0.612383
F	0.633488	1.345317	-1.1252
F	2.173189	2.45022	-0.05428
F	0.197591	2.192141	0.815603
Si	-3.55789	1.089044	0.33308
F	-5.02037	0.543546	0.682556

F	-3.29514	2.371334	1.251776
F	-3.59519	1.591239	-1.18954
C	-1.78117	-1.27816	-2.00373
C	-0.36188	-1.60121	-1.98305
H	-0.03929	-2.61386	-2.20719
H	0.345186	-0.84265	-2.29977
H	-2.08142	-0.28761	-2.33715
H	-2.50286	-2.05272	-2.24806

W-3

W	0.850348	-0.45738	-0.8555
O	0.836299	-1.27106	-2.35455
O	-1.00668	-0.13527	-0.64163
O	2.743159	-0.56567	-0.48746
O	1.110526	1.493478	-0.70609
C	0.625383	-2.04753	0.594121
C	-2.03714	0.53792	0.020437
C	-1.55536	1.355541	1.21439
H	-1.02074	0.704261	1.903753
H	-2.39697	1.806175	1.737753
H	-0.88615	2.141768	0.876128
C	-3.04304	-0.5548	0.493191
C	-2.68109	1.475826	-1.04743
F	-2.46629	-1.30118	1.45759
F	-4.15359	-0.00756	1.010661
F	-3.40288	-1.3824	-0.49399
F	-3.67584	2.205292	-0.51667
F	-3.16937	0.798232	-2.09327
F	-1.74829	2.326241	-1.50985
Si	1.911362	2.877703	-0.56976
Si	4.240631	-0.60668	0.109593
F	1.2562	3.78867	0.572997
F	1.903146	3.728297	-1.9206
F	3.440779	2.61953	-0.16673
F	4.314216	0.116913	1.533041
F	4.713333	-2.11875	0.326168
F	5.277137	0.096825	-0.87525
C	-0.28163	-3.17952	0.100039
H	0.215202	-1.57406	1.493773
H	1.610432	-2.43728	0.850152
H	-1.24811	-2.82412	-0.25287
H	-0.46718	-3.88465	0.91512
H	0.192192	-3.72475	-0.71726

W-3'

W	0.92853	-0.38499	-0.78388
O	1.06818	-0.88008	-2.40964
O	-0.90097	0.005104	-0.63109
O	2.72897	-1.00018	-0.12028
O	1.51939	1.382314	-0.1936
C	0.59498	-2.24034	0.249201
C	-1.98034	0.478494	0.129241
C	-1.55428	0.989314	1.500131
H	-1.00566	0.206254	2.020891
H	-2.42277	1.267104	2.095021
H	-0.91303	1.860274	1.386151
C	-2.97535	-0.70984	0.272981
C	-2.58792	1.640284	-0.71445
F	-2.42416	-1.65718	1.056691
F	-4.11958	-0.31323	0.849431
F	-3.26728	-1.27625	-0.90194
F	-3.60562	2.226234	-0.06886
F	-3.02356	1.232594	-1.91063
F	-1.63494	2.570564	-0.91999
Si	1.77277	2.976694	-0.19424
Si	4.22022	-0.39591	0.048161
F	0.76023	3.676584	0.828731
F	1.53484	3.619874	-1.63558
F	3.257	3.326054	0.269611
F	4.42078	0.290284	1.481551
F	5.30701	-1.56262	-0.06924
F	4.57259	0.711124	-1.05721
C	-0.38914	-3.20836	-0.38274
H	0.35569	-1.99899	1.290811
H	1.67842	-2.41804	0.129591
H	-1.3956	-2.79555	-0.46587
H	-0.45746	-4.11198	0.231121
H	-0.06194	-3.50567	-1.38009

W-4

W	-0.27724	1.505244	-0.62341
O	0.445922	3.037931	-0.79862
O	-2.00079	1.434639	-1.53808
C	2.084319	-0.60432	-0.42511
C	2.221717	-1.86591	-1.32376
C	3.382648	0.258383	-0.48026
C	1.808717	-1.01777	1.016727

H	0.899613	-1.61304	1.065171
H	1.668787	-0.12412	1.620526
H	2.635463	-1.59887	1.421801
F	3.162282	-2.70836	-0.87963
F	2.482188	-1.57694	-2.60003
F	1.038017	-2.55141	-1.31001
F	3.66603	0.684097	-1.71706
F	4.451214	-0.41653	-0.01698
F	3.216635	1.347153	0.295544
Si	-3.59798	1.357326	-1.68163
F	-4.07369	1.796451	-3.1421
F	-4.13144	-0.13709	-1.44342
F	-4.34569	2.296577	-0.62409
C	-0.58236	1.506953	1.251962
C	-0.28236	2.46442	2.355959
H	0.252706	3.342003	1.992937
H	0.325971	1.982361	3.129198
H	-1.20842	2.792737	2.839364
H	-1.13466	0.605947	1.547001
O	-1.38166	-1.25778	-0.42755
Si	-2.4973	-2.13287	0.379654
F	-3.33486	-1.10117	1.257982
F	-1.79575	-3.17775	1.368455
F	-3.46886	-2.96753	-0.56571
O	1.069681	0.1543	-1.00592
H	-0.69883	-1.71504	-0.93889

References for appendix to Chapter 4:

1. Frisch, M. J. T., G. W.; Schlegel, H. B.; Scuseria, G. E.; Robb, M. A.; Cheeseman, J. R.; Scalmani, G.; Barone, V.; Mennucci, B.; Petersson, G. A.; Nakatsuji, H.; Caricato, M.; Li, X.; Hratchian, H. P.; Izmaylov, A. F.; Bloino, J.; Zheng, G.; Sonnenberg, J. L.; Hada, M.; Ehara, M.; Toyota, K.; Fukuda, R.; Hasegawa, J.; Ishida, M.; Nakajima, T.; Honda, Y.; Kitao, O.; Nakai, H.; Vreven, T.; Montgomery, J. A.; Peralta, J. E.; Ogliaro, F.; Bearpark, M.; Heyd, J. J.; Brothers, E.; Kudin, K. N.; Staroverov, V. N.; Keith, T.; Kobayashi, R.; Normand, J.; Raghavachari, K.; Rendell, A.; Burant, J. C.; Iyengar, S. S.; Tomasi, J.; Cossi, M.; Rega, N.; Millam, J. M.; Klene, M.; Knox, J. E.; Cross, J. B.; Bakken, V.; Adamo, C.; Jaramillo, J.; Gomperts, R.; Stratmann, R. E.; Yazyev, O.; Austin, A. J.; Cammi, R.; Pomelli, C.; Ochterski, J. W.; Martin, R. L.; Morokuma, K.; Zakrzewski, V. G.; Voth, G. A.; Salvador, P.; Dannenberg, J. J.; Dapprich, S.; Daniels, A. D.; Farkas, O.; Foresman, J. B.; Ortiz, J. V.; Cioslowski, J.; Fox, D. J. *Gaussian 09, Revision D.01*, Gaussian, Inc.: Wallingford CT., 2013.
2. Becke, A. D., Density-functional thermochemistry. III. The role of exact exchange. *J. Chem. Phys.* **1993**, *98*, 5648-5652.
3. Stephens, P. J.; Devlin, F. J.; Chabalowski, C. F.; Frisch, M. J., Ab Initio Calculation of Vibrational Absorption and Circular Dichroism Spectra Using Density Functional Force Fields. *J. Phys. Chem.* **1994**, *98*, 11623-11627.
4. Grimme, S.; Antony, J.; Ehrlich, S.; Krieg, H., A consistent and accurate ab initio parametrization of density functional dispersion correction (DFT-D) for the 94 elements H-Pu. *J. Chem. Phys.* **2010**, *132*, 154104.
5. Marenich, A. V.; Cramer, C. J.; Truhlar, D. G., Universal Solvation Model Based on Solute Electron Density and on a Continuum Model of the Solvent Defined by the Bulk Dielectric Constant and Atomic Surface Tensions. *J. Phys. Chem. B* **2009**, *113*, 6378-6396.
6. Andrae, D.; Häußermann, U.; Dolg, M.; Stoll, H.; Preuß, H., Energy-adjusted ab initio pseudopotentials for the second and third row transition elements. *Theor. Chim. Acta.* **1990**, *77*, 123-141.
7. Schäfer, A.; Horn, H.; Ahlrichs, R., Fully optimized contracted Gaussian basis sets for atoms Li to Kr. *J. Chem. Phys.* **1992**, *97*, 2571-2577.
8. Schäfer, A.; Huber, C.; Ahlrichs, R., Fully optimized contracted Gaussian basis sets of triple zeta valence quality for atoms Li to Kr. *J. Chem. Phys.* **1994**, *100*, 5829-5835.

Appendix to Chapter 5

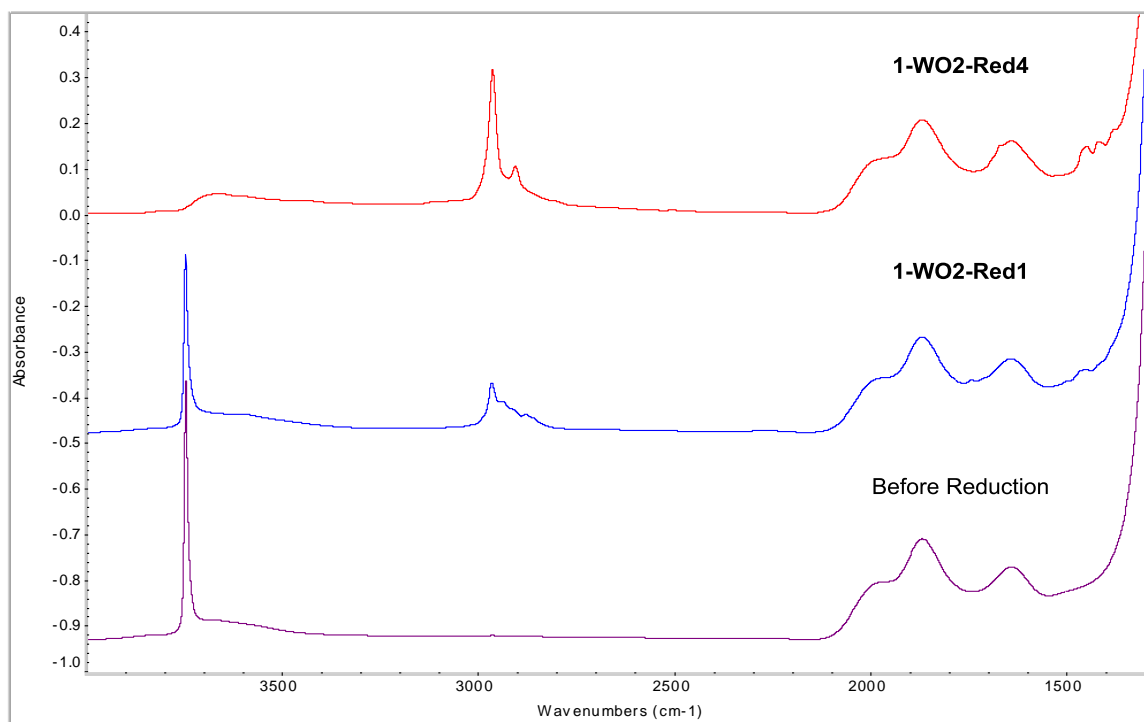


Figure A.5.1. FTIR of the materials **1-WO2-Red4** (top), **1-WO2-Red1** (middle) and before reduction (bottom).

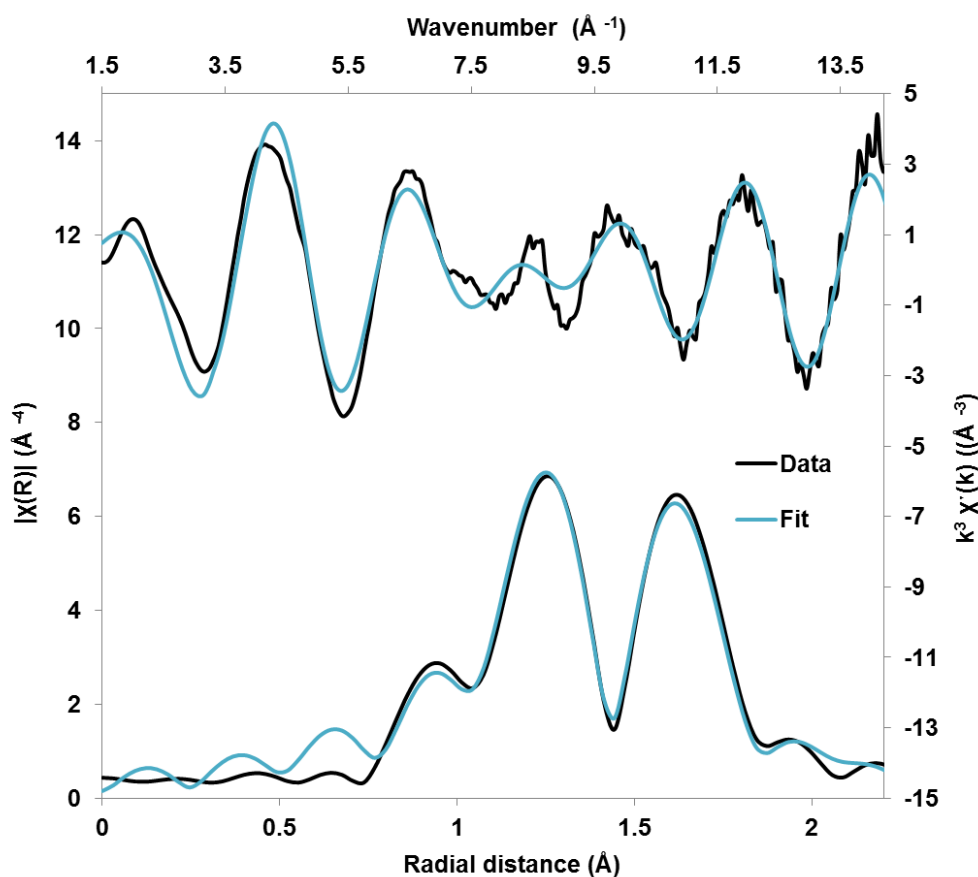


Figure A.5.2. EXAFS data (Black) and fits (Blue) in k-space (Upper; top and right axes) and R-space (Lower; bottom and left axes) of **1-WO** in W L_{III} edge.

	No. of neighbor	R (Å)	σ^2 (Å ²)
W=O	1.66 (8)	1.702 (3)	0.00153*
W—O	2.9 (1)	1.889 (4)	0.00355*

Table A.5.1. EXAFS fit parameters for **1-WO**. $S_0^2 = 0.94$; ΔE_0 (eV) = 7.6 (8); k range 1.5-14.2 Å⁻¹; R range 1-2.2 Å; k weight 3. *Fixed parameters in the fit.

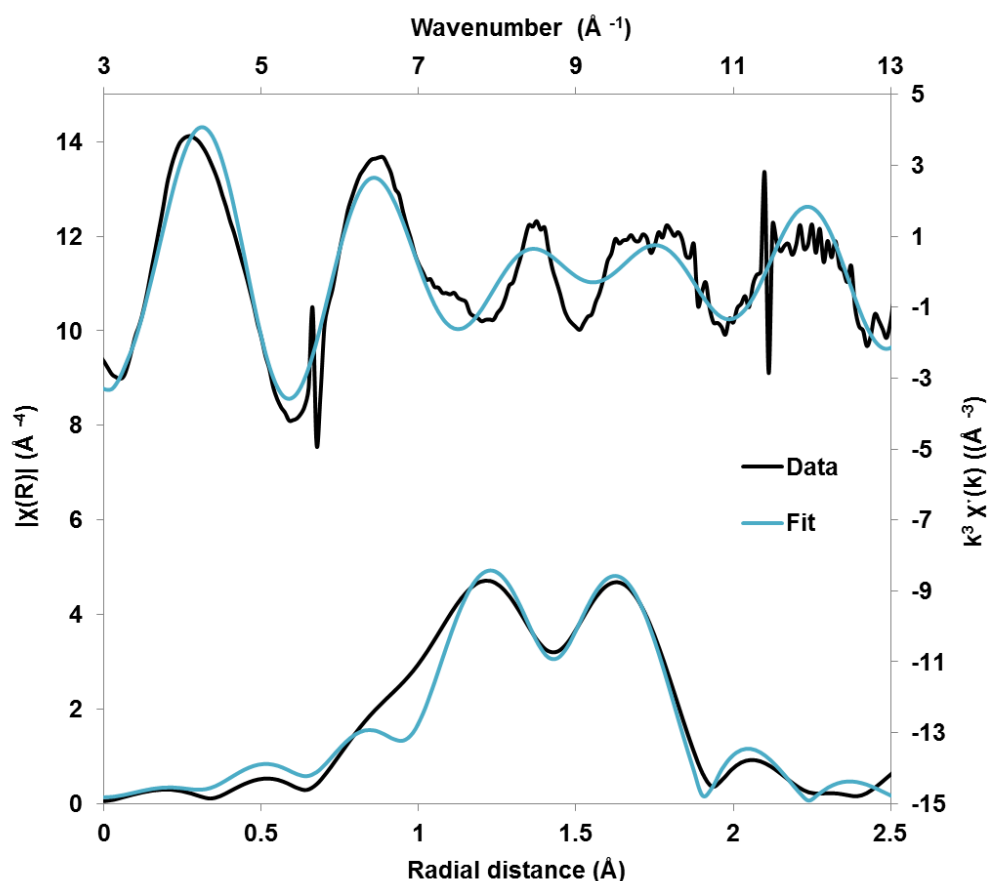


Figure A.5.3. EXAFS data (Black) and fits (Blue) in k-space (Upper; top and right axes) and R-space (Lower; bottom and left axes) of **2** in W L_{III} edge.

	No. of neighbor	R (Å)	σ^2 (Å ²)
W=O	1.2 (1)	1.71 (1)	0.00153*
W-O	2.3 (2)	1.88 (1)	0.00355*

Table A.5.2. EXAFS fit parameters for **2**. $S_0^2 = 1.2$; ΔE_0 (eV) = 7 (2); k range 3-13 Å⁻¹; R range 1-2.5 Å; k weight 3. *Fixed parameters in the fit.

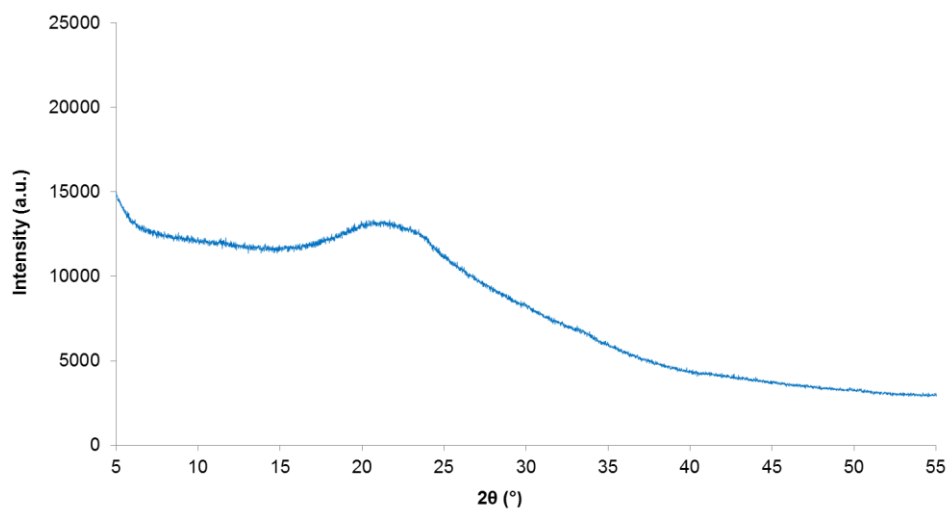


Figure A.5.4. Powder XRD of **2**

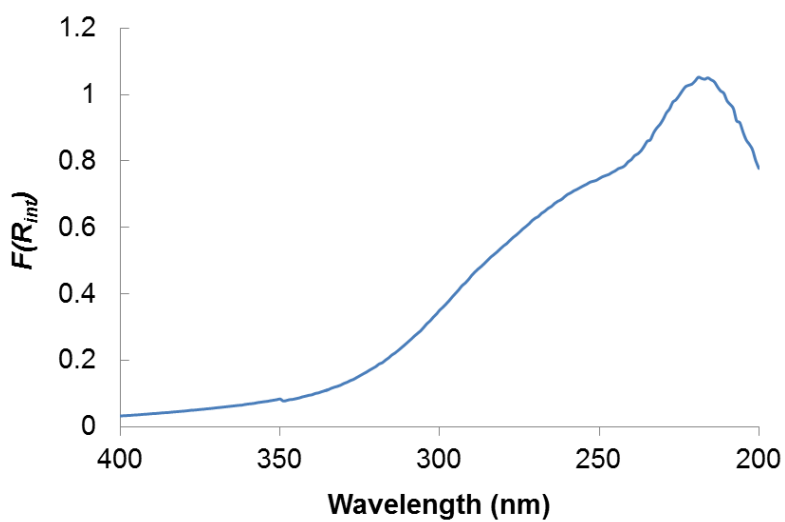


Figure A.5.5. UV-vis DRS spectra of **2**

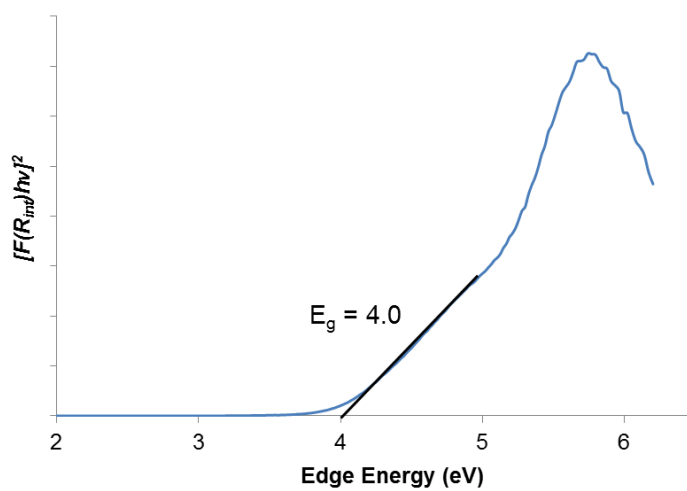


Figure A.5.6. E_g value of **2**

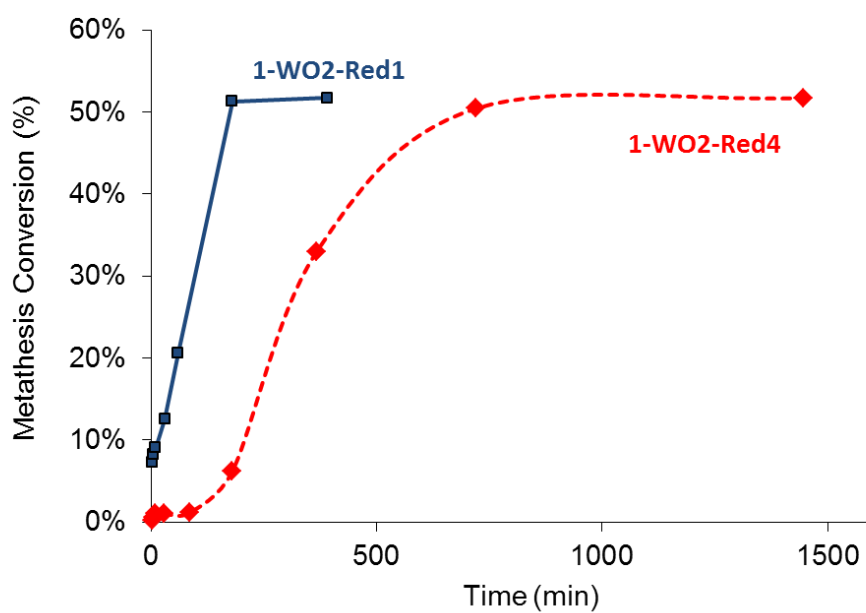


Figure A.5.7. Conversion vs time, cis-4-nonene (1000 equiv) homometathesis at 70 °C by **1-WO2-Red1** (dark blue solid line) and **1-WO2-Red4** (red dotted line).

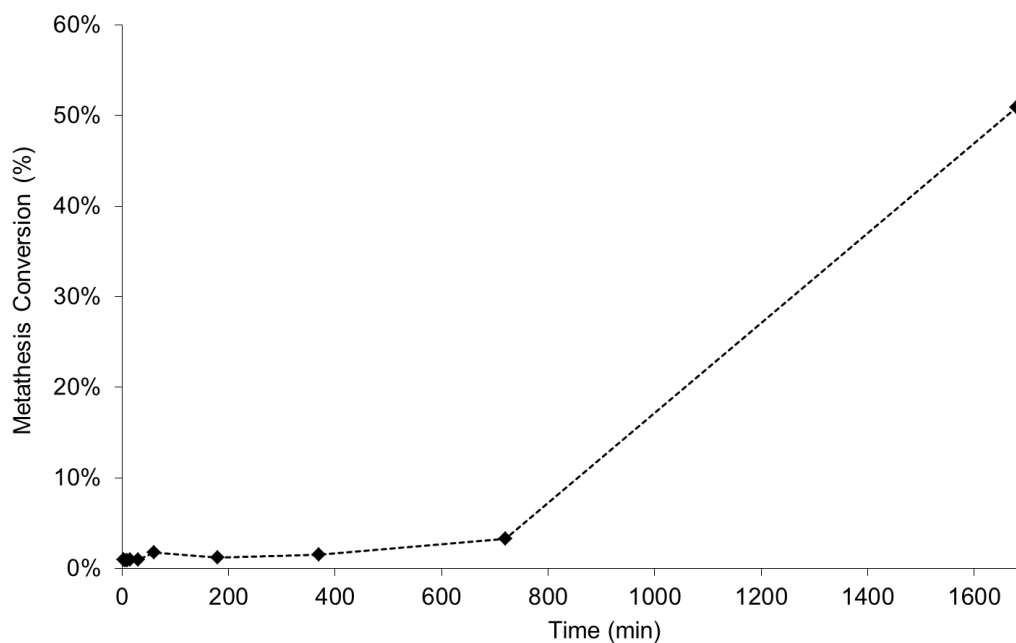


Figure A.5.8. Conversion vs time, cis-4-nonene (5000 equiv) homometathesis at 70 °C by **1-WO2-Red1**.

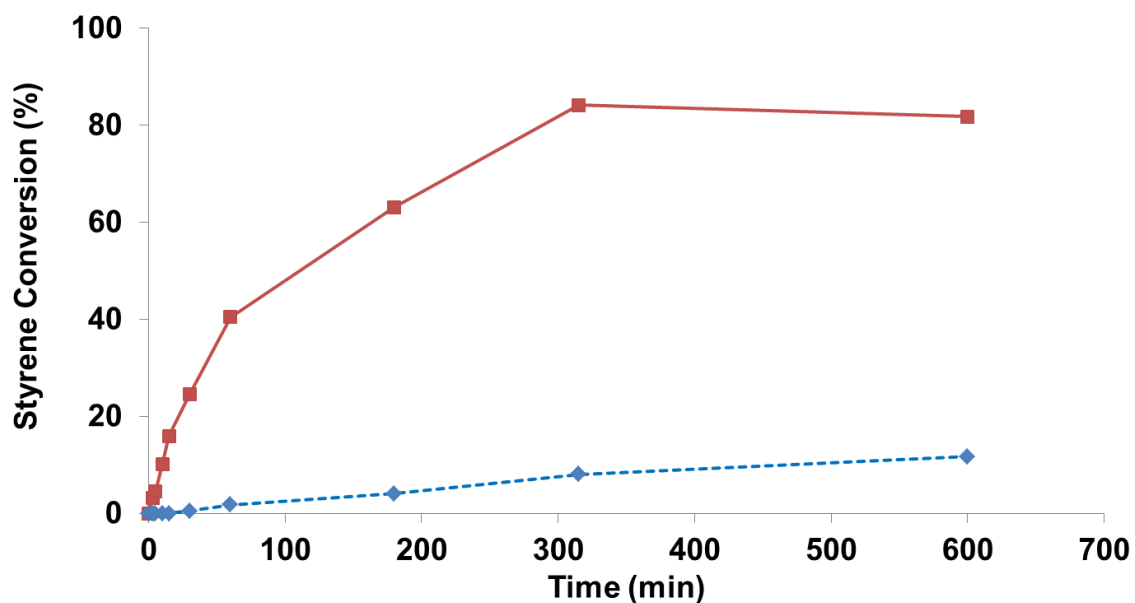


Figure A.5.9. Conversion vs time, styrene (50 equiv) homometathesis at 70 °C by **1-WO2-Red1** (red solid line) and **1-WO2-Red4** (blue dotted line).

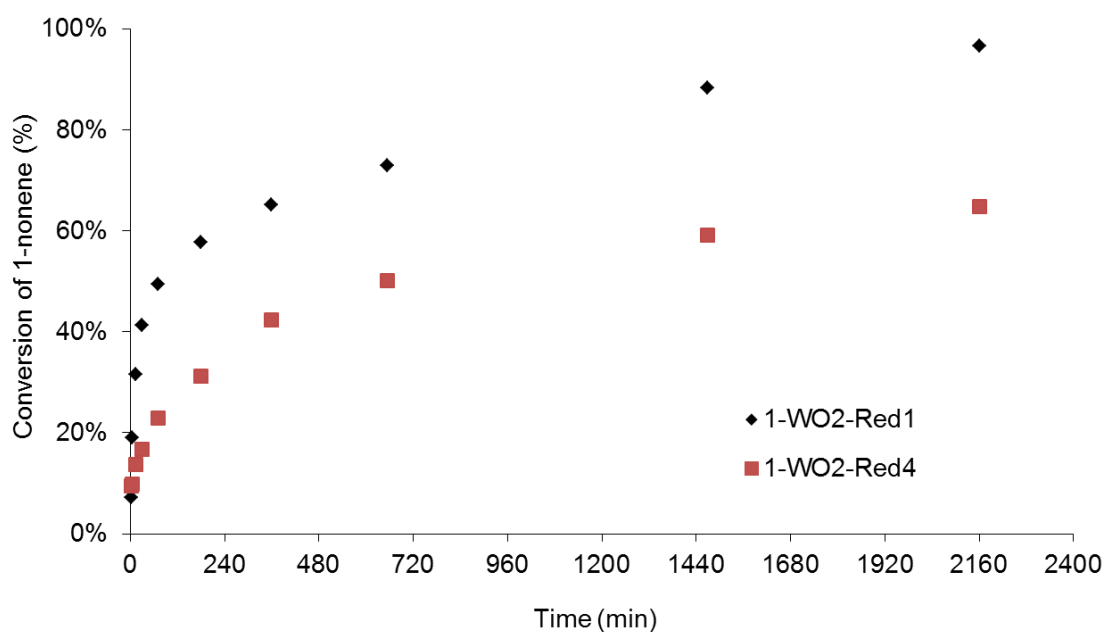


Figure A.5.10. Conversion vs time, 1-nonene (100 equiv) homometathesis at 70 °C by **1-WO2-Red1** (black diamond) and **1-WO2-Red4** (red square).

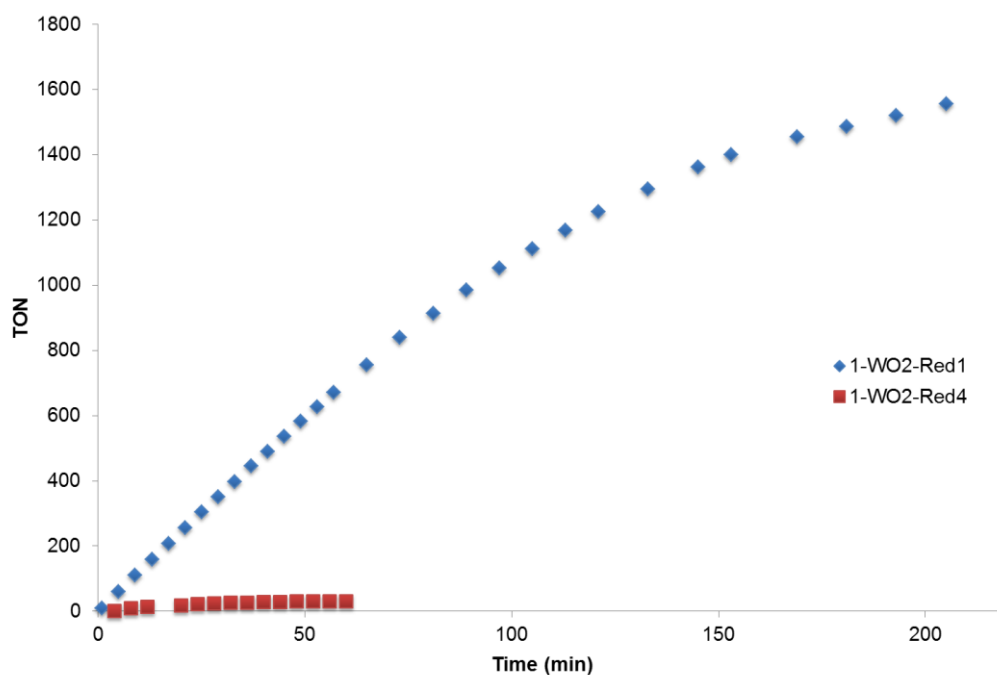


Figure A.5.11. Propene metathesis under flow condition at 70 °C by **1-WO2-Red1** (blue diamond) and **1-WO2-Red4** (red square). TON calculated by assuming all the W sites are active.

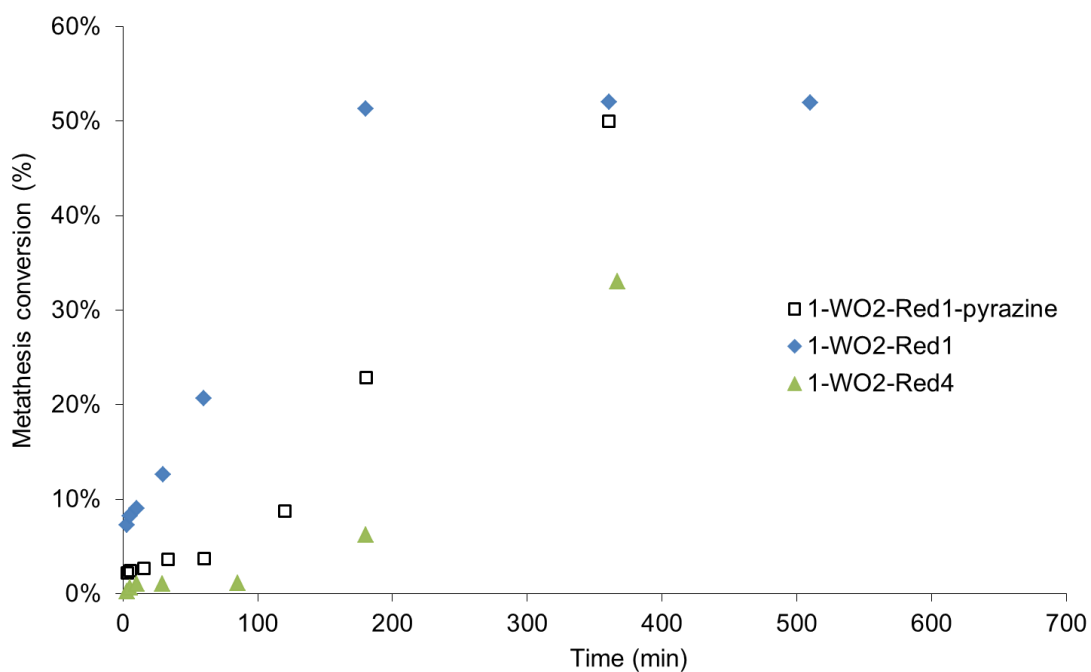


Figure A.5.12. Conversion vs time, *cis*-4-nonene (1000 equiv) homometathesis at 70 °C by **1-WO2-Red1-pyrazine** (0.5 equiv of 2,3,5,6-tetramethylpyrazine per W was added to **1-WO2-Red1**; square), **1-WO2-Red1** (blue diamond) and **1-WO2-Red4** (green triangle).

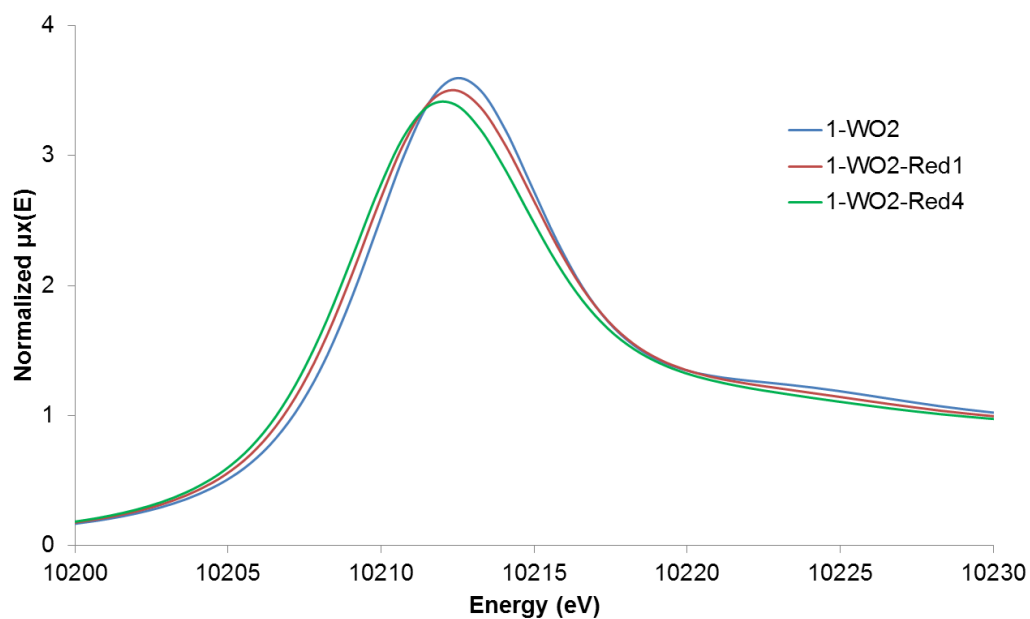


Figure A.5.13. W L_{III} edge XANES of **1-WO2** (blue), **1-WO2-Red1** (red) and **1-WO2-Red4** (green).

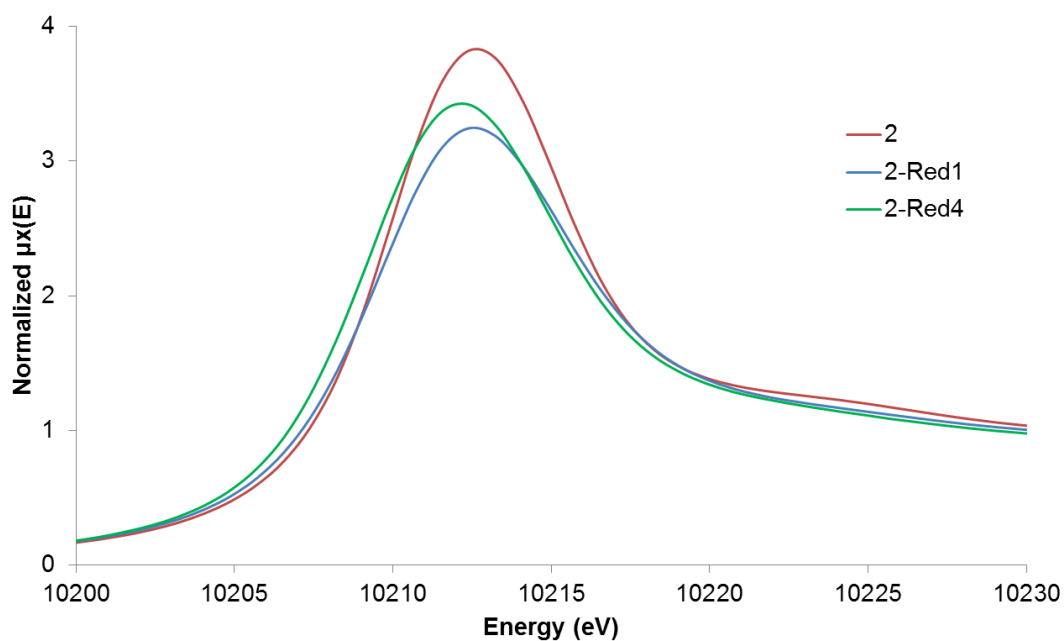


Figure A.5.14. W L_{III} edge XANES of **2** (red), **2-Red1** (blue) and **2-Red4** (green).

Sample	White line energy in W L _{III} edge (eV)
1-WO2-Red4	10212.02
1-WO2-Red1	10212.323
2-Red4	10212.159
2-Red1	10212.549
2	10212.65
1-WO2	10212.535

Table A.5.3. White line energy in W L_{III} edge XANES of different materials.

Computational details. All DFT calculations were performed with the Gaussian 09 (d1) software package.¹ Ground state and transition state geometries were optimized using the B3LYP²⁻³ functional augmented with the D3 version of Grimme's empirical dispersion correction.⁴ Solvent effects of benzene were taken into account using SMD solvation model.⁵ The SDD⁶ basis set was used for tungsten and the TZVP⁷⁻⁸ basis set for the other atoms. The frequency calculations were performed at the same level of theory. The Gibbs free energy and enthalpy were calculated at 298.15 K using the harmonic approximation for vibrational contributions.

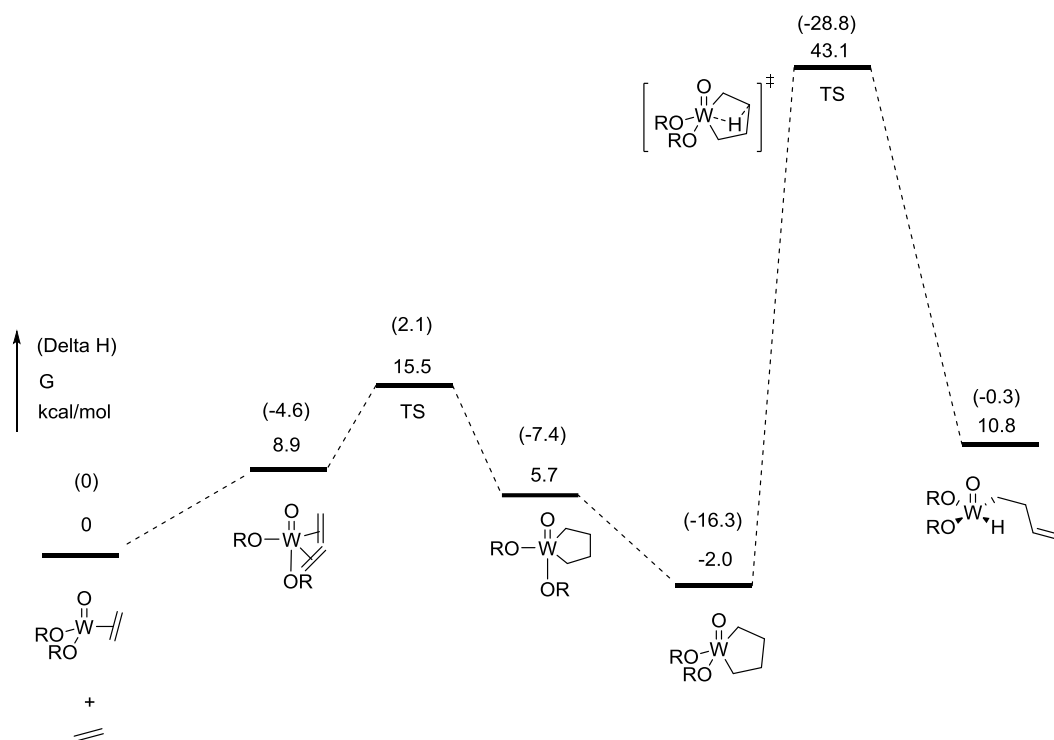


Figure A.5.15. Computed Gibbs free energies and enthalpies in parentheses at 298.15 K (in kcal mol⁻¹) for initiation pathways via ring contraction of metallacyclopentane intermediate; R = -C(CH₃)(CF₃)₂.

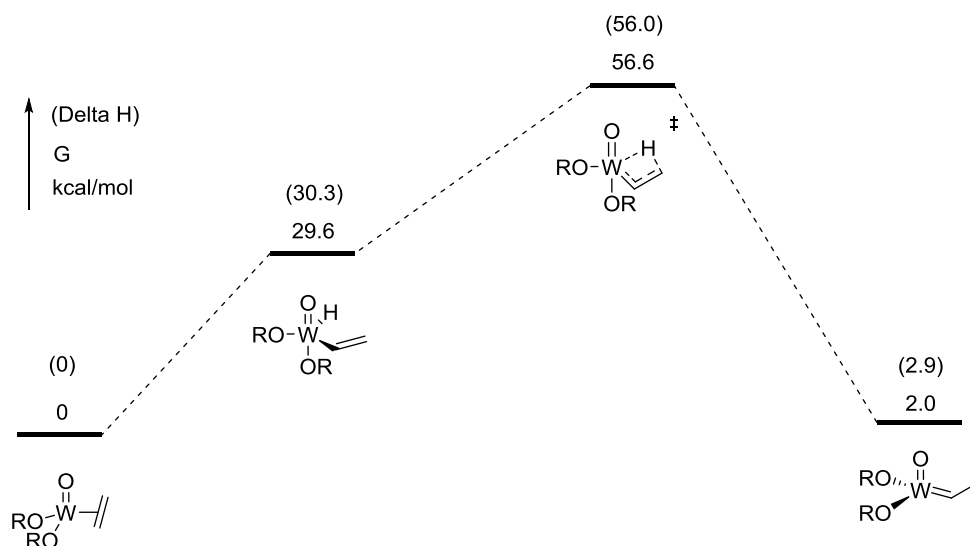


Figure A.5.16. Computed Gibbs free energies and enthalpies in parentheses at 298.15 K (in kcal mol⁻¹) for initiation pathways via vinylic C-H activation; R = -C(CH₃)(CF₃)₂.

References for appendix to Chapter 5:

1. Frisch, M. J. T., G. W.; Schlegel, H. B.; Scuseria, G. E.; Robb, M. A.; Cheeseman, J. R.; Scalmani, G.; Barone, V.; Mennucci, B.; Petersson, G. A.; Nakatsuji, H.; Caricato, M.; Li, X.; Hratchian, H. P.; Izmaylov, A. F.; Bloino, J.; Zheng, G.; Sonnenberg, J. L.; Hada, M.; Ehara, M.; Toyota, K.; Fukuda, R.; Hasegawa, J.; Ishida, M.; Nakajima, T.; Honda, Y.; Kitao, O.; Nakai, H.; Vreven, T.; Montgomery, J. A.; Peralta, J. E.; Ogliaro, F.; Bearpark, M.; Heyd, J. J.; Brothers, E.; Kudin, K. N.; Staroverov, V. N.; Keith, T.; Kobayashi, R.; Normand, J.; Raghavachari, K.; Rendell, A.; Burant, J. C.; Iyengar, S. S.; Tomasi, J.; Cossi, M.; Rega, N.; Millam, J. M.; Klene, M.; Knox, J. E.; Cross, J. B.; Bakken, V.; Adamo, C.; Jaramillo, J.; Gomperts, R.; Stratmann, R. E.; Yazyev, O.; Austin, A. J.; Cammi, R.; Pomelli, C.; Ochterski, J. W.; Martin, R. L.; Morokuma, K.; Zakrzewski, V. G.; Voth, G. A.; Salvador, P.; Dannenberg, J. J.; Dapprich, S.; Daniels, A. D.; Farkas, O.; Foresman, J. B.; Ortiz, J. V.; Cioslowski, J.; Fox, D. J. *Gaussian 09, Revision D.01*, Gaussian, Inc.: Wallingford CT., 2013.
2. Becke, A. D., Density-functional thermochemistry. III. The role of exact exchange. *J. Chem. Phys.* **1993**, *98*, 5648-5652.
3. Stephens, P. J.; Devlin, F. J.; Chabalowski, C. F.; Frisch, M. J., Ab Initio Calculation of Vibrational Absorption and Circular Dichroism Spectra Using Density Functional Force Fields. *J. Phys. Chem.* **1994**, *98*, 11623-11627.
4. Grimme, S.; Antony, J.; Ehrlich, S.; Krieg, H., A consistent and accurate ab initio parametrization of density functional dispersion correction (DFT-D) for the 94 elements H-Pu. *J. Chem. Phys.* **2010**, *132*, 154104.
5. Marenich, A. V.; Cramer, C. J.; Truhlar, D. G., Universal Solvation Model Based on Solute Electron Density and on a Continuum Model of the Solvent Defined by the Bulk Dielectric Constant and Atomic Surface Tensions. *J. Phys. Chem. B* **2009**, *113*, 6378-6396.
6. Andrae, D.; Häußermann, U.; Dolg, M.; Stoll, H.; Preuß, H., Energy-adjusted ab initio pseudopotentials for the second and third row transition elements. *Theor. Chim. Acta.* **1990**, *77*, 123-141.
7. Schäfer, A.; Horn, H.; Ahlrichs, R., Fully optimized contracted Gaussian basis sets for atoms Li to Kr. *J. Chem. Phys.* **1992**, *97*, 2571-2577.
8. Schäfer, A.; Huber, C.; Ahlrichs, R., Fully optimized contracted Gaussian basis sets of triple zeta valence quality for atoms Li to Kr. *J. Chem. Phys.* **1994**, *100*, 5829-5835.